LEABHARLANN CHOLÁISTE NA TRÍONÓIDE, BAILE ÁTHA CLIATH | TRINITY COLLEGE LIBRARY DUBLIN
Ollscoil Átha Cliath | The University of Dublin

Terms and Conditions of Use of Digitised Theses from Trinity College Library Dublin

Copyright statement

All material supplied by Trinity College Library is protected by copyright (under the Copyright and Related Rights Act, 2000 as amended) and other relevant Intellectual Property Rights. By accessing and using a Digitised Thesis from Trinity College Library you acknowledge that all Intellectual Property Rights in any Works supplied are the sole and exclusive property of the copyright and/or other IPR holder. Specific copyright holders may not be explicitly identified. Use of materials from other sources within a thesis should not be construed as a claim over them.

A non-exclusive, non-transferable licence is hereby granted to those using or reproducing, in whole or in part, the material for valid purposes, providing the copyright owners are acknowledged using the normal conventions. Where specific permission to use material is required, this is identified and such permission must be sought from the copyright holder or agency cited.

Liability statement

By using a Digitised Thesis, I accept that Trinity College Dublin bears no legal responsibility for the accuracy, legality or comprehensiveness of materials contained within the thesis, and that Trinity College Dublin accepts no liability for indirect, consequential, or incidental, damages or losses arising from use of the thesis for whatever reason. Information located in a thesis may be subject to specific use constraints, details of which may not be explicitly described. It is the responsibility of potential and actual users to be aware of such constraints and to abide by them. By making use of material from a digitised thesis, you accept these copyright and disclaimer provisions. Where it is brought to the attention of Trinity College Library that there may be a breach of copyright or other restraint, it is the policy to withdraw or take down access to a thesis while the issue is being resolved.

Access Agreement

By using a Digitised Thesis from Trinity College Library you are bound by the following Terms & Conditions. Please read them carefully.

I have read and I understand the following statement: All material supplied via a Digitised Thesis from Trinity College Library is protected by copyright and other intellectual property rights, and duplication or sale of all or part of any of a thesis is not permitted, except that material may be duplicated by you for your research use or for educational purposes in electronic or print form providing the copyright owners are acknowledged using the normal conventions. You must obtain permission for any other use. Electronic or print copies may not be offered, whether for sale or otherwise to anyone. This copy has been supplied on the understanding that it is copyright material and that no quotation from the thesis may be published without proper acknowledgement.

Structural and Biophysical Investigations of Rab GTPase Interacting Proteins

Submitted for the degree of Doctor of Philosophy

2011

Carmen Dregger

TRINITY COLLEGE
22 OCT 2012
LIBRARY DUBLIN
Thesis 9779

To my family

Thank you for being there, no matter what.

Declaration

This thesis is submitted by the undersigned to the University of Dublin for the examination of Doctorate in Philosophy. The work herein is entirely my own and has not been submitted as an exercise for a degree in any other university. The library of Trinity College Dublin has my full permission to lend or copy this thesis upon request.

Summary

Rab GTPases are important regulators of cell trafficking steps such as vesicle fusion, budding and motility. They are often described as 'on/off' switches, interacting with specific effectors when bound to GTP. Although their secondary and tertiary structures are largely conserved they bind sometimes very diverse effectors sharing little or no homology. A similar but less prodigious situation is evident with guanosine nucleotide exchange factors, proteins that interact with Rab GTPases in order to facilitate the nucleotide exchange during the Rab GTPase cycling. Research efforts over the past decade have concentrated on finding the specificity determinants of Rab GTPases as well as the mechanisms of interaction. This has resulted in the determination of several Rab/effector complexes. The interactions involved however are as yet poorly understood, and more structural information is needed, especially of Rab/effector complexes involving larger constructs or where possible with full length effectors. In addition to this there has been an astonishing lack of thermodynamic analyses of these interactions due to difficulties in obtaining soluble effector proteins without employing the technique of co-expression.

In this study, the full length Rab27-effector JFC1 was successfully expressed and purified and was used for thermodynamic analysis. The results show, that JFC1 also recognises GDP bound Rab27, and provides an insight into the importance of several residues for affinity and specificity. Moreover, the yeast-Rab GTPase Ypt32 was successfully purified and crystallised in its active form. Comparisons between this and other yeast GTPase structures reveals that one notable residue is central to this interaction. It is also shown that the switch II region of Ypt32 is probably very flexible which may be important for effector recognition.

In conclusion, the overall work represents a significant contribution to our understanding of Rab GTPases and their interactions with effectors. However, despite the identification of well over 100 effectors of Rab GTPases, the thermodynamics and kinetics of complex formation are poorly described. Along with crystal structures and cellular assays, these interactions require more detailed analyses to understand the biology of membrane trafficking in health and disease.

Acknowledgments

I would like to thank my supervisor Dr. Amir R. Khan for his advice and support throughout my thesis.

I am also very grateful for the help and support I have received from former and current lab members: Azmiri, Beto, Ed, Patrick, Shun, Tânia and Tomoko, you were not only a great help, but also made work often seem more fun than actual work. I consider myself very lucky to have been working with friends rather than colleagues. Also, I extend my thanks to everyone else in the department who was there to help and/or listen whenever needed.

A big thank you also goes to my friends and especially my family, for their support and encouragement throughout my studies and my thesis.

To Zakaria I am very grateful for encouraging me to pursue my studies and for his mental support, especially during the more difficult times of my thesis. It is amazing how a simple phone call at the right time can change so many things.

I remain grateful to all of them.

This work was funded by Science Foundation Ireland.

Table of contents

DECLARATION I
SUMMARY II
ACKNOWLEDGMENTS III
TABLE OF CONTENTS IV
TABLE OF FIGURES VII
LIST OF ABREVIATIONS IX

CHAPTER 1 INTRODUCTION

1.1. INTRACELLULAR TRAFFICKING 1
1.2. SMALL GTPASES 5
1.2.1. SMALL RAS GTPASES HAVE DIFFERENT FUNCTIONS 6
1.2.2. STRUCTURAL PROPERTIES OF SMALL RAS RELATED GTPASES 8
1.3. RAB GTPASES 12
1.3.1. IMPORTANCE OF RAB GTPASES IN TRAFFICKING 12
1.3.2. RAB GTPASES IN VESICLE FUSION 13
1.3.3. RAB GTPASES IN VESICLE BUDDING 15
1.3.4. RAB GTPASES IN VESICLE MOTILITY 15
1.3.5. COORDINATION OF DIFFERENT RAB GTPASE FUNCTIONS 16
1.3.6. RAB GTPASES AND RECEPTOR SIGNALLING 17
1.3.7. RAB GTPASES AND DISEASES 17
1.3.8. RAB GTPASE CYCLE 18
1.3.9. RAB FAMILY AND SUBFAMILY MOTIFS 20
1.4. STRUCTURAL PROPERTIES AND SPECIFICITY OF RAB GTPASES 21
1.4.1. STRUCTURAL BASIS FOR MEMBRANE TARGETING AND EXTRACTION 21
1.4.2. STRUCTURAL BASIS FOR ACTIVATION AND INACTIVATION OF RAB GTPASES 24
1.4.3. STRUCTURAL PROPERTIES OF RAB EFFECTORS 27
1.5. RAB27 SUBFAMILY 31
1.5.1. RAB27 AND DISEASES 31
1.5.2. RAB27 EFFECTOR PROTEINS 34
1.6. INTRODUCTION TO YEAST TRAFFICKING 42
1.7. RAB1 IS 'HI-JACKED' BY HOST PATHOGEN PROTEIN DRRA 47
1.8. PROPOSED STUDIES AND AIMS 51

CHAPTER 2 MATERIALS AND METHODS

2.1. MATERIALS 53
2.2. DNA MANIPULATION TECHNIQUES 53
2.2.1. PLASMID EXTRACTION 53
2.2.2. DNA ELECTROPHORESIS 53
2.2.3. SITE DIRECTED MUTAGENESIS 53
2.3. TRANSFORMATION OF CELLS 55
2.4. PROTEIN EXPRESSION 56
2.4.1. SMALL SCALE PROTEIN EXPRESSION SCREENING 56
2.4.2. LARGE SCALE PROTEIN EXPRESSION 57
2.4.3. EXPRESSION OF SELENOMETHIONINE CONTAINING PROTEIN 57
2.5. PROTEIN PURIFICATION 58
2.5.1. CELL HARVESTING AND PROTEIN EXTRACTION 58

2.5.2. Purification of Rab27a and Rab1a ... 58
2.5.3. Purification of JFC1 ... 59
2.5.4. Purification of full length DrrA ... 60
2.5.5. Purification of DrrA (residues 202-647) ... 61
2.5.6. Purification of Ypt32 ... 62
2.6. Complex formation ... 62
2.7. Nucleotide exchange ... 63
2.8. Protein analysis techniques ... 63
2.8.1. SDS-Polyacrylamide gel electrophoresis (SDS-PAGE) ... 63
2.8.2. Protein concentration determination ... 64
2.8.2.1. Nanodrop ... 64
2.8.2.2. Bradford protein assay ... 64
2.8.2.3. Bicinchoninic acid assay (BCA assay) ... 65
2.8.3. Isothermal Titration Calorimetry ... 65
2.8.4. Homology modelling of JFC1 ... 66
2.8.5. Static light scattering ... 66
2.9. Crystallisation techniques ... 66
2.9.1. Crystallisation condition screening ... 66
2.9.2. Seeding ... 67
2.10. Data collection and structure determination ... 67
2.10.1. Ypt32 crystal diffraction, data collection and refinement ... 67
2.10.2. $DrrA_{202-647}$ crystal diffraction, data collection and refinement ... 68
2.11. Sequence alignments ... 68

CHAPTER 3 RAB27 AND ITS EFFECTORS

3.1. Introduction ... 69
3.1.1. Rab27 effector complexes ... 69
3.1.2. Mutagenesis and Griscelli Disease ... 70
3.1.3. Goals ... 72
3.2. RESULTS ... 73
3.2.1. Production of a wild-type Rab27a expression plasmid ... 73
3.2.2. Rab27 – Expression and purification ... 73
3.2.3. Rab27a nucleotide exchange and HPLC analysis ... 75
3.2.4. Expression and purification of JFC1 ... 77
3.2.5. Complex formation of Rab27 with JFC1 ... 81
3.2.6. Crystallisation of JFC1 and Rab27(GppNHp)-JFC1 ... 84
3.2.7. Homology modeling and mutagenesis of Rab27a ... 85
3.2.8. Biophysical characterization of the interaction between Rab27a and JFC1 ... 87
3.2.3.1. Static light scattering ... 87
3.2.3.2. Thermodynamics of the Rab27a/JFC1 complex formation ... 88
3.3. Discussion ... 95
3.3.1. Rab27a expression and purification ... 95
3.3.2. JFC1 expression and purification ... 96
3.3.3. Formation of a Rab27a/JFC1 complex ... 97
3.3.4. Crystallisation of Rab27a/JFC1 ... 98
3.3.5. Static light scatterning ... 98
3.3.6. Thermodynamic analysis of the Rab27a – JFC1 interaction ... 99

CHAPTER 4 STRUCTURAL ANALYSIS OF THE RAB GTPASE YPT32

4.1 INTRODUCTION AND GOALS 102
4.2 RESULTS 104
4.2.1 YPT32 – EXPRESSION AND PURIFICATION 104
4.2.2 CRYSTALLISATION OF YPT32(GPPNHP) 108
4.2.3 DATA COLLECTION AND STRUCTURE DETERMINATION OF YPT32(GPPNHP) *108*
4.2.4 THE STRUCTURE OF YPT32(GPPNHP) *110*
4.2.5 COMPARISON OF YPT32(GPPNHP) WITH YPT32(GDP) *114*
4.2.6 COMPARISONS OF ACTIVE YPT32(GPPNHP) AND SEC4 ..... *116*
4.3 DISCUSSION 118
4.3.1 CRYSTALLISATION AND COMPARISONS OF ACTIVE/INACTIVE STRUCTURES *118*
4.3.2 COMPARISONS OF ACTIVE YPT32 AND SEC4 ..... *119*
4.3.3 GDI BINDING TO YPT31/32 ..... *120*

CHAPTER 5 RAB1 AND THE HOST PATHOGEN PROTEIN DRRA

5.1. INTRODUCTION OF RAB1 AND DRRA AND GOALS 123
5.2. RESULTS 124
5.2.1. PRODUCTION OF A GDP LOCKED RAB1A MUTANT 124
5.2.2. RAB1 – EXPRESSION AND PURIFICATION 124
5.2.3. DRRA FULL LENGTH – EXPRESSION AND PURIFICATION *126*
5.2.4. COMPLEX FORMATION OF RAB1A WITH DRRA *130*
5.2.5. $DRRA_{202-647}$ – EXPRESSION AND PURIFICATION *132*
5.2.6. COMPLEX FORMATION OF RAB1A WITH $DRRA_{202-647}$ *136*
5.2.7. CRYSTALLISATION OF DRRA AND RAB1/DRRA *138*
5.2.8. CRYSTALLISATION OF $DRRA_{202-647}$ AND RAB1/$DRRA_{202-647}$ *140*
5.3. DISCUSSION 142
5.3.1. RAB1A EXPRESSION AND PURIFICATION *142*
5.3.2. DRRA AND $DRRA_{202-647}$ EXPRESSION, PURIFICATION AND COMPLEX FORMATION WITH RAB1A *142*
5.3.3. CRYSTALLISATION OF DRRA, DRRA/RAB1A, $DRRA_{202-647}$ AND $DRRA_{202-647}$/RAB1A *144*

CHAPTER 6 FINAL DISCUSSION AND CONCLUSION

6.1. THERMODYNAMICS OF RAB-EFFECTOR COMPLEXES 145
6.2. STRUCTURE DETERMINATION OF YPT32 AND COMPARISON WITH OTHER YEAST TRAFFICKING PROTEINS 147
6.3. RAB-HOST PATHOGEN AND GEF INTERACTIONS 149
6.4. GENERAL IMPLICATIONS OF THE WORK PRESENTED 149

REFERENCES 153

Table of figures

Figure 1.1 Intracellular transport pathways....3
Figure 1.2 Steps involved in vesicle budding and fusion....4
Figure 1.3 The main steps involved in GTPase cycling....7
Figure 1.4 Visualization of the G-domain fold and arrangement of G-box motifs....10
Figure 1.5 NMR structure of H-Ras(GDP)....11
Figure 1.6 Subcellular localisation and function of selected Rab GTPases in an epithelial cell. 14
Figure 1.7 Structures of RabGDI and REP with prenylated Rab GTPase or RGGT. 23
Figure 1.8 Putative mechanism of Rab membrane extraction by GDI. 24
Figure 1.9 Structures of effector RBDs in complex with active Rab GTPases....30
Figure 1.10 Sequence alignment of Rab27a, Rab27b, Rab3a and Rab8a. 33
Figure 1.11 Schematic domain distribution of the 11 Rab27 effector proteins. 35
Figure 1.12 Sequence alignment of all known SHD containing Rab27 effectors....36
Figure 1.13 Structures of Rab27/Slp2 and Rab27/melanophilin....41
Figure 1.14 Structure of the Sec4/Sec2 complex. 44
Figure 1.15 Model for the Rab-mediated trafficking of vesicles to the exocyst. 45
Figure 1.16 Structures of Rab1/DrrA, Rab1. 49
Figure 1.17 Structures of DrrA fragments. 50
Figure 3.1 The purification of Rab27a. 74
Figure 3.2 Rab27a nucleotide exchange and HPLC analysis....76
Figure 3.3 12% SDS-PAGE analysis of the elution of Nus-JFC1 from the nickel resin with a multiple step imidazole gradient. 77
Figure 3.4 12% SDS-PAGE analysis of different fractions from a second nickel affinity step performed right after cleavage of the Nus-Tag. 78
Figure 3.5 Separation of Nus and JFC1 by anion exchange. 79
Figure 3.6 SDS-PAGE analysis of the different fractions obtained during the purification process of JFC1. 80
Figure 3.7 Different elution profiles of monomeric and dimeric JFC1....81
Figure 3.8 12% SDS-PAGE analysis of JFC1 and of the Rab27a-JFC1 complex after elution from the size exclusion column. 82
Figure 3.9 Complex formation of monomeric JFC1 with Rab27a....83
Figure 3.10 Rab27a/JFC1 crystals. 85
Figure 3.11 Homology model of JFC1 with Rab27. 86
Figure 3.12 Static light scattering coupled to size exclusion chromatography of the Rab27a Nus-tagged JFC1 protein complex....87
Figure 3.13 Titrations of WT Rab27a(GppNHp) into JFC1. 90
Figure 3.14 Titration of 90 μM WT Rab27a(GDP) into 11 μM Nus-JFC1. 91
Figure 3.15 Titration of 95 μM Rab27a Y8A into 6 μM JFC1 92
Figure 3.16 Titration of 65 μM Rab27a L84F+F88Y+D91G into 5 μM JFC1....93
Figure 3.17 Titration of Rab27a W73A into JFC1....94
Figure 4.1 Sequence alignment of Ypt32, Ypt31 and Sec4. 103
Figure 4.2 SDS-PAGE analysis of the amylose affinity chromatography step....105
Figure 4.3 Elution of MBP and Ypt32 from anion exchange chromatography. 106

Figure 4.4 Size exclusion chromatography of Ypt32. 107
Figure 4.5 GppNHp-Ypt32 crystals. 108
Figure 4.6 Sructure of Ypt32 with GppNHp. 110
Figure 4.7 2Fo-Fc map around GppNHp at1 σ. 111
Figure 4.8 2Fo-Fc map around switch II at 1 σ 111
Figure 4.9 Surface of the Ypt32-GppNHp binding pocket. 113
Figure 4.10 Interactions of Ypt32 with the β and γ-phosphate of GppNHp. 113
Figure 4.11 Ypt32 symmetry molecules with GppNHp at the interface. 114
Figure 4.12 Superimposition of Ypt32(GppNHp) with Ypt32(GDP) 115
Figure 4.13 Comparison of Ypt32(GppNHp) and Sec4(GppNHp). 117
Figure 4.14 Comparison of Ypt32(GDP) to Ypt31/GDI, Sec4(GDP) and Sec4/GDI 122
Figure 5.1 Purification of Rab1a Ser21Asn. 125
Figure 5.2 SDS-PAGE analysis of the first purification steps of DrrA. 126
Figure 5.3 Elution of DrrA from anion exchange. 128
Figure 5.4 Size exclusion chromatography of DrrA. 129
Figure 5.5 Complex formation of Rab1a/DrrA. 131
Figure 5.6 SDS-PAGE analysis of the first and second affinity chromatography steps of $DrrA_{202-647}$. 132
Figure 5.7 Elution of $DrrA_{202-647}$ from ion exchange chromatography. 134
Figure 5.8 Elution of $DrrA_{202-647}$ from size exclusion chromatography. 135
Figure 5.9 Complex formation of Rab1/$DrrA_{202-647}$. 137
Figure 5.10 Needle like DrrA crystals. 138
Figure 5.11 Diamond shaped DrrA crystal. 139
Figure 5.12 Diffraction pattern of DrrA. 139
Figure 5.13 $DrrA_{202-647}$ crystals. 141
Figure 5.14 Selenomethionine $DrrA_{202-647}$ crystals. 141
Figure 6.1 Crystal structure of Rab27(GDP). 148

List of abbreviations

AMP	Adenosine monophosohate
Amp	Ampicillin
APS	Advanced photon source
ATP	Adenosine triphosphate
BSA	Bovine serum albumin
BTP	Bis-tris propane
CBR	C-terminal binding region
CCV	Clathrin coated vesicle
CDR	Complementary-determining region
CMTB2	Charcot-Marie-Tooth disease type IIb
COP	Coat protein
CRMP-2	Collapsin response mediator protein-2
DIC	Dynein intermediate chain
DNA	Deoxyribonucleic acid
DTT	Dithiothreitol
EDTA	Ethylenediaminetetraacetic acid
EE	Early endosome
EGFR	Epidermal growth factor receptor
ER	Endoplasmic reticulum
ERGIC	ER-Golgi intermediate compartment
ESRF	European Synchrotron Radiation Facility
FL	Full length
FPLC	Fast protein liquid chromatography
GAP	GTPase activating protein
GDF	GDI displacement factor
GDI	Guanine nucleotide dissociation inhibitor
GDP	Guanosine diphosphate
GEF	Guanine nucleotide exchange factor
GppNHp	Guanosine-5'-(β,γ)-imidotripphosphate
G-protein	Guanine nucleotide binding protein
GTP	Guanosine triphosphate
HPLC	High-performance liquid chromatography
IC	Pre-Golgi intermediate compartment
IP	Immunoprecipitation;
IPTG	Isopropyl-ß-D-thiogalactopyranosid
Kan	Kanamycin
LB	Lysogeny broth
LCV	Legionella containing vacuole

LE	Late endosome
LIC	Light intermediate chain;
MBP	Maltose binding protein
MHD	Munc13 homology domain
MME	Monomethyl ether
MWCO	Molecular weight cut off
ND	Not determined
NMR	Nuclear magnetic resonance spectroscopy
ORF	Open reading frame
P4M	PtdIns4P binding of SidM/DrrA
PBS	Phosphate buffered saline
PCR	Polymerase chain reaction
PDB	Protein data bank
PEG	Polyethylene glycol
pI	Isoelectric point
mM	Millimolar
SDS	Sodium dodecyl sulfate
PAGE	Polyacrylamide gel electrophoresis
p-loop	Phosphate-binding-loop
PM	Plasma membrane
PMSF	Phenylmethanesulfonylfluoride
PtdIns(3)P	Phosphatidylinositol 3-phosphate
RBD	Rab binding domain
REP	Rab escort protein
RGGT	Rab geranylgeranyl transferase
RMS	Root mean square
SeMet	Selenomethionine
SGC	Structural genomics consortium
SHD	Slp homology domain
Slp	Synaptotagmin-like protein
SNARE	Soluble N-ethylmaleimide-sensitive factor attachment protein receptor
SPR	Surface Plasmon resonance
TEMED	Tetramethylethylenediamine
TGN	Trans-Golgi network
TRAPP	Transport protein particle
WT	Wild-type
Y2H	yeast two-hybrid
YT	Yeast Extract Tryptone

Chapter 1

Introduction

1.1. Intracellular trafficking

Eukaryotic cells are compartmentalised into membrane bound organelles that establish and manage functionally distinct environments. This facilitates discrete protein, lipid, nucleic acid, and molecular segregation and mediates cargo trafficking to various intra and extracellular destinations. As an example, proteins destined for different locations inside or outside the cell are initially produced by ribosomes that reside on the endoplasmic reticulum (ER). Secreted proteins are then transported through the Golgi complex for further processing and maturation. From there the proteins are transported to the plasma membrane where they are either released from the cell (exocytosis) or they remain tethered to the membrane. Figure 1.1 presents a schematic of intracellular transport pathways. In 1974 G. Palade was awarded the Nobel Prize in medicine or physiology for the discovery of the protein secretory pathway in mammals [1]. Later it was shown that the vesicular transport machinery mechanism is the same in yeast and mammals [2-3]. Knowledge of transport pathways has advanced greatly but the molecular intricacies involved remain elusive.

Trafficking inside cells not only happens for the purpose of protein secretion. Endocytosis and transport to and from the lysosome also present an important part of cargo trafficking inside the cell. To facilitate trafficking between the different cell compartments, the cargo is packed into membrane enclosed transport vesicles. These vesicles are customised, somewhat ensuring that the cargo arrives at its destination through specific and directed movement. Regulation is also required so that only proteins destined for relocation are included in the transport vesicles. Thus regulation is needed at different steps and hence many different proteins are involved in the process. This results in a vast range of research that is needed for a better understanding of cargo trafficking inside the cell.

The process of vesicle transport can be divided in four main steps (Figure 1.2.): (1) a vesicle is formed, (2) the vesicle moves towards its target where, (3) tethering and docking take place followed by, (4) fusion of the membranes and release of the cargo. Upon assembly of cargo proteins from the cytoplasm, vesicle budding is initiated and a protein coat is formed around the vesicle. The vesicle then moves towards the target by diffusion or facilitated by vesicle-associated motors that interact with the cytoskeleton of

the cell. Kinesin, dynein and myosin have all been shown to take part in motor mediated vesicle transport [4-6]. Once the vesicle reaches its destination tethering then takes place. Tethering describes the initial interaction between a vesicle and the target membrane. The protein coat was initially thought to be released from the vesicle before tethering, but more recent studies show that it is sometimes involved in initialising the tethering process and only then released to allow membrane fusion [7].

Proteins/protein complexes termed tethers or tethering factors were implicated in nearly all trafficking events [8]. Tethers, along with Rab proteins, small Ras related GTPases, are critical for the specificity of vesicle targeting and it has been proposed that tethers interact with Rab GTPases [9]. Upon tethering the vesicle membrane fuses with the target membrane. For this purpose soluble N-ethylmaleimide-sensitive factor attachment protein receptors (SNAREs) that are bound to the vesicle (v-SNARE) and the target membrane (t-SNARE) interact with each other [10].

The composition of the protein coat depends on the transport step. Three different types of coats have been identified thus far. Clathrin coats were the first to be identified [11-12] and were initially thought to be involved into most transport steps. Later studies showed that they are involved in post-Golgi locations including plasma membrane, the trans-Golgi network (TGN) and endosomes. Coat protein I (COPI) is known to take part in intra-Golgi transport as well as retrograde transport from the Golgi to the ER [13], while COPII mediates transport from the ER towards either the ER-Golgi intermediate compartment (ERGIC) or the Golgi complex [14].

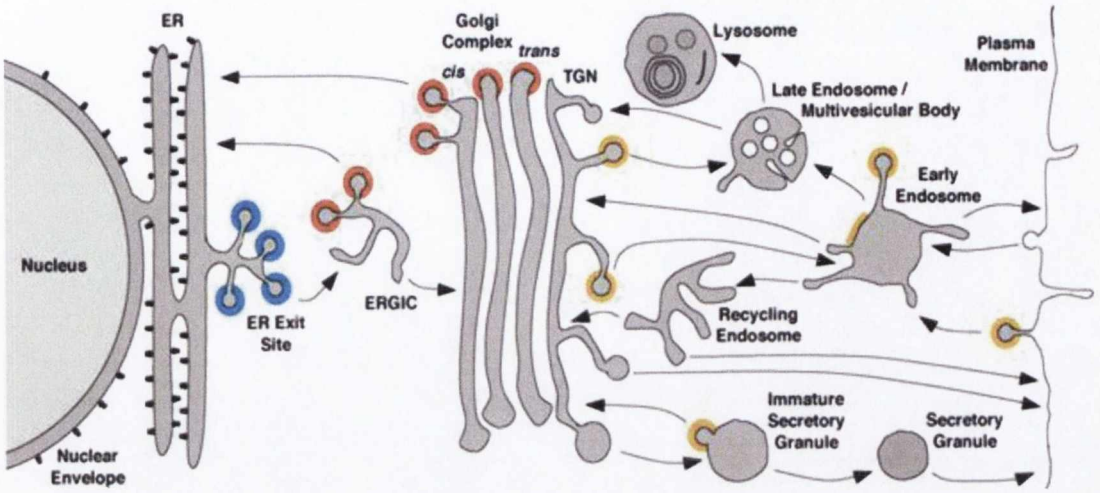

Figure 1.1 Intracellular transport pathways.
This figure shows the compartments of the secretory, lysosomal/vacuolar, and endocytic pathways with directional transport indicated by arrows. The presumed locations of protein coats (COPII (blue), COPI (red), and clathrin (orange)) are also presented.
Adapted from [15]

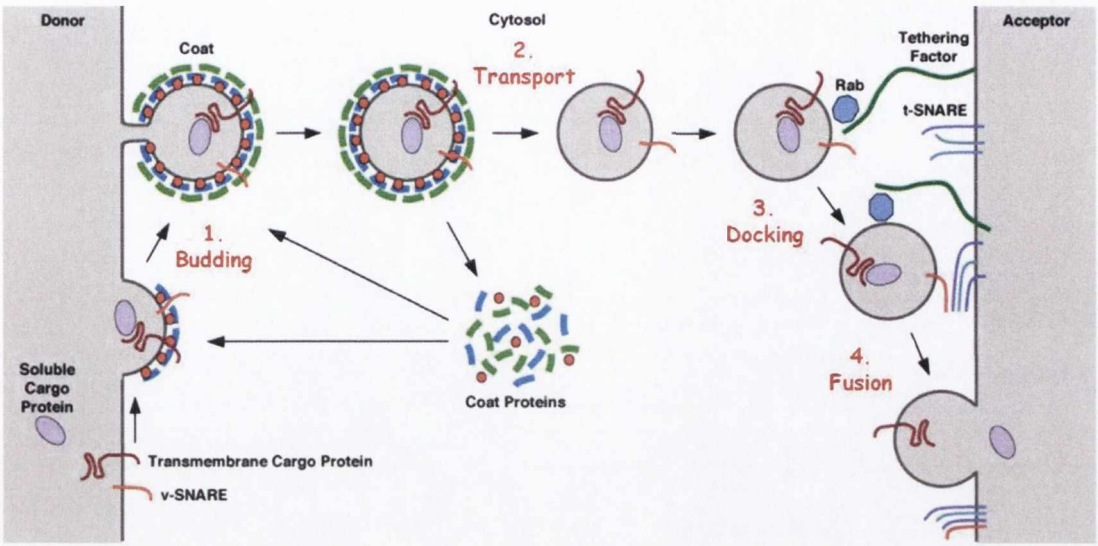

Figure 1.2 Steps involved in vesicle budding and fusion.
(1) Budding: Cargo proteins diffuse into the budding site where they are trapped with coat proteins or cargo receptors. The coat is assembled and a bud that matures into a vesicle is formed. (2) Transport: The vesicle is transported towards the acceptor membrane by associating with cytoskeletal elements and transport motors (not shown). (3) Docking: When the vesicle comes close to the target membrane it is tethered to it by the combination of a GTP bound Rab, elongated coiled-coil tethering proteins and other tethering factors (not shown). After the tethering step an R-SNARE (VAMP) assembles with a Qa-SNARE (syntaxin), Qb-SNARE (SNAP N) and Qc-SNARE (SNAP C) forming a parallel, four-helical bundle. (4) Fusion: This so called Trans-SNARE, or ternary core fusion complex leads to further approach of vesicle and target membranes, possibly driving the fusion reaction. (5) Disassembly: After fusion has occurred Rab-GDP is released from the membrane by a GDI and then recruited back to the donor membrane. The SNARE-complex is disassembled by the ATPase N-ethylmaleimide-sensitive factor and α-SNAP in order for the SNAREs to be recycled. More recent studies showed that the uncoating of the vesicle (taking place immediately after scission from the donor membrane in this schematic) takes place later during the transport process [7]. Figure from [15]

1.2. Small GTPases

Guanine nucleotide-binding proteins (G-proteins) bind and hydrolyse the guanosine nucleotide GTP. Some G-proteins, i.e. G_S1, are large and comprise of heterotrimers with subunits Gα, Gβ and Gγ [16-17]. Furthermore there are large numbers of small G-proteins and the first members of this family to be detected were the Ras GTPases. Thus small G proteins are more often termed Ras GTPases (superfamily), small GTPases (of the Ras superfamily) or small Ras related GTPases, whereas the large G-proteins are usually referred to as G-proteins. Small Ras related GTPases with evolutionary conserved orthologs have been identified in all eukaryotic organisms. In lower organisms like *Saccharomyces cerevisiae* (*S. cerevisiae*) or *Caenorhabditis elegans* (*C. elegans*) there are fewer GTPases than in mammals, for example there are 35 human Ras subfamily proteins but only 12 in *C. elegans* [18]. The small Ras related GTPases superfamily can be divided into 5 subfamilies: Ras GTPases, Rho GTPases, Ran GTPases, Arf GTPases and Rab GTPases. Small Ras related GTPases share about 30% homology with up to 55% homology in the subfamilies [19]. The subfamilies of small Ras related GTPases differ in many ways but it has been shown that all share a similar mechanism of activation and deactivation which will be discussed further.

Small Ras related GTPases are typically monomeric and are homologous to the Gα subunit of large G-proteins. Their usual size ranges from 20-25 kDa and they function as GDP/GTP-regulated molecular switches [20-21]. They have a high affinity for GDP and GTP that requires the cofactor Mg^{2+}. Since the GTP-bound forms of small Ras related GTPases are able to control the activities of their effectors, like molecular switches, they are considered active (or 'on') in the GTP bound form whereas the GDP-bound forms are considered inactive (or 'off'). With an ability to cycle between active and inactive states, small Ras related GTPases have evolved to become powerful regulators of various processes within the cell. The rate limiting factor for the protein activation is GDP-GTP exchange. Two main classes of regulatory proteins control the cycling between GDP- and GTP- bound states. Formation of the active form is facilitated by guanine-nucleotide exchange factors (GEFs) [22] while the intrinsic rate of GTP hydrolysis is accelerated by GTPase activating proteins (GAPs) [23]. In addition to these mediators, guanine nucleotide

dissociation inhibitors (GDIs) also exist. They bind to GDP-bound GTPases which prolongs the inactive state by inhibiting the release of GDP. The GTPase is released from a GDI through the activities of a GDI displacement factor (GDF) [24-26]. To date, GDIs have only been identified for Rho and Rab proteins which represent different subfamilies of small Ras related GTPases. An illustration of the GTPase cycle of Rab GTPases is shown in Figure 1.3.

1.2.1. Small Ras GTPases have different functions

Despite having structural similarities discussed in Section 1.2.2, it is important to note the distinct differences found between members of small Ras GTPase subfamilies. The effectors of each subfamily can be very distinct, and some Ras GTPases were shown to interact with more than one effector protein, for example Rab GTPases [27-28]. Apart from conserved so called G-box motifs, the sequences of small Ras GTPase subfamily members can vary greatly. The differences in sequence makeup combined with the degree of conformation flexibility of regions such as switch II has led to a diversification in the effectors recognised by these proteins. Most importantly, this has produced a diversification of function in the cell [18, 29]. The functions of the subfamilies members outlined earlier for example have distinct cellular function. The Ras subfamily of GTPases (Ras sarcoma oncoproteins) which were the first one to be identified, and was implicated in certain types of cancer [30-31]. Ras proteins are important in the regulation of cytoplasmic signalling networks that control gene expression as well as cell proliferation and differentiation. The Rho (Ras homology) subfamily proteins are closely related to the Ras subfamily. But they have been found to take part in cytoskeletal remodelling and cell polarity [32-33]. The Ran (Ras-like nuclear) proteins are involved in nucleocytoplasmic transport of proteins and RNA. Ran is the most abundant small GTPase in the cell [34]. Arf (ADP-ribosylation factor) GTPases take part in the regulation of vesicular transport. The initiation step for COPI assembly requires activation and membrane recruitment of Arf [35]. Rab GTPases (Ypt in yeast), from Ras like protein in brain or sometimes Ras associated binding, were first purified from rat brain [36]. They are important for the regulation of intracellular vesicular transport of proteins in the endocytic and secretory

pathways and are implicated in the specificity of vesicle delivery to receptor membranes [28].

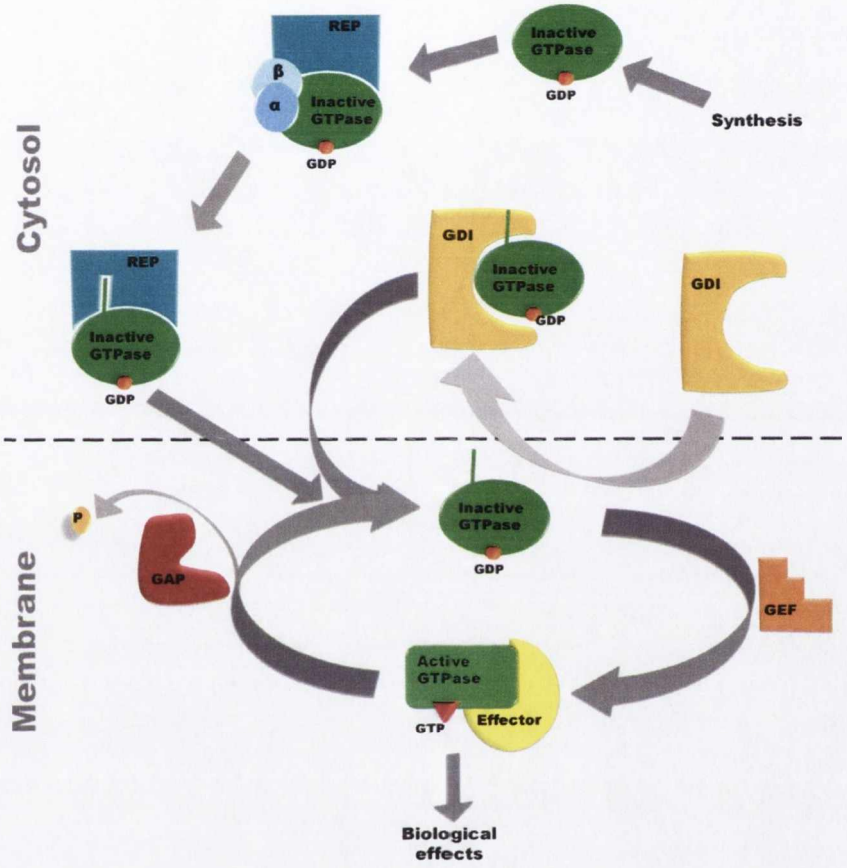

Figure 1.3 The main steps involved in GTPase cycling.
Rab GTPases are used as an example for all Ras related GTPases. Unmodified GDP-bound Rab is recognised by Rab escort protein (REP) and presented to Rab geranylgeranyl transferase (RGGT; α and β subunits) which leads to prenylation of one or two C-terminal cysteines with geranylgeranyl. Prenylated Rab GTPase is then released from RGGT but remains in complex with REP which escorts it to its distinct organelle membrane where it anchors via insertion of the hydrophobic residues. Membrane bound Rab GTPase is then activated by a GEF which exchanges GDP to GTP. Now the Rab GTPase can interact with its effectors leading to biological effects that involve the small GTPase in cell signalling or trafficking. Afterwards GTP hydrolysis is accelerated by a GAP. GDP bound Rab protein is then extracted from the membrane by GDI, which recycles the Rab GTPase to its distinct organelle membrane. Where the GDF dissociates the Rab/GDI complex and enables activation by a GEF. For simplicity the other functions of Rab proteins such as interaction with motors or effectors are not shown. (After [37])

1.2.2. Structural properties of small Ras related GTPases

The structures of many small Ras related GTPases in both active and inactive states, have been determined. This has made it possible to characterise a Ras superfamily G-domain fold which consists of a six-stranded β-sheet, five parallel with one antiparallel, framed by five α-helices [21], also see Figure 1.4. It has also been shown that small Ras related GTPases possess a universal switch mechanism [20]. Generally the overall conformation of the protein does not change upon binding to GDP or GTP, except for two regions which show distinct changes. They 'switch' their positions depending on the nucleotide bound, and are referred to as switch I (Ras residues 30-38) and switch II (Ras residues 60-67) [20, 38]. These switch regions are able to distinguish the constitution of the bound nucleotide via invariant residues that bind to the γ-phosphate of GTP [21]. But the switch regions also present an important part of the binding sites for effectors, thus coupling GTP hydrolysis directly to effector recognition and regulation.

Bourne and colleagues [39] identified conserved G-box GDP/GTP-binding motif elements that are found in all small Ras related GTPases: G1, GxxxxGKS/T; G2, T; G3, DxxGQ/H/T; G4, T/NKxD; and G5, C/SAK/L/T (where X represents any amino acid). The G1 motif is also known as the phosphate-binding-loop (p-loop). It contains a Ser or Thr which is coordinated by the Mg^{2+} ion in the active state. The p-loop mainly interacts with the β-phosphate of the nucleotide, keeping it in place within a shallow pocket at the surface of the protein [40]. Affinity studies showed it to be the most important part for the nucleotide-GTPase interaction. p-loops are common features for GTP and ATP binding sites [41]. The G2 Thr (positioned in switch I) contacts the γ-phosphate and is also coordinated by the Mg^{2+} ion in the active state. The Asp of G3 (switch II) stabilises the Mg^{2+} through interaction with a water molecule, the backbone amide of Gly contacts the γ-phosphate and the side chain of Gln serves as a catalytic residue for the intrinsic GTP hydrolysis. The conformational change in the switch regions is due to the loss of hydrogen bonds to the γ-phosphate upon GTP hydrolysis. Changing the nucleotide binding and hydrolysis properties can be done by mutating conserved G box motifs. Most commonly used are substitution of the p-loop Ser/Thr to Asn (SN or TN mutant) and the G3 Gln to Leu (QL mutant). SN or TN mutants have a disrupted Mg^{2+} binding site which results in reduced affinity for guanine nucleotides, in low Mg^{2+} concentrations especially for GTP.

This suggests a 'GDP-locked' state for these mutants [42]. QL mutants are supposedly locked in the GTP bound state. The G4 and G5 motifs are involved in interactions with the guanine base, they discriminate the nucleotide binding pocket against other nucleotides such as ATP/ADP [43]. Figure 1.4 displays the 3-dimensional arrangement of G-box motifs.

Further analysis, shows that switch I and II are not found in one designated 'on' or one designated 'off' position, but in several conformations whereas the rest of the protein does not change in conformation. The NMR structure of H-Ras bound to GDP for example reveals that especially switch II, and to a lower magnitude also switch I, are much more flexible than the rest of the protein (Figure 1.5) Although no NMR structure is available for a native GTP-bound Ras GTPase, NMR spectroscopy of Ras GTPases bound to GTP suggests that several distinct conformations exist for the switch regions [45-46]. It has been suggested that the different switch conformations, which pre-exist, are recognised by the different effectors and that effector-binding does not necessarily involve large changes in switch conformations, but that effectors preferably bind when the switch region adopts the most convenient conformation [46]. This has been shown not to be true for all Ras related GTPases. For example the structure of Rab11(GTP)/FIP2 shows that switch II undergoes a large conformational change in order to bind FIP2 [47]. Switch I is highly flexible in the GDP bound state but when bound to GTP it binds to the Mg^{2+} cofactor and a conserved threonine residue forms a hydrogen bond with the γ-phosphate of GTP which stabilises the loop [46]. Switch II is generally more ordered in the GTP state, and by definition, switch I and II adopt different conformations in the GTP versus. GDP bound states. A comparison of various crystal structures of small Ras GTPases bound to GTP and GDP revealed that the switch regions adapt a less diverse conformation in the GTP-bound form than the GDP-bound form [21], illustrating the conformational changes of the switch regions and the higher switch flexibility in the GDP-bound state. But as different proteins are compared this does not prove that the switch regions do not adapt a single conformation for each nucleotide-bound state.

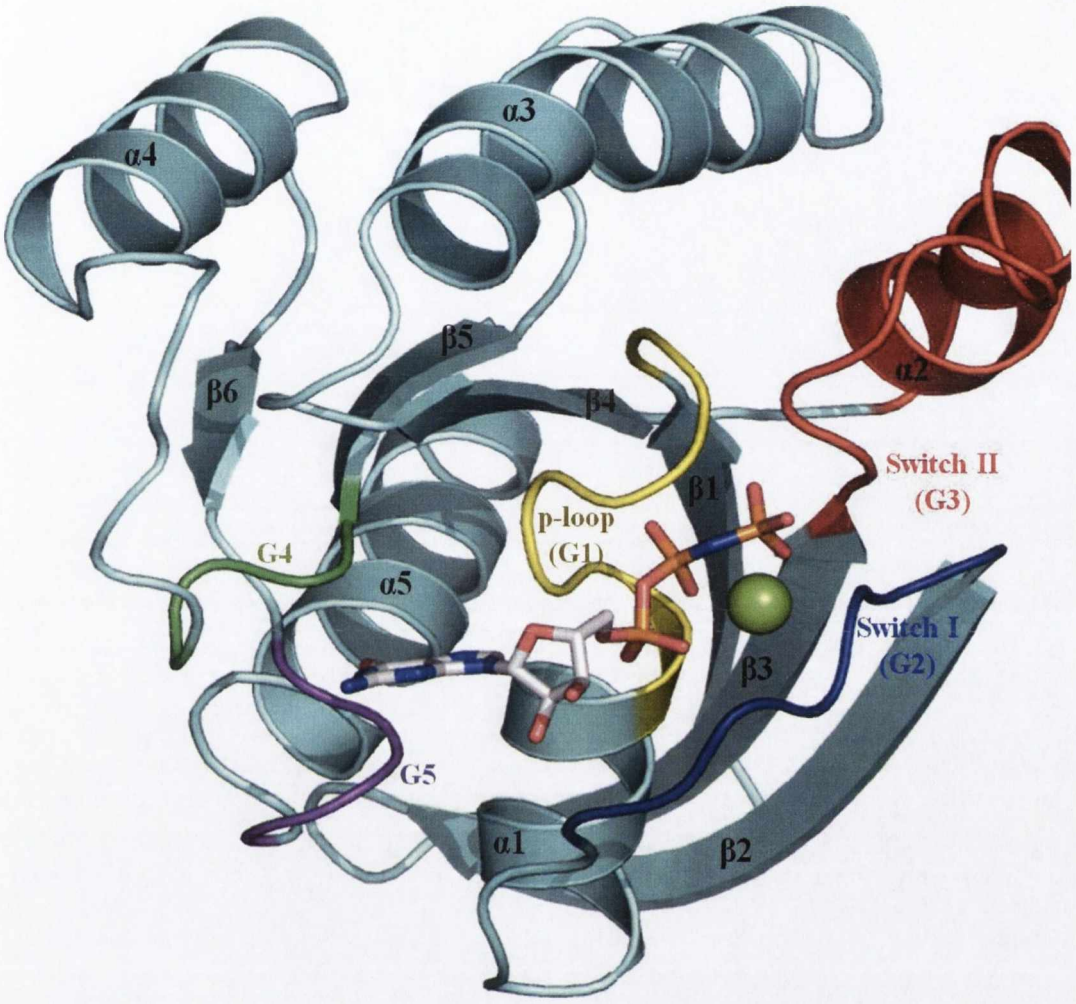

Figure 1.4 Visualization of the G-domain fold and arrangement of G-box motifs.
The structure presented is H-Ras in complex with the non-cleavable GTP analogue GppNHp. The different G-box motifs are coloured differently, GppNHp is represented as sticks and Mg^{2+} as a green sphere. PDB-file used for this figure: 5P21, [44]

Structures of different small GTPase/effector complexes indicate that the switch conformations found upon effector binding pre-exist as a repertoire of states. This would mean that the GTPases might exhibit a certain number of switch conformations that are specific for different binding surfaces. When binding to an effector, the GTPase stays in the corresponding switch conformation [46]. Small Ras GTPases have been found to bind to more than one effector. Analyses of the residues involved in the binding process showed that the interacting regions of the small Ras related GTPase are only partly the same for

different effectors, making it difficult to predict the determinants of their specificity [21, 48]. Although non switch regions have been identified to contribute to several complexes, the switch region residues present a higher multiplicity of conformations with some of their residues participating in almost all complexes formed. The high multiplicity of the switch regions is thought to be a reason for the ability of small Ras related GTPases to recognise multiple ligands and to be differentially regulated by them [21, 49].

Figure 1.5 NMR structure of H-Ras(GDP).
Carbon Cα traces of the ensemble of 20 conformations derived from the NMR structure of the GDP-bound form of H-Ras. The p-loop is coloured yellow, switch I is in blue and switch II in red. The main part of the protein, including the p-loop, is not very flexible, but near the two switch regions the Cα trace is disperse, indicating high flexibility. This is especially true for switch II which does not interact with the GDP. It is likely that a Ras(GTP) structure would show a less flexible switch II because the switch II interacts with the γ-phosphate of GTP. PDB-file used for this figure: 1CRP [50].

1.3. Rab GTPases

1.3.1. Importance of Rab GTPases in trafficking

Rab GTPases present the biggest subfamily of small Ras related GTPases with over 60 identified genes in humans and 11 in *S. cervisiae* [19]. Rab GTPases are essential for intracellular trafficking. The amount of Rab GTPase encoding genes increases significantly from yeast (11) to fly (32) to humans (over 60), which is in contrast to a relatively constant number of coat proteins, SNARE's. These observations suggest a greater regulatory requirement for vesicle-trafficking pathways with increasing complexity of the organism [51]. Expression of evolutionary conserved Rab GTPases normally takes place in all cell and tissue types. Less conserved Rab GTPases are found to function in more specific, often tissue dependent pathways [52]. Depending on the cell compartment, a unique set of Rab GTPases are found, and some Rab GTPases are only expressed in a specific subset of cells or tissues. For example Rab3a is only expressed in neurons [28, 53]. The importance of Rab GTPases in vesicle transport is highlighted by the finding that a large number of Rab isoforms are present on vesicles [54]. Furthermore Rab GTPases organise almost all trafficking processes in eukaryotic cells [27]. This is often mediated through indirect interactions with coat components, motors and SNAREs. ER-Golgi trafficking is mediated by Rab1, located at ER exit sites and the pre-Golgi intermediate compartment (IC). Rab2 is also located at the IC and might also regulate Golgi-ER trafficking. Rab6, Rab33 and Rab40 are localised in the Golgi and mediate intra-Golgi trafficking. Rab33, together with Rab24, also regulates the formation of autophagosomes. Constitutive biosynthetic trafficking from the TGN to the plasma membrane involves Rab8 that also participates in GLUT4 vesicle translocation (together with Rab10 and Rab14) as well as in ciliogenesis (with Rab17 and Rab23). Rab3, Rab26, Rab27 and Rab37 are involved in various types of exocytic events. Rab27 also mediates the translocation of melanosomes to the cell periphery. The biogenesis of melanosomes involves Rab32 and Rab38, additionally Rab32 controls mitochondrial fission. Assembly of tight junctions between epithelial cells is regulated by Rab13 whereas Rab18 controls the formation of lipid droplets. Rab22 is involved in trafficking between the TGN and early endosomes. Localised to early endosomes, phagosomes, caveosomes and the plasma membrane is Rab5, it mediates endocytosis and endosome fusion of clathrin coated vesicles (CCVs), macropinocytosis

(with Rab34), and maturation of early phagosomes (with Rab14 and Rab22). Integrin endocytosis is mediated by Rab11, Rab21 also takes part in this process. Rab11 and Rab35 mediate slow endocytic recycling through recycling endosomes, whereas Rab4 mediates fast endocytic recycling directly from early endosomes. Rab15 is not only involved in trafficking from early endosomes to recycling endosomes but also in the trafficking from apical recycling endosomes to the basolateral plasma membrane. Trafficking through the apical recycling endosomes to the apical plasma membrane is controlled by Rab17 and Rab25. Rab7 is associated to the late endosome and mediates maturation of late endosomes and phagosomes, and their fusion with lysosomes. Rab9 is also associated to the late endosome and mediates trafficking from late endosomes to the TGN [27]. Figure 1.6 presents Stenmark's summation of known localisations of Rab proteins within the cell.

1.3.2. Rab GTPases in vesicle fusion

The first evidence for Rab GTPases involvement in intracellular trafficking was reported by Salminen and Novick [55]. They mutated Sec4 (a yeast Rab GTPase) and showed that this causes an accumulation of TGN-derived vesicles destined for secretion. They concluded that this GTPase plays an essential role in controlling a late stage of the secretory pathway. It was assumed that Rab GTPases were involved in tethering and docking of transport vesicles to their target membrane but were not responsible for the specificity. The most important determinants of specificity for membrane targeting were thought to be SNAREs [56]. It has now been shown that Rab GTPases are mainly responsible for the membrane specificity of the transport vesicle via their interactions with tethers and SNAREs which is consistent with the finding that almost all known tethers interact with Rab GTPases [8, 57-59].

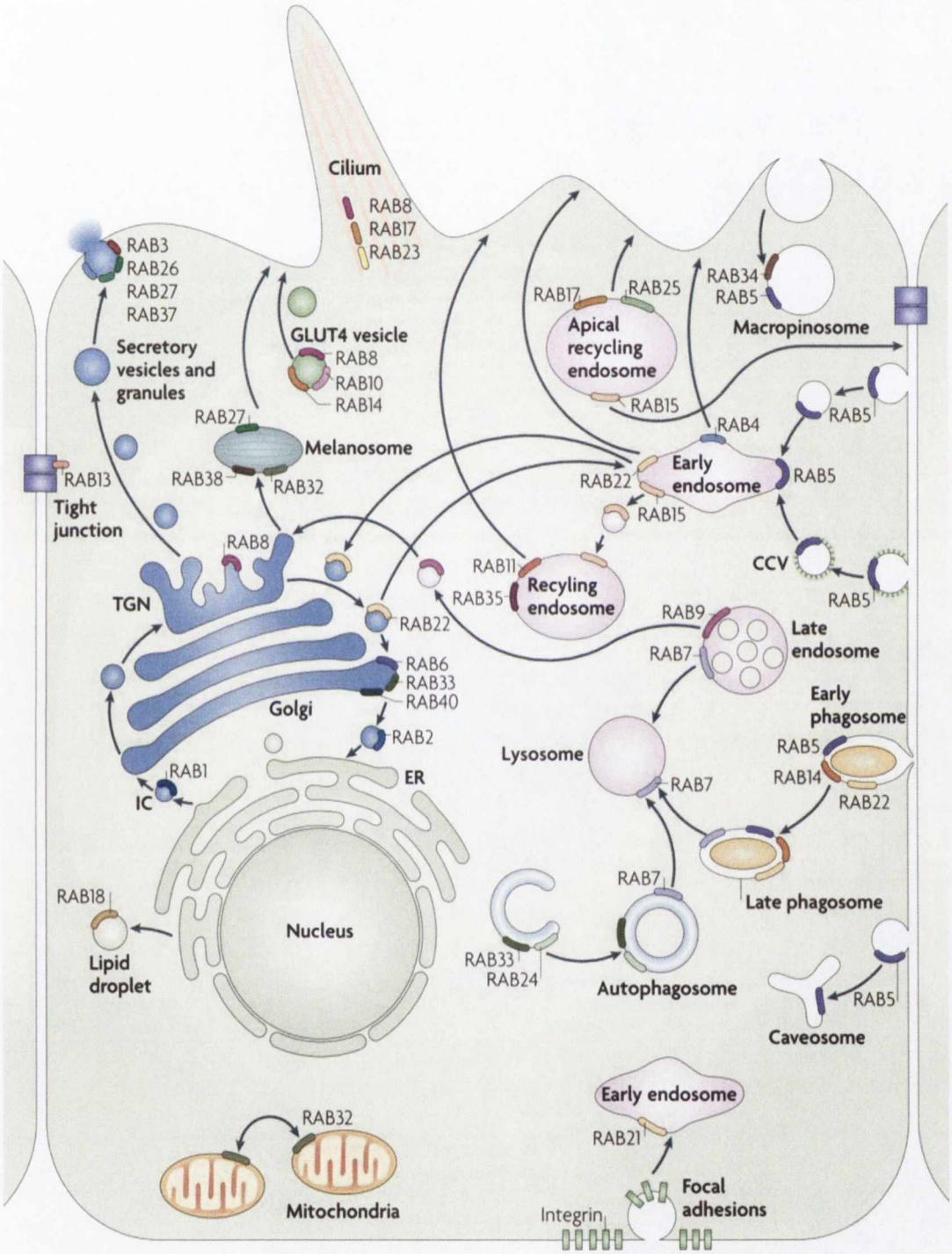

Figure 1.6 Subcellular localisation and function of selected Rab GTPases in an epithelial cell.
Figure from [27]

1.3.3. Rab GTPases in vesicle budding

Vesicles are formed by a process called vesicle budding. Transmembrane proteins that are cargo or cargo receptors associate with cytosolic coat protein complexes. Several factors are involved in the sorting of cargo destined for different locations. The coat complexes recognise different cargoes which makes the coat assembly cargo-specific. Furthermore other determinants such as membrane curvature, lipid composition as well as Rab GTPases enable specific cargo and/or coat recruitment which results in transport towards the right destination [15, 27]. It was shown for example that Rab9 significantly increases the affinity of cargo receptor TIP47 for its cargo and is thus regulating its uptake [60]. Some other Rab GTPases have been shown to be involved in vesicle budding or SNARE recruitment [60-63].

1.3.4. Rab GTPases in vesicle motility

In order to arrive at their destination, vesicles that are transported between different cell compartments have to be directed, from donor to target compartments. Several motor proteins have been implicated in this process, and involve both the microtubule and the actin network. The actin network is usually involved in transport over a shorter range whereas microtubules transport vesicles over a longer range [64]. Different motor proteins move along actins or microtubules and are thought to associate with cargo in order to transport it to its destination. Most kinesin motors move towards the plus ends of microtubules, dyneins towards the minus end [65-67]. Myosin motors (except for myosin VI) move towards the plus end of actins [68]. Myosins present a large protein family and have a variable tail domain that mediates interaction with specific cargoes [69]. Myosin V is the most efficient member of that family, it is able to slide along actin without dissociation [70]. Some Rab GTPases interact with motor proteins directly or via another protein, which highlights the importance of some Rab proteins in vesicle motility [4-5, 71]. Table 1.2 presents a summary of the different known Rab GTPase involvements with motor proteins.

Table 1.1 Rab GTPases interacting with motor proteins (adapted from[72])

Rab	Motor	Compartment	Interaction	Effector	Reference
Rab4	KIF3B	EE	IP		[73]
	LIC	EE	Y2H		[74]
Rab5	DIC	EE	IP		[75]
	KIF16B	EE	No	PI3K	[76]
Rab6	$p150^{GLUED}$	Golgi	Y2H	BicD1/2	[6, 77]
	$p50^{dynamitin}$	Golgi	Pull down		[6]
	RB6K/MKLP2	Golgi	Y2H, pull down		[78]
Rab7	Dynein/dynactin	LE/Lys	Unknown	RILP	[79]
Rab8	MyoVI	Golgi	Y2H, direct interaction	Optineurin	[80-81]
Rab11	MyoVb	Recycling compartment	Y2H		[82]
			Y2H	Fip2	[83]
Rab27a	MyoVa	Melanosome	Y2H, IP	Melanophilin/Slac2	[84-88]
	MyoVIIa	Melanosome	Pull down	MyRIP	[89-90]

DIC, dynein intermediate chain; IP, immunoprecipitation; LIC, light intermediate chain; Y2H, yeast two-hybrid

1.3.5. Coordination of different Rab GTPase functions

As described in Section 1.3.1 different Rab GTPases are found to localise to distinct sub-cellular organelles. Furthermore it was found that different Rab GTPases, that are found on the same organelle, do not mix, but stay separated from each other and present distinct microdomains (also called Rab domains [91]). Over time a transport compartment can undergo a change of the associated Rab GTPases which causes a change of other associated proteins, converting it into another compartment, as happens for instance by exchange of Rab5 for Rab7 at the interface between early and late endosomes [92-93]. This implies that a mechanism exists which enables the selection of different Rab GTPases and facilitates their positioning on different parts of the membrane. It has been proposed that this could, at least in part, be mediated by Rab effectors [27]. It remains unclear however, how the different Rab GTPases coordinate such actions. Several 'bivalent' Rab effectors were found to have separate non-overlapping binding sites for different Rab GTPases, and interaction with one Rab can results in enhanced affinity for another Rab GTPase, suggesting possible cooperativity and coordination of Rab binding and subsequent trafficking [94]. Evidence has been found that Rab GTPases also confer membrane identity

by controlling the phosphoinositide levels of their associated membranes, which would influence the recruitment of other membrane associated proteins [95-96].

1.3.6. Rab GTPases and receptor signalling

Many signaling receptors have to traverse the endocytic pathway in order to arrive at their destination, and endosomal membranes are themselves organised into compositionally and functionally specialised domains [97]. It has been shown that endocytosis is a fundamental organiser of the cell and coordinates the core variables in cell signaling (duration, intensity, integration, and spatial distribution) in order to control processes such as cell fate determination and cell migration [98]. Rab5 for example has been shown to be involved in epidermal growth factor receptor (EGFR) signaling [99]. Rab7 was found to be activated by growth factor withdrawal, suggesting it contributes to the induction of apoptosis and indicating that Rab7 dependent fusion reactions might be targeted by signaling pathways that limit growth factor-independent cell survival [100].

1.3.7. Rab GTPases and diseases

Rab GTPases have been linked to several genetic and acquired diseases, some of them through Rab-associated proteins. The Charcot-Marie-Tooth disease type IIb (CMTB2) for example is characterised by prominent sensory loss, marked distal weakness, foot deformities and there is a high frequency of ulcers occurring with associated infection. As a consequence, amputation of toes is often necessary [101]. CMTB2 is caused by mutations in Rab7, which are thought to keep the protein in a GTP locked state [102]. Other examples are defects in Rab GTPase dependent transport steps that have been linked to the Griscelli syndrome, choroideremia and osteoporosis [103-105]. Several pathogens have been reported to modulate Rab GTPase function, especially in the endocytotic pathway which is involved in host pathogen defense by fusing the phagocytes with lysosomes [106]. At least one pathogen, *Legionella pneumophilia*, was reported to 'hijack' a Rab GTPase (Rab1) along with other host proteins to its legionella containing vacuole which adopts an ER like morphology. Until recently, in contrast to Ras and Rho GTPases, Rab GTPases were not linked to cancer. However this has changed and several Rab

GTPases have been found to be aberrantly expressed in tumor cells [107]. Given their involvement in EGFR signaling, for example it is possible that altered expression of the involved Rab GTPases contributes to tumorigenesis [107]. Table 1.2 summarises all Rab GTPases that had been linked to diseases in 2011.

1.3.8. Rab GTPase cycle

After translation Rab GTPases undergo posttranslational modifications the most noteworthy being prenylation of one or two cysteins with geranylgeranyl (a C20 isoprenoid group) at their C-terminus [156]. In contrast to other small Ras related GTPases, Rab proteins do not present one prenylation motif but several: Cxxx, CC, Cxx or CCxx where x represents any amino acid. Sometimes only one cysteine residue is present for prenylation at the C-terminal. RGGT (Rab geranylgeranyl transferase) does not recognise Rab protein prenylation motifs alone, so in order to be prenylated the Rab must bind the REP (Rab escort protein), a 95 kDa protein, and only then can it be recognised as a substrate of RGGT [157]. Once prenylated, REP transfers the Rab GTPase to the membrane of its specific compartment where it is tethered to the membrane followed by activation by a GEF. It then interacts with its effectors and remains linked to the transport vesicle until the vesicle fuses with its target membrane. GTP is hydrolysed to GDP by means of a GAP and the Rab GTPase is separated from the membrane by GDI. Apart from inhibiting GDP to GTP exchange, GDIs are thought to catalyse insertion and recovery of prenylated Rab GTPases into and out of cellular membranes [158]. GDI then delivers the Rab protein back to the donor membrane, thus recycling it and completing the cycle, where the Rab-GDI dissociation involves a GDI displacement factor (GDF) [159]. Figure 1.3 depicts Rab GTPase prenylation and recycling as well as the GTPase cycle. Interestingly, GDIs are structurally related to REPs, binding Rab GTPases via interaction with a conserved 'Rab-binding platform' but GDIs do not interact with RGGT and have a very low affinity to unprenylated Rab proteins [160]. Three GDI isoforms have been isolated to date (GDIα, GDIβ and GDIγ) [149].

Table 1.2 Rab GTPases implicated in monogenic and multigenic diseases. (Adapted from [108])

RAB isoforms	Cellular locations	Functions	Diseases
Rab1 A, B	ER, Golgi	ER–Golgi trafficking	Elevated in tongue cancer [109], oculocerebrorenal syndrome [110], infections [111-112]
Rab2 A, B	ER, Golgi, PM, melanosomes	ER–Golgi trafficking	Elevated in various cancers [113-114]
Rab3 A, B, C, D	PM	Neurotransmitter release, fusion of synaptic vesicle, exocytosis (insulin), protein transport	Cancers of nervous system [115], neuro-endocrine related cancers [116], pituitary adenomas [117-118], Warburg Micro syndrome [119]
Rab4 A,B	PM	Protein transport	Obesity [120], diabetes [121]
Rab5 A, B, C	PM, EE, melanosomes	Fusion of PM to EE, protein transport	Various cancers [122-126], oculocerebrorenal syndrome [110], neurodegenerative Diseases [127-128], Huntington's disease [129], bacterial infection[130], diabetes [121]
Rab6 A, A', B	Golgi membrane	Golgi–ER trafficking	Oculocerebrorenal syndrome [110]
Rab7 A, B	LE, lysosome, phagosome, melanosomes	Late endocytic transport, maturation of phagosome	Hereditary sensory and autonomic neuropathies [131], Niemann–Pick disease type C [132], Alzheimer's disease [133-134], Chagas disease [135], thyroid carcinoma [136]
Rab8 A, B	PM	Vesicular trafficking, neurotransmitter release, dendrite extension, ciliogenesis	Melanoma [137], retinal degeneration in mice/glaucoma [138], microvillous inclusion disease [139-140], Bardet–Biedel syndrome [141]
Rab9 A, B	LE	Endosome-TGN trafficking	Niemann–Pick disease type C [132]
Rab10	PM	Neurotransmitter release, vesicular trafficking, phagosome maturation, Glut4 translocation	Type 2 diabetes [121]
Rab11 family A, B, C (Rab11C synonymous with Rab25)	Recycling endosome, Rab25 in apical recycling compartments	Long loop recycling, Rab25 implicated in integrin recycling, cell motility, ciliogenesis	Breast, lung, colon, ovarian endometrial, prostrate, bladder carcinomas [142], Rab11 implicated in Chagas disease [135], Rab11A in diabetes [121]
Rab13	Tight junction	Polarized transport, tight junction activity	Crohn's disease [143], upregulated in tuberculosis [144]
Rab23	PM	Negative regulator of Sonic Hedgehog signaling, vesicular trafficking	Carpenters syndrome [145], craniosynostosis[146], liver cancer [147], gastric cancer [148]
Rab24	ER–Golgi, LE	Autophagy	Tuberculosis [144]
Rab27 A, B	PM, melanosomes	Exocytosis	Choroidermia [149], Griscelli syndrome 2 [104], type 2 diabetes [108], breast cancer [150-152]
Rab31	PM, TGN	Anterograde transport	Metastatic breast cancer [153]
Rab33 A, B	Golgi	Autophagosome formation	Tuberculosis [144]
Rab38	Melanosomes	Melanosomal transport, docking, sorting TYRP1	Hermansky–Pudlak syndrome [154-155]

1.3.9. Rab family and subfamily motifs

Rab proteins are highly homologous, share a similar fold, and are very similar in the active (GTP) state; however they have very specific functions and unique properties. Generally every Rab GTPase has several effectors, and in turn some effectors act on more than one GTPase, while others are more specific. Rabphilin for example interacts mainly with Rab27, but can also interact with Rab3 and Rab8 whereas melanophilin only interacts with Rab27 [161]. It has been proposed that this may be a consequence of not only sequence variation but also the ability to form different conformations which distinguish Rab GTPases from each other [9]. In order to clarify how Rab GTPases account for their specificity several studies have been performed. One approach concentrated on the identification of distinguishing Rab GTPases features within subfamilies. Finding conserved sequence motifs would enable identification of differences that are likely to account for the specificity. Through sequence alignments of Rab GTPases several Rab family sequences (RabF) were identified: RabF1 = IGVDF [162-163] RabF2 = KLQIW RabF3 = RFrsiT RabF4 = YYRGA RabF5 = LVYDIT [163]. F1, F3 and F4 are found in the switch domains. These motifs, together with the nucleotide binding and variation in prenylation motifs allow for Rab GTPases distinctions to be made between superfamily members, such as Ras and Ran. Defining and categorising these motifs helped in the identification of unknown Rab GTPases and also provided support for the idea that the switch regions, in addition to the other motifs mentioned, determine the specificity of binding to their effectors. Furthermore this analysis allowed the organisation of Rab GTPases into phylogenetic groups. These groups contain Rab subfamilies which tend to have similar function or are in fact isoforms [164]. Different authors refer to a different number of phylogenetic groups, Pereira-Leal and Seabra [163] make the point that it is difficult to draw a line between subgroups especially when it is unclear exactly how much homology is required to categorise two related proteins as isoforms (as for Rab1a and Rab1b for example). Pereira-Leal and Seabra identified 11 Rab subfamilies, while two other separate groups identified 10 [165-166].

1.4. Structural properties and specificity of Rab GTPases

It is difficult to understand the underlying mechanisms employed in Rab GTPase-effector interactions, especially because it is hard to identify common sequences and structures in effectors. As a result structural analysis of Rab GTPase-effector interactions are very important in order to have a better understanding of trafficking mechanisms; combined with measurements of affinities and kinetics and mutational analysis they will allow understanding the processes taking place at the molecular level [51, 167].

As described for the superfamily of small Ras related GTPases, Rab GTPases are found to have less ordered switch regions in the GDP bound state, and very diverse conformations. In the active state, the conformations of Rab GTPases are much more similar. These observations present a conundrum – as discussed below, crystal structures of Rab-effector complexes (from our lab and others`, i.e. [47, 168-169]) have revealed that the switch regions of active Rab GTPases are the key determinants of specificity, despite similar sequences and conformation. This dilemma is, at least partially, explained by the finding that Rab-effector specificity is very subtle, and dependent on a single or a few amino acid variants and also dependent on conformational heterogeneity (side chain and backbone) of highly conserved switch residues, but further analysis is necessary in order to understand the system quantitatively [167].

1.4.1. Structural basis for membrane targeting and extraction

As described in section 1.2.1 and 1.3.8 prenylated RabGTPases interact with RabGDI in their GDP-bound form when not bound to membranes [170-171]. They also retrieve prenylated Rab proteins from membranes and return them to their membrane of origin [171-172].

Several crystallographic structures of RabGDI and REP, in complex and alone have been determined [24, 173-177]. The overall architectures of RabGDI and REP are similar (Figure 1.7). Both have two distinct domains designated domain I and II. Domain II is comprised of approximately 100 residues and entirely helical, whereas the larger (~340 residues) domain I contains several β-sheets and some conserved characteristics which are

involved in Rab GTPase binding, including the so called 'Rab-binding platform' (RBP) [177-180]. This platform is adjacent to the switch and interswitch regions of the bound Rab. Through structural and sequence analysis Goody and colleagues identified a motif that consists of a large aliphatic residue followed by a polar amino acid, followed in most cases by a second large aliphatic residue and has been termed the 'AxA box' [37]. This motif is found in a non-conserved position within the hypervariable C-terminal extension of Rab GTPases and it interacts with the so-called 'C-terminal binding region' (CBR) of domain I. Another part of domain I that interacts with the hypervariable C-terminal region is the 'Mobile effector loop' (MEL). Domain II contains a distinct prenyl group pocket into which one geranylgeranyl binds. If the Rab GTPase is double prenylated, the first prenyl group binds differently to the pocket in domain II and the second prenyl covers the first which leaves it partly exposed [24, 173-176]. Despite their structural similarities only REP interacts with RGGT. This is due to only two substitutions at the interaction interface of domain II [181].

Based on structural and biophysical data of Rab-GDI interactions a model explaining the mechanism in which prenylated Rab GTPases are extracted from the membrane was suggested [175], also see Figure 1.8. GDI recognises the membrane bound Rab GTPase and forms an initial low affinity complex via the Rab-binding platform. Binding of the conserved AxA box with the CBR then increases the affinity of the complex and as a result of structural adjustments to this the prenyl binding pocket of GDI is opened. This pocket would be located close to the membrane inserted prenyl groups of the Rab GTPase and as a result of the now high affinity of the GDI-Rab complex the prenyl groups are extracted from the membrane.

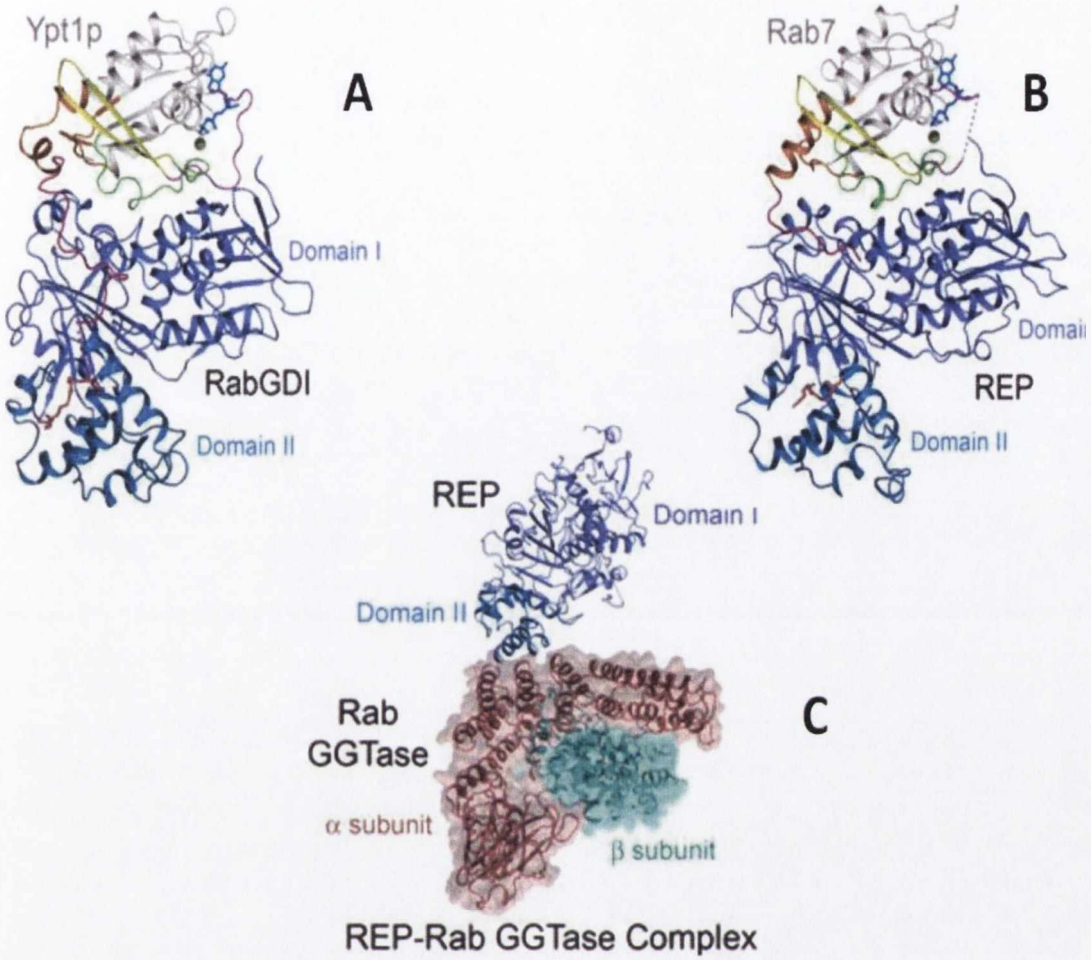

Figure 1.7 Structures of RabGDI and REP with prenylated Rab GTPase or RGGT.
RabGDI and REP are shown in darker blue shades; Rab GTPases in grey with switch I in lavender, switch II in green, interswitch regions in yellow, complementary-determining regions (CDRs) in orange and C-terminal regions in purple. CDRs are discussed further in Section 1.4.3. Panel A: Structure of RabGDI in complex with mono-prenylated Ypt1p (PDB ID 1UKV, [173]). Panel B: Structure of REP in complex with mono-prenylated Rab7. The Rab-REP interaction interface and position of the prenyl binding pocket are very similar to the Rab-GDI interface shown in A (PDB ID 1VG0, [174]). Panel C: Structure of REP in complex with RGGT (PDB ID 1LTX, [182]). The domain II of the REP interacts with the α subunit of RGGT in a manner which orients the Rab-binding platform in a position that enables the Rab C-terminus to interact with the active site in the β subunit. Figure adapted from [166].

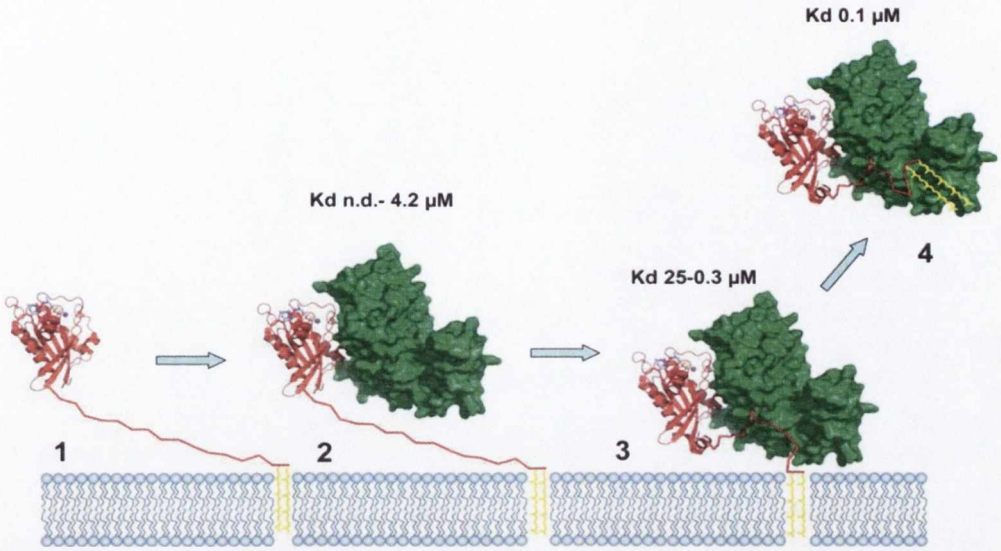

Figure 1.8 Putative mechanism of Rab membrane extraction by GDI.
1. Rab is anchored in the membrane. **2.** First recognition and low affinity complex formation via Rab-binding platform interactions. **3.** Further interactions result in a higher affinity of the complex, the prenyl binding pocket opens and since it is located close to the membrane anchored residues lipid transfer occurs. **4.** The high affinity Rab-GDI complex is released from the membrane. Rab GTPase in red with yellow geranlygeranyl groups, GDI in green. Figure adapted from [175].

1.4.2. Structural basis for activation and inactivation of Rab GTPases

In order for the Rab GTPase to be activated, the GDP has to be exchanged with GTP. For this, the Rab/GDI complex has to be dissociated from the GDI first. As described in sections 1.2 and 1.3.8 the dissociation from GDI and the membrane recruitment of Rab GTPases are thought to be catalyzed by GDFs [183]. Only few GDFs have been identified so far, out of which one is the integral membrane protein Ypt-interacting protein 3 (Yip3) [25]. Subsequent research revealed that a family of Yips exists, and it has been proposed that these proteins serve as GDFs for the targeting of Rab GTPases in eukaryotic cells [184]. A general model for GDF function has also been suggested: The GDF recognises the Rab/GDI complex. The prenyl groups of the Rab GTPase might then be transferred from the GDI to the GDF which causes a conformational change in GDI that leads to its release. The Rab GTPase could then be transferred onto the adjacent membrane surface where the nucleotide exchange occurs [178]. This hypothesis still remains to be further investigated and has not been supported by a structure yet.

The high affinity of the Rab GTPase for GDP prevents a fast nucleotide exchange and GEFs catalyse this reaction accelerating it by several orders of magnitude [185]. The general mechanism can be described as a series of fast reaction steps [21]. Upon binding of the GEF to the Rab-nucleotide complex a Rab/nucleotide/GEF complex is formed. Binding of the GEF destabilises the interaction between the Rab GTPase and the nucleotide by opening the nucleotide binding pocket via movements of one or both switches [186]. The GEF stabilises the nucleotide free Rab GTPase and when a nucleotide binds the series of reactions is reversed. In the cell the GTP concentration is much higher than that of GDP, therefore GTP is much more likely to bind the Rab GTPase. Hence a GEF does not really act as nucleotide exchange protein, its function is better described as a catalyst that increases the rate at which the equilibrium between the Rab(GDP) and Rab(GTP) is reached [21]. GEFs have been found to be structurally very diverse, they range from small molecules over large modular proteins to multiprotein complexes. This makes it hard to identify them by amino acid and sequence analysis [186]. In contrast to this Rho-GEFs for example can be identified by their Dbl-homology or DOCK domain. Some similarities for Rab-GEFs of the same Rab-family could be identified. For example the GEF Rabex-5 contains a Vps9 domain. This domain has been found in other proteins as well and Vsp9 domain containing proteins have been shown to act on members of the Rab5 subfamily [187]. The structure of the Rab5-family GTPase Rab21 has been solved in complex with the Rabex-5 Vps9 domain [188]. The Vps9 domain was found to be in a novel fold of six α-helices. The interaction with Rab21 results in an open state of switch I. An aspartate residue of Rabex-5 interacts with the conserved lysine in the p-loop (G1-motif GxxxxGK(S/T)) as well as the conserved glycine of switch II (G3-motif DxxGQ/H/T). This interaction mimics the interactions of the Rab GTPase with the γ-phosphate of GTP, thus stabilising the nucleotide free form of the GTPase. A comparison of Rab21(GDP) with the nucleotide free Rab21 lead to the suggestion that the GDP release is initiated by disruption of the Mg^{2+} binding site together with an electrostatic repulsion between the phosphate and the Rabex-5 aspartate residue. Other Rab/GEF structures revealed that the reaction is a common GEF mechanism although the high diversity of Rab-GEFs leads to differences in the details [189]. Another Rab/GEF structure is that of the Rab8 yeast homologue Sec4 in complex with its GEF Sec2 [190-191]. Here the nucleotide release is

achieved in a different way. The GEF-domain of Sec2 interacts with the C-terminal end of switch I in a manner that forces the hydrophobic residue isoleucine into the Mg^{2+} binding site. In addition a conserved interaction between the guanosine base and a phenylalanine residue located at the N-terminus of switch I is also disturbed. A very interesting discovery was the fact, that the *Legionella pneumophila* (*L. Pneumophilia*) protein DrrA (SidM) has a combined GDF and GEF activity for Rab1 [192-194]. Although further research revealed that the GDF function of DrrA was reported incorrectly, the GEF function could be structurally described [195-197]. The structure revealed a big conformational change of switch I that is displaced upon binding to DrrA. In general it can be said that GEFs enable the nucleotide exchange by interacting with the p-loop and the switch regions of the Rab GTPases, competing with the nucleotide to bind the GTPase [198-199] and that this general mechanism is different for individual GEFs.

Rab GTPases possess an intrinsical GTP hydrolysis mechanism. A nucleophilic water molecule approaches the GTP γ-phosphate, the nucleophilic attack releases inorganic phosphate and this reaction depends on a magnesium ion. The details of the mechanism with regards to the transition state of the reaction are somewhat controversial [200-201]. However, this intrinsic reaction is slow (rate constants of 10^{-1} to $3 \cdot 10^{-3}$ min^{-1}) and is accelerated by up to five orders of magnitude through interaction with GTPase activating proteins (GAPs) [202]. A characteristic protein domain could be identified for GAPs, it shared some sequence similarities with the human oncogene Tre2, with *S. cervisiae* Bub2 and with *S. pombe* Cdc16 and was therefore termed the TBC domain [203-208]. Description of this common domain enabled identification of GAPs by amino acid and sequence analysis. Only one GAP without a TBC domain has been identified so far, it is the Rab3GAP1/Rab3GAP2 complex [209].

The TBC domain comprises six sequence motifs designated A to F [208]. Three of these motifs contain invariant so-called signature sequences: RxxxW in motif A; IxxDxxR in motif B; and YxQ in motif C. The TBC domain is fully α-helical, and adopts 'V' shaped conformation [204]. It is also worth noting that highly similar TBC domains differ in their C-terminal subdomain which is most likely to contribute to Rab specificity [210].

Initially it was believed that the GTP hydrolysis catalysis mechanism of the TBC domain proteins for Rab GTPases would be the same as for Ras GTPases. This hydrolysis

mechanism involves an arginine finger of the TBC domain and a conserved glutamine residue from the Ras GTPase [211-212]. However, the first structure of a Rab/GAP complex showed that this mechanism was slightly different for Rab GAPs [213]. Here both residues, arginine and glutamine, were provided by the TBC domain while the conserved Rab glutamine interacts with the TBC domain and is important for positioning the TBC domain glutamine. Positioning of the Glutamine of the TBC domain ensures the coordination of a water molecule for a nucleophilic attack on the γ- phosphate [214]. This nucleophilic attack causes a shift of negative charge from the γ- to the β-phosphate of the nucleotide, a charge distribution closer to GDP than to GTP [215]. The arginine provided by the TBC-domain compensates this negative charge and this reduces the activation energy for the β - γ bond cleavage. In addition to this the movement of the arginine into the binding pocket 'pushes' water molecules out of the pocket, thus increasing the entropy for the reaction [216-217]. The inorganic phosphate released during the hydrolysis reaction can fuse back to form GTP again or become the leaving group and therefore its release is the rate-limiting step of this reaction [215].

1.4.3. Structural properties of Rab effectors

Once activated by a GAP, each Rab GTPase is thought to have several effectors and most effectors are specific for one Rab GTPase. More than 20 effectors have been identified for Rab5 alone [218]. Hence the number of Rab effectors is far greater than the number of Rab GTPases. It is possible to identify small families of homologous Rab-binding domains (RBD) but apart from that, their effectors do not share much sequence homology and have great structural diversity [9, 166]. Rab effectors can be integral and peripheral membrane proteins, cytosolic proteins or complexes and do not employ the same recognition mechanisms or functional activities [219]. Effectors with very different structures can be specific for the same Rab GTPase. Rab27 for example has several effectors that all contain a similar Rab-binding domain, but two of its effectors have a very different amino acid sequence with an unknown Rab binding domain [220]. This diversity, plus the vast functional range of Rab GTPases presents an enormous challenge for the elucidation of cellular trafficking pathways. The identification and characterisation of Rab

effectors and their mechanisms of interaction with Rab GTPases is an important goal and will without doubt provide molecular insights into many intracellular trafficking related diseases. Considering that there is little sequence homology, sequence analysis approaches provide very limited information for identifying new Rab-effectors. To date effectors have largely been identified experimentally, mainly utilising yeast-hybrid assays and GST-pull down assays [221]. Once identified effectors require in-depth structural analysis to identify the specificity determinants and mechanisms involved in Rab GTPase recognition and function.

A comparison of 10 Rab GTPases structures and their effectors focuses our attention on the conformational differences found in the interaction of Rab GTPases their effectors. It also helps to unearth some related types of interaction (Figure 1.9) Lee and colleagues established that Rab GTPase interactions with their effectors usually involve the conserved switch/interswitch regions with at least one residue of the hydrophobic triad. This manner of interaction seems to be present in all structures and can be considered a set of general recognition determinants characteristic of the Rab GTPase family. A characteristic shared by all but two Rab binding domains, is an α helical structure [166, 222-223].

Structural analysis of Rab/effector complexes revealed conserved residues of a 'hydrophobic triad' (interswitch Phe and Trp and switch II Tyr), located near the switch/interswitch junction, and these are found to adopt very different conformations in the GTP-bound state. It has been suggested that this is one of the major reasons for Rab GTPase specificity for recognition of different effectors in the GTP bound state and presents a family recognition motif for Rab GTPase effectors [186, 224]. Additionally, several other specificity determinants have been proposed. These include complementary-determining regions (CDRs) and the identification of subfamily motifs that are conserved within the subfamilies [163, 168]. The CDRs were initially identified in a structure of the Rab3a/Rabphilin complex and they are located N-terminal to the β1, between α3 and β5 (SF3) and near the C-terminal end of α5 [168]. CDRs and subfamily motifs seem to be crucial for some interactions but are not generally involved in every interaction. Altogether this shows that even subtle variations, especially within the switch regions, can produce

very distinct surfaces in order to obtain the required specificity and these interactions are further enhanced by interactions of nonconserved regions of Rab GTPases with the effector [9]. Sometimes the variations in the switch regions are not that subtle. The structure of GTP-Rab11 in complex with FIP2 revealed a large rearrangement of switch II in order to bind FIP2. The importance of such switch flexibility was not observed for active Rab GTPases until that point and it underlines the importance of the switch region conformation for effector binding [47]. This structure also provided some evidence that the notion that Ras related GTPase effectors recognise a pre-existing switch conformation is not strictly true.

Although there has been sporadic elucidation of affinities and kinetics between Rab/effector complexes and analysis of the impact of mutations in both binding partners [i.e. 225, 226], more data is needed in order to identify specificity determinants for Rab GTPase/effector complexes.

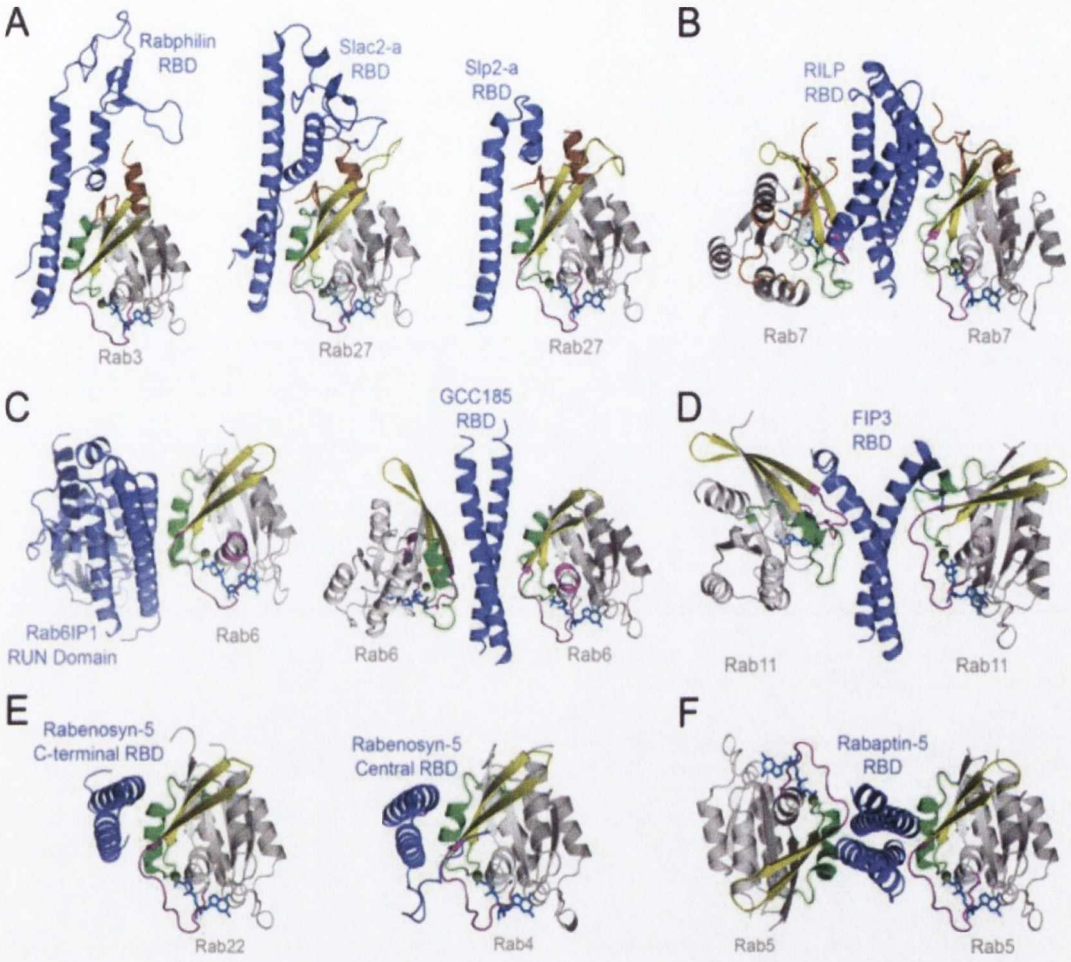

Figure 1.9 Structures of effector RBDs in complex with active Rab GTPases.
Panel A: The RBDs form an extended interface with the Rab GTPases in which switch/interswitch regions and all three CDRs are involved. Panel B: The effector RBD consists of interleaved helical hairpins, the 2:2 complex interacts via switch/interswitch regions and the N-terminal CDR of Rab7. Panel C: Although structurally different the two effectors induce similar switch/interswitch conformations. Panel D: Binding of the FIP3 RBD to Rab11 causes a substantial conformational change of the switch II region. Panel E: Different RBDs of the same effector (Rabenosyn-5) both interact with the switch/interswitch regions of Rab22 and Rab4 in a similar manner. Panel F: The C-terminal RBD of Rabaptin-5 interacts with the switch/interswitch regions of Rab5 in a similar manner to that described in Section E above, but by formation of a 2:2 complex. Figure adapted from [166].
The following PDB-files were used by Lee and colleagues to produce this figure: 1ZBD (Rabphilin-3A/Rab3A [168]); 2ZET (Slac2-a/Rab27B [169]); 3BC1 (Slp2-a/Rab27a [227]); 1YHN (RILP/Rab7 [228]); 3CWZ (Rab6IP1/Rab6A [229]); 3BBP (GCC185/Rab6A [230]); 2HV8 (FIP3/Rab11A [231]); 1Z0J (Rabenosyn-5/Rab22A [232]); 1Z0K (Rabenosyn-5/Rab4 [232]); 1TU3 (Rabaptin-5/Rab5A [233]).

1.5. Rab27 subfamily

The human Rab27 subfamily consists of two proteins, Rab27a and Rab27b that are 81% similar. A sequence alignment of both proteins with closely related Rab8 and Rab3 visualizes the high conservation of the parts that are usually involved in interactions with effectors (Figure 1.10). Both, Rab27a and Rab27b, are involved in the control of regulated secretion [234]. Rab27a and Rab27b are widely expressed in different cell types with both proteins present in some cells/tissues and only one protein present in others [235-236] and they both act through different effector proteins in a cell dependent manner [85, 237-238]. Rab27b for example, is highly expressed in brain tissue, whereas Rab27a is barely detected [239]. It has been shown that they are at least partly functionally redundant [240-241] however it is also clear that they can function in very distinct roles. Ostrowski and colleagues for instance reported that they have different subcellular localisations in HeLa cells where they take part in regulation of exosome secretion [242]. A summary of the localisation of Rab27 subfamily members is given in Table 1.3.

1.5.1. Rab27 and diseases

Rab27 has been linked to the following hereditary and acquired diseases: Choroidermia, breast cancer, and Griscelli syndrome 2. Due to its involvement in insulin release it is also suspected to be involved in type II diabetes [108].

Choroideremia is caused by a deviant geranylgeranylation of Rab27a by REP1 in the retinal pigment epithelium. This is thought to be the reason for degeneration of the retinal pigment epithelium and the adjacent choroid and retinal photoreceptor cell layers, leading to blindness, [52, 103, 243].

Rab27a also has been shown to act as a mediator of invasion and metastasis promotion in human breast cancer cells [150]. In addition to this Rab27b has been reported to regulate invasive growth and metastasis in estrogen receptor-positive breast cancer cell lines. Its increased expression is associated with poor prognosis in humans and proven to be a generalised feature of human tumors [151-152]. The Griscelli syndrome is a human autosomal recessive disorder that causes pigment abnormalities, neurological defects and in many cases immunological disorders that include haemophagocytic syndrome and

defective exocytosis of lytic granules from cytotoxic T lymphocytes [244-245]. Several mutations of RAB27A have been linked to the Griscelli syndrome type 2 causing mutations of W73G, L130P, A152P and in addition there are a number of nonsense and frame shift mutations [104]. These mutations result in the loss of the interaction between Rab27a and melanophilin, which in turn disturbs melanosome transport in melanocytes. Other Griscelli syndrome types are caused by mutations in MYO5A (encoding the motor protein myosin Va), Griscelli syndrome type 1, or MLPH (encoding the Rab27a effector melanophilin), Griscelli syndrome type 3 [246]. All types thus disturb the melanosome transport, but it is only Griscelli syndrome type 2 patients which present with haemophagocytic lymphohistiocytosis.

Table 1.3: Different cell types that express Rab27 subfamily members and the relevant effectors.
Modified from [234].

Cell types/types of secretion or membrane trafficking	Putative Rab effectors or binding proteins
Rab27a	
Endocrine cells/hormone secretion chromaffin and PC12 cells	Granuphilin, rabphilin, MyRIP, Noc2 [234]
Pituitary cells	Granuphilin [234]
Pancreatic β cells and cell lines	Granuphilin, Slp5, MyRIP, Noc2 [234]
Pancreatic α cells and their cell lines	Slp2-a[234]
Gastric surface mucous cells/mucus secretion	Slp2-a [234]
Melanocytes/melanosome anchoring	Melanophilin, Slp2-a [234]
Platelets/dense granule exocytosis	Munc13-4 [234]
CTLs/cytotoxic granule exocytosis	Munc13-4 [234]
Mast cells/histamine release	Munc13-4 [234]
Granulocytes/azurophilic granule exocytosis	JFC1, Munc13-4 [247]
Endothelial cells/Weibel-Palade body exocytosis	MyRIP [248]
Prostate carcinoma cells/prostate-specific marker secretion	JFC1 [234]
Epithelial cells/epithelial sodium channel transport	Slp5, Munc13-4 [234]
Rab27b	
Pituitary and AtT-20 cells	Granuphilin[234]
Mast cells/histamine release	ND
Parotid acinar cells/amylase release	Granuphilin-a, MyRIP, Noc2 [234]
Pancreatic acinar cells/zymogen granule exocytosis	ND
Platelets/dense granule exocytosis	Munc13-4 [234]
Axons/ selective anterograde transport of TrkB	JFC1 [249]

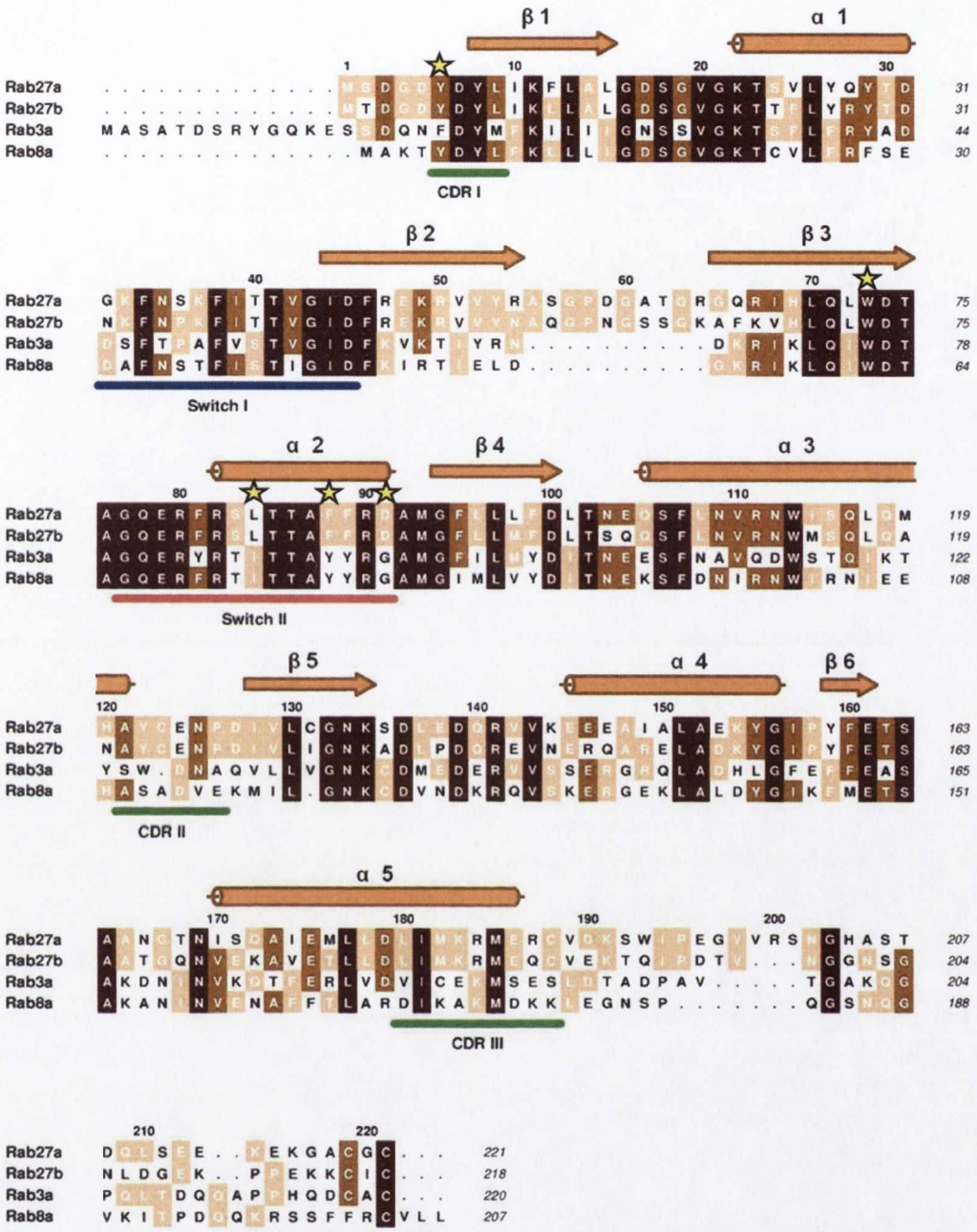

Figure 1.10 Sequence alignment of Rab27a, Rab27b, Rab3a and Rab8a.
Rab27 and Rab8 sequences are from human, Rab3 is from rat. Conserved residues of the SHDs are highlighted in black and least conserved residues (50%) are in light brown with a gradient from dark to light depending on the conservation. Switch I is underlined in blue, switch II in red and the CDRs are underlined in green. Residues that were chosen for mutational analysis are designed by a star.
The closely related sequences, especially of Rab27a and Rab27b from the Rab27 subfamily are highly conserved, with the most diverse regions being the interswitch region and the C-termini.

1.5.1. Rab27 effector proteins

In total there are 12 known effectors of Rab27 subfamily members: exophilin1/rabphilin, exophilin2/granuphilin/Slp4, exophilin3/melanophilin/Slac2-a, exophilin4/Slp2 exophilin5/Slac2-b, exophilin6/Slp3, exophilin7/JFC1/Slp1, exophilin8/MyRIP/Slac2-c, exophilin9/Slp5, Noc2, Munc13-4 and coronin3. Both, Rab27a and Rab27b, can interact with each of these effectors, although this is somewhat restrained by their differing tissue localisations [84, 161, 220]. The effector proteins can be divided into groups, depending on their structures and/or affinities [238]. The first group contains members of the synaptotagmin-like protein (Slp) family. They have several domains in common: a C-terminal tandem C2 domain (C2A and C2B domain) linked by a sequence of differing lengths to an N-terminal Slp homology domain (SHD) [250-251]. The SHD is composed of two conserved α-helical regions (SHD I and SHD II). These domains are either linked directly to each other or they are found separated by a zinc-binding motif, related to the FYVE domain. The FYVE-like domain is a phosphatidylinositol 3-phosphate (PtdIns(3)P) -binding domain that binds zinc, however it is noteworthy that the FYVE-like domain of rabphilin does not bind PtdIns(3)P [252-253] and additionally it was shown that it is not required to bind Rab27 [254]. The second group, synaptotagmin-like protein homologue lacking C2 domains (Slac2), does have SHDs but no C2 domains [250]. The previously described features are found in ten of the twelve Rab27 effectors and when they were first identified other authors named them exophilins (exocytosis-associated rabphilin3/granuphilin-like proteins) [255]. Some of the previously described effectors interact only with Rab27 (melanophilin, Slp2, Slac2-b and Slp3) whereas Noc2, rabphilin, granuphilin and JFC1 have been shown to bind to Rab3 and/or Rab8 [161, 256] [257]. Two effector proteins however stand out over the other ten. Munc13-4 consists of two separate C2 domains and two so called Munc13 homology domains (MHD1 and MHD2). As yet the Rab binding domain of Munc13-4 has not been identified [220, 238]. Coronin 3 is an effector of Rab27 that interacts only with its GDP bound form, here as well no Rab-binding domain has been identified ([258]. Figure 1.11 depicts the different domains of Rab27 effectors (except for coronin 3) and further information regarding the effector proteins will be discussed further.

Sequence alignments of all SHD-containing Rab27 effectors reveals, that the SHD I is rather conserved, but the SHD II only contains few conserved residues (Figure 1.12).

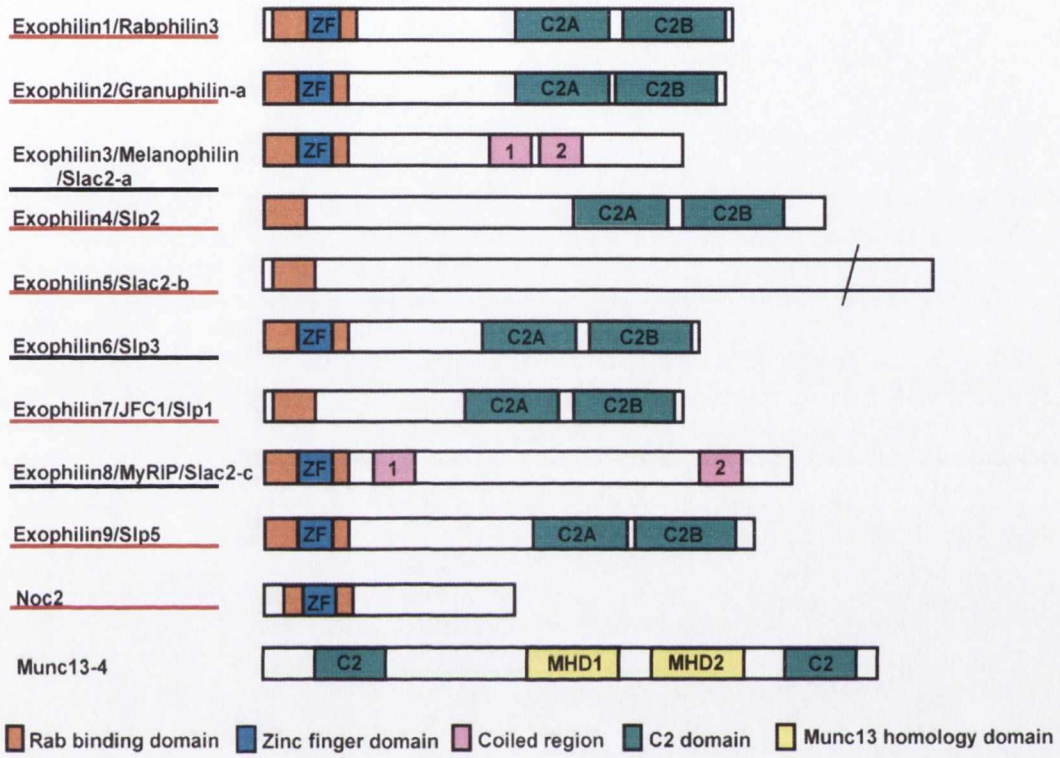

Figure 1.11 Schematic domain distribution of the 11 Rab27 effector proteins.
The amino acid numbers shown on the right are of effector proteins from mice, numbers for humans are given in brackets. Effectors that have been determined to belong to a so called 'high affinity group' are underlined red and 'low affinity group' effectors in black. Modified from [259].

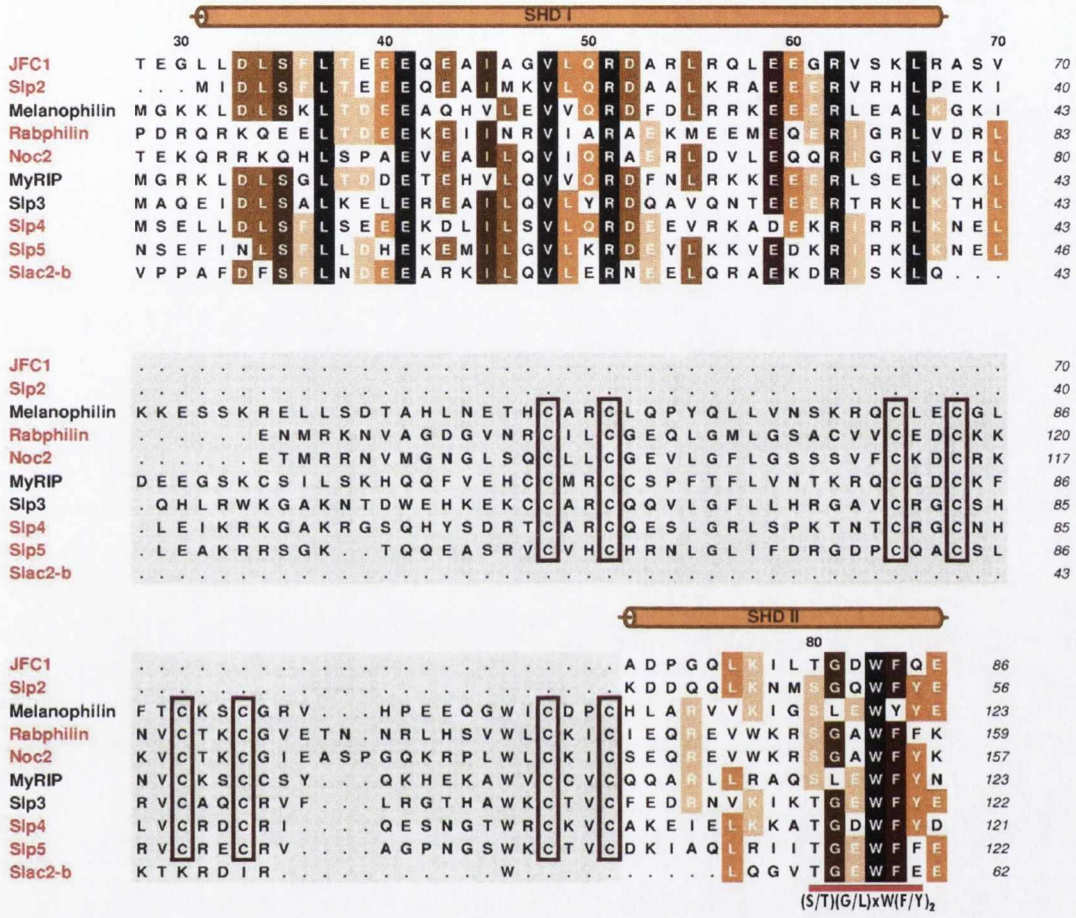

Figure 1.12 Sequence alignment of all known SHD containing Rab27 effectors.
The names of high affinity group effectors are in red and that of low affinity group effectors in black. Conserved residues of the SHDs are in black and least conserved residues (50%) are in light brown with a gradient from dark to light depending on the conservation. SHD I and SHD II are depicted by cylinders above the first sequence line. The numbers above the sequences are from JFC1. The FYVE-like linker domain that is only present in some effectors is highlighted in grey, with the cysteine residues that are responsible for zinc binding in boxes. The (S/T)(G/L)xW(F/Y)$_2$ motif is underlined in red. Especially the SHD I contains several highly conserved residues, the most conserved part of the SHD II is the (S/T)(G/L)xW(F/Y)$_2$ motif.

Rabphilin was shown to be a Rab3 effector protein when first discovered and is therefore sometimes referred to as rabphilin3 [260]. In 2002, its interaction with Rab27 was first documented [261]. Later it was shown that a Rab27/rabphilin/SNAP-25 protein complex connects the secretory vesicle and the plasma membrane in neuroendocrine and neuronal cells [262].

Granuphilin was the second Rab27 effector protein to be discovered, it mediates the docking of insulin granules to the plasma membrane [259]. Since it is more similar to the other SHD containing effector proteins than rabphilin, it has enabled the identification of other Rab27 effectors by sequence comparisons [255, 263]. Interestingly, granuphilin was reported to interact with Rab27a Thr23Asn (inactive form) as well as Rab27a Gln78Leu (active form) but only with the active forms of Rab3a and Rab8a [264]. It has been proposed that the interaction of granuphilin with Rab27 in its GDP bound form results in inhibition of dense-core vesicle exocytosis.

MyRIP/Slac2-c was first identified as a myosin VIIa partner that is involved in recruiting retinal melanosomes [90]. It can interact with myosinV as well, and thus links Rab27 to motor proteins [89].

Munc13-4 has been identified as a Rab27 effector protein despite the absence of a known Rab27 binding region [220]. It has been identified as the limiting factor for platelet granule release and hemostasis, loss of its function has been linked to hemophagocytotic lymphohistiocytosis type 3, which is caused by phagocytosis by macrophages of erythrocytes, leukocytes, platelets, and their precursors in bone marrow and other tissues [265-267].

Melanophilin/Slac2-a links Rab27a with myosin Va and is thus involved in the melanosome transfer from microtubules to actin filaments and then the actin based melanosome transport [84, 261, 268]. The SHD I of melanophilin has been shown to be a critical determinant of GTP-dependent specific binding to Rab27 whereas the SHD II is not necessary for the interaction [254].

The structure of the melanophilin Rab binding domain in complex with Rab27b was solved in 2008 [169]. Tyr6 from Rab CDR I and three residues from switch II of Rab27

(Leu84, Phe88, and Asp91) were identified as the minimum determinants of melanophilin binding to Rab27. Those residues interact with the melanophilin SHD I and when the sequences of all SHD containing Rab27 effector proteins were compared it was revealed that the amino acids involved directly in the interaction with Rab27 were mainly conserved but some differences were found, for instance Val18 and Val22 of melanophilin were conserved in MyRIP, which is also a low affinity group member. In high affinity group members isoleucine or leucine was present instead. The authors concluded that the combination of those sequence alterations might be the reason for different Rab27 affinities.

Slp2 has been shown to be involved in localising melanosomes and glucagon granules toward the plasma membrane by the affinity of its C2A domain for membrane phospholipids. After the actin based melanosome transport mediated by melanophilin, Slp2-a interacts with Rab27a resulting in anchoring of melanosomes to the plasma membrane [269-270]. The structure of Rab27a/Slp2 revealed that the Rab27a residue Tyr122 (in the CDR II) was a key residue for effector selectivity. Rab27 Tyr122 shows a stacking interaction with Slp2 Phe54 located in the $(S/T)(G/L)xW(F/Y)_2$ motif which is characteristic of the SHD II and was previously described as a structural determinant for the interaction of Rab3a with rabphilin [168]. Contrary to melanophilin, the SHD II of Slp2 is therefore likely to be important for the Rab27/effector interaction. The invariant hydrophobic triad found in Rab GTPases, composed of Phe46 and Trp73 from the interswitch region and Phe88 from the switch II element in Rab27, was found likely to be essential for effector recognition. Most of the Rab27-Slp2 interface involves the SHD I of Slp2 and interswitch and N-terminal regions of Rab27. The switch regions themselves are not that much involved in the interaction.

JFC1 was discovered as a protein that binds to the p67(phox) component of NADPH oxidase [271]. It could be shown that JFC1 binds and hydrolyses ATP in a magnesium dependent way, it does not have an affinity for GTP. The ATP binding site of JFC1 is predicted to adopt a Bergerat fold but structural analysis is needed in order to confirm this [272-273]. Later on, JFC1 was identified as a Rab27 effector. It contains a C-terminal tandem C2 domain and possesses SHD I and SHD II in its N-terminal region, but

no FYVE-related domain is separating the two SHD domains [85]. It localises to the plasma membrane via its C2A domain, that specifically binds to PtdIns(3,4,5)P3. JFC1 is also phosphorylated by Akt, which is thought to control the cellular localisation of JFC1 and probably initiate its recycling but the phosphorylation has been shown to have no effect on Rab27 binding [274]. Additionally to Rab27, JFC1 interacts with Rab8, controlling Rab8 membrane dynamics [256]. Hattula and colleagues found, that JFC1 interacts stronger with Rab8 than Rab27 whereas others reported a weaker binding to Rab8 than to Rab27 [261]. JFC1 has also been linked to the motor protein Kinesin-1 in a multiprotein complex [249]. Rab27/JFC1 form a complex with the cargo receptor collapsin response mediator protein-2 (CRMP-2). JFC1 also binds directly to the growth factor receptor TrkB in a Rab27 dependent manner. Another protein of this complex, CRMP-2 interacts with Kinesin-1; therefore this complex regulates the axonal transport of neutrophin receptor containing vesicles.

It has been reported that JFC1 does not bind Rab27a Thr23Asn, but does bind wild-type Rab27(GDP) [264, 274]. However, no biophysical data is available, therefore it is unknown if there is a difference in affinity of JFC1 for active/inactive Rab27 or not.

Recently a new protein was detected to bind to Rab27(GDP), but not Rab27(GppNHp), coronin3 [258]. Because this interaction regulates the endocytosis of insulin granule membranes, it does fall under the category of a Rab effector, although it does not bind to Rab27(GppNHp) which is part of the definition of Rab effectors. Coronin3 does not have common domains with other known Rab27 effectors.

The functions and mechanisms of the remaining Rab27 effector proteins remain elusive at the moment and therefore no further information has been included.

One study [225] investigated differences in binding affinities of all SHD containing effectors for Rab27a. A high affinity group containing JFC1, Slp2, granuphilin, Slp5, Slac2-b, rabphilin, and Noc2 and a low affinity group containing Slp3, melanophilin, and MyRIP have been identified. Kinetic analysis using surface plasmon resonance (SPR) was performed with melanophilin SHD, Slp4-a SHD and MyRIP SHD and the resulting equilibrium dissociation constants were determined to be 13.4, 19.2 and 112 nM

respectively. The other effectors were attributed to the low or high affinity groups based on immunoblots.

The binding of Rab27a mutants to its effectors has also been investigated, with the main focus being melanophilin/Slac2-a [169, 261]. The following residues were amongst those mutated: Rab27 L84I+F88Y+D91G which effectively transforms the switch II region to that of Rab3 and Rab8. The W73G, L130P, and A152P mutants are found in Rab27a of Griscelli syndrome type II patients. Rab27a L130P and A152P mutants did not interact with any of the effectors, whereas W73G and L84I+F88Y+D91G disrupted interactions with low affinity group effectors only but still allowed interaction with high affinity effectors (shown with immunoblotting). This suggests that these residues are important for the specificity in some effectors but not others. Further kinetic investigation of wild type versus mutants would shed light not just on the nature of these Rab effector complex interactions, but also on the functional implications of some of the natural mutants found in diseased states.

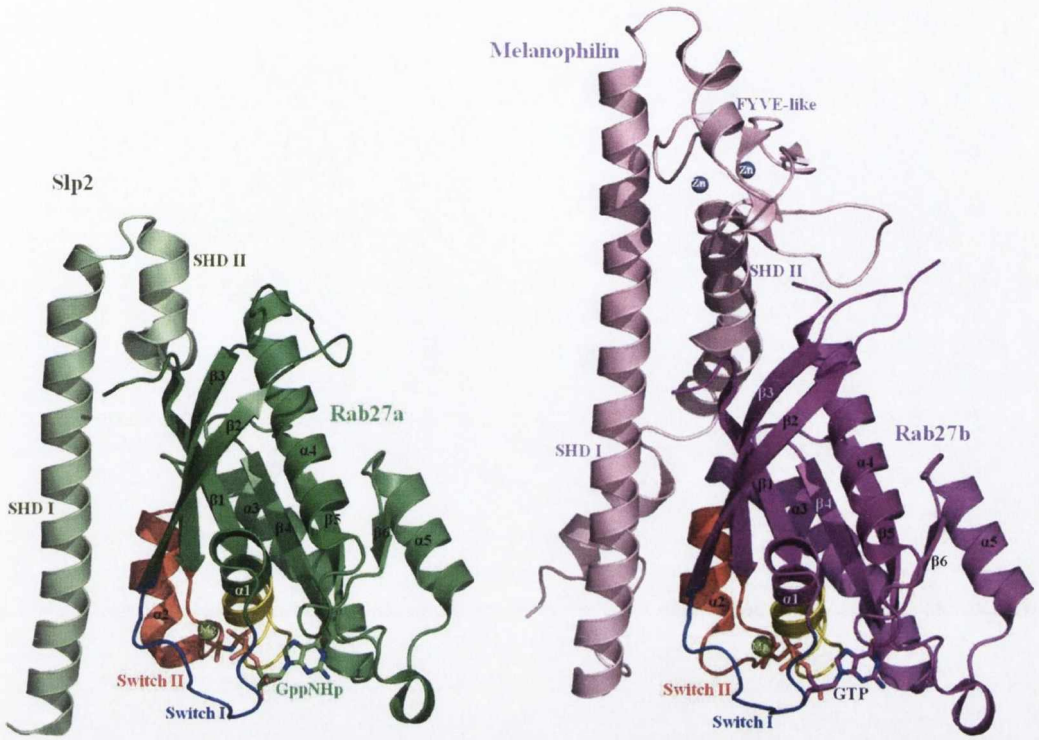

Figure 1.13 Structures of Rab27/Slp2 and Rab27/melanophilin.
Rab27a/Slp2 is in green with Rab27 in dark and Slp2 in light green, Rab27b/melanophilin is in purple with Rab27 in dark and melanophilin in light purple. Switch I is in red, switch II in blue, the p-loop in yellow, nucleotides are shown as sticks, Mg^{2+} as green spheres and Zn^{2+} as blue spheres.
Both effectors are helical, SHD I and SHD II are connected with a short loop in Slp2 whereas the FYVE-like domain connects them in melanophilin. The main binding interface is formed between the effector SHDs and the switch, interswitch and CDRs of Rab27 for both complexes. The melanophilin FYVE-like domain also interacts with the Rab27b but the residues involved are not conserved in Rab27a. Since melanophilin binds to Rab27a and Rab27b it is unlikely that the interaction is essential for the interaction.
The following PDB-files were used for this figure: 2ZET (Rab27b/melanophilin [169]) and 3BC1 (Rab27a/Slp2 [227]).

1.6. Introduction to yeast trafficking

The main trafficking processes are conserved from yeast to human, but in contrast to other eukaryotic cells only eleven Rab GTPases have been identified in budding yeast [275]. Ypt GTPases usually share 54-71% sequence identity with their closest mammalian homologues and this conserved homology also extends on a functional basis. Ypt1 for example mediates ER to Golgi trafficking [276] as does its homologue Rab1 [277]. Ypt51, Ypt52 and Ypt53 have a similar function as their mammalian counterpart Rab5 in the early endocytic pathway [278]. Ypt1, Sec4 and Ypt31 and Ypt32 are essential for cell viability. Ypt31 and Ypt32 are homologues of Rab11, they share 81% sequence identity and 90% similarity and are functionally redundant [61]. Given their high sequence identities and redundant functions, RabGTPases will occasionally be referred to as Ypt31/32, denoting a single functional unit. Sec4 does not have a functional mammalian homologue, its closest homologue is Rab8 which plays a similar but more specialised role in trafficking [279]. With such similarities between human and yeast Rab GTPases, *S. cervisiae* is often used to identify trafficking systems and the Ypt/effector interaction mechanisms. Results from such studies have expanded our knowledge of equivalent mammalian Rab/effector interactions. The transport mechanisms regulated by yeast Rab GTPases are summarised in Table 1.4: Functions of yeast Rab GTPases

Even though the first Ypt GTPases and their involvement in trafficking were discovered almost three decades ago [55, 280], new functions are constantly being discovered, one of the latest being the involvement of Ypt1 in late Golgi transport [281]. Several findings indicate that Ypt GTPases not only regulate transport but also modulate each other. The Ypt GEF Transport protein particle (TRAPP) was found to be a Ypt1 GEF as well as Ypt31/32 and it was suggested that this might coordinate the function of these GTPases' entry and exit from the Golgi [282]. The fact that both GTPases are activated by the same complex suggested the presence of a signaling cascade that directs membrane traffic through the secretory pathway [283]. In addition to this, the Ypt31/32 effector Sec2 is a Sec4 GEF [284-285]. This possibility was even further strengthened by the findings from other GEF cascades in mammalians in which one Rab GTPase, in its GTP-bound state, recruits the GEF that activates the next Rab GTPase along the pathway [93, 284]. Recently it was reported that a counter-current GAP cascade serves to restrict the spatial

and temporal overlap of two Rabs, Ypt1 and Ypt32 on the exocytic pathway in *S. cerevisiae* [92]. The same group suggested that GEF cascades which work together with counter current GAP cascades would be able to generate a programmed series of Rab GTPase conversions that regulate the choreography of membrane traffic.

Another interesting finding was that the localisation and half-life of the Ypt31/32 downstream effector Rcy1 (mediating plasma membrane recycling and involved in phosphorylation and/or ubiquitination) is regulated by Ypt31/32 itself [286]. The same study found that Ypt31/32 and Rcy1 mediate endosome-to-Golgi transport and proposed that Ypt31/32 GTPases regulate the function of Rcy1 in the phosphorylation and/or ubiquitination of proteins that recycle through the Golgi.

Cis Golgi cisternae mature to Trans Golgi cisternae, a process that involves a change of the attached Ypt GTPase. Ypt1, which is found on cis Golgi cisternae is replaced by Ypt31/32[93] [287]. Ypt31/32 is required for the vesicle formation from the Trans Golgi [61, 288]. It interacts directly with the myosin V motor Myo2, recruiting it to the vesicle [289-290]. At the Trans Golgi phosphatidylinositol 4-phosphate (PI4P) is present on the membrane and promotes the recruitment of the Ypt31/32 effector Sec2 [291]. Sec2 itself is a GEF for Sec4, another Yeast Rab GTPase and thus Sec4 is subsequently recruited to the vesicle [284-285]. It could be shown that Ypt31/32 and Sec4 bind to different parts of Sec2. Ypt31/32 requires residues 161–374 for the interaction whereas Sec4 binding occurs between residues 1-161 [284]. The structure of the Sec4/Sec2 complex has been solved [190]. Sec4 was found in the typical G-domain fold of GTPases and the Sec2 GEF domain adapts a fold of 2 coiled-coiled α-helices (Figure 1.14). The coiled coil packing is disrupted between residues 94 and 119 of both monomers and this is the interaction site with Sec4. Especially the switch regions of Sec4 are involved in the interactions with Sec2. A comparison of Sec2 bound Sec4 with Sec4(GDP) and Sec4(GppNHp) reveals that the switch regions seem to be reordered upon binding to Sec2 [190]. The remodeling of the switch regions leads to an open nucleotide binding pocket. Although different in details the overall mechanism employed by GEFs for the nucleotide exchange (described in section 1.4.2.) is the same.

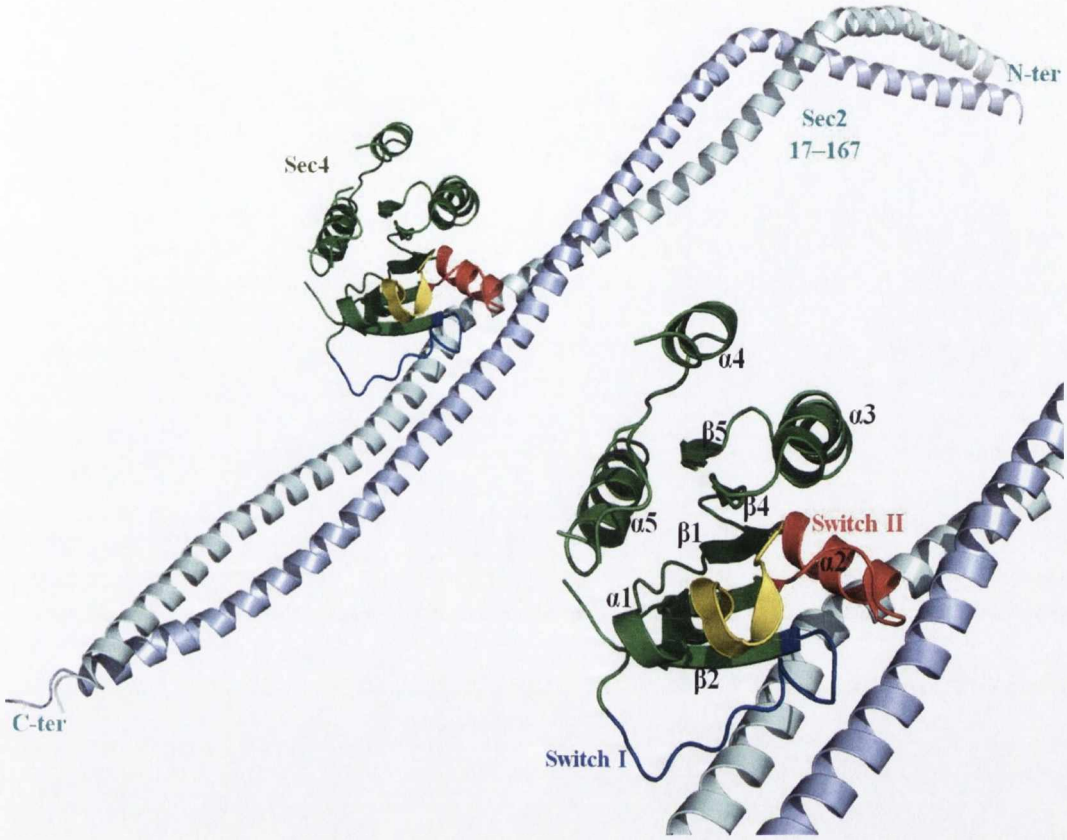

Figure 1.14 Structure of the Sec4/Sec2 complex.
Sec4 is in green with the p-loop in yellow, switch I in blue and switch II-α2 in red. The two Sec2 molecules are shown in light blue shades. The Sec2 GEF domain (residues 17-167) adopts the conformation of a coiled coil made of two Sec2 GEF domain molecules. Sec4 adopts the overall fold of GTPases. The interaction between Sec2 and Sec4 mainly involves the switch regions of Sec4 and a part of Sec2 (residues 94-119) where the packing of the coiled coil is disrupted. The interaction leads to an opening of the nucleotide binding pocket, enabling nucleotide exchange.
PDB-file used for this figure: 2OCY [190].

Sec4 also binds to Myo2, using the same interaction site as Ypt31/32 [292-293]. Ypt31/32 is released and the PI4P concentration diminishes as well [291]. Sec2 and Sec4 both interact with the subunit of the exocyst tethering complex Sec15 and this interaction is inhibited as long as PI4P is present on the vesicle membrane [291, 294-295]. Additionally, the lab of Lois Weisman together our own lab recently showed that Sec15 can bind directly bind to Myo2 at a site that is different from the Ypt31/32/Sec4 binding site [292]. Thus

Myo2 is attached to the secretory vesicle through direct binding to several Rab proteins, starting from the vesicle formation (Ypt31/32) and proceeding to Sec4, until it directly attaches to the exocyst *via* Sec15 [292]. A model for the trafficking pathway, published in collaboration with the laboratory of Lois Weisman, is shown in Figure 1.15.

In mammalian cells the Ypt31/32 homologue Rab11 has been shown to bind to so called FIP proteins (Rab11-Family of Interacting Proteins), FIP2 and FIP3, which in turn interact with motor proteins [83, 296-297]. The closest Sec4 homologues are Rab8 and Rab10, which both interact with myosin V [297-299]. Hence the processes involved in secretory vesicle trafficking in yeast are also found in mammalian cells, although they are more complex than in yeast.

Having resolved the steps that are necessary for vesicle secretion in yeast, it will now be interesting to include structural information about the interactions that take place. Structures of Ypt1 and Sec4 alone or in complex with effectors have been solved. A Ypt31-GDI structure is also available on the protein data bank, which is the only existing YPT31/32 structure resolved thus far.

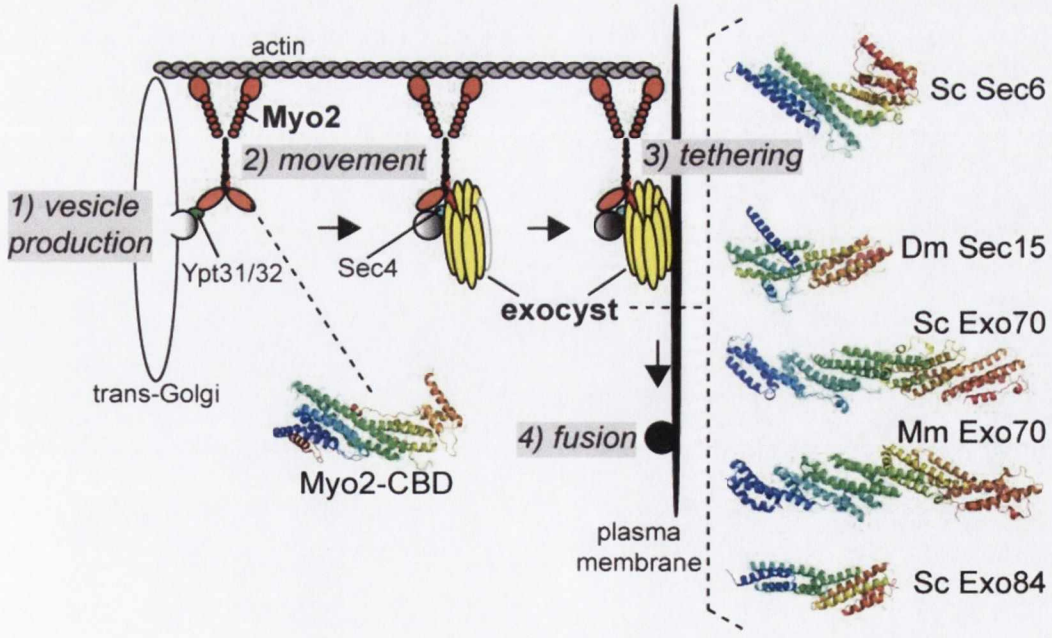

Figure 1.15 Model for the Rab-mediated trafficking of vesicles to the exocyst.
Ypt31/32 co-ordinates exit from Golgi, while Sec4 mediates later stages involving Sec15 and the exocyst. The vectorial transfer is facilitated by myosin.

Table 1.4: Functions of yeast Rab GTPases

Ypt	Transport steps regulated	Reference
Ypt1	ER-to-Golgi and cis-to-medial-to-trans; retrograde to ER	[276, 280-281, 300]
Sec4	Golgi to plasma membrane	[55]
Ypt31 **Ypt32**	Between and from Golgi compartments; Myo2 dependent motility	[61, 288, 290]
Ypt51 **Ypt52** **Ypt53**	Plasma membrane to early endosome , early to late endosome, Golgi to early endosome,	[278, 301]
Ypt6	Late Golgi, endosome	[302]
Ypt7	Late endosome to vacuole, vacuole-vacuole fusion	[303]
Ypt10	Endocytosis	[165]
Ypt11	ER and Golgi inheritance during budding	[165, 304]

1.7. Rab1 is 'hi-jacked' by host pathogen protein DrrA

The Rab GTPase Rab1 is a regulator of ER to Goli transport [305]. It is usually found on membranes of both, the ER and Golgi compartments [277]. Not only is it necessary for the initial step of exporting proteins from the ER, it is also required for the transport between Cis- and Medial-Golgi compartments and obligatory in order to maintain a functional Golgi complex [306].

Legionella pneumophilia is a bacterial pathogen that causes both Legionnaires' disease, which leads to pneumonia, and Pontiac fever, an illness that resembles acute influenza [307]. After infecting its eukaryotic host cells *L. pneumophilia* replicates inside a specialised organelle, morphologically similar to the ER. This bacteria has been shown to modulate the transport of so called Legionella containing vacuole (LCV) [308]. Among the 566 different host proteins found on the LCV membrane is Rab1. It is recruited to the LCV within minutes of *L. pneumophilia* uptake into the host cell [309-310]. Two separate groups identified the protein responsible for Rab1 recruitment and named it SidM and DrrA respectively and both names are currently used in the literature [192, 311], however here it will be referred to as DrrA.

DrrA shares little sequence identity with other proteins and homologues are difficult to identify via sequence alignments. DrrA seems to be anchored to the LCV via interaction of its C-terminal region with phosphatidylinositol 4-phosphate (PtdIns(4)P) [312]. The domain was called P4M domain for PtdIns4P binding of SidM/DrrA and comprises residues 520-647. It could also been shown that a domain of residues 340-520 has a guanosine nucleotide exchange activity, and also functions as a GDF [193-194]. However it became apparent later on that the GDF activity is a result of the GEF activity [195]. The higher affinity of DrrA for Rab1 over the affinity of GDI favors the complex formation with DrrA thus making a GDF activity unnecessary. The function of the N-terminal domain of DrrA, residues 1-340, remained unknown until the determination of its structure. It has an adenosine monophosphate (AMP)–transferring activity towards the switch II region of Rab1 [313]. A threonine residue is AMPylated which prevents the access of GAPs and thus the catalysis of nucleotide hydrolysis. The AMPylation is also thought to prevent interaction of Rab1 with at least some host effectors of Rab1 [313].

Several structures of DrrA and Rab1/DrrA have been solved recently [195, 197, 313-314]. Different length DrrA fragments were employed but a full length structure of DrrA has not been solved yet. The structures revealed that DrrA is found in a hitherto unknown fold. The GEF domain adopts a raft like structure that is formed by 8 α helices (Figure 1.16 A and Figure 1.17 A). The nucleotide exchange mechanism employed by DrrA involves a huge conformational change of switch I (Figure 1.16). This results in an opening of the nucleotide pocket towards the solvent. The membrane anchoring P4M domain is comprised of 5 α-helices and like the GEF domain does not contain any β-strands (Figure 1.17 A). The fold of the N-terminal AMPylation domain resembles that of glutamine synthetase adenylyl transferase, both proteins share the catalytically important sequence motif $G(x)_{11}DxD$ and a similar overall fold [313]. The structural resemblance with glutamine synthetase adenylyl transferase was the key factor for identifying the function of the N-terminal domain of DrrA.

Research conducted within the last few years has given insights on how host pathogens can employ host proteins for their purposes. The example of DrrA shows that bacterial proteins often combine several functions in one protein in order to successfully replicate in their host organism. It also emphasises the importance to solve structures of proteins/protein domains with unknown function since this can be the key to identifying this function.

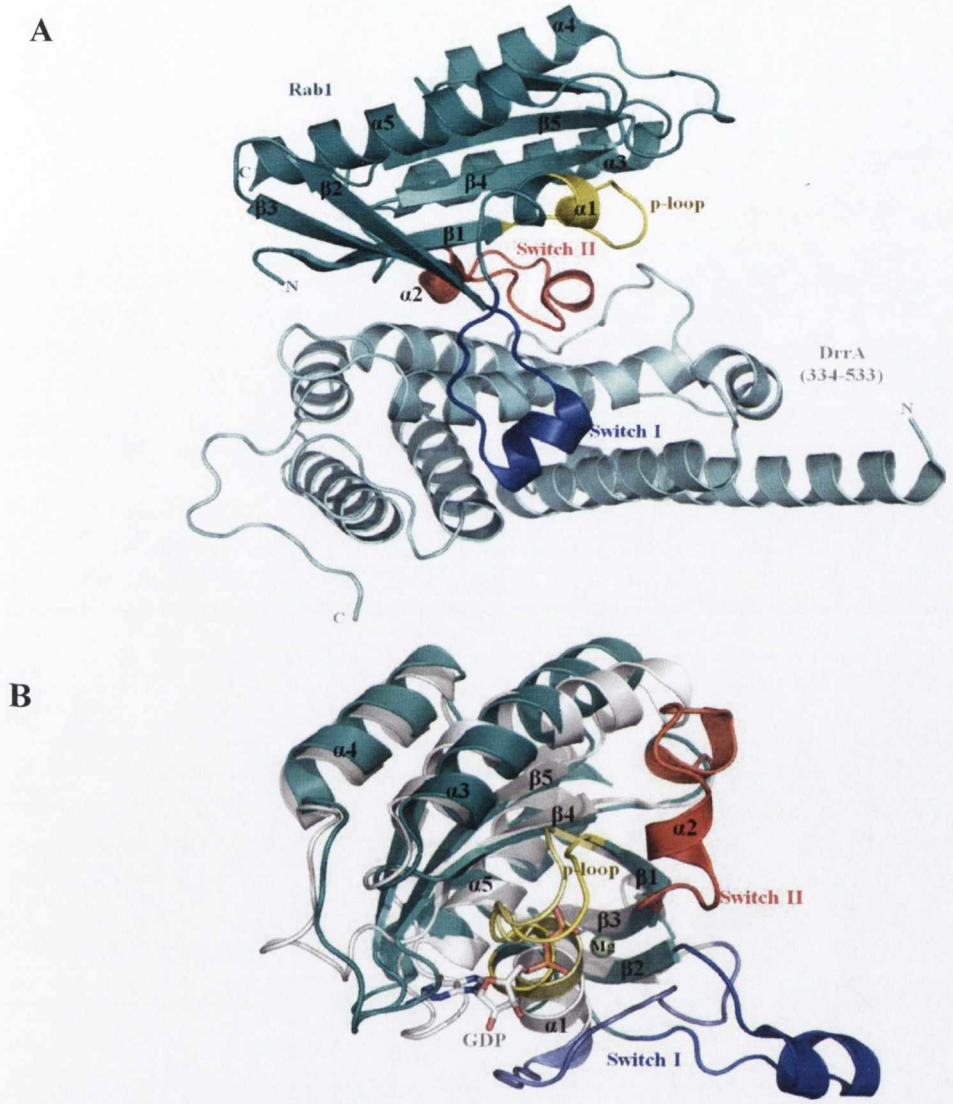

Figure 1.16 Structures of Rab1/DrrA, Rab1.
The p-loop is shown in yellow, switch I in blue, switch II in red, the nucleotide is shown as sticks and Mg^{2+} as a sphere. Panel A: Rab1/DrrA complex. Rab 1 is shown in cyan and $DrrA_{334-533}$ in light blue. Upon binding to DrrA switch I opens up from the nucleotide binding pocket and forms a helix that interacts with DrrA. Panel B: Comparison of Rab1a(GDP) with Rab1b when bound to DrrA. The Rab1 taken from the structure with DrrA is in cyan, Rab1(GDP) in grey. The overall conformation of Rab1 when bound to DrrA is the same as of Rab1(GDP). The α3 helix changes its position, as does the p-loop, but those changes are by far not as dramatic as the repositioning of switch I. Switch II is disordered in the structure of Rab1(GDP), the interaction with DrrA stabilises it. PDB-files used for this figure: 2WWX (Rab1/$DrrA_{334-533}$ [314]); 2FOL (Rab1(GDP) [SGC]).

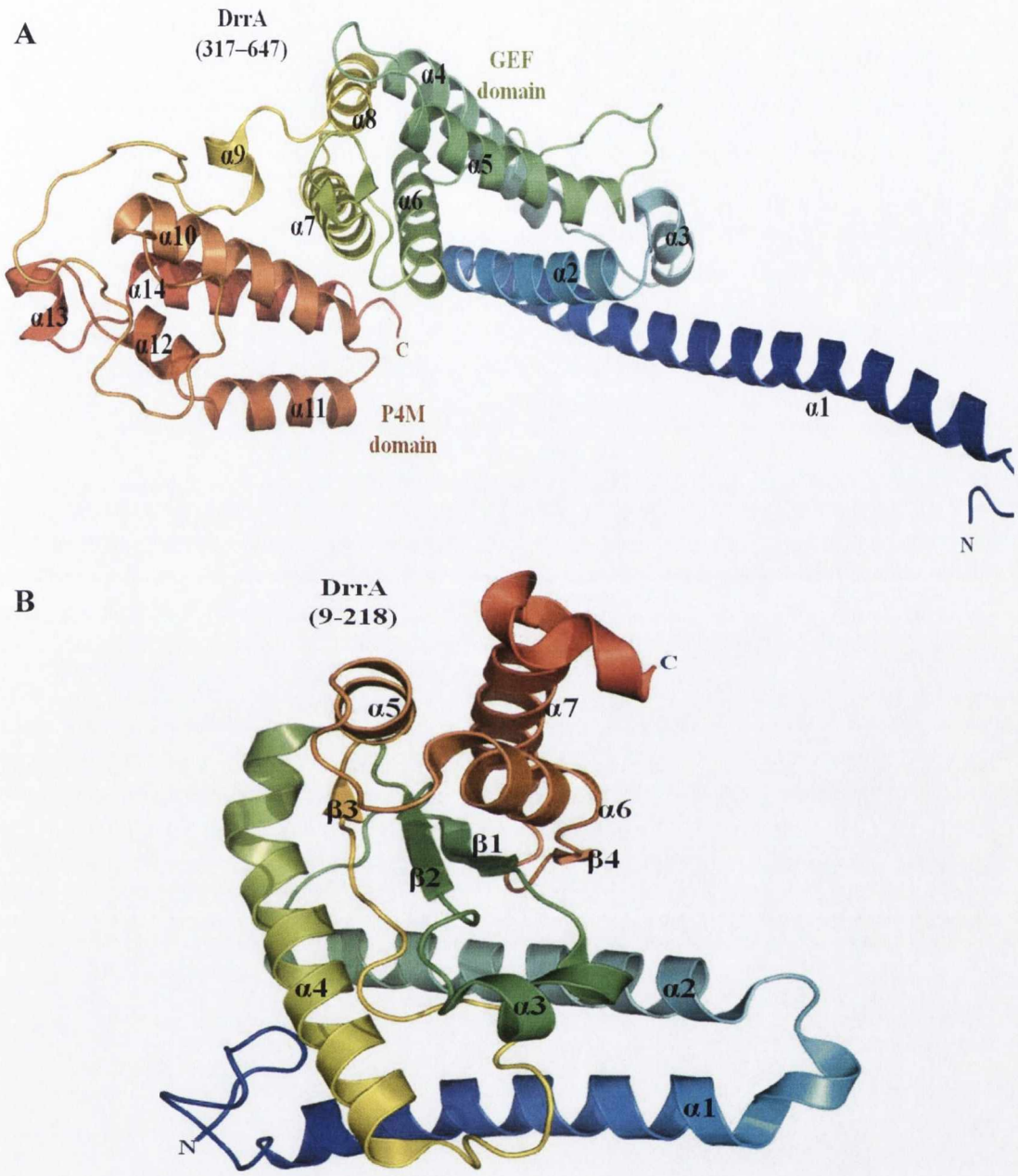

Figure 1.17 Structures of DrrA fragments.
Panel A: Structure of $DrrA_{317-647}$. This structure shows the Rab1 interacting GEF domain as well as the P4M domain that is involved in the anchoring of DrrA to the membrane. These domains are solely comprised of α-helices. Panel B: structure of the N-terminal AMPylation domain of DrrA. The catalytic domain is located between β1 and β2, here in dark green. PDB-files used for this figure: 3LOM ($DrrA_{317-647}$ [197]); 3NKU ($DrrA_{16-215}$ [313]).

1.8. Proposed studies and aims

Even though a considerable amount of research has provided insights into the specificity determinants for Rab/effector complexes, more information is needed for thorough understanding of Rab biology. Structural analysis of more complete fragments of effectors and other regulatory proteins in complex with Rabs are required for a better understanding of their detailed mechanisms in regulating cell dynamics. Effectors are modular – the RBD is responsible for cellular localisation, but the additional domains exert biological effects. Currently, there exists no structure of a Rab with the complete effector polypeptide – the vast majority of effectors have only had their RBD, generally a short a-helical motif (30-40 residues), in complex with their cognate Rab, as can be observed in Figure 1.9. The largest complex thus far is the Rab6 complex with Rab6-interacting protein 1 (R6IP1), which is a 380-residue fragment of the effector that is only 1/3 of the total proteins [229]. The structure revealed the mechanism by which the 'PLAT domain' (acronym) could regulate lipid attachment. Furthermore, the thermodynamic and kinetic parameters are key to understanding the biological function of Rab complexes in vesicle trafficking.

Our lab's work began with Rab27 and effectors since, at the time, no crystals structure of a Rab27/effector complex had been determined. Since then, two crystal structures have emerged; Rab27a/Slp2 [227] and Rab27b/melanophilin [169]. Nevertheless, the structure of Rab27/JFC1 remains interesting for several reasons. Firstly, no crystal structure of a complete effector has yet been determined (the Rab27 complexes involved the RBD of effectors), and JFC1 may be amenable to crystallisation of the complete complex. Also, the soluble behavior of the effector allowed thermodynamic studies, which could now be extrapolated to the known structures in order to understand the significance of Rab/effector interfaces. Previous structural studies of Rab27/effector and the related Rab3/effector complexes all involved co-expression of the effector RBD to obtain soluble complexes for structural studies.

Other projects of our lab involve the investigation of yeast trafficking Rab GTPases as well as host pathogen – host interactions involving Rab GTPases.

The individual goals of the various projects are listed below.

1. Crystallisation and thermodynamic studies of the complete JFC1 in complex with Rab27
2. Crystallisation of Ypt32 and clarification of its role in yeast vesicle trafficking
3. Crystallisation of DrrA in complex with Rab1

Chapter 2

Materials and Methods

2.1. Materials

Reagents used were of analytical grade where possible and generally obtained from Sigma-Aldrich unless specified otherwise.

2.2. DNA manipulation techniques

2.2.1. Plasmid extraction

LB medium (ForMedium), 5 ml containing the appropriate selective antibiotic was inoculated with a single colony of *E.coli XL1-Blue* cells harbouring the plasmid of interest and grown over night at 37°C (310 K) with shaking at 120 rpm. Cells were then harvested by centrifugation at 4000 g in a bench top centrifuge, and the supernatant removed. Plasmids were purified using the 'PureYield Plasmid Miniprep System' (Promega) using the protocol outlined by the manufacturers. When DNA sequencing was required, 5 µg of the extracted plasmids were sent to Source Bioscience Dublin for sequencing.

2.2.2. DNA electrophoresis

DNA was analysed by electrophoresis through 1% agarose gels containing 0.5 ug/ml ethidium bromide. Gels were prepared by melting 100 ml of a 1% (w/v) agarose (Promega) in TAE buffer (40mM Tris-HCl, 20 mM acetic acid, 1mM EDTA pH 8.5). The melted gel was poured and allowed to set in an ATTO AE-6100 gel box. Samples in volumes up to 20 µl (containing up to 50 ng DNA) were mixed with loading dye (0.4% orange G 0.03% bromophenol blue, 0.03% xylene cyanol, 15% Ficoll, 0.62% SDS, 50 mM EDTA, 10 mM Tris-HCl pH8). Samples were electrophoresed at 100 V for approximately 50-60 minutes.

2.2.3. Site directed mutagenesis

Stock solutions of primers (10 pmol/µl), template DNA (10 ng/µl), dNTPs (5 mM) were prepared and used in PCR amplification reactions. Phusion High-Fidelity DNA Polymerase and Phusion HF Buffer containing 1.5 mM $MgCl_2$ NEB was the polymerase of

choice. Used primers are shown in Table 2.1. The PCR reaction was run using the following conditions: initial denaturation at 95°C for 90 sec followed by 18 cycles of denaturation (30 sec at 95°C) primer annealing (60 sec at 55°C) and extension (5.5 min at 68°C). The final step was a 7 minute long elongation at 68°C before cooling the products at 4°C until the samples were recovered.

A synthetic open reading frame (ORF) of Rab1a (GeneArt) was used as template DNA. This construct encoded the active locked Rab1a mutation (Q66L). Using site directed mutagenesis this template was used to produce the wild type (wt) Rab1a form (Gln66). From the wild type a further mutation (S21N) was introduced to produce Rab1a encoding the GDP locked form.

The synthetic ORF of Rab27a Ser123/Ser188 (GeneArt) was used as template DNA for mutations in order to obtain the wild type sequence (Cys123/Cys188). Rab27a Ser123/Ser188 was first mutated to Rab27a Cys123/Ser188 which was then used as a template to obtain Rab27a Cys123/Cys188 (wt). The resulting wild type Rab27a was used as a template for the following mutations: Y8A; W73G; W73A; L84I+F88Y+D91G (r3mut).

Table 2.1 Forward primers used in various amplification reactions

Template	Primer Name	Sequence	Vector
Rab1			
	L66Q FP	GGGATACCGCAGGCCAGGAACGTTTTCGTAC	pET 15b
	S21N FP	GCGGTGTTGGTAAAAACTGTCTGCTGCTGCG	pET 15b
Rab27			
	S123C-FP	CTGCAGATGCATGCATATTGCGAAAATCCGGATATTGTTC	pET 28b
	S188C-FP	GAAACGTATGGAACGTTGCGTTGATAAAAGCTGGTAATA AGG	pET 28b
	rY8A-FP	GTCCGATGGCGATTATGATGCTCTGATTAAATTTCTGGCC C	pET 28b
	rW73G-FP	GTATTCATCTGCAGCTGGGGGATACCGCAGGTCAAG	pET 28b
	rW73A-FP	GTATTCATCTGCAGCTGGCGGATACCGCAGGTCAAG	pET 28b
	r3mut-FP	CGTTTTCGTAGCATTACCACCGCATATTTTCGTGGTGCAA TGGGTTTTCTGC	pET 28b

2.3. Transformation of cells

Plasmids were transformed into 50 µl competent *E. coli* BL21 DE3 using a heat shock method. To the host cells 10 – 50 ng of the plasmid was added and the suspension was incubated on ice for 20 minutes followed by a 45 second heat shock at 42°C (315 K). The suspension was then incubated on ice for a further 2 minutes. To the cell suspension 1 ml of LB (ForMedium) was then added and the mixture was incubated at 37°C (310 K) for 1 hour with shaking at 120 rpm. The cells were then harvested through brief centrifugation at in a bench top centrifuge and 900 µl of the supernatant was removed. Cells were resuspended in the remaining medium and were spread onto LB agar plates containing selective antibiotics for each plasmid transformed. Plates were incubated over night at 37°C (310 K) and then stored at 4°C (277 K). Selective antibiotics used were ampicillin (Amp) at a final concentration of 100 µg/ml and kanamycin (Kan) at a final concentration of 35 µg/ml agar or liquid medium. Table 2.2 shows details of each construct used.

Table 2.2 Details of constructs used in this study

Construct	Size (kDa)	Supplier	Vector	Selective antibiotic	Protease (tag-cleavage)	Tag	Expression temperature
DrrA (1-647, FL)	73.4	GeneArt	pET 15b	Amp	Thrombin	His	37°C (310 K)
DrrA (202-647)	50.5	In-house	pNIC28 -Bsa4	Kan	rTEV	His	25°C (298 K)
Rab1a (1-175)	19.8	GeneArt	pET 15b	Kan	Thrombin	His	37°C (310 K)
Ypt32 (1-184)	20.3	Lois Weisman, University of Michigan	pMAL	Kan	rTEV	MBP	37°C (310 K)
Rab27a (1-193)	22	GeneArt	pET 28b	Kan	Thrombin	His	37°C (310 K)
JFC1 (1-562, FL)	62	In-house	pLIC-Nus	Amp	rTEV	Nus-His	18°C (291 K)

FL, full length; Amp, Ampicillin; Kan, Kanamycin

2.4. Protein expression

2.4.1. Small scale protein expression screening

Small scale expression screening of construct was performed before expressing the proteins of interest in large litre cultures, to establish whether or not the protein of interest was expressed and soluble. Starter cultures were prepared by inoculating 1 ml LB (1 µl of the selective antibiotic) with a colony from freshly transformed BL21 DE3 cells and growth at 37°C (310 K) over night. An aliquot (100 µl) of the overnight culture was then used to inoculate a 5 ml volume of 2xYT or LB. The culture was then incubated at 37°C (310 K) with shaking at 140 rpm until the OD_{600nm} reached 0.6 absorbance units. At this point a glycerol stock of this culture was made by mixing 400 µl of 50% glycerol with 300 µl of bacterial solution and flash frozen in liquid nitrogen before storing at -80°C (193 K). The remaining 4.7 ml culture was then induced through addition of IPTG (final concentrations of 0.3 mM IPTG when inducing at for 25°C (298 K) and 0.2 mM IPTG when inducing at 18°C (291 K)). Protein expression was usually induced for 3 hours at 37°C (310 K), 5 hours at 25°C (298 K) and 18 hours at 18°C (291 K). Cells were harvested by centrifugation at 7,000g and the supernatant decanted. Cells were lysed in 1 ml extraction buffer (20 mM Imidazole, 300 mM NaCl, 5 mM $MgCl_2$, 10 mM β-Mercaptoethanol, 10 mM Tris-Cl pH 7.5). The pellet was then resuspended in 500 µl of double distilled water. To the supernatant 40 µl of a 50% Ni^{2+}-ChroMatrix slurry (Jena) was added and mixed gently for 5 minutes on a rotating disk mixer (60 rpm) at 4°C (277 K). This solution was then centrifuged at 800 rpm on a bench top microcentrifuge for 3 minutes and the supernatant discarded. The Ni^{2+}-ChroMatrix beads were then washed by adding in 1000 µl extraction buffer and allowed to mix on a rotating disk and harvested by centrifugation as described above. The Ni^{2+}-ChroMatrix beads with bound his tagged target protein was then prepared for analysis on SDS polyacrylamide gel electrophoresis (described in Section 2.8.1) by adding 10 µl 6 x SDS-PAGE sample buffer to the bead pellet. Of the insoluble fraction, 5 µl in 5 µl loading buffer were loaded.

2.4.2. Large scale protein expression

A 10 ml overnight culture was prepared by adding 10 µl of the selective antibody to 10 ml sterile LB media (ForMedium) which was then inoculated with *E.coli* BL21 DE3 containing the plasmid for expression of the protein of interest. Overnight cultures were grown in a shaker incubator at 37°C (310 K) and 120 rpm. The following day 1 ml of the selective antibiotic was added to 1 liter of sterile 2xYT enriched expression media (ForMedium) in a 3 liter Erlenmeyer flask and this solution was then inoculated by the overnight culture. This culture was shaken at 37°C (310 K) and 120 rpm until the OD_{600nm} was between 0.6 and 0.8. Protein overexpression was then induced by adding 0.5 mM IPTG (ForMedium) and cells were harvested after 3 to 4 hour induction.

For proteins requiring expression at lower temperatures ($DrrA_{202-647}$ at 25°C (298 K) and JFC1 at 18°C (291 K)) the flask was transferred to an incubator shaker at 25°C (298 K) (or 18°C (291 K)) when the OD_{600nm} reached 0.4. When the OD_{600nm} was between 0.6 and 0.8, protein overexpression was induced by adding a final concentration of 300 µM (or 200 µM) IPTG. After 5 hours (or 18 hours) of induction cells were harvested.

2.4.3. Expression of selenomethionine containing protein

A 10 ml overnight culture was prepared by adding 10 µl of the selective antibiotic to 10 ml sterile LB media (ForMedium) which was then inoculated with *E.coli* BL21 DE3 harbouring the plasmid of interest. Overnight cultures were grown in an incubation shaker at 37°C (310 K) and at 140 rpm. The following morning a filtered nutrient mix was added to 1 liter SeMet Medium Base (Molecular Dimensions) as well as the selective antibiotic. The media was then preheated at 37°C (310 K) and after 30 minutes the overnight culture was added. Cells were grown at 37°C (310 K) with shaking at 140 rpm until the OD_{600nm} reached 0.5. Amino acids were then added to the media as follows: 100 mg of Lys, Thr, Phe; 50 mg of Leu, Ile, Val; 50 mg of SeMet (L-stereoisomer). If necessary the culture was then moved to a different temperature and after 15 minutes protein expression was induced with a final concentration of 400µM IPTG.

2.5. Protein purification

2.5.1. Cell harvesting and protein extraction

Cell harvesting was performed by centrifuging for 10 min at 4°C (277 K) and at 4000 g. The supernatant was discarded and the pellet was resolubilised in PBS and centrifuged again for 10 min at 4°C (277 K) and 4000 g. The supernatant was discarded and the pellet frozen at -80°C (193 K) or immediately lysed by sonication for purification of the induced protein.

2.5.2. Purification of Rab27a and Rab1a

For extraction, a cell pellet from a 1 litre culture (Section 2.4.2) was resuspended in 20 ml of extraction buffer (20 mM Imidazole, 300 mM NaCl, 5 mM $MgCl_2$, 10 mM β-Mercaptoethanol, 10 mM Tris-Cl pH 7.5) containing 0.5 mM PMSF (Fluka). Resuspended cells were then sonicated on ice with a duty output of 35% and a power output of 4, over 4 cycles with 1 minute sonication bursts followed by 1 minute incubating on ice. The resulting lysate was then centrifuged for 30 min at 4°C (277 K) and at 18,000 g. The supernatant was filtered with a Filtropour S filter (Sarstedt), poresize 0.45 µm, in order to remove remaining cellular debris and the remaining pellet was discarded. A gravity column was filled with 2 ml Ni^{2+}-ChroMatrix resin (Jena bioscience) and equilibrated with extraction buffer. The filtered cell lysate was then loaded onto the column by gravity flow followed by rigorous washing with 100 ml of extraction buffer. Bound protein was eluted from the column with elution buffer (200 mM Imidazole, 300 mM NaCl, 5 mM $MgCl_2$, 10 mM β-mercaptoethanol, 10 mM Tris-Cl pH 7.5). Cleavage of the His-tag was performed on addition of 10 units/ml of thrombin (GE Healthcare) while dialysing overnight (Thermo Scientific Snakeskin Dialysis Membrane (7 kDa MWCO)) against 150 mM NaCl, 5 mM $MgCl_2$ 10 mM β-mercaptoethanol, 10 mM Tris-Cl, pH 8. After dialysis the NaCl concentration of the Rab protein solution was adjusted to a final concentration of 300 mM NaCl and 20 mM imidazole. A second Ni^{2+}-ChroMatrix affinity chromatography step was performed by incubating 2 ml Ni^{2+} resin with the protein solution for at least 15 minutes. The solution was then loaded into a gravity column and flow through and extraction buffer

wash fractions that contained the cleaved protein were harvested. If the Rab was to be used for complex formation no further purification was performed and the protein was stored at -80°C (193 K) if required. Protein that was to be used for thermodynamics was concentrated if needed and loaded onto a Superdex-200 16/60 size exclusion column (mounted on AKTAbasic FPLC, GE Healthcare) equilibrated with 100 mM NaCl, 5 mM $MgCl_2$, 1 mM DTT and 10 mM Tris-Cl, pH 7.5. The purity of the protein was checked at each step by analysing with SDS-PAGE (described in Section 2.8.1).

2.5.3. Purification of JFC1

The pellet from a 2 litre induced culture (Section 2.4.2) was resuspended in 40 ml of extraction buffer (300 mM NaCl, 5 mM $MgCl_2$, 10 mM β-mercaptoethanol, 10 mM Tris-Cl, pH 7.5) containing 0.5 mM PMSF (Fluka). Resuspended cells were then sonicated as described in Section 2.5.2. The resulting cell lysates was then centrifuged at 18,000 g for 40 min at 4°C (277 K). The supernatant was filtered with a Filtropour S filter (Sarstedt), poresize 0.45 µm, in order to remove remaining cellular debris and the remaining pellet was discarded. A gravity column containing 3 ml Ni^{2+}-ChroMatrix resin (Jena bioscience) was equilibrated with extraction buffer. The filtered cell lysate was then loaded onto the column and washing with 100 ml of extraction buffer. Bound protein was eluted from the column with elution buffer (200 mM Imidazole, 300 mM NaCl, 5 mM $MgCl_2$, 10 mM β-mercaptoethanol, 10 mM Tris-Cl, pH 7.5). Cleavage of the His-tag was achieved by addition of 10 µg rTEV protease per mg fusion protein and the mix was dialysed over night against 200 mM NaCl, 5 mM $MgCl_2$, 10 mM β-mercaptoethanol, 10 mM Tris-Cl, pH 8 (Thermo Scientific Snakeskin Dialysis Membrane (7 kDa MWCO)). The dialysed and cleaved JFC1 protein solution was then dialysed further into a 100 times volume of low salt buffer (10 mM NaCl, 5 mM MgCl2, 1 mM DTT, 10 mM Tris-Cl, pH 7.5) for 2 hours. The protein solution was then loaded onto a MonoQ 5/50 anion exchange column connected to an AKTAbasic FPLC, GE Healthcare. Elution was performed with a linear salt gradient to 1 M NaCl. Eluted fractions containing JFC1 were combined, the NaCl concentration was adjusted to 300 mM and 20 mM imidazole was also added and the protein solution was subsequently loaded onto a 2 ml bed volume of Ni^{2+} ChroMatrix, prequilibrated extraction

buffer (20 mM Imidazole, 300 mM NaCl, 5 mM $MgCl_2$, 10 mM β-mercaptoethanol, 10 mM Tris-Cl pH 7.5). The same buffer was also used to wash the column after loading the protein solution. Flow through and washing fractions containing JFC1 were then combined, and concentrated when necessary before loading onto a Superdex-200 size exclusion column (GE Healthcare), equilibrated in 100 mM NaCl, 5 mM $MgCl_2$, 1 mM DTT and 10 mM Tris-Cl pH 7.5. The purity of the protein was analysed at each step using SDS-PAGE (described in Section 2.8.1).

2.5.4. Purification of full length DrrA

A cell pellet from a 1 litre induced culture (Section 2.4.2) was resuspended in 20 ml of extraction buffer (10 mM imidazole, 300 mM NaCl, 5 mM $MgCl_2$, 10 mM β-mercaptoethanol, 10 mM Tris-Cl pH 7.5) containing 0.5 mM PMSF (Fluka). The cell suspension was then sonicated as described in Section 2.5.2. The cell lysate was then centrifuged at 18,000g for 40 min at 4°C (277 K). The supernatant was filtered with a Filtropour S filter (Sarstedt), poresize 0.45 μm. The filtrate was loaded onto a gravity flow column containing 2 ml Ni^{2+}-ChroMatrix resin prequilibrated with extraction buffer and washed with 100 ml of extraction buffer. Protein was then eluted from the column using 50 mM imidazole, 300 mM NaCl, 5 mM $MgCl_2$, 10 mM β-mercaptoethanol, 10 mM Tris-Cl, pH 7.5 as elution buffer. Cleavage of the His-tag was performed in the presence of 10 units/ml of thrombin (GE Healthcare) while dialysing overnight against 10 mM Tris-Cl, 150 mM NaCl, 5 mM $MgCl_2$ and 10 mM β-mercaptoethanol, pH 8. After dialysis the the DrrA protein solution was adjusted to a final concentration of 300 mM NaCl and 10 mM imidazole. A second Ni^{2+}-ChroMatrix affinity chromatography step was performed by incubating 2 ml Ni^{2+} resin with the protein solution for at least 15 minutes. The solution was then loaded into a gravity column and the flow through containing the cleaved DrrA protein was retained. The combined fractions were dialysed into a low salt buffer (10 mM NaCl, 5 mM $MgCl_2$, 1 mM DTT, 10 mM Tris-Cl, pH 7.5) for at least 2 hours and then loaded onto a MonoQ 5/50 anion exchange column (mounted on AKTAbasic FPLC, GE Healthcare). Elution from the column was performed with a linear salt gradient to 1 M NaCl. Elution fractions containing DrrA were loaded onto a Superdex-200 16/60 size

exclusion column (mounted on AKTAbasic FPLC, GE Healthcare) equilibrated with 100 mM NaCl, 1 mM DTT and 10 mM Tris-Cl pH 7.5. The purity of the protein was analysed at each step using SDS-PAGE (described in Section 2.8.1).

2.5.5. Purification of DrrA (residues 202-647)

A cell pellet from 1 litre induced culture (Section 2.4.2) was resuspended in 20 ml of extraction buffer (20 mM imidazole, 300 mM NaCl, 5 mM $MgCl_2$, 10 mM β-mercaptoethanol, 10 mM Tris-Cl, pH 7.5) containing 0.5 mM PMSF (Fluka). The cell resuspension was sonicated, centrifuged and the resulting supernatant filtered as described in Section 2.5.2. A gravity column was filled with 2 ml Ni^{2+}-ChroMatrix resin and equilibrated with extraction buffer. The filtered cell lysate was then loaded onto the column by gravity flow and washed with 100 ml of extraction buffer. Bound protein was eluted from the column with elution buffer (200 mM Imidazole, 300 mM NaCl, 5 mM $MgCl_2$, 10 mM β-mercaptoethanol, 10 mM Tris-Cl, pH 7.5). Cleavage of the His-tag was performed in the presence 10 μg rTEV protease per mg protein while dialysing overnight against 10 mM Tris-Cl, 200 mM NaCl, 5 mM $MgCl_2$ and 10 mM β-mercaptoethanol pH 8. The dialysed protein sample had its final concentration of NaCl and imidazole adjusted to 300 mM and 20 mM respectively. A second Ni^{2+}-ChroMatrix affinity chromatography step was performed by incubating 2 ml Ni^{2+} resin with the protein solution for at least 15 minutes. The slurry was then loaded into a gravity column and the flow through containing the cleaved protein was retained. The protein sample was then dialysed into 100 times volume low salt buffer (10 mM NaCl, 5 mM MgCl2, 1 mM DTT, 10 mM Tris-Cl, pH 7.5) for 2 hours and then loaded onto a MonoS 5/50 anion exchange column (mounted on AKTAbasic FPLC, GE Healthcare). Elution from the column was performed with a linear salt gradient to 1 M NaCl. Elution fractions containing the protein were loaded onto a Superdex-200 16/60 size exclusion column (mounted on AKTAbasic FPLC, GE Healthcare) equilibrated with 100 mM NaCl, 1 mM DTT and 10 mM Tris-Cl pH 7.5. The purity of the protein was analysed at each step using SDS-PAGE (described in Section 2.8.1).

2.5.6. Purification of Ypt32

A cell pellet from 1 litre IPTG induced culture (Section 2.4.2) was resuspended in 20 ml of 'MBP extraction buffer' (200 mM NaCl, 20 mM Tris-Cl, pH 8). For 20 ml of lysate 4 ml of amylose resin (NEB) were used. The resin was poured into a gravity column and equilibrated with 20 ml MBP extraction buffer. The cell lysate was then loaded onto the amylase resin by gravity flow and washed with 60 ml of MBP extraction buffer. The protein of interest was then eluted with MBP elution buffer (10 mM maltose, 200 mM NaCl, 10 mM Tris-Cl, pH 7.7). The MBP-tag was cleaved with 10 µg rTEV protease per mg protein by dialysing the protein solution over night into 200 mM NaCl, 10 mM β-mercaptoethanol, 20 mM Tris-Cl, pH 8. Following the overnight dialysis the dialysis tube was transferred into a 100 times volume of low salt buffer (10 mM NaCl, 5 mM MgCl2, 1 mM DTT, 10 mM Tris-Cl, pH 8) for 2 hours. The Ypt32 protein solution was then loaded onto a MonoQ 5/50 anion exchange column. Elution from the column was performed with a linear salt gradient to 1 M NaCl. Elution fractions containing DrrA were loaded onto a Superdex-200 16/60 size exclusion column equilibrated with 100 mM NaCl, 5 mM $MgCl_2$, 1 mM DTT and 10 mM Tris-Cl, pH 8. The purity of the protein was assessed at each step by SDS-PAGE analysis (described in Section 2.8.1).

2.6. Complex formation

A protein-protein complex was formed between Rab27a(GppNHp) or Rab27a(GDP) and JFC1 by incubating JFC1 with an excess of nucleotide exchanged Rab27a (exchange process is described in Section 2.8). This complex incubation solution was then loaded onto a Superdex-200 16/60 size exclusion column equilibrated with 100 mM NaCl, 5 mM $MgCl_2$, 1 mM DTT and 10 mM Tris-Cl, pH 7.5. The eluted peak fractions were analysed by SDS-PAGE for the presence of JFC1 and Rab27a in the same fraction. Similarly, DrrA was incubated with an excess amount of the Rab1a S21N mutant protein and the solution was processed in the same manner as JFC1/Rab27a complex.

2.7. Nucleotide exchange

Nucleotide exchange was performed by incubating the protein with 5 mM EDTA and then removing the $MgCl_2$ and EDTA from the protein solution with a PD10 desalting column (GE Healthcare). Then a 5 fold concentration of GppNHp or GDP, and 5 mM $MgCl_2$ (final concentration) was added to the protein solution.

The efficiency of nucleotide exchange was determined by HPLC, using a Dionex, Umltimate 3000 system with a Discovery C18 column (Supelco) attached. The column was equilibrated with HPLC running buffer (0.1 M KH_2PO_4, 5 mM tetrabutyl ammonium hydrogen sulfate, 8% acetonitrile, pH 6.5). Samples (containing 0.5-1 mg/ml protein in 100 mM NaCl, 5 mM $MgCl_2$, 1 mM DTT and 10 mM Tris-Cl, pH 7.5) and standards of GDP, GppNHp (containing 10 µM nucleotide in sample buffer) and GTP (5 µM in sample buffer) were prepared by incubating at 98°C (371 K) for 3 minutes followed by centrifugation at 13,000 rpm for 30 minutes. To 100 µl of supernatant 50 µl of HPLC buffer were added and 50 µl of this solution was injected onto the column, a run lasted 20 minutes with an isocratic gradient of HPLC buffer. Data processing was performed using Chromeleon software (Dionex).

2.8. Protein analysis techniques

2.8.1. SDS-Polyacrylamide gel electrophoresis (SDS-PAGE)

The presence and purity of proteins was analysed by SDS-PAGE [315] using Tris-Cl/Glycine gels on a mini-slab size electrophoresis system (ATTO corporation). Briefly, protein solutions were mixed with SDS containing sample buffer (2% (w/v) SDS, 0.5% (v/v) 2-mercaptoethanol, 25 mM Tris-Cl pH 6.8, 0.0012% bromophenol blue and 10~% (v/v) glycerol) and boiled at 370 K and then spun down by flash centrifugation. Typically 15 µl protein sample containing 5-10 µg protein and 10 µl protein molecular weight marker 14-116 kDa (Jena Bioscience) were loaded onto an acrylamide gel and run at constant current of 25 mA. The 12% acrylamide resolving gel (10 ml) was made by mixing the following components; 3.3 ml H_2O, 4 ml 30 % Bis Acrylamide mix (National Diagnostics) 0.1 ml 10% SDS, 2.5 ml 2.5M Tris-HCl (pH 8.8) 0.1 ml 10% ammonium persulphate, 4µl

TEMED) The 5% acrylamide stacking gel (4 ml) was made by mixing the following components; 2.7 ml H_2O, 0.67 ml of 30 % Bis Acrylamide mix (National Diagnostics) 0.04 ml of 10% SDS, 0.5 ml of 1.5M Tris-HCl (pH 6.8) 0.04 ml of 10% ammonium persulphate, 4µl TEMED) The electrophoresis buffer contained 400 mM glycine, 0.1% (w/v) SDS, 50 mM Tris-HCl pH 8.3. In order to visualise the protein bands the gels were briefly washed with water and then stained with Instant Blue (Molecular Dimensions Inc.).

2.8.2. Protein concentration determination

Several methods were used in order to determine the concentration of proteins in solution.

2.8.2.1. Nanodrop

The NanoDrop ND-1000 was used to determine the protein concentration at 280 nm. For this purpose 2 µl protein solution was loaded onto the measurement pedestal and the absorption was measured. To obtain the concentration the Lambert-Beer equation was used.

$$A = E \cdot b \cdot c$$

A is the absorbance represented in absorbance units (A), E is the wavelength-dependent molar extinction coefficient with units of liter/mol-cm, b is the path length in cm, and c is the analyte concentration in moles/liter.

2.8.2.2. Bradford protein assay

Bovine serum albumin (BSA) standard solutions at the following concentrations were prepared in 0.15 M NaCl: 0, 200, 400, 600, 800 and 1000 µg/ml. Samples were diluted with 0.15 M NaCl where necessary so as to lie within the concentration of protein standards. To 20 µl of each sample 480 µl of Quick Start Bradford dye reagent was added and the solution was mixed thoroughly. After incubation for 5 minutes at room temperature the absorbance of each solution at 595 nm was measured. A standard curve was produced by plotting the absorbance of the standard solutions versus their concentrations and calculating a line through linear regression in Microsoft Excel. The equation for the linear regression line was then used to calculate the concentration of the samples.

In order to detect protein in eluted samples a colour change in 1 x Bradford reagent (BioRad) when mixed with the sample was used. This was done by pipetting 2 µl of the eluate into 30 µl Bradford reagent.

2.8.2.3. Bicinchoninic acid assay (BCA assay)

The QuantiPro BCA assay kit (Sigma) was used as described in the kit's protocol. The working reagent was prepared by mixing 25 parts of buffer A (Na_2CO_3, $Na_2C_4H_4O_6$, $NaHCO_3$ in 0.2 M NaOH pH 11.25) with 25 parts of buffer B (4% (w/v) bicinchoninic acid pH 8) and 1 part of reagent C (4% (w/v) $CuSO_4 \cdot 5H_2O$).

Standard solutions were prepared with 0.5, 5, 10, 20 and 30 µg/ml BSA and protein samples were diluted if necessary. The same buffer of the protein sample itself was used to make dilutions and also used as a blank. 1 ml of each standard and sample was added to 1 ml of the working reagent. The solutions were then incubated at 333 K for 1 hour. The absorption was measured at 562 nm. A standard curve was produced by plotting the absorbance of the standard solutions versus their concentrations and calculating a linear regression line using Microsoft Excel. The equation of the standard line was then used to calculate the concentration of the samples.

2.8.3. Isothermal Titration Calorimetry

Calorimetric measurements were performed using the ITC-200 instrument (MicroCal, Inc). Purified and nucleotide exchanged Rab27 (wt or mutant) and JFC1 were dialysed against 100 mM NaCl, 1 mM DTT and 10 mM Tris-Cl pH 7.5. Rab27 proteins were concentrated to approximately 100 µM and JFC1 to 10 µM.

Titrations were performed at 293 K with JFC1 in the reference cell and Rab27 in the syringe.

Concentrations were usually 6-10 µM in the cell and 50-100 µM in the syringe. Data analyses by peak integration and curve fitting were performed using the Origin software 7.0, and curves were fitted to a single-site binding model to give the binding constant (K_d), enthalpy change (ΔH), and entropy (ΔS) of complex formation.

2.8.4. Homology modelling of JFC1

The coordinates of the Slp2-RBD were obtained from the protein data bank (www.rcsb.org [316]; PDB ID 3BC1 [227]). The amino acid sequence of the Slp2 RBD was then aligned with that of the JFC1-RBD and 3BC1 was then used as a template to model the JFC1-RBD using the molecular operation environment (MOE; Chemical Computing Group, Montréal, Canada). The resulting structure was validated with Procheck [317] and via superimposition with the reference molecule using the secondary structure matching algorithm in Coot [318].

2.8.5. Static light scattering

A Superdex-200 10/300 size exclusion column (GE Healthcare), equilibrated with buffer (10 mM Tris-HCl pH 7.5 supplemented with 100 mM NaCl, 1mM DTT) was loaded with purified proteins (typically 0.1-0.5 mg total). The FPLC system was connected in-line with the miniDAWN multiangle light-scattering system, followed by an Optilab refractometer (Wyatt Technologies). Processing of data and absolute molecular mass calculations were performed using ASTRA software (Wyatt Technologies).

2.9. Crystallisation techniques

2.9.1. Crystallisation condition screening

Protein samples that were considered sufficiently pure by SDS-PAGE analyses were subjected to crystallisation trials. Typically proteins were concentrated to between 5 and 20 mg/ml using concentrators of suitable molecular weight cut offs (Amicon or Pierce). Initial screening for crystallisation was achieved using sparse matrix screening using the sitting drop vapor diffusion method at 18°C (291 K). Drops containing 100 nl of protein sample (in the buffer of the final purification step) at concentrations between 5 and 20 mg/ml and 100 nl of a reservoir solution were set up in 96-well sitting drop plates using a Mosquito robot (TTP Labtech). Usually two drops with one lower and one higher protein concentration were set up per condition. The reservoir volume was 70 µl. Commercial screens with 96 different conditions from Jena Bioscience, Molecular Dimensions and

Quiagen were used. If a potential crystallisation condition hit was achieved the condition crystal growth was optimised in a grid screen. Grid screens were set up in Linbro 24-well plates using hanging drop vapor diffusion methods with a reservoir volume of 500 µl.

2.9.2. Seeding

Different seeding techniques were used. Streak seeding was performed by touching crystals in a drop with a seeding tool (Hampton research) and streaking the needle through a new drop. Cross seeding was performed by transferring a drop containing crystals, into a microcentrifugation tube containing 50-100 µl of the reservoir solution. This solution was shaken vigorously for 10 sec and the thus produced seed stock solution was then used to set up crystallisation drops with 1 µl seed stock solution and 1 µl protein solution. Alternatively the seed stock solution was also used for streak seeding.

2.10. Data collection and structure determination

2.10.1. Ypt32 crystal diffraction, data collection and refinement

Diffraction data were collected at beamline BM14 at 0.9784 Å the European Synchrotron Radiation Facility (ESRF) in Grenoble, France using the oscillation method under cryogenic conditions. Prevention of ice formation was obtained by soaking the crystals in a cryoprotectant solution containing 25% xylitol before flash freezing them at 100K. The obtained data was integrated and scaled using the XDS package [319]. The structure of Ypt32 with GppNHp was solved by molecular replacement using MolRep [320], with a Ypt32 GDP structure that had previously been solved in the lab as search model (www.pdb.org [316]; PDB ID 3RWO, [321]). The structures were refined in reciprocal space using Refmac5 [322]. MolRep and Refmac5 are available through the CCP4 suite [323]. Structures were optimised in real space with the program Coot [318]. Part of the model and GppNHp were manually built by alternating cycles of model building with Coot and refinement with Refmac5. Water molecules were built with Coot. Pictures of molecules and electronic densities were prepared using PyMOL [324].

2.10.2. DrrA202-647 crystal diffraction, data collection and refinement

Diffraction data were collected at beamline 24ID-C at the advanced photon source, Chicago, USA using the oscillation method under cryogenic conditions. Prevention of ice formation was obtained by soaking the crystals in a cryoprotectant solution containing 20% glycerol before flash freezing them at 100K. The obtained data was integrated and scaled using the HKL2000 package [325] Phases were determined with molecular replacement using MolRep [320], and PDB ID 3JZ9 (www.rcsb.org [316]; [195]) as template.

2.11. Sequence alignments

Sequences for alignment were obtained from the database UniProtKB (http://www.uniprot.org). Protein sequences were aligned using Multiple Sequence Comparison by Log- Expectation [MUSCLE, 326] and images of the alignment were produced using the program ALINE [327].

Chapter 3

Rab27 and its effectors

3.1. Introduction

3.1.1. Rab27 effector complexes

Rab27/effector complexes are involved in various steps of exocytosis. Depending on the cell type, Rab27 recruits a distinct effector to vesicles *via* a highly conserved RBD on the effector protein. Sometimes Rab27 interacts with more than one effector in succession [269]. From the 12 identified effectors, some additionally bind to Rab3 and/or Rab8 [161, 256-257]. One effector exclusively binds to GDP-bound Rab27 [258].
From many studies of the interactions between Rab GTPases and their effectors, it can be concluded that most Rab/effector interactions involve helical domains of the effector [166]. There are two exceptions to this general rule the Early Endosomal Autoantigen 1 (EEA1; [222]) and the Lowe Syndrome protein OCRL1 [223], which have non-helical RBDs. Importantly, despite approximately 10 Rab/effector structures, there is very little information regarding the thermodynamics and kinetics of effector recruitment. Since many crystallisation studies were performed by co-expression of Rab/effectors to enable soluble expression, it has not been possible to understand the strength of Rab/effector interfaces and the contribution of various residues to the binding affinities.

To date, two Rab27/effector structures have been solved [169, 227] and several mutational studies have been performed that helped identify residues that might be important for Rab27 specificity. Interestingly, the Rab27 effectors were divided into a high affinity and low affinity group from initial analyses of the binding affinities [169, 225, 261]. Surface plasmon resonance data was obtained with the Rab binding domains of three out of the twelve effectors (Slp2-a SHD, Slp4-a SHD and Slac2-a SHD, [225]).

The two structures of Rab27/effecor-RBDs solved so far, combined with mutational analysis, revealed that the two α-helixes of the SHDs both contribute to the interaction but with differing importance for each complex [169, 227]. The structure of Rab27a/melanophilin the melanophilin contact areas identified involved the coiled coil of the SHD I, the motif of the SHD II and the FYVE-like zinc binding domain and the Rab27 contact areas involved the switch, interswitch and CDR regions. The residues that are important for the interaction of melanophilin with Rab27 are Tyr6 from Rab CDR I (that forms a hydrogen bond with melanophilin E32) and three residues from switch II of Rab27

(Leu84, Phe88, and Asp91). They were identified as the minimum determinants of melanophilin binding to Rab27 with hydrogen bonding between Rab27 Asp91 and melanophilin Arg29 and melanophilin Gly133. Although the side chain of Rab27 Tyr122 interacted with melanophilin Trp120 and melanophilin Tyr121 from the $(S/T)(G/L)xW(F/Y)_2$ motif, this interaction was not necessary for complex formation. This is different for the interaction of Rab27 with Slp2. Here Rab27 Tyr122 of the $(S/T)(G/L)xW(F/Y)_2$ motif from the SHDII, that stacks with Slp2 Phe54, is a key residue for the interaction. The invariant hydrophobic triad found in Rab GTPases (Phe46 and Trp73 from the interswitch region and Phe88 from the switch II element in Rab27) seemed to be essential for effector recognition as they form, together with several more Rab27 residues, an extended hydrophobic cluster that contacts the SHD I of Slp2. Most of the Rab27-Slp2 interface involves the SHD I of Slp2 and interswitch and N-terminal regions of Rab27. The switch regions themselves though are not much involved in the interaction which might be the reason for interaction of granuphilin and JFC1 with GTP and GDP Rab27.

According to Fukuda [225] SHD containing effectors can be separated into a high affinity group (JFC1, Slp2, granuphilin, Slp5, Slac2-b, rabphilin, and Noc2) and a low affinity group (Slp3, melanophilin and MyRIP). Kinetic analysis by surface plasmon resonance was used to determine the equilibrium dissociation constant for three effectors, Slp2-a SHD (13.4 nM), granuphilin SHD (19.2 nM) and melanophilin (112 nM). Attribution of the other effectors to the high or low affinity groups was based on immunoblots. Therefore no biophysical data is available to support the classification. Different affinities of effectors for one Rab GTPase would be a way to enable sequential interaction of the different effectors with the same Rab GTPase and a hierarchy in Rab27 effectors would be one way to achieve this.

3.1.2. Mutagenesis and Griscelli Disease

Several missense mutations of Rab27 are found in Griscelli syndrome type II patients, namely W73G, L130P, and A152P. The L130P and A152P mutations disrupt GTP and GDP binding, and are thought to disrupt proper folding of Rab27. When the protein

contains either of these mutations, it will not interact with its effectors [225, 328]. Trp73 is part of the hydrophobic triad, and the W73G mutation presumably abolishes interactions with melanophilin, MyRIP, and Slp3-a. However, interactions of Rab27 (W73G) with other effectors such as JFC1 and granulophilin are not apparently affected by this mutation, at least when tested by GST pull down experiments [225].

Tyr8 of CDR I is conserved in Rab GTPases and has been reported to be important for the interaction of Rab27 with Slp2 [227] but does not seem to have any importance for the Rab27/melanophilin interaction. The interaction with Slp2 is mainly mediated by Met49, and in JFC1 the analogous residue is Leu79. Homology modeling of JFC1 carried in the course of this study suggests that the hydrophobic interaction might be even stronger. A Rab27 Y8A mutant and its thermodynamic investigation might shed light onto the importance of this residue for the interaction. If it is essential for the interaction with JFC1, the affinity would strongly diminish.

Some Rab27 effectors, amongst which is JFC1, have also been reported to bind to other Rab GTPases. Studies have revealed that the residues Leu84, Phe88 and Asp91 are specific for Rab27. When those residues were mutated to the analogous residues in Rab3 and Rab8 (L84I, F88Y and D91G) it appeared that the interaction between Rab27 and JFC1 was not affected, whereas Slp2 seemed to bind with less affinity and melanophilin did not bind at all [225]. These conclusions were made using immunoblotting techniques, which are not quantitative. Further analysis is needed in order to confirm that the triple mutant binds JFC1 with the same affinity as the wild type, especially because there is controversy about the affinities of JFC1 for Rab27 *vs.* Rab8 [256, 261]. Measuring the affinity of WT Rab27 and a triple mutant (L84I+F88Y+D91G) that resembles Rab8 may give more insight Rab/effector specificity.

It has also been reported that GDP-locked Rab27 (mutant T23N) retains binding to granuphilin [264]. Further complicating the issue is the observed binding of JFC1 Rab27 in the GDP form in vitro, but not to the GDP-locked T23N mutant of Rab27 [274]. It is possible that the WT Rab27 did contain some GTP and that the interaction with JFC1 was therefore detected. However, a Rab27 effector - Coronin 3 - that exclusively interacts with Rab27(GDP) has been reported as well [258]. This is contradictory to the commonly

accepted view of Rab GTPase specificity for effectors. Investigation of the thermodynamics involved in this mechanism would provide quantitative numbers for such interactions and enable better comparison of the interaction between Rab27(GTP) and Rab27(GDP).

3.1.3. Goals

No full length Rab effector structure is known so far. It would be a major step in the understanding of how effector proteins exert their biological function if we could visualize a complete Rab/effector complex. Because JFC1 has also been reported to have an ATP-binding site, possibly adopting a Bergerat-fold, and the three-dimensional structure would enable its visualisation. An analysis of the structure of the Rab27/JFC1 SHD is very likely to resemble the other two structures that have already been solved. However, the small differences in amino acid position or a different amino acid in one place can be very important for the interaction. Detecting those small differences and also a comparison to the unbound Rab27 forms, would doubtlessly add to the knowledge about specificity and affinity determinants for Rab/effector interactions, which is needed in order to understand the biology of vesicle trafficking.

Isothermal titration calorimetry is a technique that enables the determination of the equilibrium dissociation constant as well as determination of stoichiometry, enthalpy and entropy. It is therefore a powerful method to investigate the thermodynamics of protein-protein interactions and was hence the method of our choice for the investigation of the interaction of active and inactive Rab27 as well as several Rab27 mutants with the effector protein JFC1.

3.2. RESULTS

3.2.1. Production of a wild-type Rab27a expression plasmid

The Rab27a construct available in the laboratory (purchased from Geneart AG) had two mutated residues incorporated, namely Ser123 and Ser188, which are actually cysteine in the wild-type Rab27a sequence. Therefore the first step was to mutate these serines back to cysteine. This side directed mutagenesis was performed in two steps, firstly mutating Ser123 to cysteine and secondly, using the resulting plasmid as a template for the mutation of serine 188 back to cysteine. Once nucleotide sequencing confirmed that the Rab27a wild type sequence had been obtained, the protein was expressed and purified. Site directed mutagenesis methods are discussed in Section 2.2.3.

3.2.2. Rab27 – Expression and purification

WT Rab27a was expressed at 37°C (310 K) and purified as described in the sections 2.4.2., 2.5.1. and 2.5.2. For initial purification nickel affinity chromatography was performed, followed by cleavage of the His-Tag. A second Ni^{2+}-affinity column was then used to remove the His-Tag and proteins that co-purified during the first affinity chromatography step. Size exclusion chromatography was used to remove soluble aggregates and 'polish' the protein. Rab27a eluted at 90 ml from the Superdex 200 16/60 column and SDS-PAGE analysis, Figure 3.1.

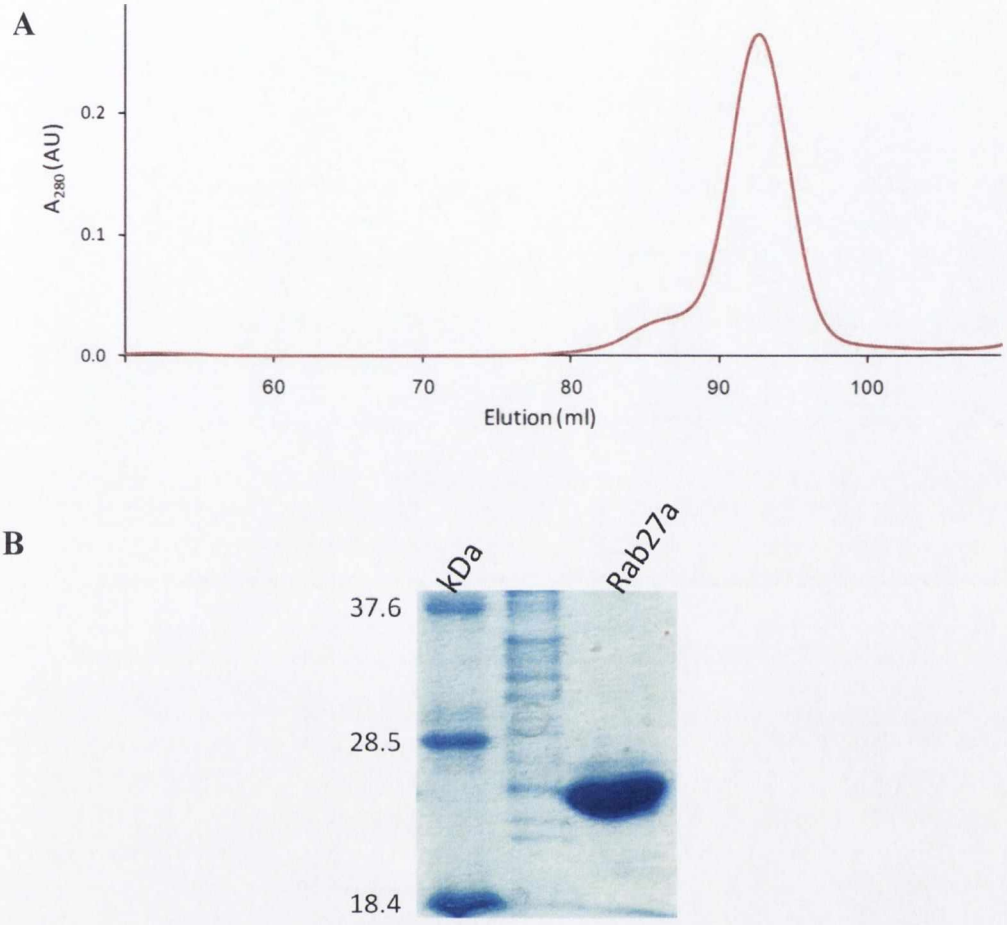

Figure 3.1 The purification of Rab27a.
Following cleavage of the 6xHis tag (Section 2.5.2) the Rab27a protein was loaded onto a Superdex-200 16/60 size exclusion column equilibrated with 100 mM NaCl, 5 mM $MgCl_2$, 1 mM DTT and 10 mM Tris-Cl, pH 7.5. The purity of the protein was checked at each step by analysing with SDS-PAGE. Panel A: Elution profile of Rab27a from a Superdex 200 column. Rab27 elutes at 90 ml. Panel B: 12% SDS-PAGE analysis of the elution peak of Rab27a. 10µl of the Rab27a peak fraction as eluted from the Superdex SX200 column were loaded. Molecular weight markers were from Jena.

3.2.3. Rab27a nucleotide exchange and HPLC analysis

Wild type Rab27a has a catalytic activity and hydrolyses GTP to GDP. Therefore the purified Rab27a would supposedly be in complex with no or only a very small amount of GTP. Depending on the required form of Rab27a (active or inactive), a nucleotide exchange with GppNHp (a non hydrolysable GTP analogue) or GDP was performed, as described in material and methods section 2.7. Analysis with High-Performance Liquid Chromatography (HPLC) was the method of choice to reveal how well the nucleotide exchange worked. In order to test the effectivity of the nucleotide exchange, the protein samples had to be denaturated by boiling, followed by removal of the protein debris from the solution by centrifugation. The supernatant then contained the nucleotide that had been bound to the protein before its denaturation. The column was equilibrated with HPLC running buffer (0.1 M KH_2PO_4, 5 mM tetrabutyl ammonium hydrogen sulfate, 8% acetonitrile, pH 6.5). Samples (containing 0.5-1 mg/ml protein in 100 mM NaCl, 5 mM $MgCl_2$, 1 mM DTT and 10 mM Tris-Cl, pH 7.5) and standards of GDP, GppNHp (containing 10 µM nucleotide in sample buffer) and GTP (5 µM in sample buffer) were prepared by incubating at 98°C (371 K) for 3 minutes followed by centrifugation at 13,000 rpm for 30 minutes. To 100 µl of supernatant 50 µl of HPLC buffer were added and 50 µl of this solution was injected onto the column, a run lasted 20 minutes with an isocratic mobile phase of HPLC buffer. The elution profiles of standards and nucleotide extracted from Rab27a are shown in Figure 3.3 A. GDP and GppNHp elute close to each other but the peaks are still distinguishable. The elution profile of GDP has one single peak at 6.8 minutes and GTP having a single peak at 9 minutes whereas GppNHp elutes in two peaks, the first at 6.2 minutes, and a second peak at 7.6 minutes. Reversed phase chromatography revealed that the nucleotide exchange was not 100% successful but most of the Rab27a had GppNHp bound and some still GDP (Figure 3.2 A). A test sample with non-exchanged Rab27a contained almost 100% GDP, therefore a nucleotide exchange with GDP was not essential when Rab27a with GDP bound was required.

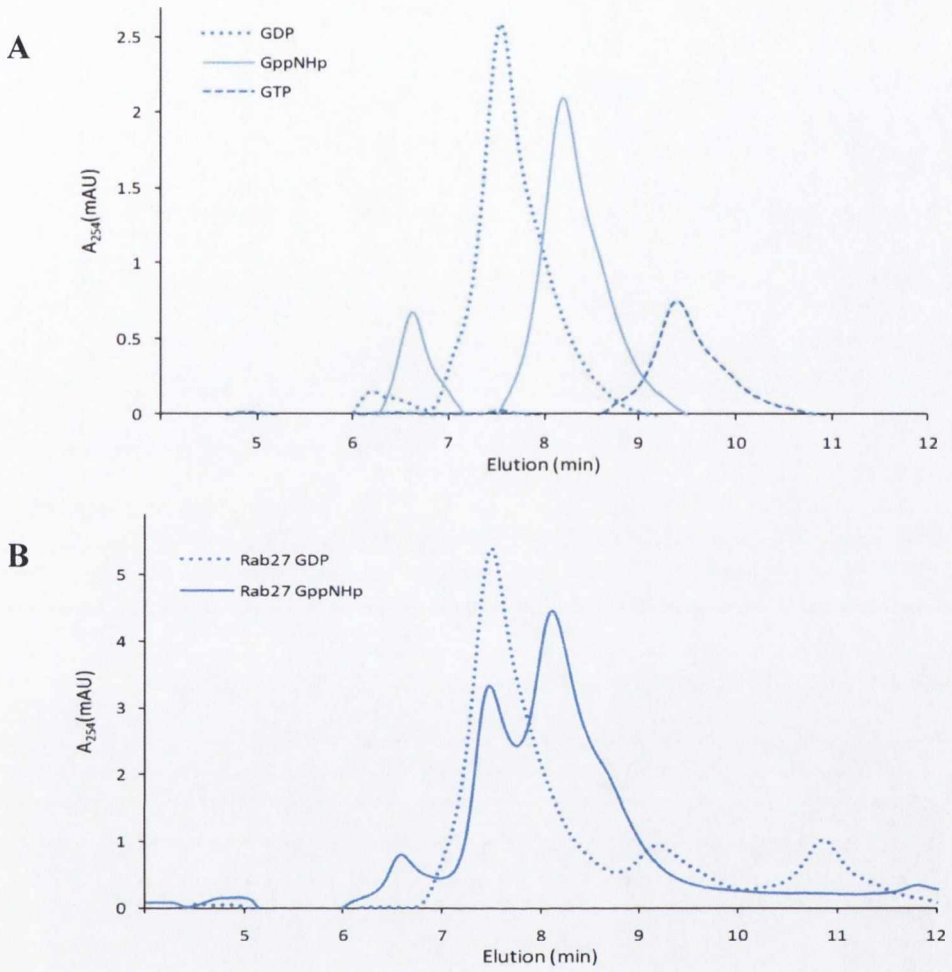

Figure 3.2 Rab27a nucleotide exchange and HPLC analysis.
Samples were loaded onto the C18 column as described in Section 3.1.3. Nucleotides were eluted with an isocratic flow of 0.1 M KH_2PO_4, 5 mM tetrabutyl ammonium hydrogen sulfate, 8% acetonitrile, pH 6.5.
Panel A: Elution profile of the different nucleotide standards from the C18 column. The absorbance was measured at 254 nm. GDP elutes after 6.8 minutes, GppNHp elutes with 2 peaks, one after 6.2 and one after 7.6 minutes and GTP elutes after 9 minutes. GDP and GppNHp were used at 10 µM, GTP at 5 µM.
Panel B: Example of elution profiles of nucleotides from Rab27 samples (absorbance at 254 nm). To obtain the Rab27-GDP form a nucleotide exchange was not necessary. To obtain Rab27 bound to mainly GppNHp a nucleotide exchange was necessary. Rab27 that has been nucleotide exchanged with GppNHp does still contain GDP.

3.2.4. Expression and purification of JFC1

A plasmid encoding Nus-tagged JFC1 had been produced in-house. It was expressed at 18°C (291 K) and purified as described in 2.4.2. 2.5.1. and 2.5.3. Briefly, an initial nickel affinity chromatography step was performed (Figure 3.3) followed by cleavage of the Nus-Tag over night. The protein solution was dialysed into a low salt buffer (10 mM NaCl, 5 mM $MgCl_2$, 1 mM DTT, 10 mM Tris-Cl, pH 7.5) and loaded onto an anion exchange column. The proteins were eluted from the column using a gradient up to 600 mM NaCl. The elution profiles shown in Figure 3.4 and Figure 3.5 reveal that JFC1 is easily separated from the Nus-tag by anion exchange chromatography, and both proteins run approximately at the expected sizes of 62 kDa for JFC1 and 57 kDa for the his tagged Nus.

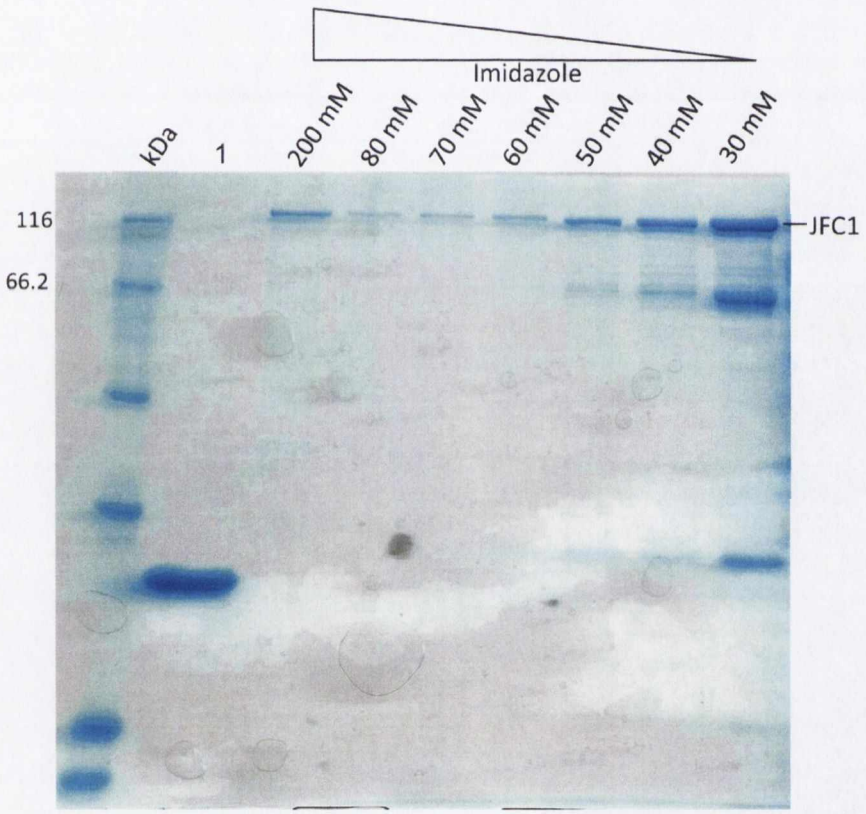

Figure 3.3 12% SDS-PAGE analysis of the elution of Nus-JFC1 from the nickel resin with a multiple step imidazole gradient.
The nickel resin was washed with 30 mM imidazole until no more protein could be detected in the flow through. Then this was repeated with the next higher concentration of 40 mM imidazole until a concentration of 80 mM imidazole was reached, then a last wash step was performed with 200 mM imidazole. JFC1 eluted at all imidazole concentrations. Lane 1 is unrelated to this project.

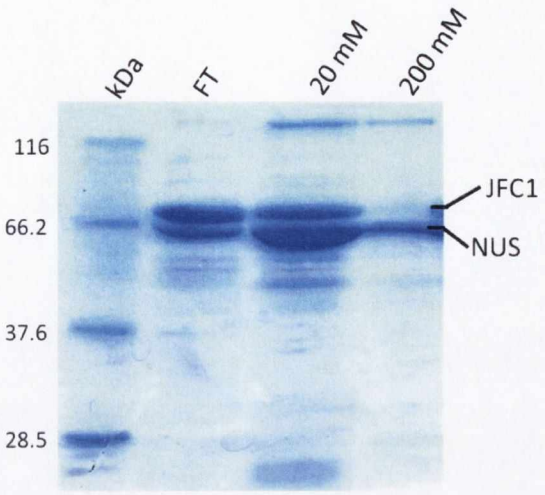

Figure 3.4 12% SDS-PAGE analysis of different fractions from a second nickel affinity step performed right after cleavage of the Nus-Tag.
The 61.9 kDa JFC1 and the 57 kDa Nus both do elute within the flow through (FT) and in a wash with 20 mM imidazole. A 200 mM imidazole wash contains only Nus.

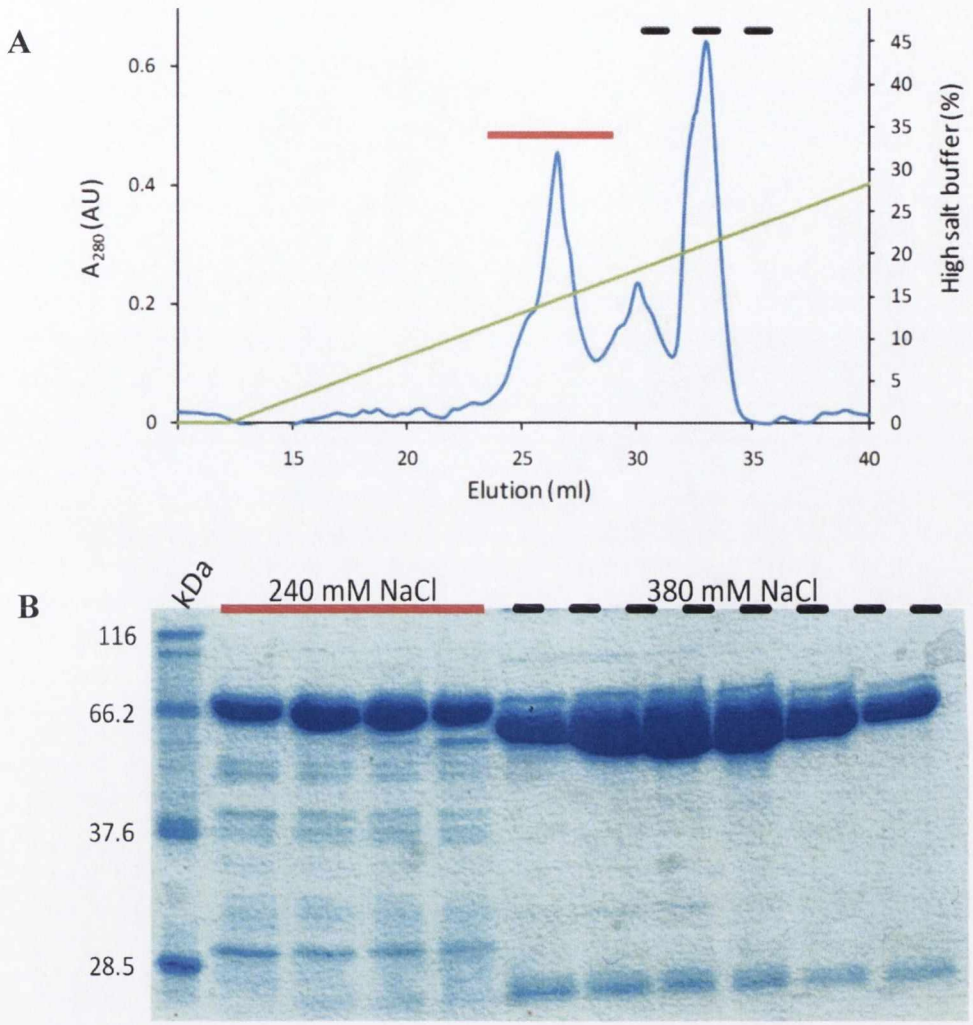

Figure 3.5 Separation of Nus and JFC1 by anion exchange.
Purified and rTEV cleaved Nus-JFC1 fusion protein was loaded onto a MonoQ 5/50 anion exchange column. Elution was performed with a linear salt gradient to 600 mM NaCl (30%) in 10 mM NaCl, 5 mM $MgCl_2$, 1 mM DTT, 10 mM Tris-Cl, pH 7.5. Panel A: Elution profile of JFC1 and the Nus tag from anion exchange. JFC1 elutes at 240 mM NaCl and Nus at 380 mM NaCl. Panel B: 12 % SDS-PAGE analysis of JFC1 and the Nus-Tag from anion exchange peaks.

After the anion exchange chromatography JFC1 is still relatively impure. In order to improve the purity a second nickel affinity chromatography step was introduced at this state in order to improve protein purity (Figure 3.6). After the second nickel affinity chromatography the protein was concentrated and a final size exclusion chromatography step was performed. Interestingly JFC1 eluted at different volumes from a Superdex 200 16/60 column. The first peak was observed eluting at 62 ml whereas the second peak eluted at 73 ml (Figure 3.7). For the following results it is assumed that the peak at 62 ml contained a dimeric form of JFC1 and the peak at 73 ml a monomeric form. After size exclusion chromatography JFC1 was relatively pure (Figure 3.8) and used for complex formation with Rab27a. The protein was also used for subsequent biophysical analysis.

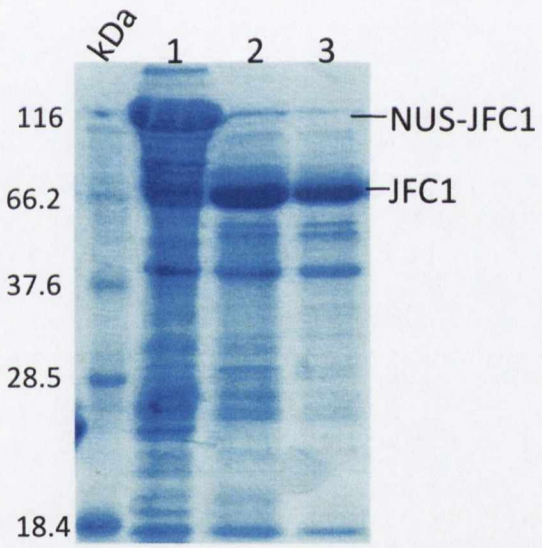

Figure 3.6 SDS-PAGE analysis of the different fractions obtained during the purification process of JFC1.
Lane 1 is from a first nickel affinity elution step. Lane 2 is from combined peak fractions from the anion exchange chromatography step outlined in section 2.5.3. Lane 3 is the flow through of the second nickel affinity step. The 2nd nickel affinity does improve the purity slightly.

3.2.5. Complex formation of Rab27 with JFC1

Rab27a that had been obtained as described above was then used to form a complex with its effector JFC1. For this purpose JFC1 was incubated with Rab27a at a ratio of 1 µM to 2 µM. This was necessary because the complex formation would not shift the elution peak of JFC1 sufficiently to allow separation of the complex from excess JFC1. Active (GppNHp-bound) Rab27a bound to the monomeric form of JFC1 but not the dimeric one (Figure 3.9). SDS-PAGE analysis revealed that the complex still contained some impurities (Figure 3.8) but it was decided to use it for crystallisation trials.

It was also detected that the inactive Rab27a(GDP) bound JFC1.

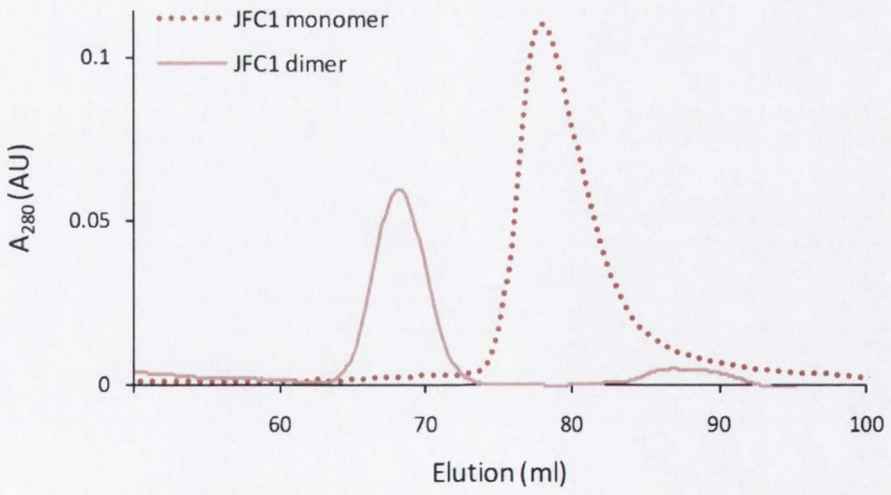

Figure 3.7 Different elution profiles of monomeric and dimeric JFC1.
Monomeric JFC1 elutes at 73 ml whereas dimeric JFC1 elutes at 62 ml.

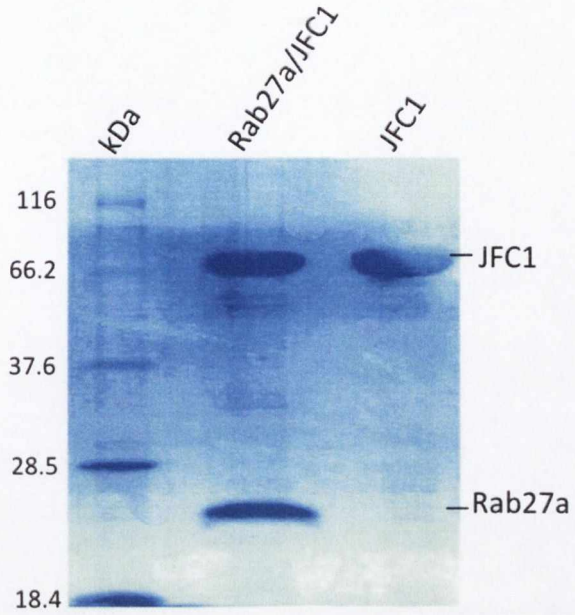

Figure 3.8 12% SDS-PAGE analysis of JFC1 and of the Rab27a-JFC1 complex after elution from the size exclusion column.
Most contaminants have been removed.

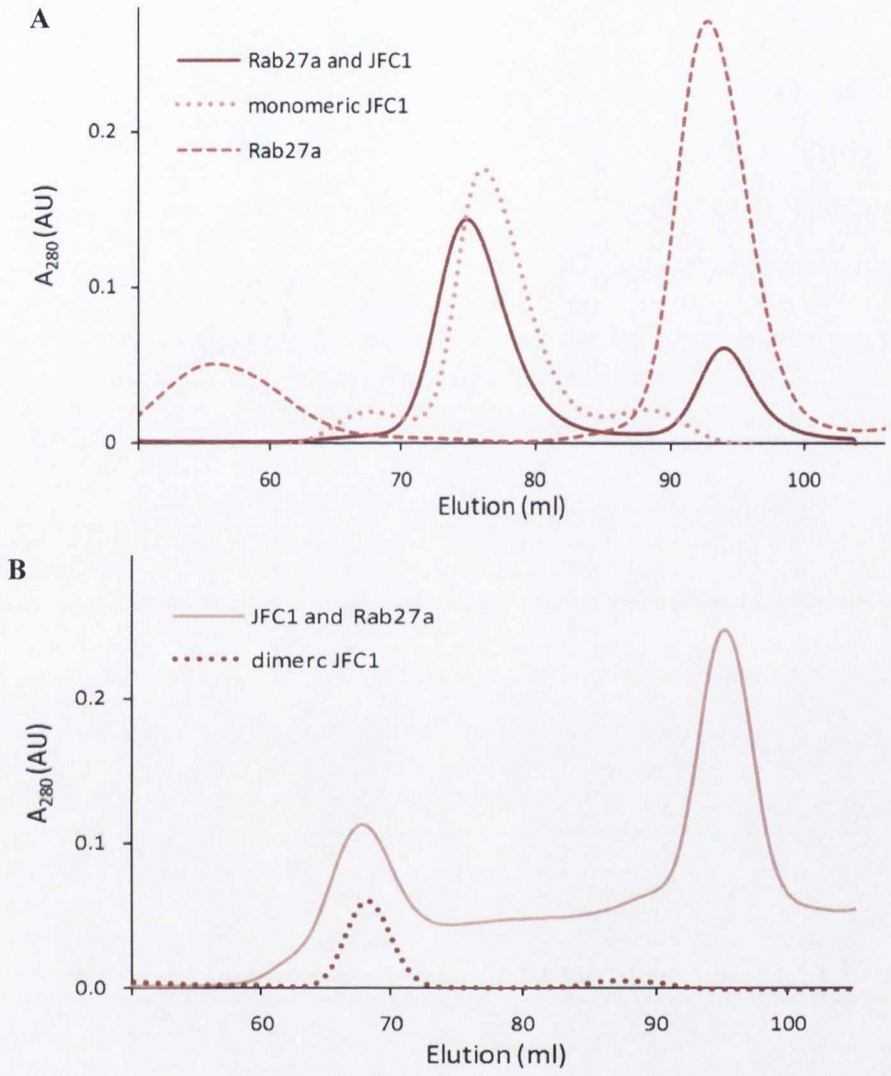

Figure 3.9 Complex formation of monomeric JFC1 with Rab27a.
Panel A: Complex formation of Rab27-GppNHp with JFC1. The complex elutes slightly faster (70 ml) than JFC1 alone (72 ml). Rab27 that is in excess and thus does not interact with JFC1 elutes at 90 ml. The elution profile of Rab27 alone (dashed line) does show soluble aggregates which elute at 48 ml.
Panel B: Elution profile of dimeric JFC1 with Rab27. Rab27 does not interact with JFC1, thus no peak shift is detected.

3.2.6. Crystallisation of JFC1 and Rab27(GppNHp)-JFC1

Purified Rab27a(GppNHP)/JFC1 complex as well as JFC1 and Rab27(GppNHp) were then used to set up initial crystallisation screens. For this purpose the proteins were concentrated up to 12 mg/ml. Because GppNHp absorbance, that has a maximum at 254 nm, interfered with the concentration determination at 280 nm, the concentration was determined with Bradford protein assay or BCA assay.

Several commercially available sparse matrix and grid screens were set up with concentrations of 12 mg/ml, 10 mg/ml, 8 mg/ml and 4 mg/ml for the protein complex and concentrations of 10 mg/ml and 5 mg/ml were used for JFC1 (section 2.9). No hits were observed for JFC1 or Rab27a(GppNHp). After six weeks crystals were observed for the Rab27a(GppNHp)-JFC1 complex in two conditions of the Structure Screen namely conditions E4 and E10 (Molecular Dimensions). Figure 3.10 shows the crystals obtained in condition E10 (0.01 M $NiCl_2$, 0.1 M Tris pH 8.5, 20% w/v PEG 2000 MME). These crystals have a rectangular shape and are approximately 10 - 20 µm in length. The crystals observed in condition E4 (0.2 M $MgCl_2$, 0.1 M Tris pH 8.5, 3.4 M 1,6-hexanediol) are similar to those presented in the picture, but much smaller and are difficult to photograph. Although large amounts of grid screens have been set up, these crystals have yet to be reproduced.

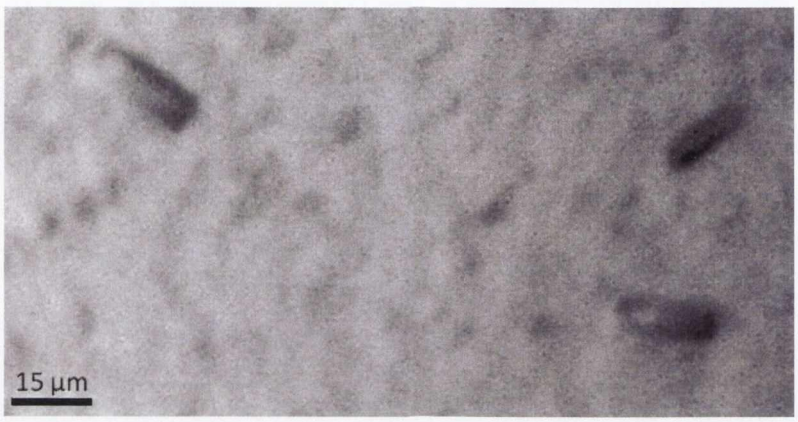

Figure 3.10 Rab27a/JFC1 crystals.
Crystals were obtained in the Molecular Dimensions E10 condition of the Structure Screen (0.01 M $NiCl_2$, 0.1 M Tris pH 8.5, 20% w/v PEG 2000 MME). Drops were set up with 8 mg/ml solution of the Rab27(GppNHp) JFC1 complex.

3.2.7. Homology modeling and mutagenesis of Rab27a

Mutants were designed on the basis of homology modeling of the JFC1-RBD complex which was created in silico using the structure of Slp2/Rab27a (Figure 3.11). With this model and through an extensive review of the literature, potentially functionally important residues were identified. The homology model revealed that Trp73 is placed in the centre of a large hydrophobic interface of Rab27 and JFC1. Thus it is likely that the loss of this residue does result in an effect on the interaction. Leu84, Phe88 and Asp91 are different residues in Rab3 and Rab8 (L84I, F88Y and D91G) and had been shown to be important for the specificity of the interaction of Rab27 with melanophilin. Phe8 is involved in hydrophobic stacking at a second interface (Figure 3.11) and seems to be important for the Rab27 – Slp2 interaction.

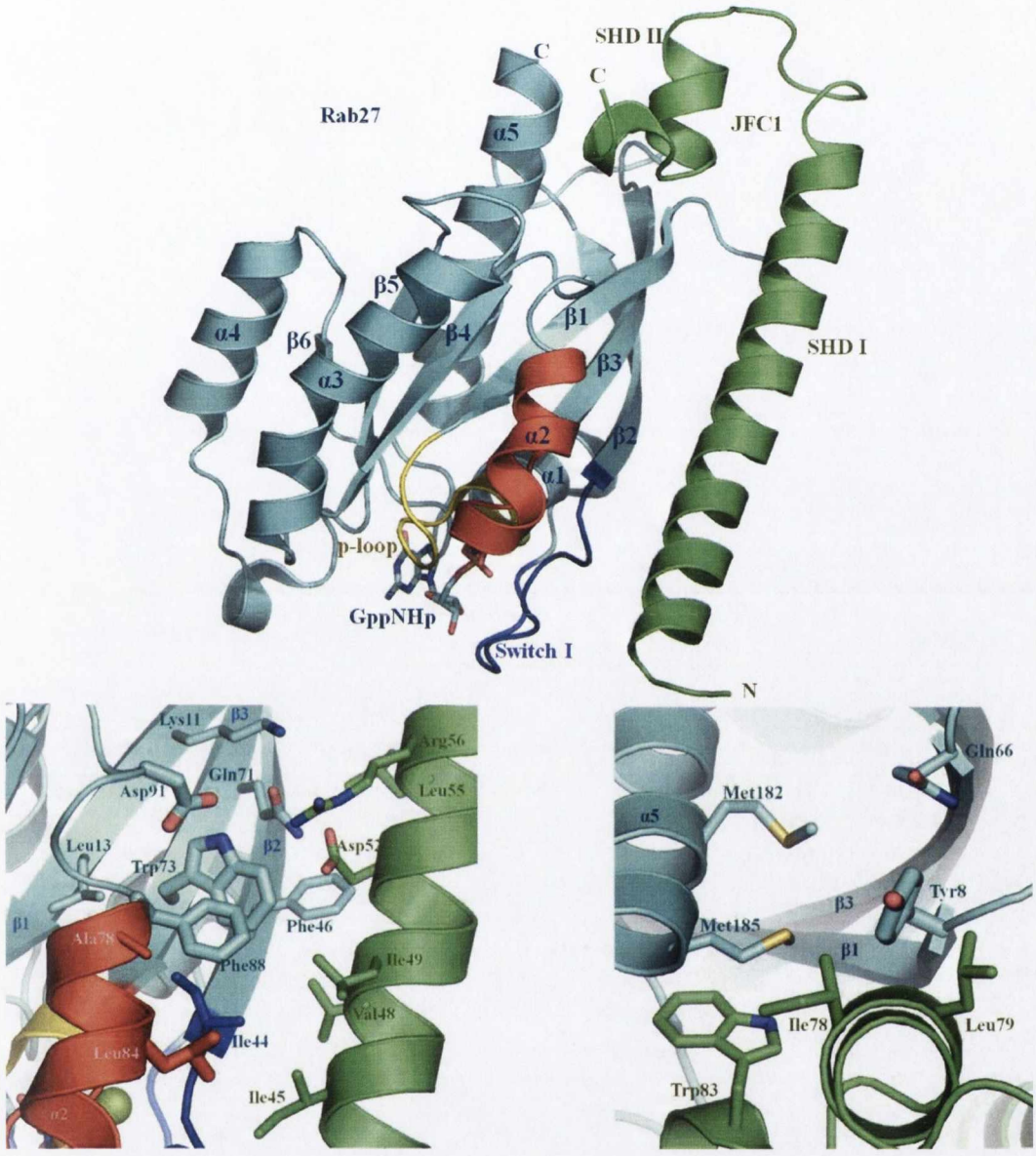

Figure 3.11 Homology model of JFC1 with Rab27.
JFC1 is shown in green and Rab27 in light blue with the p-loop in yellow, the switch I in dark blue, switch II in red, chosen residues and GppNHp as sticks and Mg^{2+} as a sphere. Sticks of residues chosen later for mutational analysis are slightly thicker than others. The model accounts for JFC1 residues 35-86. Panel A gives an overview of the binding interface of Rab27/JFC1 with the large SHD I helix and the smaller SHD II. Panel B shows residues present at the binding interface with SHD I that are important for the mutational analysis. Panel C shows residues present at the binding interface with SHD II, Tyr8 was chosen for mutational analysis later on.

It was decided to create the following Rab27a mutants: W73G and W73A, Y8A and a triple mutant with L84I+F88Y+D91G. Only W73A, Y8A and L84I+F88Y+D91G were successfully expressed and purified.

3.2.8. Biophysical characterization of the interaction between Rab27a and JFC1

3.2.3.1. Static light scattering

In order to find out about the nature of the complex formed, static light scattering was performed coupled to a size exclusion chromatography as described in Section 2.8.5. The mass of the eluted Rab27a/Nus-JFC1 complex was calculated to be 140,000 g/mol (140 kDa) (Figure 3.12).

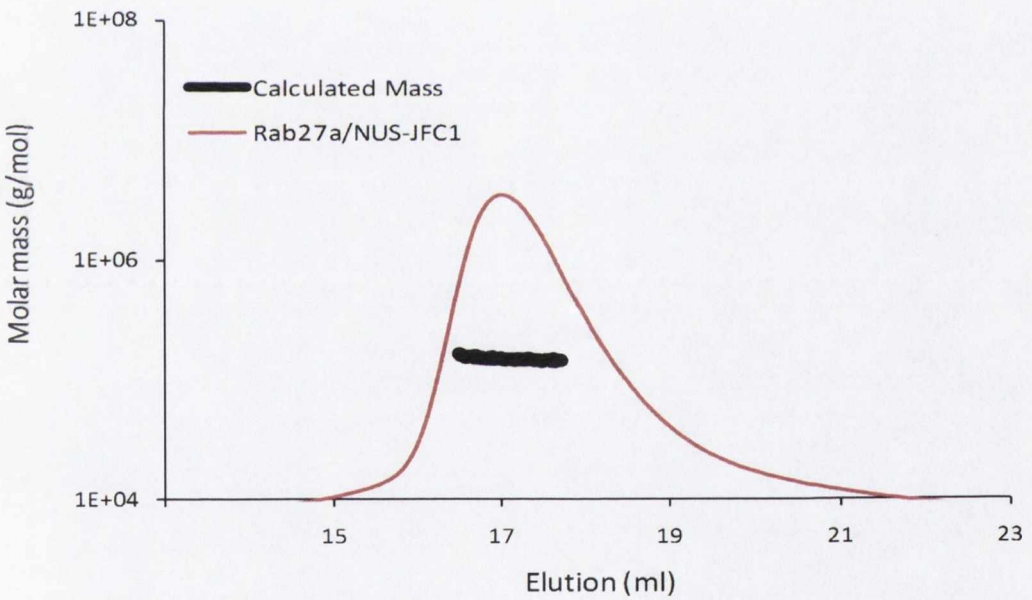

Figure 3.12 Static light scattering coupled to size exclusion chromatography of the Rab27a Nus-tagged JFC1 protein complex.
The molar mass of the elution peak from the size exclusion column is calculated to be 140 kDa. (See section 2.8.5.)

3.2.3.2. Thermodynamics of the Rab27a/JFC1 complex formation

Isothermal titration calorimetry was selected as a quantitative approach to determine the thermodynamic properties behind Rab27a and JFC1 complex formation. The following wild type Rab27a(GppNHp), Rab27a(GDP) and the selected mutants, Rab27a W73A (GppNHp), Rab27a Y8A(GppNHp) and finally the triple mutant Rab27a L84I+F88Y+D91G(GppNHp) were titrated into JFC1 or Nus tagged JFC1.

It is very important for correct results that the exact protein concentrations are known. Several methods were tested and the Bradford protein assay and the BCA assay were both tested and found to be consistent.

Examples of titration profiles are shown in Figure 3.13 to Figure 3.17 and values obtained from those titrations are presented in Table 1.3. WT Rab27a(GppNHp) binds JFC1 in the low nanomolar range, the average from two titrations was resulted in a Kd of 67 nM. WT Rab27a(GDP) did interact with JFC1 as well, and with a K_d of 46 nM the affinity was as high as that of WT Rab27a(GppNHp). Rab27a Y8A did reveal a K_d of 296 nM which is 5 times less than WT Rab27a. The K_d of Rab27a L84F+F88Y+D91G was 330 nM and thus about 6 times weaker than that of WT Rab27a. Mutating Rab27a Trp73 to Ala had the strongest effect on the interaction, resulting in a K_d of 613 nM which is more than eight times lower than that of WT Rab27a.

Table 3.1 ITC results from titrations with WT Rab27a(GppNHp), WT Rab27a(GDP) and Rab27a mutants.
The corresponding figures are given in brackets

Rab27	K_d (μM)	ΔH (kcal/mol)	ΔS (cal/mol/deg)	N
WT(GppNHp) (Figure 3.13 A)	0.097	-15.1	-19.5	1.1
WT(GppNHp) (Figure 3.13 B)	0.037	-11.9	-6.4	0.7
WTGDP) (Figure 3.14)	0.046	-19.1	-34.4	0.8
Y8A (Figure 3.15)	0.296	-14.3	-18.8	1.0
L84F+F88Y +D91G (Figure 3.16)	0.313	-27.7	-64.8	0.90
W73A (Figure 3.17)	0.613	-12.9	-15.7	1.2

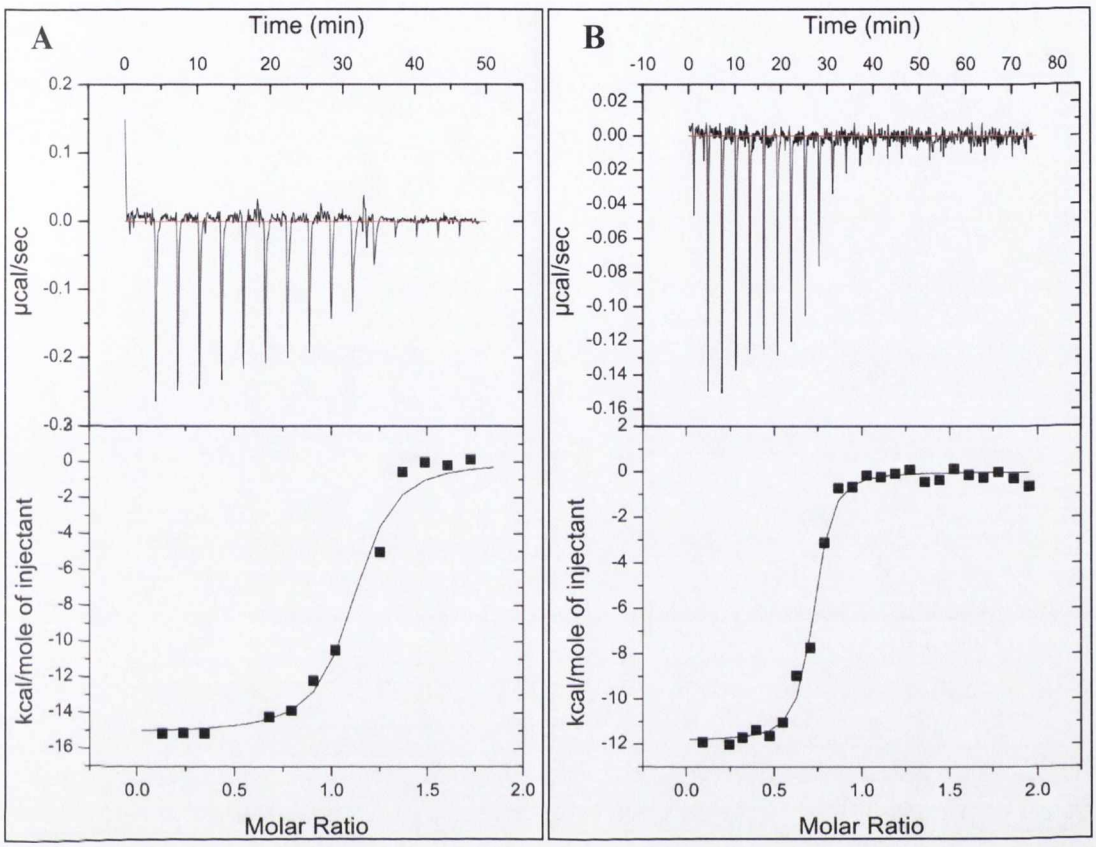

Figure 3.13 Titrations of WT Rab27a(GppNHp) into JFC1.
Panel A: Titration of 120 µM WT Rab27a(GppNHp) into 10 µM Nus-JFC1.
Panel B: Titration of 100 µM WT Rab27a(GppNHp) into 10 µM JFC1.

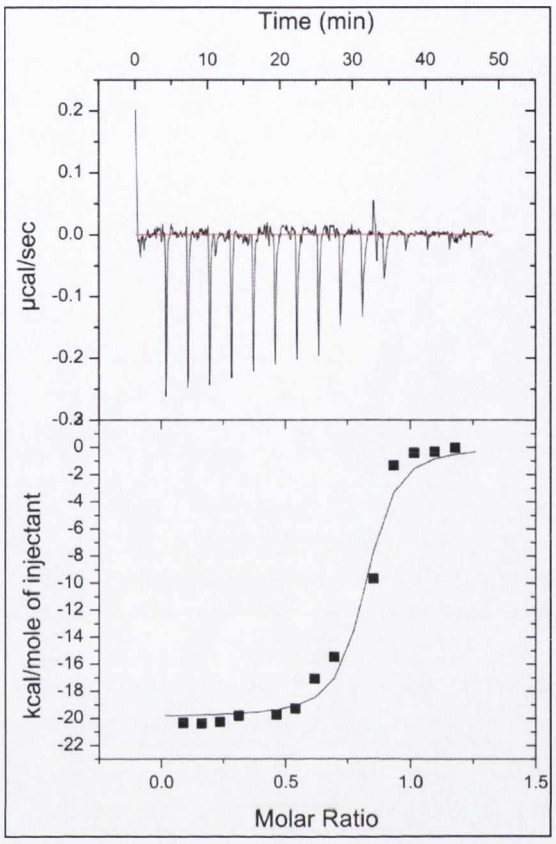

Figure 3.14 Titration of 90 µM WT Rab27a(GDP) into 11 µM Nus-JFC1.

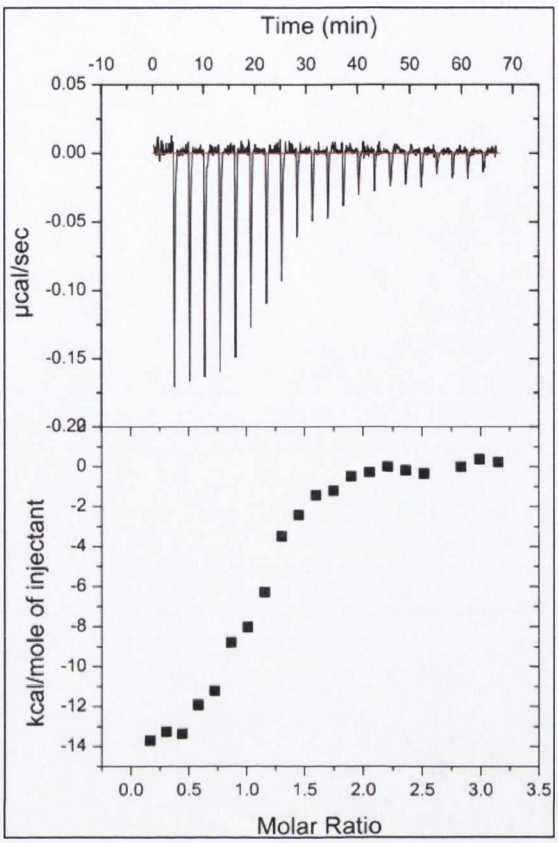

Figure 3.15 Titration of 95 µM Rab27a Y8A into 6 µM JFC1.

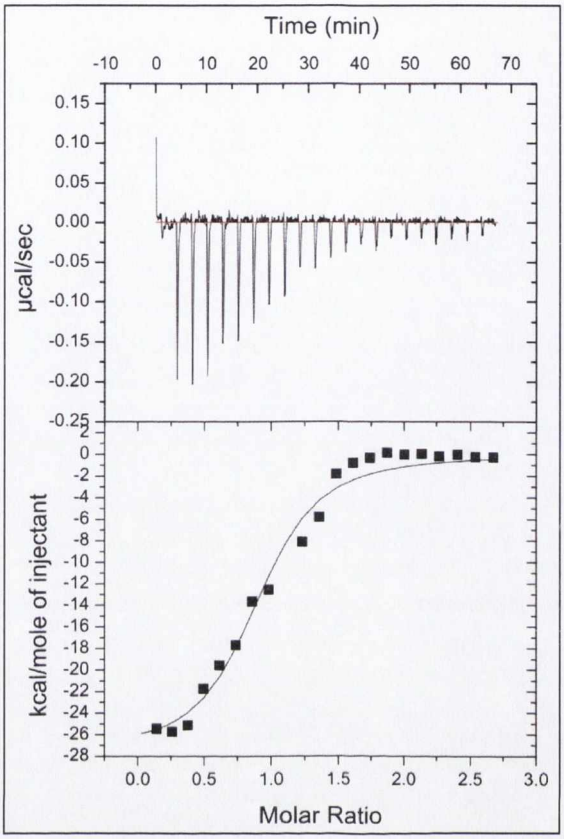

Figure 3.16 Titration of 65 µM Rab27a L84F+F88Y+D91G into 5 µM JFC1.

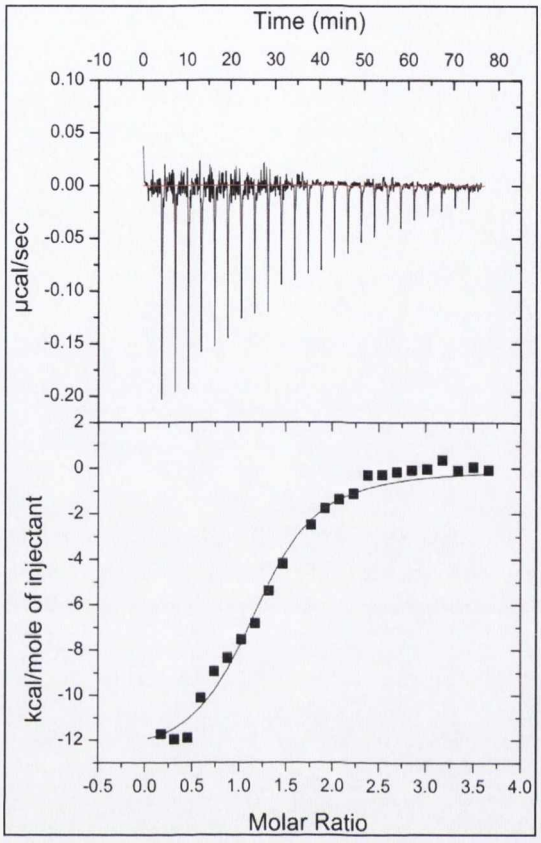

Figure 3.17 Titration of 108 µM Rab27a W73A into 6 µM JFC1.

3.3. Discussion

3.3.1. Rab27a expression and purification

The Rab27a construct that had been used for previous studies by our group contained two mutated residues: C123S and C188S. Those two cysteine residues can lead to the formation of a disulfide bond, as was observed in the crystal structure of Rab27a(GDP) [329]. This disulfide bond changes the conformation of the α3-β5 loop, which is involved in the effector recognition process. In order to obtain crystals of the Rab27b/Slp2 complex, the formation of the disulfide bond had to be prevented by mutating the involved cysteine residues to serine [227]. This construct was used in our group as well in order to improve crystals of a Rab27a/MyRIP complex. However it became clear that this did not improve the crystal formation of Rab27a/MyRIP. It was therefore decided to use a wild-type Rab27a for the Rab27a/JFC1 studies. After successfully mutating the Rab27a sequence back to the wild-type form, the protein was then expressed in order to be used for structural and thermodynamical studies.

Rab27a was expressed without its C-terminal region (expression of residues 1-193 out of 221), because this region is the flexible tail of the protein that anchors to the membrane with the geranylgeranyl groups. Most Rab GTPases that are not used for studies with REP or GDI are expressed without their C-terminal tail region, for example most Rab GTPase structures in the protein data bank do not contain this region. The purification of Rab27a proved to be straightforward with three consecutive purification steps. The elution volume of the 22 kDa protein from the size exclusion column was 90 ml which is the volume that would be expected for a monomeric protein this size (Figure 3.1 A). After the last step SDS-PAGE analysis of the concentrated protein reveals no detectable contaminants and can be used for crystallisation as well as thermodynamic assays (Figure 3.1 B).

In order to obtain the active or inactive form of Rab27a, a nucleotide exchange had to be performed. Because of the intrinsic hydrolysis activity of Rab GTPases, that would hydrolyse GTP to GDP, the GTP analogue GppNHp was chosen. GppNHp contains a nitrogen atom at the position of the oxygen atom that links the β to the γ phosphate of GTP. This disables hydrolysis of the γ phosphate and a GppNHp bound protein is therefore locked in the active state. After a nucleotide exchange Rab27a was mainly in the GppNHp

bound form, although some GDP was still present as well, and could be used to form a complex with an effector or for thermodynamical analysis of the active state. Rab27a that had been freshly purified was shown to contain no GTP and was thus in the inactive state. (Figure 3.2)

3.3.2. JFC1 expression and purification

The expression and purification of JFC1 proved to be more challenging. JFC1 was expressed with a Nus-tag. NusA is an *E.coli* protein that has been shown to greatly enhance the solubility of target insoluble proteins [330] and the construct used in this study contained an N-terminal hexa histidine-tag that enabled purification with affinity chromatography. The Nus-JFC1 purification showed to be very sensitive towards the amount of imidazole present in the used buffers. The standard protocol used for initial purification of a protein uses an extraction and wash buffer for the first nickel affinity step that contains 10 to 20 mM imidazole in order to prevent non-specific interactions between proteins and the nickel resin. It became apparent however that the imidazole at this level led to heavy bleeding of the protein from the nickel resin. This could be reduced when no imidazole was used in the buffers for extraction and wash steps. As the Nus-JFC1 seemed to bind weakly to the nickel resin, an imidazole gradient with several steps was performed in order to find out if it was possible to eliminate contaminants by eluting the protein from the column at a low imidazole concentration. For this purpose the column was washed with buffer that contained a certain amount of imidazole until no more protein was detected to elute. Elution fractions from each step were analysed by SDS-PAGE (Figure 3.3) which revealed that most Nus-JFC1 eluted at an imidazole concentration of 30 mM, along with a considerable amount of what seems to be cleaved JFC1. But even though the nickel resin was washed with each buffer until no more protein eluted, Nus-JFC1 eluted at higher imidazole concentrations. Therefore it was decided to elute the protein with a single step gradient of 200 mM imidazole. According to standard protocol the cleavage of the Nus-tag was followed by a second nickel affinity chromatography step. SDS-PAGE analysis of the elution fractions revealed, that the Nus-Tag was not retained efficiently by the nickel resin (Figure 3.4). Most of the Tag eluted with JFC1. It was thus decided to separate the JFC1 from its tag in another way. The theoretical isoelectric point of JFC1 is 5.32 whereas that of

Nus is 4.65. Therefore it was decided to try separating the two proteins by anion exchange chromatography prior to a second nickel affinity step. Following the Nus-tag cleavage, the protein solution was directly dialysed into a low salt buffer and loaded onto an anion exchange column. The elution profile shown in Figure 3.5 A reveals that the two proteins are easily separated by anion exchange, but SDS-PAGE reveals that JFC1 is still relatively impure. In order to improve the purity a second nickel affinity chromatography step was introduced at this state. The SDS-PAGE analysis of the flow through from a second nickel affinity step reveals that the purity can be slightly improved (Figure 3.6). The last purification step was size exclusion chromatography. The 62 kDa, full length JFC1 would be expected to elute at 73 ml and an elution at 62 ml corresponds to approximately double the molecular weight of JFC1 (Figure 3.7). Hence the two elution peaks represent two different species of protein, possibly one monomeric and one dimeric. The buffers used for all purifications were the same but a test showed that the dimeric form of JFC1 seemed to occur after freezing of the bacterial pellet prior to extraction of the protein and when the pellet was very large and the resolubilised pellet was very concentrated in the extraction buffer. It is likely that the dimerisation of JFC1 is due to misfolding caused by freezing and/or sonication. However this last step further enhanced the JFC1 purity; although contaminant proteins are still present (Figure 3.8). From four litres of bacterial culture usually 1-2 mg of pure protein could be obtained. Because of the low yield it was decided to use the protein for further experiments, as introducing further purification steps would decrease the yield even further.

3.3.3. Formation of a Rab27a/JFC1 complex

After successful purification of Rab27a and JFC1 the Rab27a/JFC1 complex was formed. When the complex formation was attempted with monomeric JFC1, the complex was formed with the GppNHp- and the GDP-bound form of Rab27a (Figure 3.9 A). This shows that JFC1 does indeed interact with both forms of Rab27, active and inactive. It had previously been shown that the inactive mutant (T23N) does not bind JFC1 [264] but another study shows that the GDP-bound wild-type does [274]. Our result confirms this latter finding. This is especially interesting because Rab GTPases with mutations of the

analogous residue are commonly used to prove that an effector protein does not interact with the GDP-bound Rab GTPase. Ideally it would have to be confirmed that a Rab27 T23N does not interact with JFC1 when both proteins are prepared the same manner as presented here. An explanation for this could be the fact that the threonine to asparagines mutation causes a disrupted Mg^{2+} binding site resulting in reduced affinity for guanine nucleotides [42]. Alternatively, Thr23 may directly interact with the effector JFC1. GppNHp-bound Rab27a bound to the monomeric form of JFC1, but not the dimeric one (Figure 3.9 B), which also hints at the fact that the dimeric form might have its Rab-binding region involved in the dimerisation , or that it is mis-folded. SDS-PAGE analysis of the complex reveals that the contaminants present in JFC1 are also present in the purified complex (Figure 3.8). Because of the low yield it was attempted to crystallise a Rab27a(GppNHp)/JFC1 complex without further improving the purification.

3.3.4. Crystallisation of Rab27a/JFC1

It was possible to obtain crystals in two conditions that are slightly different; they both contain the same buffer and low molecular alcohols and different salts. The condition yielding the crystals shown in Figure 3.10 contains 0.01 M $NiCl_2$ which is a very low salt concentration. It is still possible that salt crystals have been formed, but the fact that similar crystals were found in a similar condition as well as the difficulties to reproduce the crystals suggest that they are actually protein crystals. Until now the small crystals could not be harvested and shipped to a synchrotron in order to check for diffraction and ideally collect a native data set.

3.3.5. Static light scatterning

Static light scattering of the Rab27a/Nus-JFC1 revealed a molar mass of 147,000 g/mol (147 kDa) which roughly corresponds to the expected molecular mass of a monomer of the complex (i.e. 141 kDa; Figure 3.12). It can therefore be concluded that the complex formed by Rab27a and Nus-JFC1 is a 1:1 complex.

3.3.6. Thermodynamic analysis of the Rab27a – JFC1 interaction

The aim of this study was not only to crystallise the Rab27a-JFC1 complex, but also to characterise the interaction thermodynamically using active and inactive Rab27a and Rab27a mutants. Since Rab27 had been reported to recruit effectors in its active and inactive form, and we had observed this as well, we attempted to see if there was a difference in the affinities of JFC1 for active and inactive Rab27. From two titrations with Rab27(GppNHp) into JFC1 two different values were obtained for the K_d, 97 nM and 37 nM (Table 3.1, Figure 3.13). The values for all other parameters also differ from each other. The stoichiometry (N) obtained from isothermal titration calorimetry is a good indicator if the values obtained are precise. Since we had determined the Rab27a/JFC1 complex to have a 1:1 stoichiometry N should ideally be 1. If the protein concentration provided is not correct, this has an impact on determination of all values and an incorrect value for the stoichiometry can be an indicator for this. One reason for the different values of the dissociation constant could be caused by the fact that JFC1 contained some contaminants, and thus the real concentration of JFC1 was in reality lower than determined. Another problem was the low signal to noise ratio, caused by the low protein concentration used. Fluctuations of the baseline thus had more impact on the value obtained from integration of the peaks and might have caused the differences. Although the signal to noise ratio was higher than ideally should be the case, it was still within a reasonable range, and therefore repeating the titration with purer protein would possibly improve the accuracy. For this purpose more purification steps would have to be introduced, which would require a larger expression volume. Even though the values for the experiment are not a perfect match, it can still be shown that the affinity is in within the low nanomolar range.

The K_d of Rab27(GDP)/JFC1 was determined to be 46 nM. This is within the same low nanomolar range as for Rab27(GppNHp)/JFC1. In order to obtain a more reliable value the titration will have to be repeated several times, but the result obtained hints strongly at the fact, that the affinity of JFC1 for active and inactive Rab27a is approximately the same. Improving the nucleotide exchange procedure for obtaining Rab27(GppNHp) might lead to a slightly stronger affinity of Rab27(GppNHp)/JFC1.

The first mutant chosen was Rab27a Y8A. Tyr8 is positioned in the CDR I of Rab27a and has been reported to be important for the interaction of Rab27a with Slp2 [227]. The homology model shows that it is involved in hydrophobic interaction with Ile78 and Leu79 of JFC1 and also Met185 of Rab27a (Figure 3.11). This hydrophobic interaction pattern is lost when the residue is mutated, but the position is not within the mayor interface and thus does not disturb other interactions. We expected a reduced affinity. Indeed the K_d of 296 nM obtained from one titration indicates that the affinity is at least three times lower compared to the affinities obtained for wild-type Rab27a. The hydrophobic interactions involving Tyr8 are not necessary for the interaction to take place, but they may contribute significantly to the overall interaction.

JFC1 had been reported to bind Rab8 addition to Rab27 with some controversy about which interaction is stronger [256, 261]. It has previously been shown that Rab27 L84I, F88Y and D91G are important for the specificity of Rab27 versus Rab3/Rab8. The homology model revealed that the residues are part of the main interaction surface (Figure 3.11). L84I and F88Y do not present big changes, the residues stay hydrophobic and only the space occupied by them slightly changes. Asp91 has a negative charge and is in proximity to JFC1 Arg56 and Asp52. It is highly possible that these residues do contact each other by means of hydrogen bonds *via* a water molecule as is the case in the Rab27a/Slp2 structure. Mutating Asp91 to glycine would prevent hydrogen bonding and therefore lead to a loss in affinity. Therefore we expected a decrease in affinity of JFC1 for the mutant. Indeed the titration of Rab27a L84I+F88Y+D91G into JFC1 affirmed this assumption, giving a K_d of 313 nM, but since this value is derived from one titration, more titrations are needed in order to confirm it. The individual contributions to the binding affinity would require single mutagenesis and subsequent binding studies.

Rab27a W73G that is found in patients with the Griscelli syndrome type II. The mutated protein does abolish the interaction with several effectors (melanophilin, MyRIP and Slp3) but seems to bind to the other Rab27 effectors [225]. A comparison between the structures of Rab27/melanophilin and Rab27/Slp2 does not reveal a reason why the mutation should have a fatal effect on the interaction with melanophilin but not Slp2. Because JFC1 had been shown to bind the Rab27 W73G mutant beforehand, we

hypothesised that the binding would still take place but that the impact on the affinity would be considerable. Currently, we have only been able to produce a W73A mutant. The homology model revealed that this mutant is very likely to have the same effect as W73G, and if anything, the glycine mutation would be more severe. When the tryptophan is changed to alanine the hydrophobic surface at the middle of the protein-protein interface is lost the same as when the residue is mutated to glycine. Isothermal titration calorimetry revealed that the interaction affinity was indeed much reduced compared to the wild-type Rab27. The K_d came to 613 nM and is thus closer to the low micromolar range.

Chapter 4

Structural analysis of the Rab GTPase Ypt32

4.1 Introduction and goals

The yeast Rab GTPases Ypt31/32 are involved in the formation of vesicles from the Trans Golgi, where they recruit the effector Sec2 (which also acts as a Sec4 GEF) as well as the myosin V motor protein Myo2 [289-290] [285]. Sec2 binding sites for the two functionally distinct Rabs, Ypt31/32 and Sec4, are situated on distinct segments of a coiled-coil region of Sec2 [190]. The subsequently recruited Sec4 also binds to Myo2. The affinities of Sec4 and Ypt32 for Myo2 were determined using surface plasmon resonance which revealed that Sec4 has a modestly greater affinity for Myo2 than Ypt32. Both affinities were in the low micromolar range, and it was observed that Myo2 contains overlapping binding sites for Ypt31/32 and Sec4.

In summary, Ypt31/32 and Sec4 have distinct functions in vesicle trafficking, but they bind to common interacting proteins, including the effector Myo2. Excluding the prenylated tails, Ypt32 and Sec4 share 48% identities (68% homology) in their globular domains (Figure 4.1). Although Ypt31 has been crystallised in complex with GDI, the structure of uncomplexed Ypt31/32 has not been determined. Here, the structures of Ypt32(GDP) and Ypt32(GTP) are presented. Active Ypt31 and Sec4 are compared and their switch I and II regions are analysed in order to understand the molecular basis for their distinct functions in the transport of exocytic vesicles. In addition, the structures are compared to the complex Ypt31/GDI, which represents the conformation of Ypt31(GDP) following membrane extraction. Analyses of the inactive and active structures are presented here seamlessly, but it is important to emphasise that my specific role was the expression, purification, crystallisation and structure determination of Ypt32(GTP). The work involving inactive Ypt32(GDP) was performed by Dr. Azmiri Sultana, and the functional analyses of the proteins was a collaboration with the laboratory of Prof. Lois Weisman (University of Michigan).

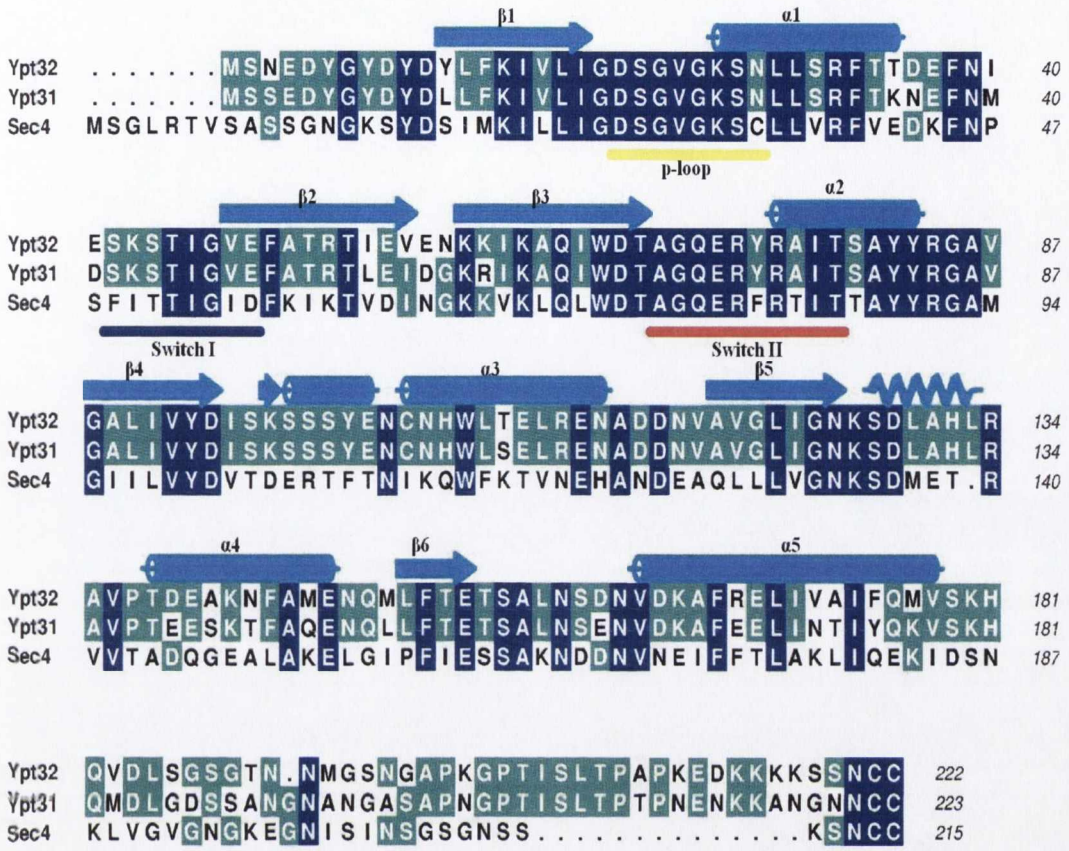

Figure 4.1 Sequence alignment of Ypt32, Ypt31 and Sec4.
Conserved residues are shown in dark blue when conserved in all sequences and light blue when conserved in two sequences. The secondary structure elements are as found in the Ypt32(GppNHp) structure and the p-loop and switch regions are underlined.

4.2 Results

4.2.1 Ypt32 – Expression and purification

Ypt32 was expressed and purified as described in section 2.5.6. The first purification step was affinity chromatography with amylose resin, followed by cleavage of the MBP-Tag overnight. SDS-PAGE analysis of the elution fraction from the amylose resin shows that the cleaved MBP-Tag is present as well (Figure 4.2). After the Tag-cleavage the protein solution was dialysed into a low salt buffer (10 mM NaCl, 5 mM $MgCl_2$, 1 mM DTT, 10 mM Tris-Cl, pH 8) and then anion exchange chromatography was performed. MBP eluted from the column at 120 mM NaCl and Ypt32 at 230 mM NaCl. As can be observed in Figure 4.3 A, the peaks are close together and SDS-PAGE analysis reveals that a small amount of MBP is still present in the Ypt32 elution fraction (Figure 4.3 B). The Ypt32 elution peak fraction was then injected into a pre-equilibrated size exclusion column and eluted at 92 ml which is the expected elution volume for the 20.5 kDa protein. SDS-PAGE analysis revealed that the MBP had been eliminated and no contaminants could be detected (Figure 4.4).

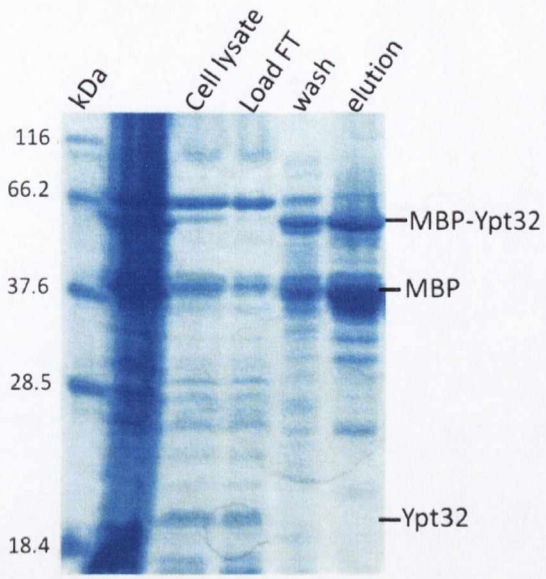

Figure 4.2 SDS-PAGE analysis of the amylose affinity chromatography step.
A part of the MBP-Ypt32 fusion protein is found in the flow through (FT) when the column is loaded with the bacterial cell lysate. Some more detaches from the column during the wash step. The eluted fraction contains MBP-Ypt32 but also a large amount of MBP. Only a small amount of cleaved Ypt32 is detected throughout the affinity chromatography.

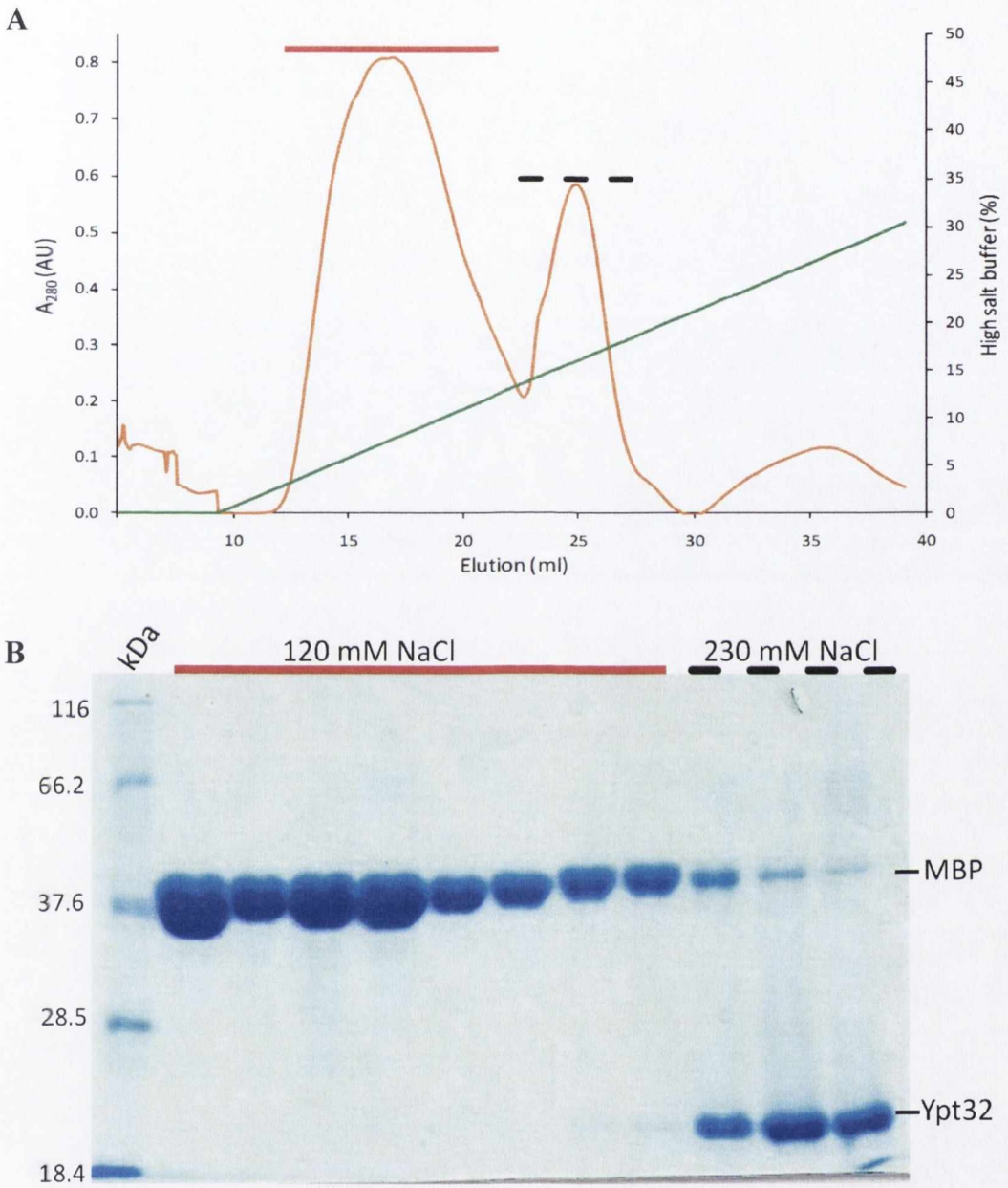

Figure 4.3 Elution of MBP and Ypt32 from anion exchange chromatography.
Panel A: During a gradient with high salt buffer up to 1M NaCl (100% high salt) in 5 mM $MgCl_2$, 1 mM DTT, 10 mM Tris-Cl, pH 8, MBP elutes at 120 mM NaCl and Ypt32 at 230 mM NaCl. The two protein peaks are close together.
Panel B: SDS-PAGE analysis of the elution peaks presented in panel A. The first peak can be identified as MBP and the second peak fraction contains mainly Ypt32 as well as some MBP.

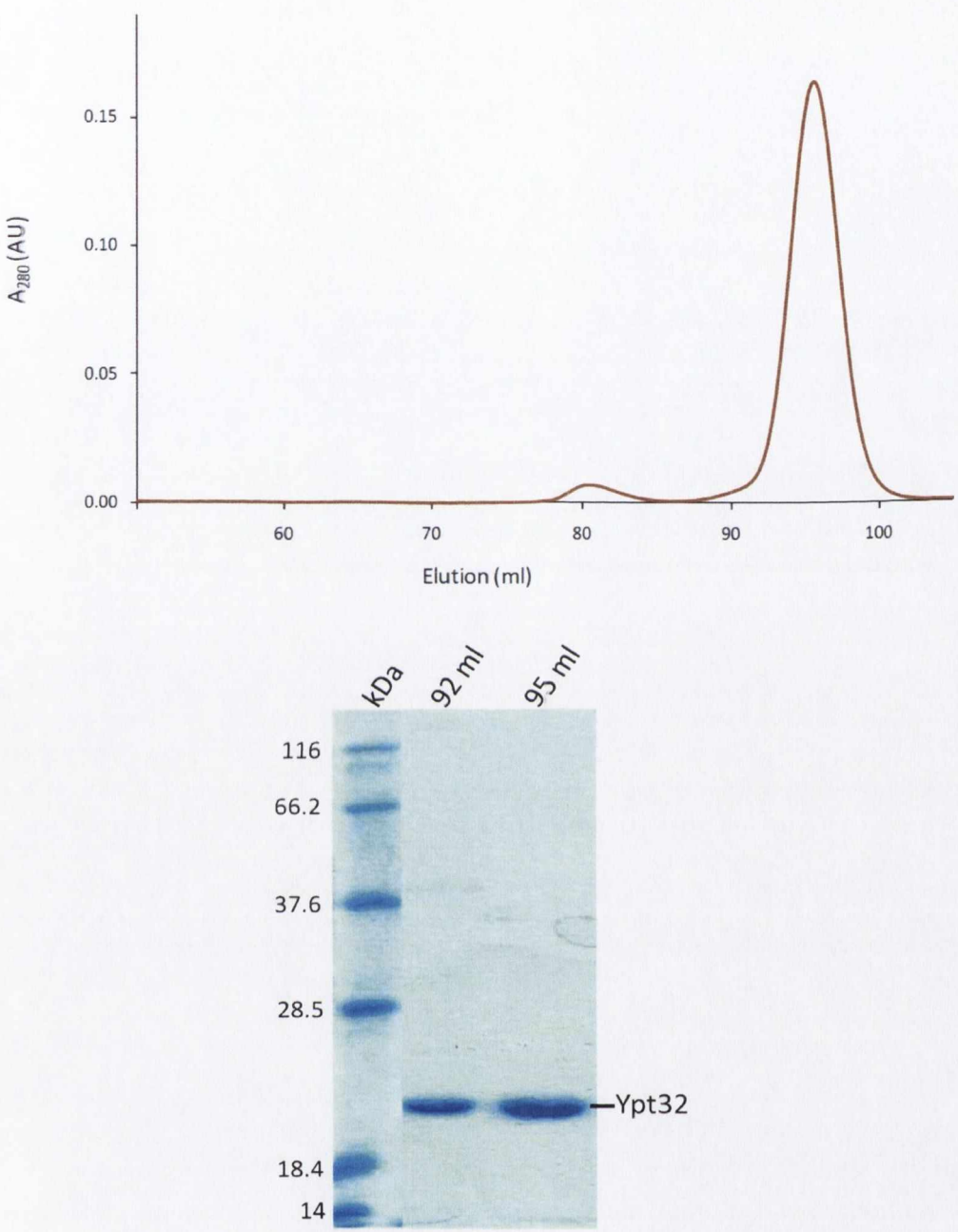

Figure 4.4 Size exclusion chromatography of Ypt32.
Panel A: Elution profile of Ypt32 from the size exclusion column. Ypt32 elutes at 92 ml.
Panel B: SDS-PAGE analysis of size exclusion peak fractions. No contaminants can be detected.

4.2.2 Crystallisation of Ypt32(GppNHp)

Purified Ypt32 was incubated on ice with a tenfold excess of GppNHp for 30 minutes and then subjected to crystallisation trials. Several initial crystals were found in two conditions, 0.2 M $MgCl_2$, 0.1 M HEPES pH 7.0, 20 % w/v PEG 6000 and 0.2 M $MgCl_2$, 0.1 M MES pH 6.0 20 % w/v PEG 6000 (Figure 4.5 A). Optimisation of these resulted in small rod-like shaped crystals (in 0.2 M $MgCl_2$, 0.1 M MES pH 6 and 20 % w/v PEG 6000; Figure 4.5 B) as well as bigger diamond shaped crystals (in 0.2 M $MgCl_2$, 0.1 M HEPES pH 7 and 15 % w/v PEG 6000 + streak seeding; Figure 4.5 C). One diamond shaped crystal was used for structure determination of GppNHp bound Ypt32.

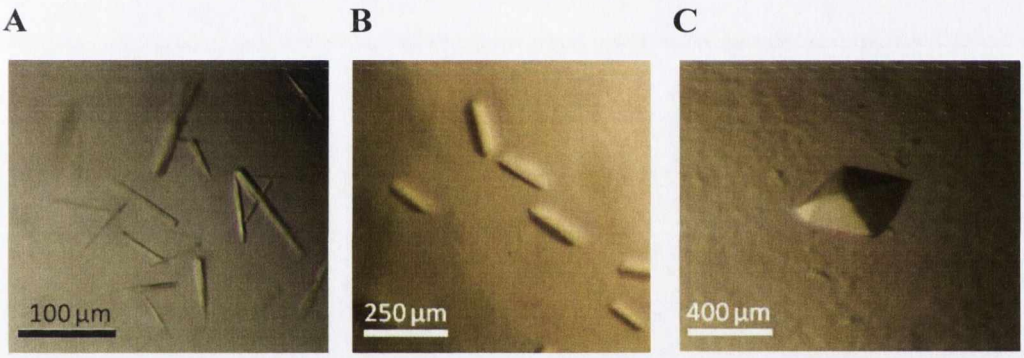

Figure 4.5 GppNHp-Ypt32 crystals.
Panel A: Initial crystals (0.2 M $MgCl_2$, 0.1 M MES pH 6.0 20 % w/v PEG 6000)
Panel B: Optimised crystals (0.2 M $MgCl_2$, 0.1 M MES pH 6 and 20 % w/v PEG 6000)
Panel C: Optimised crystal obtained with seeding, used for data collection (in 0.2 M $MgCl_2$, 0.1 M HEPES pH 7 and 15 % w/v PEG 6000 + streak seeding)

4.2.3 Data collection and structure determination of Ypt32(GppNHp)

The crystal diffracted X-rays to 2.0 Å resolution on beamline BM14 at ESRF. It belongs to the orthorhombic spacegroup $P2_12_12_1$ with one molecule in the asymmetric unit and the following unit cell parameters: a = 47.09 Å, b = 49.89 Å, c = 90.66 Å and $\alpha = \beta = \gamma = 90°C$. A summary of the data collection and refinement statics is given in Table 4.1.

Table 4.1 Data collection and refinement statistics.	
Data Collection	
Beamline	BM14
Wavelength (Å)	0.9784
Space group a, b, c (Å); α β γ	$P2_12_12_1$ 47.09, 49.89, 90.66; 90°
R_{sym} (%)	6.9 (44.6)
Molecules in Asymmetric unit	1
I/SigI	23.57 (4.24)
No. of observations	106280 (14395)
No. of unique reflections	14958 (1991)
Completeness (%)	99.6 (100)
Multiplicity	7.1 (7.2)
Wilson B factor (Å^2)	17.2
Refinement	
Resolution (Å)	45.33-2.0
R_{work} (%)	19.4
R_{free} (%)	24.0
Number of amino acids (in the ASU)	179
Number of atoms (in the ASU)	
Protein	1458
Ligand	66
Metal ions (Mg)	1
Water	192
B factor (Å^2)	
Protein overall	16.11
Protein main chains	15.36
Protein side chains	16.85
Ligand	21.88
Metal ions (Mg)	27.07
Solvent	22.07
Deviations from ideals (r.m.s.d.)	
Bond length (Å)	0.010
Bond angle (°)	2.014
Ramachandran plot (%)	
Most favoured region	93.4
Additional allowed region	6.6
Generously allowed region	0.0
Disallowed region	0.0
Values in brackets are for the highest resolution shell (2.0-2.1 Å)	

4.2.4 The structure of Ypt32(GppNHp)

The final model of Ypt32 with GppNHp was refined using data to 2.0 Å and data has been deposited at the protein data bank, PDB ID 3RWM [321]. The overall structure of Ypt32-GppNHp resembles that of other Ras related GTPases (Figure 4.6): five parallel and one antiparallel β-strands, framed by five α-helices. The nucleotide GppNHp was well defined by the electron density in the binding pocket (Figure 4.7), only the side chains of residues Tyr75 and Arg76 in the α-2 helix adjacent to switch II were disordered but the main chain was clearly defined in electron density maps (Figure 4.8).

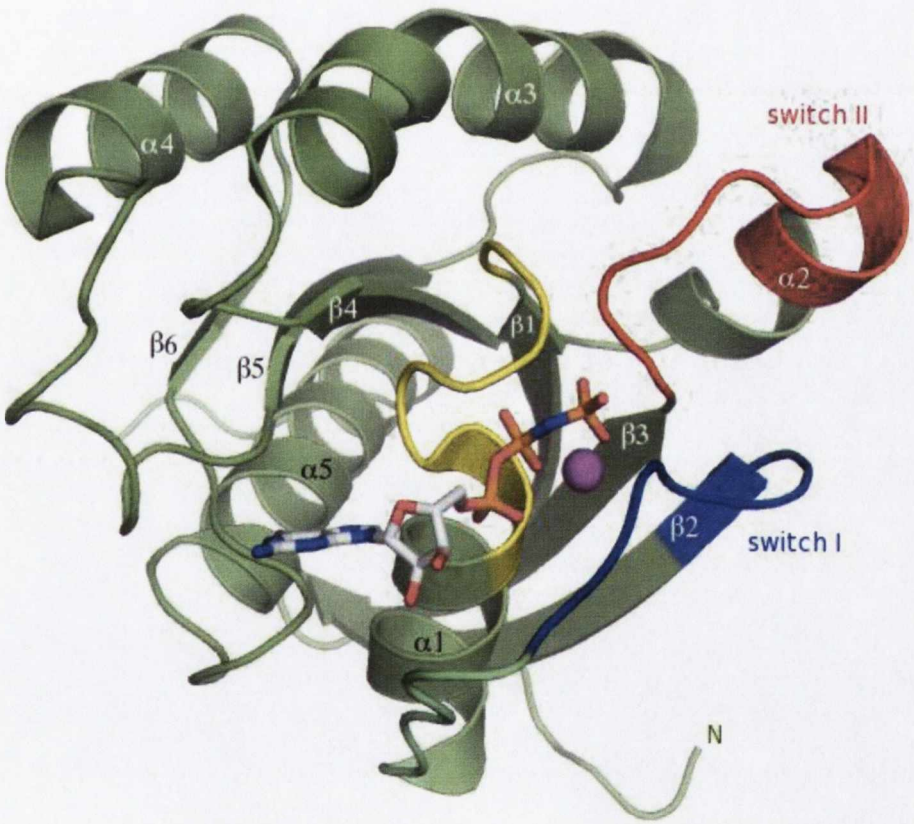

Figure 4.6 Sructure of Ypt32 with GppNHp.
GppNHp is shown as sticks, Mg^{2+} as a sphere. The p-loop is colored yellow, switch I is in dark blue and switch II with part of the adjacent α2 helix in red. α-helices and β-sheets are numbered according to their occurrence from N-ter to C-ter. Ypt32 adapts the typical G-fold.

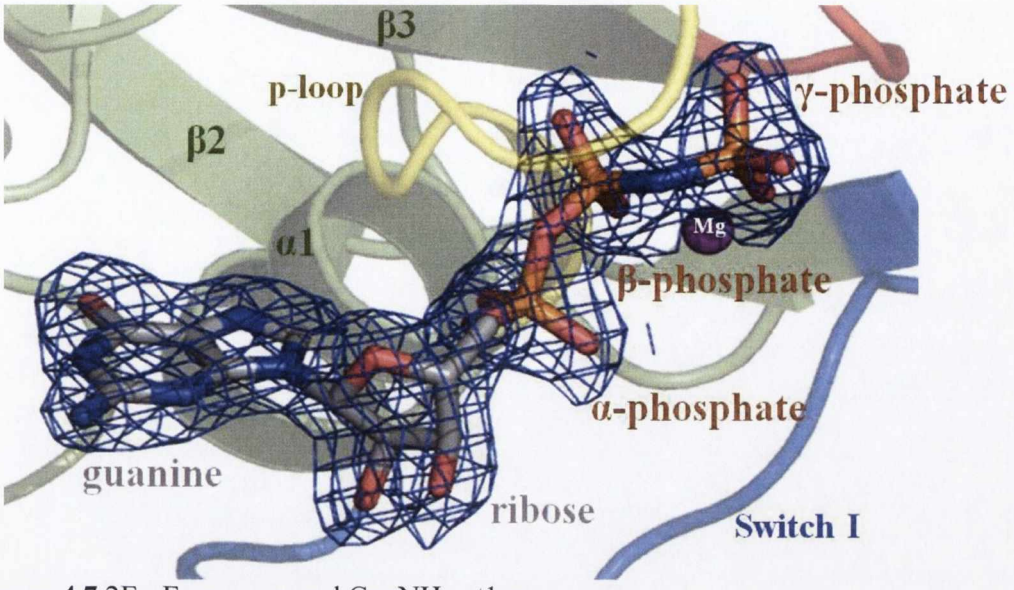

Figure 4.7 2Fo-Fc map around GppNHp at1 σ.
Switch I is in blue, switch II in red, the p-loop in yellow, Mg^{2+} is shown as a sphere, GppNHp as sticks and the 2Fo-Fc map as a blue mesh. The electron density clearly defines the GppNHp molecule including the γ-phosphate.

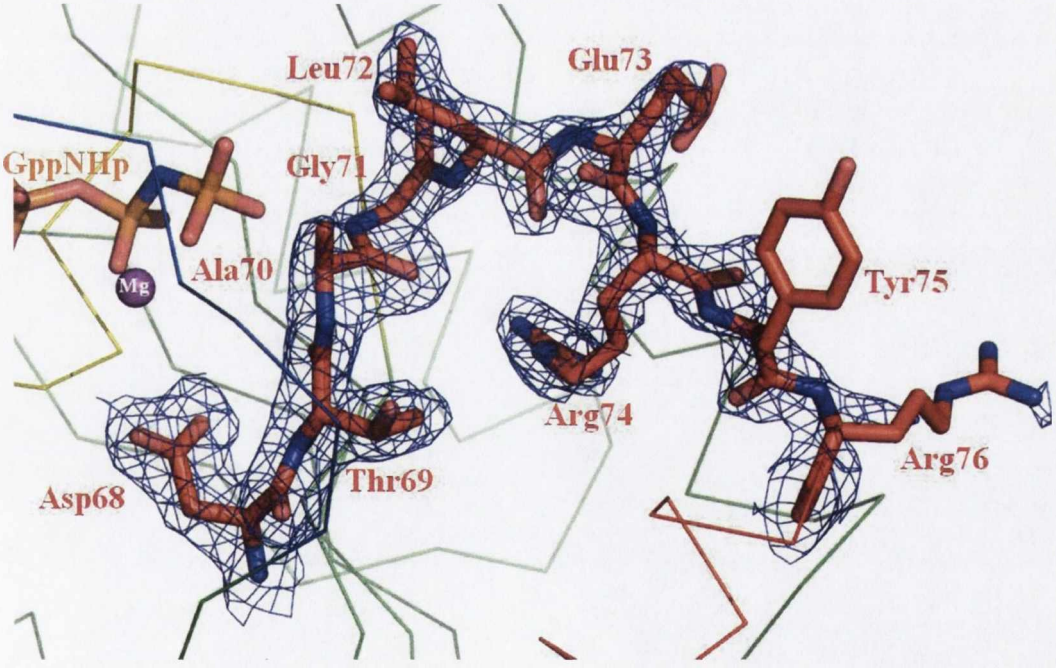

Figure 4.8 2Fo-Fc map around switch II at 1 σ.
The protein is shown as ribbon with colours as in Figure 4.7. The switch II region and part of the α2 helix is shown as sticks, as is the GppNHp. The main chain is well defined by the electron density but the side chains of residues Tyr75 and Arg76 in the α2 helix adjacent to switch II could not be built.

GppNHp binding involves hydrophobic as well as polar interactions. In Figure 4.9 the surface of Ypt32 is coloured accordingly to the charges of the adjacent amino acids. The G-box motif amino acids involved in GppNHp phosphate binding are shown in Figure 4.10. Ser27 (G1), located in the p-loop, and Thr45 (G2), located in switch I, are coordinated by the GppNHp cofactor Mg^{2+} that itself interacts with the β and γ phosphate of GppNHp. Asp68 (G3), located in switch II, interacts with Mg^{2+} *via* two hydrogen bonds, the first one from Asp68 to a water molecule and the second from the water molecule towards the Mg^{2+}. Likewise the backbone amide of Gly71 interacts with the γ phosphate by hydrogen bonding via a water molecule. The side chain of Asp129 (G4) forms a hydrogen bond with the NH_2 of guanine. Another polar interaction is the formation of a hydrogen bond between the guanine carbonyl and the backbone amide of Ala157. Hydrophobic residues pointing into the guanine binding pocket are Ile40, Phe38 and Ala157. They are all oriented towards the imidazole part of the guanosine.

A second GppNHp molecule is found to bind at the interface of two crystallographically-related Ypt32 proteins (Figure 4.11). Its position is away from the nucleotide binding pocket. It interacts with the N-terminal region and the β2-β3 loop of one Ypt32 molecule. The interactions with the other Ypt32 molecule involve the α3-β5 loop and α4-β6 loop.

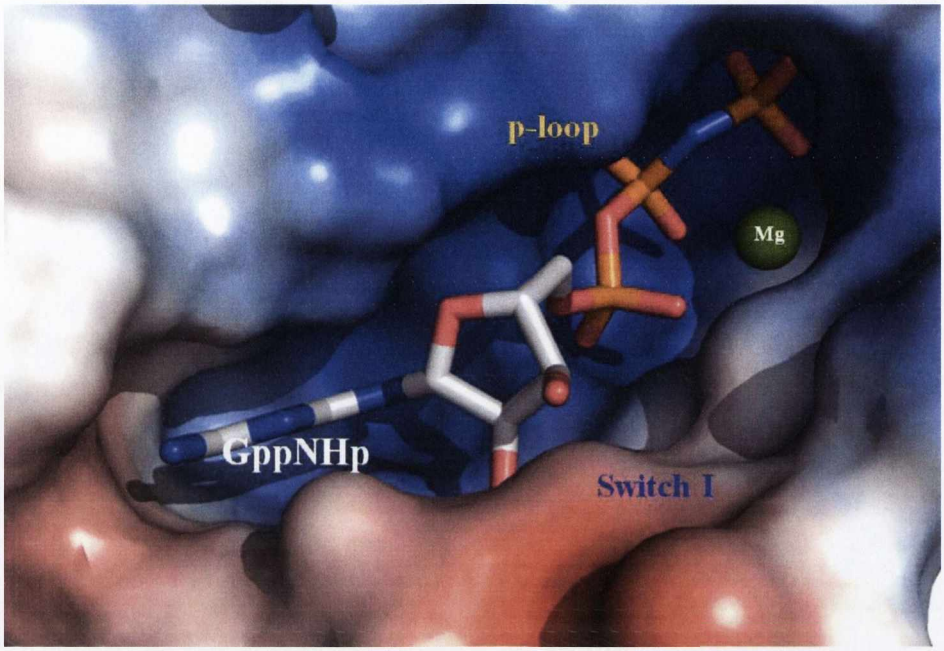

Figure 4.9 Surface of the Ypt32-GppNHp binding pocket.
Negative charged surface residues are in red, positive charged ones in blue.

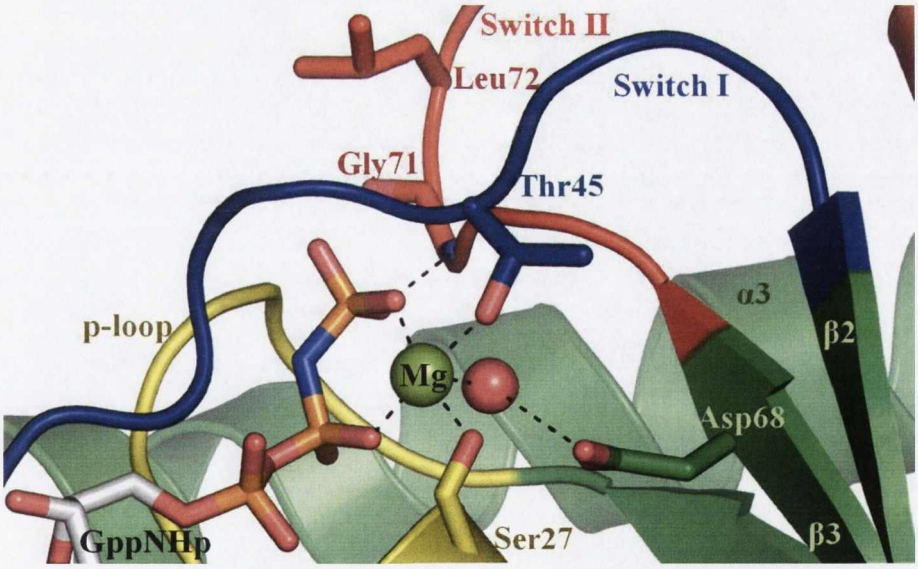

Figure 4.10 Interactions of Ypt32 with the β and γ-phosphate of GppNHp.
Switch I is in blue, switch II in red, the p-loop in yellow, Mg^{2+} and a water molecule are shown as spheres, GppNHp and highlighted residues as sticks. Ser27 from the p-loop and Thr45 from switch I coordinate the $Mg2^{+}$ ion that itself coordinates the β and γ-phosphate of GppNHp. The backbone NH of Gly71 from switch II coordinates the γ-phosphate directly whereas Asp68 interacts with the Mg^{2+} ion via a water molecule.

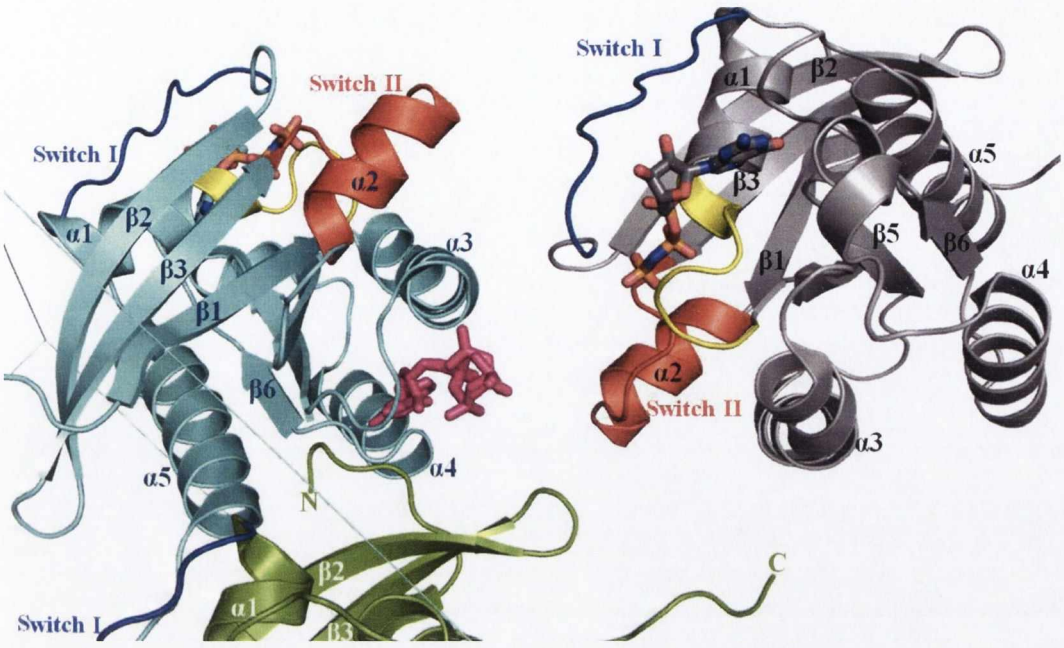

Figure 4.11 Ypt32 symmetry molecules with GppNHp at the interface.
Switch I is in blue, switch II in red, the p-loop in yellow, GppNHp as sticks, the GppNHp molecule positioned at the interface between two Ypt32 molecules is coloured pink. Its position is not close to a nucleotide binding pocket. The interactions involve the N-terminal region and the β2-β3 loop of one Ypt32 molecule as well as the α3-β5 loop and α4-β6 loop of the other Ypt32 molecule.

4.2.5 Comparison of Ypt32(GppNHp) with Ypt32(GDP)

Comparing the Ypt32(GppNHp) structure to a Ypt32(GDP) structure that had recently been solved in our group (PDB ID 3RWO, [321]) revealed no change in the overall structure. Only the conformation of the switch regions changes (Figure 4.12) Upon GppNHp binding the switch I main chain moves closer to the nucleotide, Thr45 is flipped 180° so that its side chain can interact with the γ-phosphate. The conformation of switch II changes even more drastically. It moves 6 Å towards the γ-phosphate and the p-loop, enabling the interaction of the backbone NH of Gly71 with the γ-phosphate.

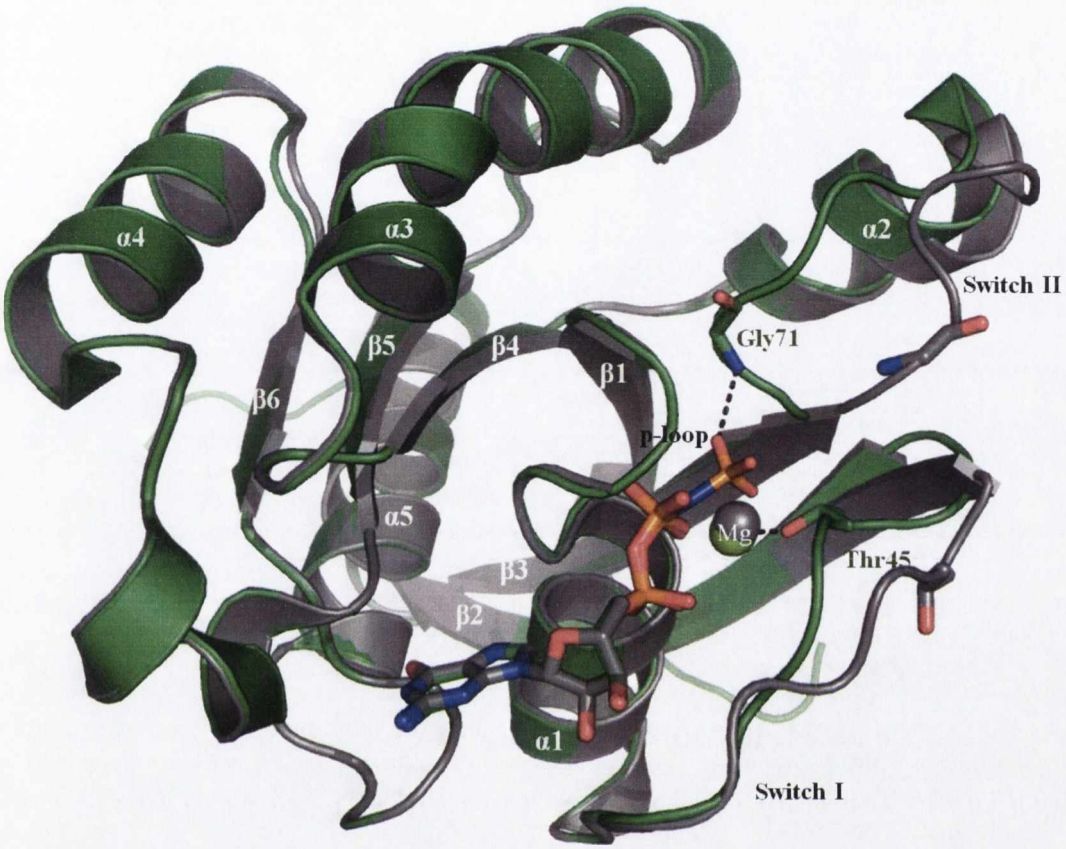

Figure 4.12 Superimposition of Ypt32(GppNHp) with Ypt32(GDP).
Nucleotides and important residues are shown as sticks and Mg^{2+} as spheres. Ypt32(GDP) is shown in grey, Ypt32(GppNHp) is coloured green. Interactions between the nucleotide and Mg^{2+} are depicted by dashes.
The overall structure is very similar, but distinct changes can be observed in the switch regions. Thr45 is flipped 180° enabling interaction with the γ-phosphate via hydrogen bonding with Mg^{2+}. Switch II moves 6 Å towards the γ-phosphate and the p-loop, enabling the interaction of the backbone NH of Gly71 with the γ-phosphate.

4.2.6 Comparisons of active Ypt32(GppNHp) and Sec4

Sec4 comes next in the Rab-cascade, and also binds Sec2 and Myo2. Aligning the sequences of Ypt32 and Sec4 reveals that the switch I region is highly conserved and the switch II regions are almost identical (Figure 4.1). Excluding the C-termini, that usually are very diverse in Rab GTPases, they share 48% identities with 68% homology. A superimposition of the structures of Ypt32(GppNHp) and Sec4(GppNHp) (PDB ID 1G17, [219]) using the secondary structure matching algorithm in Coot [318] results in a root-mean-square deviation of 1.14 Å for the 163 common Cα atoms. The overall confirmation is very similar, only switch II has a different conformation (Figure 4.13 A). Although the main chain conformation is conserved in switch I, the side chains are partly different and adapt diverse conformations. Despite the highly conserved sequence, the switch II regions adapt very different conformations. The Ypt32- switch II – α2 moves further out such that the distance equivalent Cα atoms of Ypt32-Arg76 and Sec4-Arg83 amounts to 7.8 Å. The Ypt32 structure reveals the existence of a salt bridge of 2.7 Å between Arg74 of switch II and Glu110 from the α3-helix.

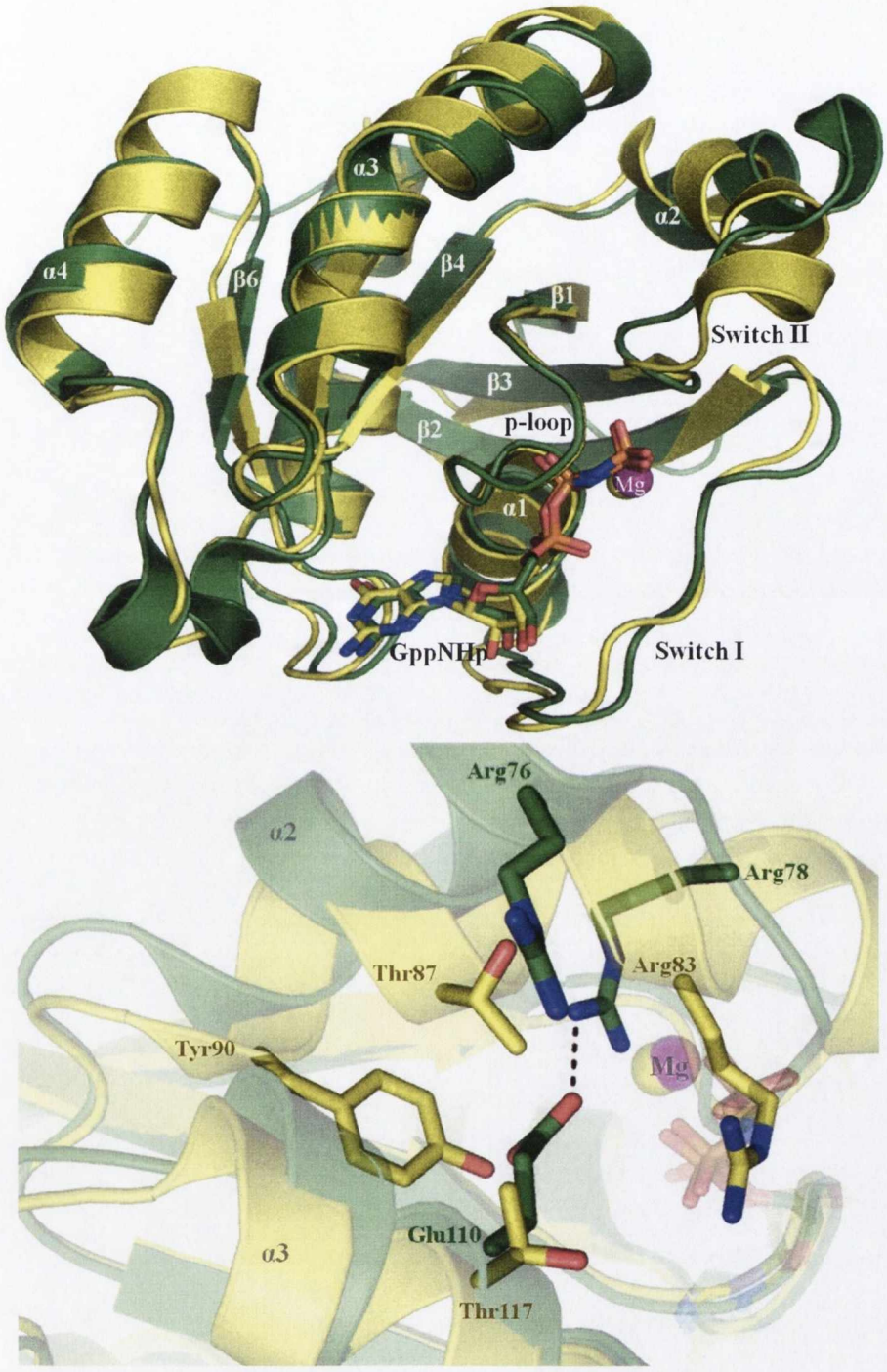

Figure 4.13 Comparison of Ypt32(GppNHp) and Sec4(GppNHp).
Ypt32 is coloured green and Sec4 yellow. Nucleotides and important residues are shown as sticks. Panel A: The overall conformation is similar, except for switch II and the adjacent α3-helix. Panel B: The switch II Arg78 forms a salt bridge to Glu110 of the α3-helix. In Sec4 Thr117 corresponds to Ypt32-Glu110. Thr117 is packed against Tyr90 and Thr87.

4.3 Discussion

4.3.1 Crystallisation and comparisons of active/inactive structures

Ypt32 was successfully expressed, purified and crystallised allowing determination of its structure. Seeding improved the crystallisation and led to large, well diffracting crystals. Interestingly the active mutant had to be incubated with GppNHp prior to crystallisation; otherwise GDP was observed in the nucleotide binding pocket. This indicates that the mutation of Q72L does not always inhibit the hydrolysis of GTP to GDP. Although the side chains of Tyr75 and Arg76 could not be found in the electron density, the main chain was well defined (Figure 4.8). If a part of a molecule is very mobile, this part cannot always be observed in the electron density because the atoms move and hence their diffraction cannot be sourced to a specific location in the crystal. Both side chains are part of the switch II region, and the switch regions with especially switch II of GTPases have been shown to be very mobile [21, 46]. It is therefore not very surprising that the electron density of these regions is not well ordered. The high mobility of this region is also reflected in higher B-factors of approximately 50 $Å^2$ as opposed to the 20-30 $Å^2$ found for most of the protein.

One additional GppNHp molecule was found on the interface of two crystallographically-related Ypt32 proteins (Figure 4.11). It is possible that it binds to a second nucleotide binding pocket. However, two Ypt32 molecules are involved in the interaction and especially the phosphates are very mobile, indicating loose binding. The GppNHp concentration in the crystallisation solution was very high (10 fold excess). Taken together this suggests that the second GppNHp molecule is probably a crystal induced artefact and does not have any relevant function.

GppNHp is a homologue of GTP that cannot be hydrolysed. The presence of GppNHp should induce the same fold and interactions as does binding to GTP. The interactions involved in the binding of GppNHp to Ypt32 are mainly of polar character (Figure 4.9). The conserved G-box motif residues are all involved into polar interactions with the nucleotide which indicates that this is common among all G-proteins. The only parts of Ypt32 that change their conformation upon GTP-binding are the switch regions (Figure 4.6). Lack of the γ-phosphate during GDP binding results in fewer interactions with

the nucleotide and thus the switch conformation changes.This is a common mechanism in G-proteins [21] and the results show that Ypt32 is not an exception to this.

4.3.2 Comparisons of Active Ypt32 and Sec4

Post-Golgi vesicle transport involves several proteins, Sec2 is an effector of Ypt32 and a GEF for Sec4, and therefore Sec4 is also recruited to the vesicle [284-285]. Indeed Ypt32 and Sec4 interact with Myo2 at the same site with the possibility that the interaction follows a similar mechanism [292]. A comparison of active Ypt32 with active Sec4 reveals that the switch I region has a similar conformation when observing the main chain, but the variation of the sequence results in diverse chemistry that is displayed for effector recognition. Most importantly in Ypt32 a positively charged Lys43 is present in contrast to the hydrophobic analogue Ile50 in Sec4. The divergence in composition (despite identical conformation) may play a part in the detailed interaction with effectors, such as Myo2.

In direct contrast to a conserved switch I conformation and divergent chemistry, the switch II conformation is highly divergent despite a highly conserved composition, with only two conservative amino acid substitutions (Figure 4.1). Indeed, this region is the most divergent in conformation upon alignment of Ypt32 and Sec4. The root-mean-square (rms) deviation of 163 Cα atoms upon superposition using the secondary structure matching algorithm in COOT [318] is 1.14 Å. The equivalent Ca atoms of Arg76 (Ypt32) and Arg83 (Sec4) reside 7.8 Å apart following the alignment. This major difference is caused by a GTP-dependant salt bridge between Arg78 (switch II) and Glu110 (α3 helix) that positions the switch II further away from the α3 helix compared to the switch II position in Sec4 (Figure 4.13). The α3 helix is divergent in RabGTPases and part of the RabSF3 motif [163]. The amino acid in the equivalent position of Glu110 is Thr117 in Sec4. Thr117 is involved in hydrophobic packing with Thr87 and Tyr90. Thus, the α3 helix influences the switch II conformation, resulting in two different recognition surfaces for effectors.

4.3.3 GDI binding to Ypt31/32

Ongoing work in our lab included the determination of the Ypt32(GDP) structure. Because of the high sequence identity and functional redundancy of Ypt31 and Ypt32 the Ypt32(GDP) structure was compared to the structure of Ypt31 in complex with GDI [321]. This comparison revealed that the switch II helix (or α2) undergoes a significant conformational re-arrangement upon binding to domain I of GDI (Figure 4.14 A and B). The different switch conformations of Rab GTPases in GDP-bound versus GTP-bound form are most likely the reason for the recognition of the GDP-bound Rab and not the GTP-bound by GDI [178]. The structure comparison between Ypt32(GDP) and Ypt32(GppNHp) revealed a conformational change of especially switch II. Thus the switch II position of Ypt32(GDP) very possibly facilitates binding to GDI.

When compared to other Rab(GDP) structures, it was revealed that the switch II helix is one turn shorter in Sec4(GDP) and Ypt1(GDP) than in Ypt32(GDP) [321]. The structure of Sec4(GDP) depicts two distinct conformations of the four molecules in the asymmetric unit [219]. When compared to the structure of Sec4(GDP)/GDI it is revealed that the conformation of two Sec4 molecules is almost identical to the conformation of Sec4 when bound to GDI (Figure 4.14 C). Binding of Sec4 to GDI thus seems to involve much less conformational changes than Ypt31/32 to GDI. In addition Sec4(GDP) also has a higher affinity for GDI (K_d = 0.33 μM) than Ypt31/32(GDP) (K_d = 18.9 μM and 1.5 μM respectively) [175]. The Ypt31/32 affinity to GDI is an order of magnitude weaker than Sec4/GDI, which could be explained by a possibly increased thermodynamic penalty caused by remodeling of switch II in Ypt31/32 in contrast to an almost 'rigid dock' of Sec4 to GDI.

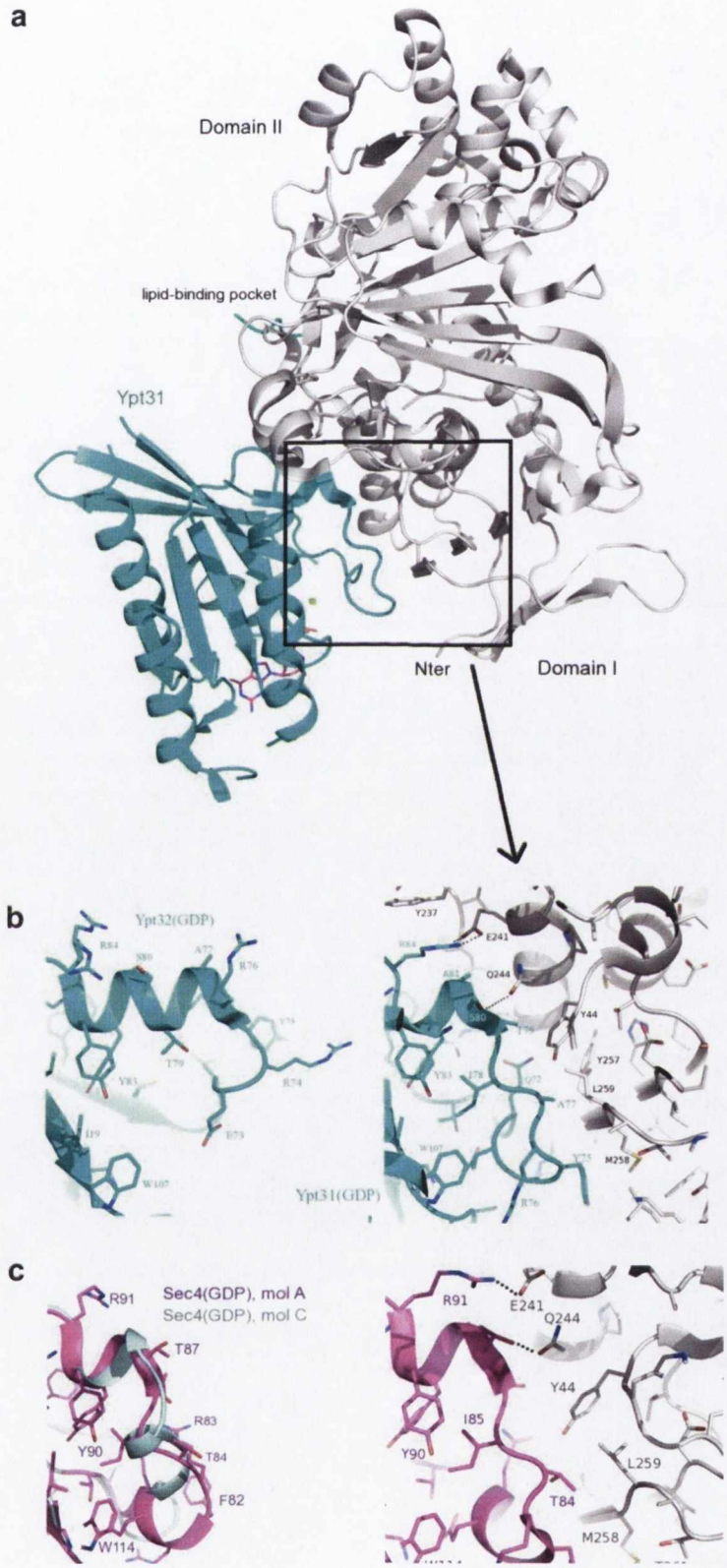
a
Domain II
lipid-binding pocket
Ypt31
Nter
Domain I
b
Ypt32(GDP)
Ypt31(GDP)
c
Sec4(GDP), mol A
Sec4(GDP), mol C
R91
T87
R83
Y90
T84
F82
W114
E241
Q244
Y44
I85
L259
M258

Figure 4.14 Comparison of Ypt32(GDP) to Ypt31/GDI, Sec4(GDP) and Sec4/GDI.
GDI is in grey, Ypt31/32 in cyan, Sec4 in pink and light blue.
Panel A: Structure of Ypt31/GDI. The RBP is emphasised by the rectangle.
Panel B: Left, uncomplexed Ypt32(GDP); right Ypt32(GDP)/GDI, corresponding to the region indicated by the rectangle. Observation of the loss of one helical turn of switch II is facilitated by showing bound and unbound Ypt with the same orientation and scale.
Panel C: Left, superimposition of both conformations found in uncomplexed Sec4(GDP) (molecule A and C); right Sec4(GDP)/GDI complex. Sec4(GDP) bound to GDI has almost the same conformation as molecule A of uncomplexed Sec4(GDP).
Figure from [321]; PDB-files used for this figure: Ypt31(GDP)/GDI 3CPJ, [175]; Sec4(GDP) 1G16 [219]; Sec4(GDP)/GDI 3CPH [175]; Ypt32(GDP) 3RWO [321]

Chapter 5

Rab1 and the host pathogen protein DrrA

5.1. Introduction of Rab1 and DrrA and goals

Rab1 is a regulator of ER to Golgi trafficking and usually found to reside on the membranes of these compartments [277, 305]. The host pathogen L. pneumophilia is capable of 'hi-jacking' host proteins, creating a LCV that is morphologically similar to the ER [308-310]. One of the proteins involved in this mechanism is DrrA that recruits Rab1 to the LCV where it is activated by nucleotide exchange mediated by the GEF activity of DrrA as well as AMPylated by a different domain of the same protein.

When our group started working with DrrA the membrane anchoring function of the P4M domain as well as the AMPylation function had not been discovered yet. It was further thought, that apart from being a GEF, DrrA was also a GDF [192-193]. No structure of any of these domains had been solved. Structural analysis of DrrA promised to give more insight into the mechanisms employed by this unusual protein as well as enabling the identification of the functions of its C-terminal and N-terminal domains. In addition to this it would be an exciting opportunity to investigate the mechanism employed by DrrA for its GEF and GDF activity. However, during the course of this work several other groups published structures and more information about the functions of DrrA [195-197, 312, 331]. The only challenge that has not been successfully overcome yet is the structure determination of the full length protein.

Our initial goal was to determine the structure of full length DrrA with or without Rab1, but the structure determination of smaller fragments of DrrA was considered as an alternative. When the first structures of DrrA fragments were published, we concentrated our efforts fully on the determination of the structure of full length DrrA, with and without Rab1.

5.2. Results

5.2.1. Production of a GDP locked Rab1a mutant

Rab1a Q66L is in a GTP locked state. DrrA interacts with the inactive, GDP bound form. Since our lab had the active form of Rab1a, it was first mutated back to the wild type sequence (L66Q). After this had been successfully performed the wild type Rab1a plasmid was used for a S21N mutation. The resulting product was then used for further studies of Rab1a-DrrA interactions.

5.2.2. Rab1 – Expression and purification

Rab1a S21N was expressed at 37°C (310 K) and purified as described in the sections 2.4.2, 2.5.1 and 2.5.2. For initial purification nickel affinity chromatography was performed, followed by cleavage of the His-Tag. A second Ni-affinity column was then used to remove the His-Tag and proteins that co-purified during the first affinity chromatography step. Size exclusion chromatography was used to remove soluble aggregates and 'polish' the protein. The 19.8 kDa Rab1a eluted at 70 ml from the Superdex-75 column (Figure 5.1 A). SDS-PAGE analysis shows that the protein is purer after each purification step and that no contaminants can be detected after the last step (Figure 5.1 B).

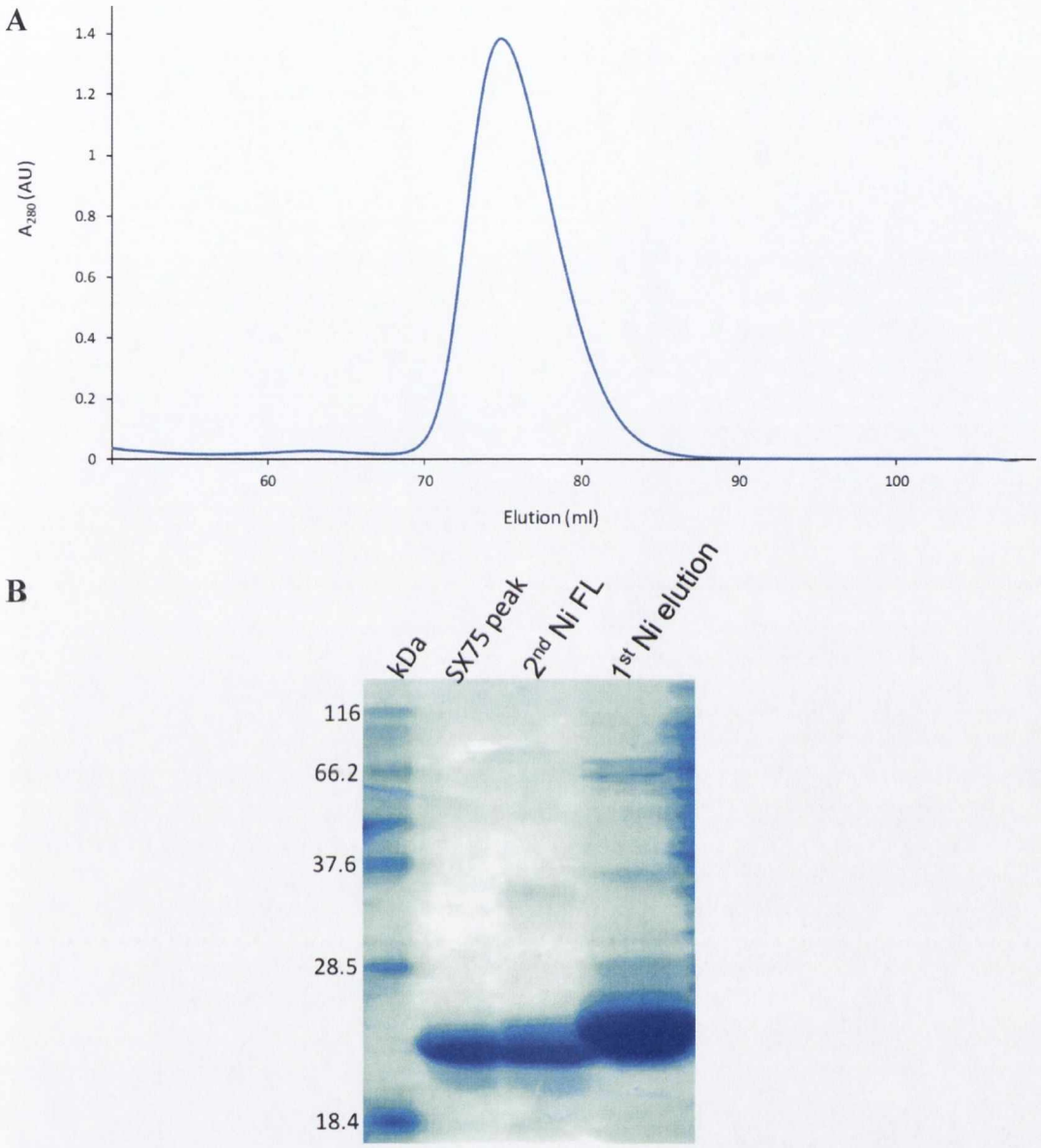

Figure 5.1 Purification of Rab1a Ser21Asn.
Panel A: Elution profile of Rab1a from a Superdex-75 size exclusion column. Rab1a elutes at 70 ml.
Panel B: SDS-PAGE analysis of the Rab1a containing fractions after each purification step. After size exclusion no other bands can be detected on the SDS-PAGE.

5.2.3. DrrA full length – Expression and purification

DrrA was expressed and purified as described in sections 2.4.2., 2.5.1. and 2.5.4. For initial purification Nickel affinity chromatography was performed (Figure 5.2). This was followed by cleavage of the His-Tag. A second Ni-affinity column was then used to remove the His-Tag and proteins that co-purified during the first affinity chromatography. SDS-PAGE reveals that the solution contains significant amounts of contaminant proteins after this second purification step (Figure 5.2).

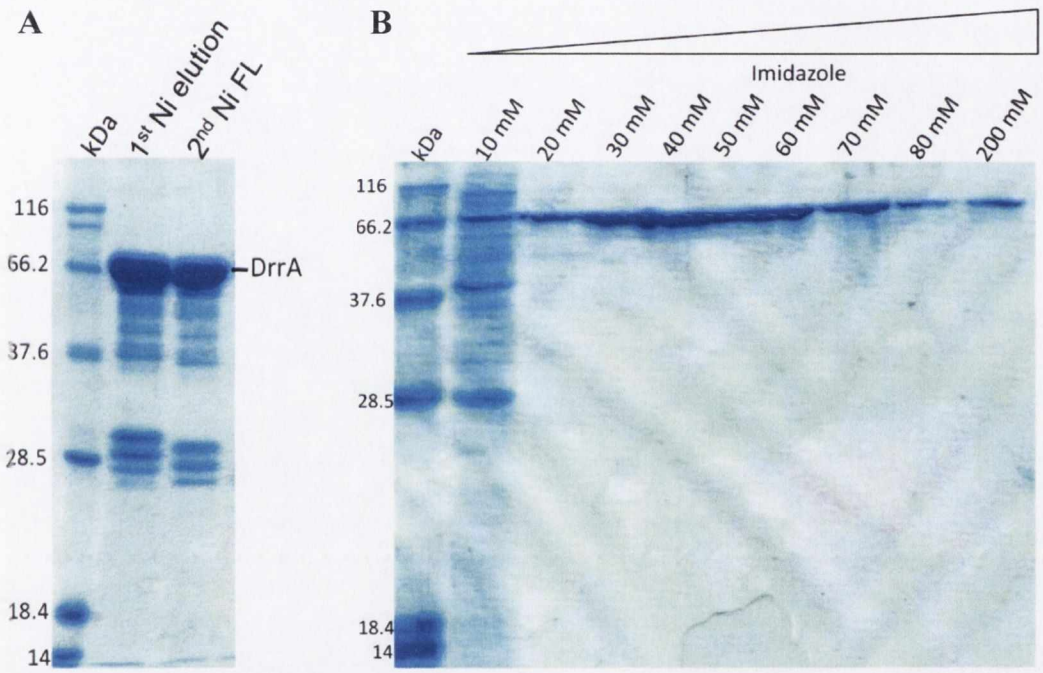

Figure 5.2 SDS-PAGE analysis of the first purification steps of DrrA.
Panel A: The eluted fraction from the first nickel affinity chromatography with 50 mM imidazole reveals several undesired bands. The flow through fraction of the second Ni affinity chromatography improves the purity slightly but still contaminating proteins are found.
Panel B: Step gradient elution of DrrA. The nickel resin was washed with 100 ml of 10 mM imidazole. Then the resin was washed subsequently with 10 ml extraction buffer containing ascending concentrations of Imidazole. DrrA eluted at all imidazole concentrations with most of the protein having eluted after washing with 60 ml Imidazole.

The protein solution was then dialysed into a low salt buffer (10 mM NaCl, 5 mM $MgCl_2$, 1 mM DTT, 10 mM Tris-Cl, pH 7.5) and loaded onto an anion exchange column. The protein was eluted from the column using a gradient up to 1 M NaCl and DrrA eluted at a concentration of 175 mM NaCl (Figure 5.3). SDS-PAGE analysis of the elution peak reveals that several contaminating proteins cannot be removed with this technique and the higher the salt concentration in the elution peak, the more contaminants are present. The less contaminants containing part of the elution peak from anion exchange chromatography was then further purified with a final size exclusion chromatography step. The 73.4 kDa protein eluted after 77 ml and the elution peak had a shoulder (Figure 5.4 A). SDS-PAGE analysis of the elution peak revealed that the DrrA that eluted with the main peak contained significantly less contaminants than before, but DrrA that eluted within the shoulder did contain more contaminants, one contaminant band is as strong as the DrrA band (Figure 5.4 B) indicating that the two proteins have a similar concentration. The elution fractions that contained the least amount of contaminating proteins were used for further studies.

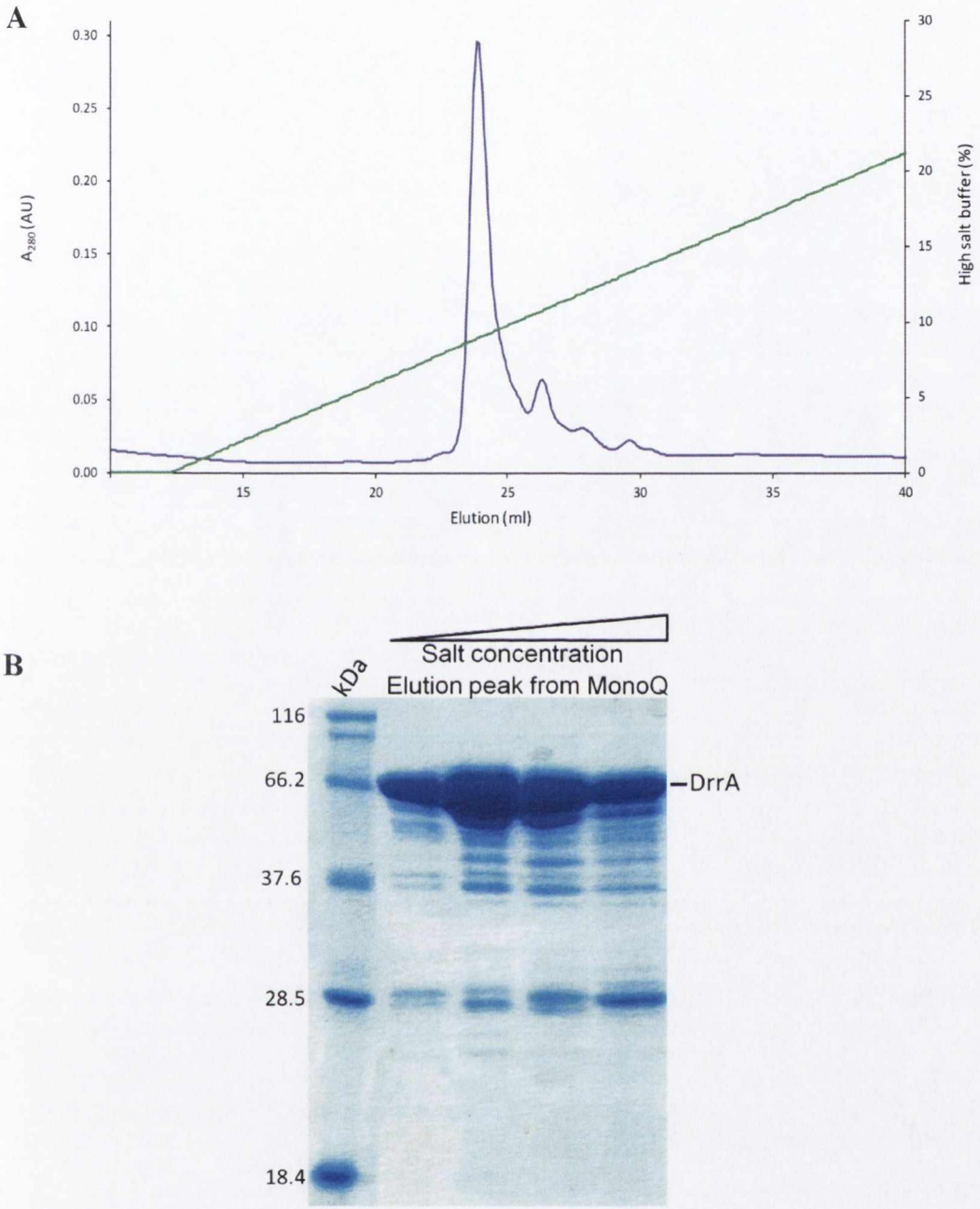

Figure 5.3 Elution of DrrA from anion exchange.
The DrrA containing flow through fraction from a second affinity chromatography was loaded onto a MonoQ 5/50 anion exchange column. Elution was performed with a linear salt gradient to 1 M NaCl (50%) in 10 mM NaCl, 5 mM $MgCl_2$, 1 mM DTT, 10 mM Tris-Cl, pH 7.5.
Panel A: Elution profile of DrrA from anion exchange, DrrA eluted at 175 mM NaCl.
Panel B: SDS-PAGE analysis of the DrrA elution peak from anion exchange. The higher the salt concentration during the elution the more impurities are detected.

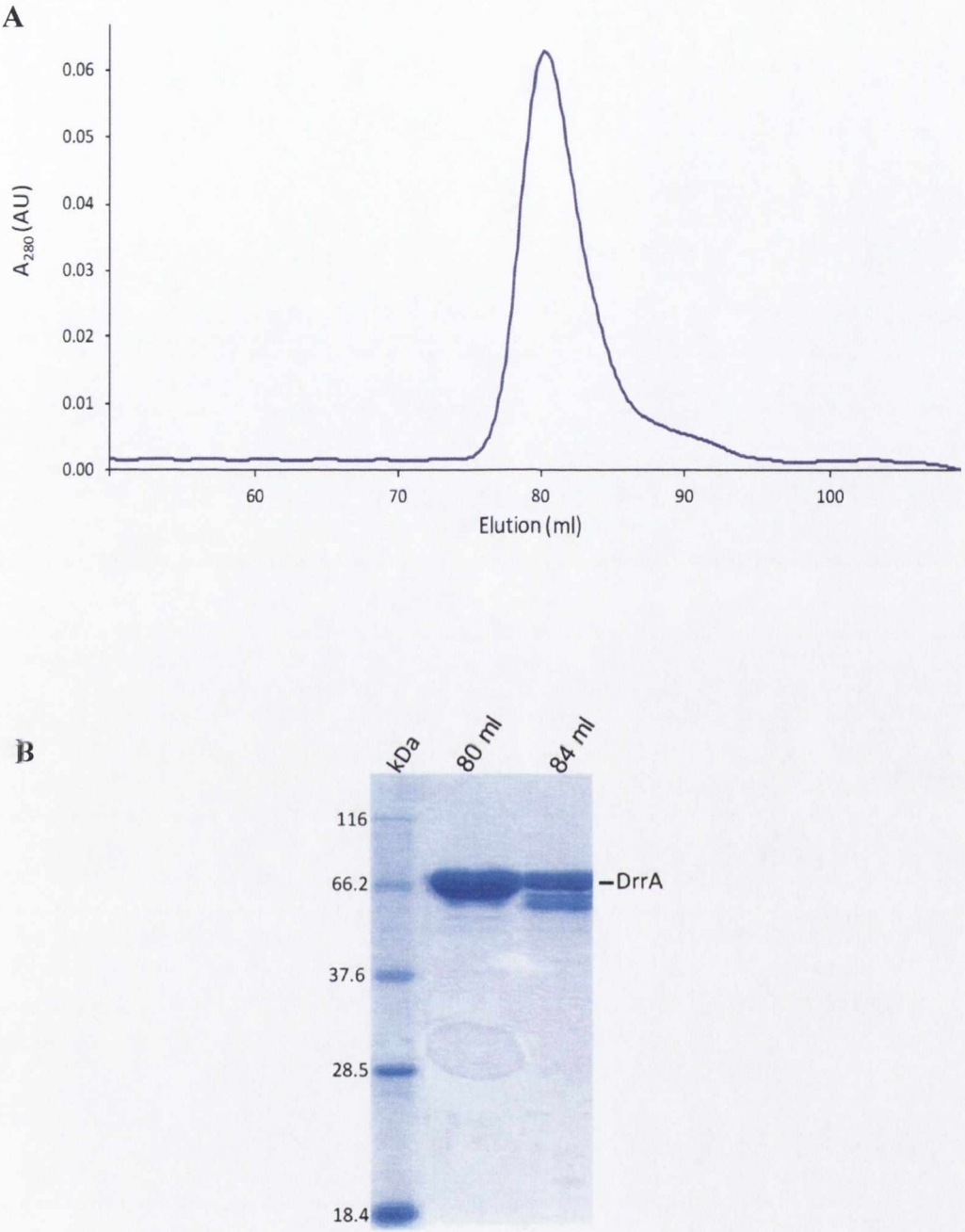

Figure 5.4 Size exclusion chromatography of DrrA.
Panel A: Elution profile of DrrA from a Superdex-200 column. The 73 kDa protein elutes after 77 ml and the elution peak has a shoulder.
Panel B: SDS-PAGE analysis of the DrrA elution peak from the size exclusion column. The main peak fraction contains only few impurities whereas the DrrA that elutes within the shoulder of the peak contains more contaminants.

5.2.4. Complex formation of Rab1a with DrrA

Rab1a S21N that had been obtained as described above was then used to form a complex with DrrA. For this purpose DrrA was incubated with Rab1a at a ratio of 1 µM to 2 µM. This was necessary because the complex formation would not shift the elution peak of DrrA sufficiently to allow separation of the complex from excess DrrA. In order to separate the complex from excess Rab1a size exclusion chromatography was performed. The 93 kDa Rab1a/DrrA complex eluted after 73 ml, when compared to the elution profile of DrrA alone a shift of the peak can be detected. Excess Rab1a elutes after 92 ml (Figure 5.5 A). SDS-PAGE analysis revealed that the complex still contained a few impurities (Figure 5.9 B).

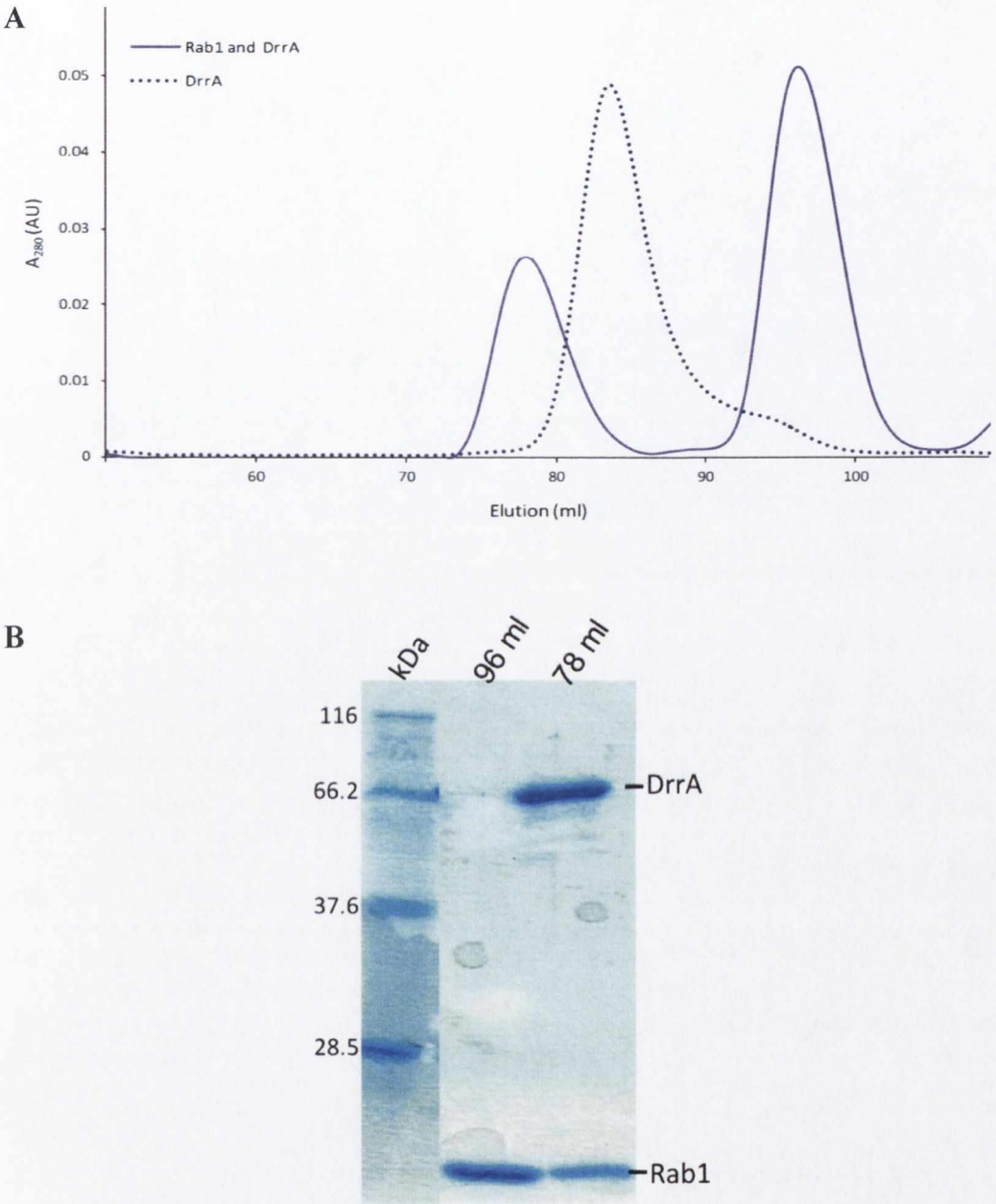

Figure 5.5 Complex formation of Rab1a/DrrA.
Panel A: Elution profiles of DrrA/Rab1a and DrrA from a Superdex-200 column. The 93 kDa complex elutes after 73 ml, which is faster than DrrA alone (77 ml). Rab1a that is in excess and thus does not interact with DrrA elutes at 92 ml.
Panel B: SDS-PAGE analysis of the elution peak maxima fractions from size exclusion chromatography with Rab1a and DrrA. The peak that starts eluting at 77 ml contains DrrA and Rab1a, proving that a complex has been formed, whereas unbound Rab1a elutes at 92 ml.

5.2.5. DrrA 202-647 – Expression and purification

$DrrA_{202-647}$ was expressed and purified as described in section 2.4.2., 2.5.1. and 2.5.5. For initial purification Nickel affinity chromatography was performed. This was followed by cleavage of the His-Tag. A second Ni-affinity column was then used to remove the His-Tag, the used protease and proteins that co-purified during the first affinity chromatography. SDS-PAGE of the two affinity chromatography steps reveals that the solution contains significant contaminants after this second purification step (Figure 5.6).

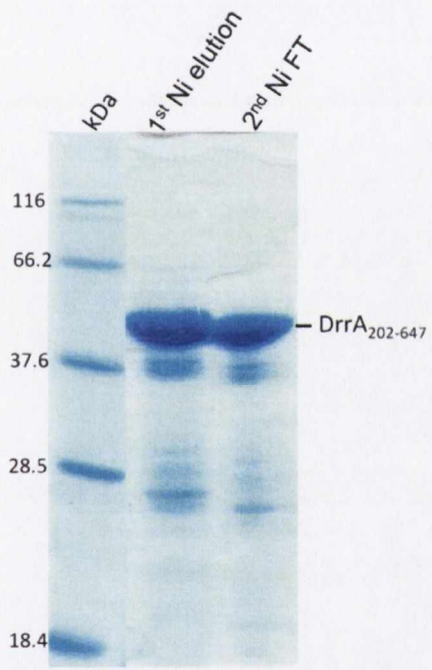

Figure 5.6 SDS-PAGE analysis of the first and second affinity chromatography steps of $DrrA_{202-647}$.
The elution fraction of the first nickel affinity step contains mainly $DrrA_{202-647}$ but also many undesired contaminant proteins. The flow through fraction of the second nickel affinity step contains cut $DrrA_{202-647}$ and the purity is slightly improved.

The protein solution was then dialysed into a low salt buffer (10 mM NaCl, 5 mM $MgCl_2$, 1 mM DTT, 10 mM Tris-Cl, pH 7.5) and loaded onto a cation exchange column. The protein was eluted from the column using a gradient up to 500 mM NaCl and $DrrA_{202-647}$ eluted at 230 mM NaCl (Figure 5.7). SDS-PAGE analysis of the elution peak reveals that the higher the salt concentration in the elution peak, the more contaminants are present. The less contaminants containing part of the elution peak from anion exchange chromatography was then further purified with a final size exclusion chromatography step. The 50.5 kDa $DrrA_{202-647}$ eluted after 73 ml and the elution peak had a shoulder (Figure 5.8 A). SDS-PAGE analysis of the elution peak revealed that the $DrrA_{202-647}$ that eluted within the first peak elution fractions contained less contaminant proteins than the $DrrA_{202-647}$ that eluted within later fractions, especially the fractions from the peak shoulder (Figure 5.8 B). The elution fractions that contained the least amount of contaminant proteins were used for further studies.

Selenomethionine containing $DrrA_{202-647}$ was produced as described in section 2.4.3 and purified in the same way as $DrrA_{202-647}$. During the purification process the selenomethionine $DrrA_{202-647}$ behaved like native $DrrA_{202-647}$.

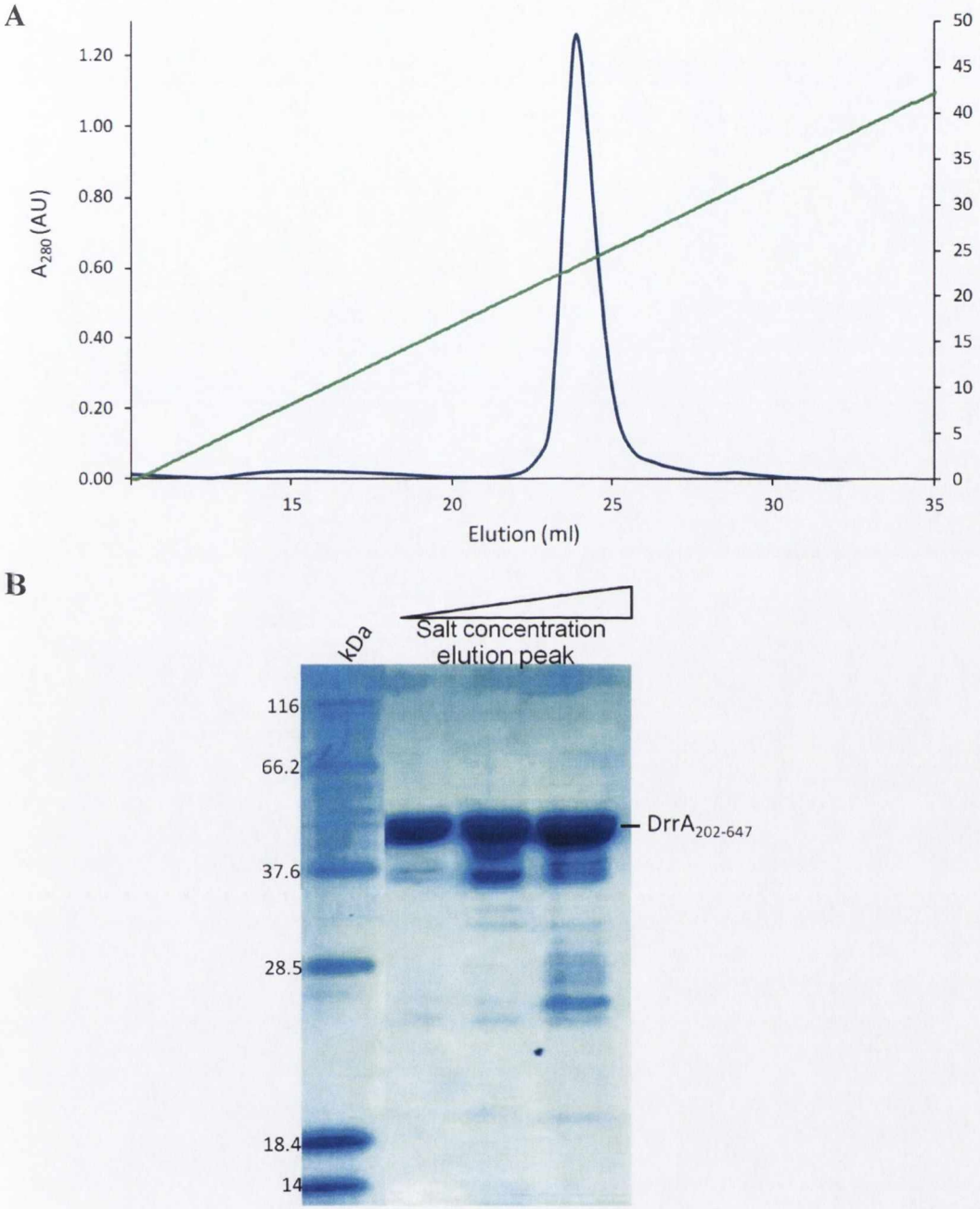

Figure 5.7 Elution of $DrrA_{202-647}$ from ion exchange chromatography.
The $DrrA_{202-647}$ containing flow through fraction from a second affinity chromatography was loaded onto a MonoS 5/50 cation exchange column. Elution was performed with a linear salt gradient to 500 mM NaCl (50%) in 10 mM NaCl, 5 mM MgCl2, 1 mM DTT, 10 mM Tris-Cl, pH 7.5.
Panel A: $DrrA_{202-647}$ elutes at 230 mM NaCl.
Panel B: SDS-PAGE analysis of the elution peak reveals that with rising salt concentration during the elution, more proteins co-elute with $DrrA_{202-647}$.

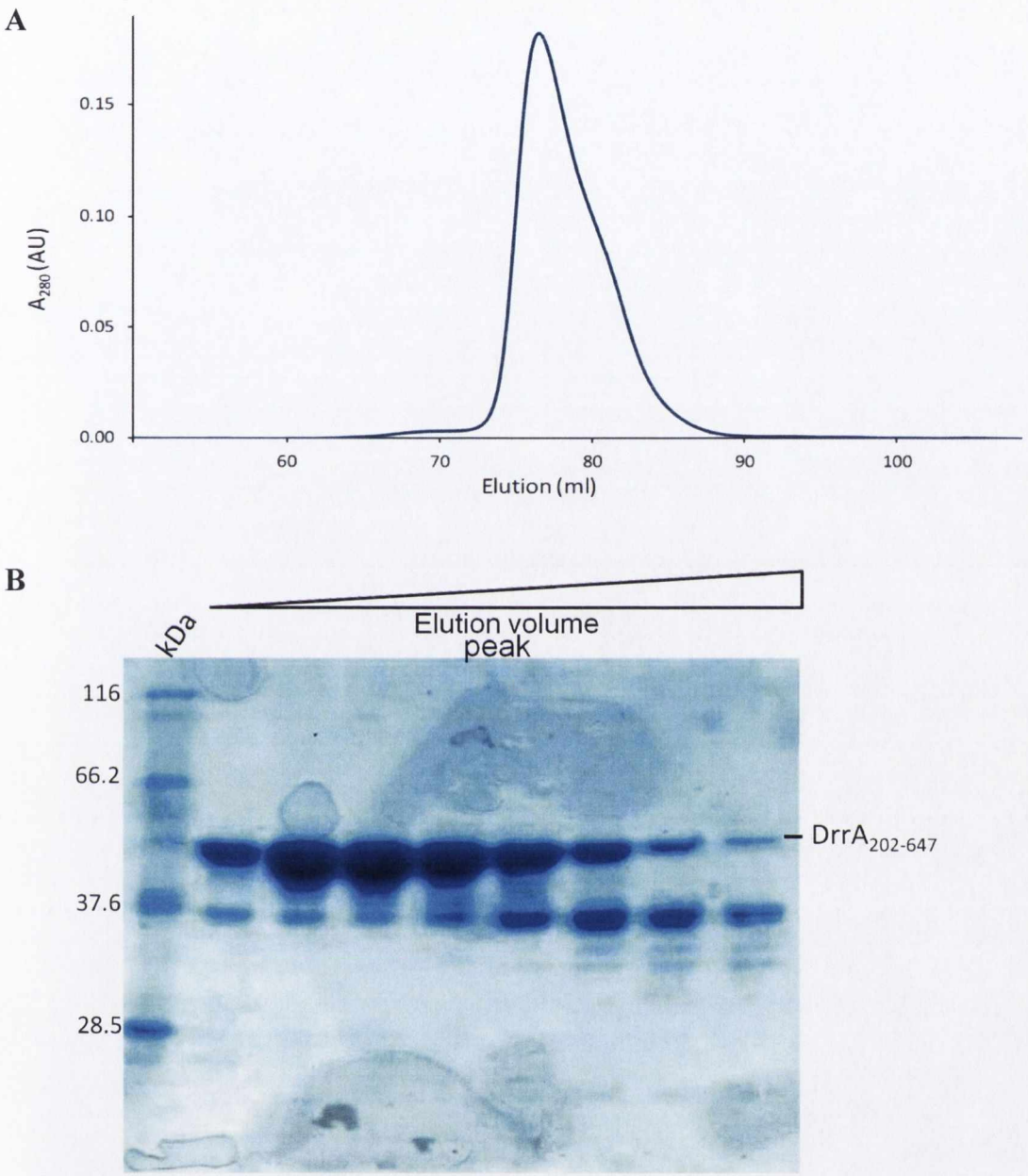

Figure 5.8 Elution of $DrrA_{202-647}$ from size exclusion chromatography.
Panel A: Elution profile of $DrrA_{202-647}$ from a Superdex-200 column. The 50.5 kDa protein elutes from 73 ml onwards, the elution peak has a large shoulder.
Panel B: SDS-PAGE analysis of the elution peak from size exclusion chromatography. The peak fractions closer to 73 ml contain less contaminant proteins than those that elute within the shoulder.

5.2.6. Complex formation of Rab1a with $DrrA_{202-647}$

Rab1a S21N that had been obtained as described above was then used to form a complex with $DrrA_{202-647}$. For this purpose $DrrA_{202-647}$ was incubated with Rab1a at a ratio of 1 µM to 2 µM. In order to separate the complex from excess Rab1 size exclusion chromatography was performed. The 70 kDa Rab1/$DrrA_{202-647}$ complex eluted after 70 ml, when compared to the elutioin profile of $DrrA_{202-647}$ alone a shift of the peak can be detected. Excess Rab1a elutes after 91 ml (Figure 5.5 A). SDS-PAGE analysis revealed that the complex still contained contaminant proteins.

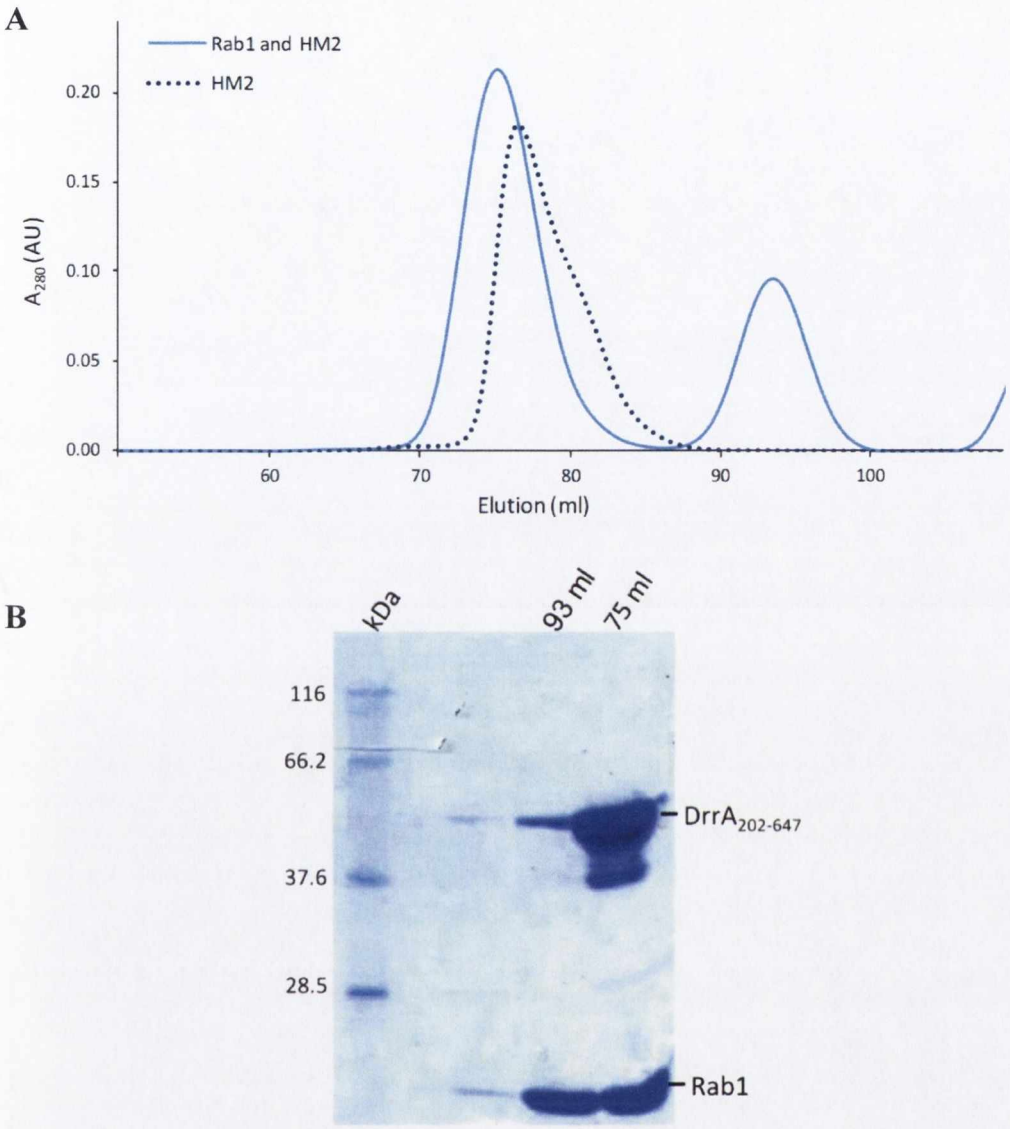

Figure 5.9 Complex formation of Rab1/$DrrA_{202-647}$.
Panel A: Elution profiles of $DrrA_{202-647}$/Rab1 and $DrrA_{202-647}$ from a Superdex-200 column. The 70 kDa complex elutes after 70 ml, which is faster than $DrrA_{202-647}$ alone (73 ml). Rab1 that is in excess and thus does not interact with DrrA elutes at 92 ml.
Panel B: SDS-PAGE analysis of the elution peak maxima fractions from size exclusion chromatography with Rab1 and $DrrA_{202-647}$. The peak that starts eluting at 70 ml contains $DrrA_{202-647}$ and Rab1, proving that a complex has been formed, whereas unbound Rab1 elutes at 92 ml.

5.2.7. Crystallisation of DrrA and Rab1/DrrA

DrrA and Rab1a/DrrA that had been purified as described in sections 5.2.2, 5.2.3 and 5.2.4 were subjected to crystallisation trials. For this purpose the proteins were concentrated up to 15 mg/ml. Several commercially available sparse matrix and grid screens were set up with varying concentrations of DrrA and Rab1a/DrrA as described in section 2.9. No hits were observed for Rab1a/DrrA but for DrrA several initial hits could be obtained. In two very similar conditions (0.2 M Na_2SO_4, 20 % PEG 3350, 0.1 M Bis Tris propane (BTP) pH 7.5 or pH 8.5) needle like crystals were observed after one to three days (Figure 5.10). Optimisation led to bigger and better separated crystals. Cube or diamond shaped crystals could be observed in a different condition after six to eight weeks (0.2 M NaBr, 20 % PEG 3350, 0.1 M BTP pH 7.5; Figure 5.11). One crystal diffracted to 7 Å in the APS (Figure 5.12). Until now those crystals could not be repeated in a customised screen.

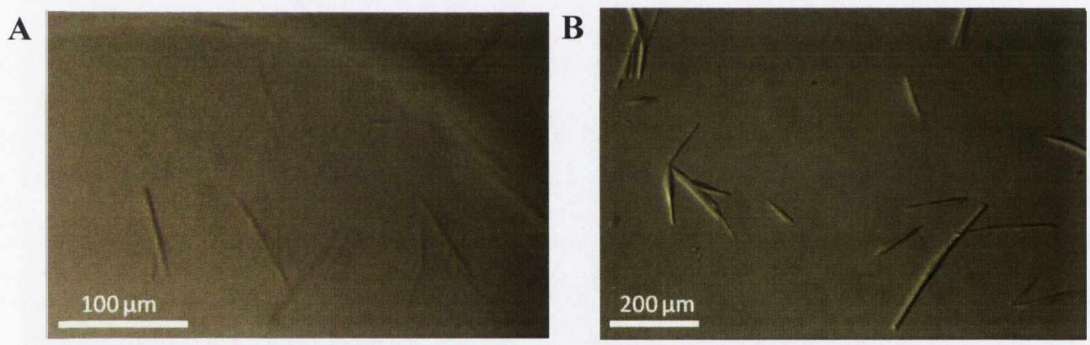

Figure 5.10 Needle like DrrA crystals.
Panel A: Crystals obtained in an initial commercial screen. Those crystals were obtained in two similar conditions; 0.2 M Na_2SO_4, 20 % PEG 3350, 0.1 M Bis Tris propane (BTP) pH 7.5 or pH 8.5.
Panel B: Crystals obtained in a customised grid screen with in 0.2 M $MgSO_4$ 20% PEG 3350 0.1 M BTP pH 7.5. Compared to the initial crystals the optimised crystals are bigger.

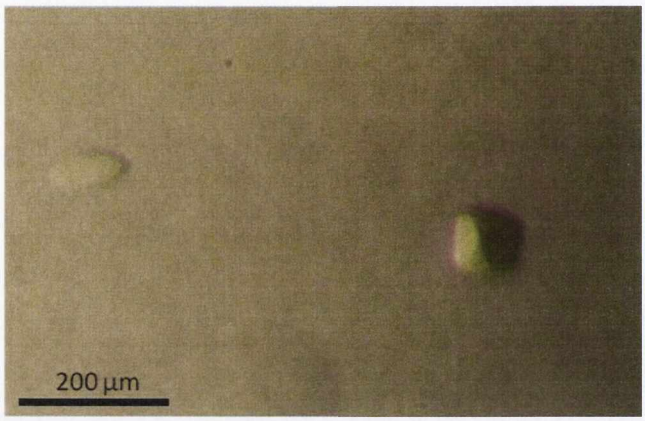

Figure 5.11 Diamond shaped DrrA crystal.
The diamond shaped crystals could be observed six to eight weeks after set up of the screens. The condition (0.2 M NaBr, 20 % PEG 3350, 0.1 M BTP pH 7.5) is also similar to the conditions in which needle like crystals were observed. Initial diffraction to 7 Å could be collected at the APS.

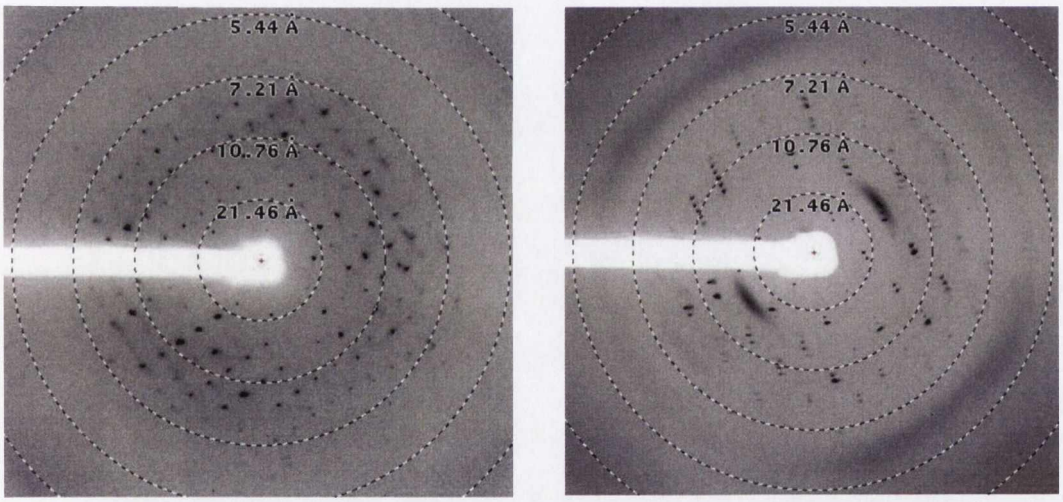

Figure 5.12 Diffraction pattern of DrrA.
Panel A: Diffraction spots can be found up to a resolution of 7 Å, with single spots up to almost 5 Å. Some spots are very clear whereas others seem to be a bit smeared.
Panel B: Diffractiion of DrrA when the crystal is turned 45°. At this angle the crystal does not diffract as far as seen in the previous image. Some spots are broad and smeary.

5.2.8. Crystallisation of $DrrA_{202-647}$ and Rab1/$DrrA_{202-647}$

$DrrA_{202-647}$ and Rab1a/$DrrA_{202-647}$ that had been purified as described in sections 5.2.2, 5.2.5 and 5.2.6 was concentrated up to 15 mg/ml and used for crystallisation trials. Several commercially available sparse matrix and grid screens were set up with varying concentrations of $DrrA_{202-647}$ and Rab1a/$DrrA_{202-647}$ as described in section 2.9. Initial crystals could be obtained in a condition similar to the condition found for $DrrA_{FL}$ (0.1 M BTP pH 7.5 and 20 % PEG 3350). The crystals were needle like or very thin plates (Figure 5.13 A). It was possible to optimise these crystals in 0.1 M MgSO4, 12% PEG 10 000, 0.1 M Tris pH 8 (Figure 5.13 B) and they diffracted up to 8 Å.

Selenomethionine $DrrA_{202-647}$ was also subjected to crystallisation trials. Initial plate shaped crystals were obtained in 0.5 M $LiSO_4$, 15 % PEG 8000 (Figure 5.14). Crystal growth could not be reproduced in larger drops or customised grid screens. These initial crystals diffracted up to 4.5 Å at 24ID-C (APS, Chicago) and it was possible to solve the structure using molecular replacement.

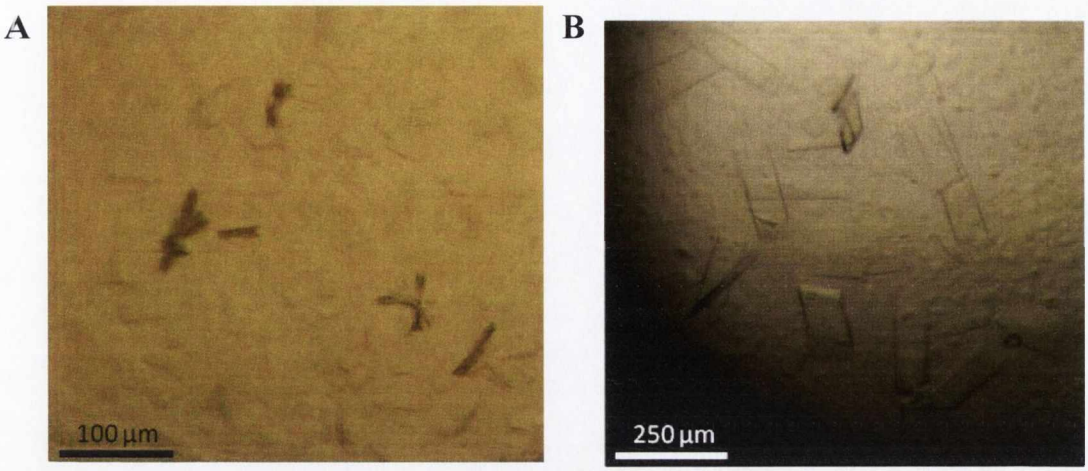

Figure 5.13 $DrrA_{202-647}$ crystals.
Panel A: Initial crystals of $DrrA_{202-647}$ observed in 0.1 M BTP pH 7.5 and 20 % PEG 3350. Some needle clusters are present as well as very thin plates that are almost undetectable in the picture.
Panel B: Optimised crystals of $DrrA_{202-647}$ in 0.1 M $MgSO_4$, 12% PEG 10 000, 0.1 M Tris pH 8 that diffract up to 8 Å at BM14 (ESRF, Grenoble).

Figure 5.14 Selenomethionine $DrrA_{202-647}$ crystals.
The plate shaped crystals were observed in a commercial screen (0.5 M $LiSO_4$, 15 % PEG 8000) and diffracted up to 4.5 Å at 24ID-C (APS, Chicago).

5.3. Discussion

5.3.1. Rab1a expression and purification

Once Rab1a had been mutated to the GDP locked form (S21N), the protein could be expressed for structural studies with DrrA. Like Ypt32 and Rab27a presented here and also like in most studies, the Rab1a construct used did not contain the C-terminal region. Rab1a behaved as expected during purification and the elution profile from the size exclusion chromatography indicates that it is present in a monomeric form (Figure 5.1 A). No contaminating proteins could be observed when the purity of the protein was analysed with SDS-PAGE (Figure 5.1 B).

5.3.2. DrrA and DrrA$_{202-647}$ expression, purification and complex formation with Rab1a

The His-tagged DrrA protein was highly expressed in *E.coli*, but the purification proved to be difficult. The initial purification step for His-tagged proteins is usually affinity chromatography. DrrA seemed to be sensitive towards the imidazole concentration present in the used buffers. It seemed that even at a low amount of imidazole the protein eluted from the column and a wash step with 20 mM imidazole containing buffer prior to elution led to loss of a large amount of protein. A step gradient elution showed that the interaction of DrrA with the nickel resin was indeed not very strong. The protein bled off the resin even at imidazole concentrations as low as 10-20 mM and 30 mM imidazole already eluted a large amount of protein (Figure 5.2 B). In order to avoid heavy loss of protein but to minimise the amount of contaminants present in the DrrA elution fraction, it was decided to extract the protein and wash the nickel resin with 10 mM imidazole containing buffer instead of 20 mM. An elution step with 50 mM imidazole was chosen so that contaminating proteins did not co-elute but sticked to the resin. The eluted fraction from the nickel resin still contained several contaminant proteins. However SDS-PAGE analysis of the flow through fraction of affinity chromatography after cutting the His-tag reveals that most contaminant bands have a lower size than after the first affinity chromatography (Figure 5.2 A). This indicates that the contaminating proteins are in fact degradation

products of DrrA that do contain a His-tag that is cut off by the protease, as happens with the full length DrrA. The degradation products are present from the first purification step onwards and do not seem to accumulate which indicates that the degradation takes place during protein expression or extraction, but stops latest once the cell lysate has been separated from the protein of interest. The next purification step after affinity chromatography was anion exchange. DrrA eluted from the column when the salt gradient reached 175 mM NaCl (Figure 5.3 A). The steep gradient led to an increasing salt concentration while DrrA was still eluting from the column which led to elution of contaminants together with DrrA (Figure 5.3 B). However most of the bands that appear on the SDS-PAGE with rising salt concentration are present in the first fraction as well and as the concentration of eluted DrrA rises, their concentration rises as well. This is possibly due to the fact that most contaminants are probably degradation products of full length DrrA and are therefore likely to have properties similar to those of full length DrrA. The size exclusion chromatography that is then performed with the less contaminant containing DrrA eliminates most of the other proteins present in the elution peak from anion exchange (Figure 5.4). Although a part of the DrrA elutes with a strong contaminant within the shoulder of the DrrA elution peak, the bigger part does contain only few contaminants. SDS-PAGE analysis reveals several weak contaminants in the fractions that contains the peak maxima but is relatively pure.

$DrrA_{202-647}$ includes the Rab-binding domain (residues 340 - 520; [193-194]) and was thus appropriate for complex formation. It behaved in a similar way as full length DrrA during the purification process. The only difference was that a cation exchange column had to be used instead of an anion exchange column for full length DrrA indicating that the isoelectric point of the smaller DrrA construct had changed. SDS-PAGE analysis of the elution peak from size exclusion seems to reveal a higher amount of contaminants, but the overall concentration of $DrrA_{202-647}$ is higher and it is therefore only normal that a higher concentration of contaminating proteins is also detected.

It was possible to form a complex of both DrrA constructs with Rab1a. The same low amounts of contaminants that were found in purified DrrA and $DrrA_{202-647}$ were present in the elution fractions of the complex (Figure 5.5 and Figure 5.9).

5.3.3. Crystallisation of DrrA, DrrA/Rab1a, DrrA202-647 and DrrA202-647/Rab1a

Although no crystals could be obtained for the complexes, it was possible to crystallise $DrrA_{202-647}$ and DrrA. The data set collected from a $DrrA_{202-647}$ crystal had a resolution of 4.5 Å. This is not enough to identify each atom's position in the electron density, however the overall conformation and the course of the main chain can be observed. Just after collection of this data set, the first structures of DrrA fragments with and without Rab1a were published [195-197]. The DrrA fragments were as follows: Schoebel and colleagues: 340-533; Suh and colleagues: 317-533; Zhu and colleagues: 195-550 in the structure of the complex and 317-647 of DrrA alone. This study used a DrrA construct with the residues 202-647. Superimposition of Rab1/$DrrA_{195-550}$ and $DrrA_{317-647}$ with the unrefined $DrrA_{202-647}$ structure revealed that the conformation of all three DrrA constructs was very similar. This means that the structure of the construct used here had been solved at a higher resolution than obtained by us thus far, therefore no further trials for higher diffracting crystals were set up and the existing data was not refined. The effort was targeted onto the crystallisation of full length DrrA. A structure of the N-terminus is known since the end of 2010 [313] but this structure is of a only the N-terminus (9-218) and therefore the full length DrrA still remains to be crystallised. Only recently this was successfully accomplished within the work presented here. Two types of crystals could be obtained. One crystal type (Figure 5.10) has not been proven to be a protein crystal yet, but its appearance and touch strongly suggest it is. It was possible to observe an initial diffraction pattern for the other crystal (Figure 5.11), but no complete data set at a high enough resolution that would permit structure determination has been collected yet.

Chapter 6

Final discussion and conclusion

6.1. Thermodynamics of Rab-effector complexes

The thermodynamic studies presented here are the first for detailed studies of Rab27 and its interactions with effectors. The technical difficulties associated with expression of soluble, full-length effectors, has also been overcome in this project. Although the effector is not perfectly pure, JFC1 has been purified to reasonable homogeneity and the the values for affinities can be reproducibly measured by isothermal titration calorimetry.

Fukuda had determined K_d values for three other Rab effectors and separated them into two groups, a high affinity group (K_d of 13.4 and 19.2 nM) and a low affinity group (K_d of 112 nM) [225]. The results obtained for WT Rab27 (46 nM) are in between those values. It is therefore difficult to confirm the affiliation of JFC1 to the so called 'low affinity group'. Possibly there are no different affinity groups but an affinity gradient, at least *in vitro*. In the cell, there are likely additional factors like the localisation in the cell and the relevant concentrations. As there was a fraction of protein associated with GDP, it is likely that a K_d of 46 nM is the upper limit of the interaction, and the interaction is somewhat stronger than this value. However, the GDP impurity is unlikely to lead to a 5-fold difference in K_d, especially given the observation that Rab27(GDP) retains significant binding affinity to JFC1.

Mutagenesis and comparisons of binding affinities can give insight into the importance that residues might have for complex formation. Here we could show that Tyr8 does contribute significantly to the affinity at the binding interface with JFC1. Tyr8 is conserved in Rab GTPases, indicating that its presence is not important for the specificity determination, but definitely for the formation of a tight complex. Asp91 has been shown to be important for the specificity of some effectors for Rab27. The fact that JFC1 is able to interact with Rab8 as well as Rab27, indicates that the residue might not be of a high importance for the recognition of Rab27 by JFC1. Here we show that the mutation, in the context of the triple mutant L84I+F88Y+D91G, still has a considerable effect. Rab27 and Rab8 can be co-localised within the cell [27, 256], this indicates that the interaction with Rab27 may be preferred if the proteins are present at similar concentrations. However, the affinity of Rab8 and JFC1 requires measurement to provide more insight into the structural basis for Rab/effector specificity.

The impact of the W73G mutation on the interaction of Rab27 with melanophilin was known to be devastating, but other Rab27 regulated pathways are not interrupted. Our results show, that the residue is of importance for a tight Rab27/effector interaction. The reduced affinity of a mutant can be expected for all Rab27/effector complexes, although in some effectors this loss can be compensated by the high contribution of other residues for the binding, whereas this is not the case in melanophilin, MyRIP and Slp3. An alanine scanning mutagenesis of residues identified to be important for some Rab27/effector interactions combined with an analysis of the thermodynamics would provide the different contributions of each towards the overall affinity and thus enable to qualitatively identify important residues.

It seems that there is no significant difference in binding affinity of JFC1 for active and inactive Rab27. A comparison of the switch regions of a Rab27(GDP) structure (PDB ID 2IEY [329]) with the known Rab27/effector structures does not provide information about a conformational change because the Rab27(GDP) structure shows a swapped dimer, a result of crystallisation [329], also see Figure 6.1. The swapped dimer arises from a non-canonical 'protruding' conformation of switch and interswitch regions that mediate dimerisation during crystal lattice formation [329]. The entire segment from β2 to β3 unravels and forms a domain-swapped homodimeric interface. However, the solution state of Rab27(GDP) is not dimeric, as evidenced by gel-filtration, pull-down, dynamic light scattering and small-angle X-ray diffraction [329]. Therefore, the relevance of the 'open' conformation is unclear, although most Rabs in their GDP state reveal significantly more flexibility in switch I. The solved Rab27/effector structures and our homology model reveal that the switch regions are involved in the interaction, but are not the only components. Because active and inactive Rab27 are recognised by JFC1 with similar affinities, it is possible that the switches involved in the binding have the same conformation, no matter which nucleotide is bound. Presuming that the switch/interswitch regions are flexible in the GDP state, it is possible that JFC1 binds to a pre-existing conformer that resembles the GTP-state, at an entropic cost. This would be consistent with the high negative ΔS observed upon complex formation between Rab27(GDP) and JFC1 (Table 3.1). On the other hand, the structure of uncomplexed Rab27(GppNHp) has not been determined. This structure needs to be visualised in order to complete the structural

and thermodynamic comparisons of GTP *vs.* GDP selectivity in Rab27 recognition by JFC1.

The biological implications of the relatively strong affinity between Rab27(GDP) and JFC1 remain to be elucidated. It has recently been observed that the interaction between the effector granuphilin and Rab27(GDP) is important for dense core vesicle exocytosis [264]. Moreover Rab27(GDP) is specifically recognised by coronin3, and this interaction has been shown to be important for the endocytosis of insulin granule membranes [258]. Previously a Rab(GDP) effector had also been reported for Rab11 [332]. The general wisdom is that an effector is defined as a GTP-dependent Rab-interacting protein that subsequently exerts a biological effect. However, the interactions between Rabs and interacting proteins may require consideration on a more individual basis, rather than a generalised conceptual view that may not hold true for all interacting proteins. Rab27 T23N does not interact with JFC1 but WT Rab27(GDP) does, which suggests that the mutation itself, rather than the nucleotide, is a determinant of binding [333]. Therefore, these studies imply caution when interpreting data from expression of GTP- and GDP-locked forms of Rabs in cells.

6.2. Structure determination of Ypt32 and comparison with other yeast trafficking proteins

A comparison of the structures of Ypt32(GppNHp) and Sec4(GppNHp) was performed in order to identify the determinants for effector recognition. It could be concluded that the α3 helix influences the switch II conformation, resulting in two different recognition surfaces for effectors. Both proteins interact with Myo2 at the same interface (and similar affinities) but with different domains of Sec2 as well as different other effectors [284-285, 292]. Interestingly the salt bridge forming Glu110 is conserved in all yeast Rab GTPases except for Sec4, where the corresponding residue is Thr117. However, mutational analysis suggests that Glu110/Thr117 is not the only residue important for different effector recognition by these GTPases [321].

It is possible that binding to Myo2 induces a change of the switch II region in one or both GTPases, that results in a common switch II conformation. Large conformational changes of the switch II region upon effector binding could be observed for human Rab11 in complex with Rab11-Family interacting proteins (FIP) FIP2 and FIP3 [47, 231, 334]. However, all other known Rab/effector complexes involve a pre-formed switch I/II conformation that effectively docks onto the Rab-binding domain of effectors [166]. The other possibility is that Ypt32 and Sec4 have different ways of recognising Myo2. Indeed their distinct roles in vesicle delivery and different binding affinities to Myo2 suggest that subtle differences in binding are possible, despite binding to an overlapping region of Myo2 [292]. Interestingly we could show, that switch II of Ypt32(GDP) undergoes a dramatic conformational change upon binding to GDI whereas the interaction of GDI with Sec4(GDP) requires few conformational changes of Sec4. This might be an indicator for a

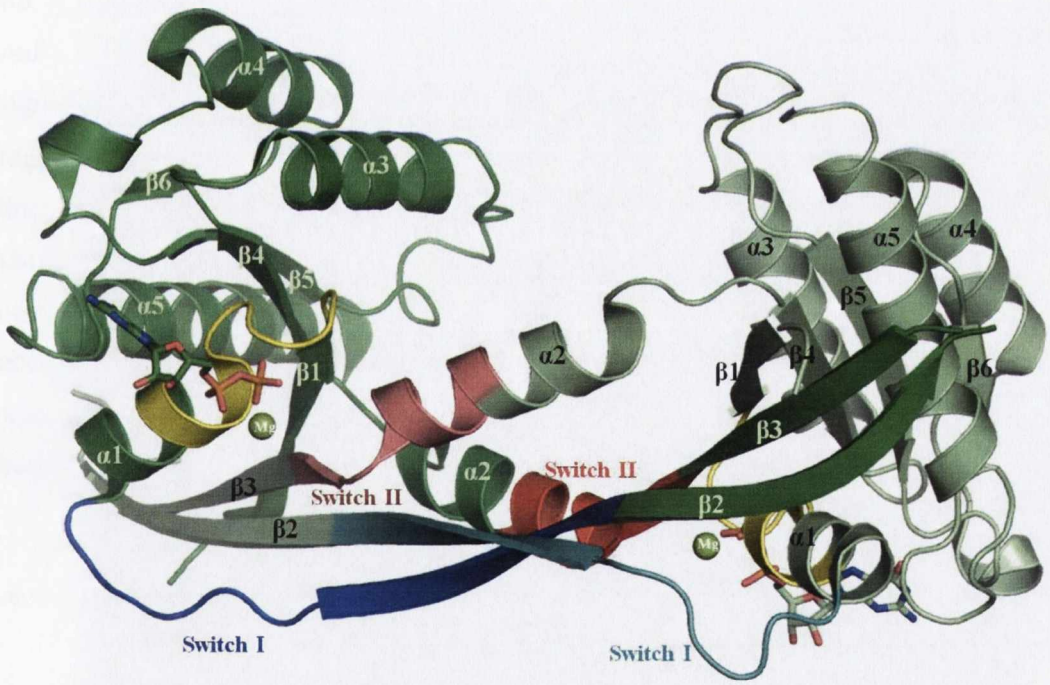

Figure 6.1 Crystal structure of Rab27(GDP).
Rab27 is shown in green, the p-loop in yellow, switch I in blue, switch II in red, GDP as sticks and Mg^{2+} as a green sphere. The first Rab27 molecule is depicted in darker colours and the second in light colours. The structure of Rab27(GDP) forms a swapped dimer upon crystallisation. The swapped dimer conformation involves the switch and interswitch regions; they mediate dimerisation during crystal lattice formation. PDB-file used for this figure: 2IF0, [329].

general higher flexibility of the Ypt32 switch II region. However it has to be taken into account that the GTP-bound form of a Rab GTPase is characterised by interactions between switch II and the γ-phosphate, and this is likely to reduce the switch flexibility compared to the GDP-bound form.

The question of how Myo2 recognises both GTPases, at different steps of the trafficking pathway, requires further investigation. More information is necessary – ideally, structures of Ypt32/Myo2 as well as Sec4/Myo2 – in order to understand the details of the Myo2 interaction site.

6.3. Rab-host pathogen and GEF interactions

The work presented here describes the crystallisation of a DrrA fragment (202-647) and full length DrrA. Although protein crystals could be obtained for both, the crystals could not be used for the collection of high resolution data. While crystal optimisation was ongoing, other groups published several structures of DrrA fragments and Rab1/DrrA-fragments [195-197, 313]. However no structure of full length DrrA has been solved so far. Since it has been shown that in addition to the GEF domain, DrrA possesses an additional AMPylation domain an observation of the 3-dimensional arrangement of all domains together might give more insight on how Rab1 is interacts with both domains [313]. Very recently, I was able to grow improved DrrA crystals (Figure 5.10), but no diffraction experiments have been performed on these, at this stage. However there is a possibility that these crystals will enable us to solve the structure of full length DrrA in the near future.

6.4. General implications of the work presented

The projects described in this work have focused on the identification of specificity determinants and mechanisms employed in interactions of Rab GTPases with various protein partners. Methods employed were crystallisation for structure determination and thermodynamic analyses. Over the course of this work it became clear, that the initial challenge of obtaining pure protein for those analyses was difficult to overcome, especially when using full length interaction partners of Rab GTPases. A review of the Rab/effector

structures deposited at the PDB (http://www.rcsb.org [316]) reveals that most Rab-effector complexes investigated structurally have to be obtained by co-expression of the partners. Therefore, despite approximately 10 Rab/effector structures, there is very little information regarding the thermodynamics and kinetics of effector recruitment. Hence it has not been possible to understand the strength of Rab/effector interfaces and the contribution of various residues to the binding affinities. Employing the bacterial protein Nus-A as a fusion protein for solubilisation as described by De Marco and colleagues [335], soluble expression of the full length Rab27 effector JFC1 was achieved. This enabled the investigation of the affinity determinants of one Rab-effector pair (Rab27-JFC1). The Nus-fusion technique seems promising in order to obtain other soluble Rab effectors that could then be used for thermodynamic analysis of the interactions employed by Rab/effector complexes.

Thermodynamic analysis enabled insights into the recognition mechanism employed by Rab/effector complexes. It was possible to confirm that a tryptophan mutation with a devastating impact on some Rab/effector complexes [104] does indeed reduce the affinity of our model system, Rab27/JFC1, to a significant extent. Our results emphasise the need of more thermodynamic analyses of Rab/effector complexes in order to improve our understanding of the biology. One interesting observation to emerge from this work is the significant residual affinity of Rab27(GDP) for JFC1. Some 'effectors' do interact with GDP-bound Rab [258, 264]. JFC1 had been the subject of controversy, as it had been reported to bind to WT Rab27 but not Rab27 T23N [274]. This study clearly shows a strong interaction between Rab27(GDP) and JFC1. The question is raised whether mutation of the p-loop serine or threonine to asparagine should be the method of choice for simulation of GDP-bound Rab. It is thought that this mutation disrupts the Mg^{2+} and that this reduces the affinity especially for GTP [42]. It is a possibility that at least in some Rab GTPases this mutation does not result in a correct simulation of the WT-GDP-bound Rab. It has to be noted that the GDP-locked mutant Rab27 T23N did bind granuphilin and coronin3 [258, 264], meaning that use of the T23N mutant only led to misleading results for the Rab27/JFC1 interaction. In any case these various studies bring into question the perception of Rab GTPases as 'on/off' switches [27-28, 336], although the reported interactions might just be very few exceptions from the general rule. Moreover, it is

important to consider the context of these interactions. If the binding of GDP dissociation inhibitor (GDI) is very tight for Rab27(GDP), then JFC1 and other effectors would be effectively out-competed and Rab27 would be extracted from the lipid bilayer. Thus, JFC1 would show an apparent GTP-dependence, although the relevant affinities are similar. This possibility necessitates the biophysical analyses of the interactions between GDI and Rab27, which unfortunately have not been performed to date. There are, however, very thorough structural and biophysical studies of yeast Rabs with GDI [24, 175]. The affinity between GDI and Sec4(GDP) is sub-nanomolar, implying that at least some Rabs are bound very tightly by GDI, whereas the interactions between Rab/effector complexes are generally weak with rapid on/off kinetics [226, 337].

In conclusion, the overall work represents a significant contribution to our understanding of Rab GTPases and their interactions with effectors. The wide range of Rab/effector affinities also raises key questions regarding the biology of vesicle trafficking. Placing the affinity of the W73A mutant of Rab27 into context, the affinity to JFC1 (K_d = 613 nM) is actually quite respectable, relative to other active Rab/effector complexes. For example, it is similar to the affinities between Rab11 and its effectors [47, 231, 334]. Some of the Rab11 effectors also contain a myosin binding site for aiding in vesicle transport. For example Rip11 and FIP2 have been shown to be involved into interactions with myosin V [338-340]. Although JFC1 does not link Rab27 to myosin, it has been reported to be involved in a multiprotein complex that mediates the interaction with kinesin [249]. In addition to this, melanophilin and other proteins with JFC1-like RBDs bind to myosin and mediate cargo transport. Thus, biological activity such as binding to myosin does not necessarily correlate with a requirement for higher affinity. However, a general observation is that Rab effectors that appear to act primarily in a tethering role appear to have relatively weak molecular interactions. In particular, the on/off rates of Rab6 with numerous effectors are fast, presumably to enable promiscuity and avoid becoming trapped. The association of Rab27 with actin or kinesin may require a tighter binding, e.g. for long-range vectorial transfer of vesicles. However, despite the identification of well over 100 effectors of Rab GTPases, the thermodynamics and kinetics of complex formation are poorly described.

Along with crystal structures and cellular assays, these interactions require more detailed analyses to understand the biology of membrane trafficking in health and disease.

References

1. Palade, G., *Intracellular aspects of the process of protein synthesis.* Science, 1975. **189**(4200): p. 347-58.
2. Griff, I.C., Schekman, R., Rothman, J.E., and Kaiser, C.A., *The yeast SEC17 gene product is functionally equivalent to mammalian alpha-SNAP protein.* The Journal of Biological Chemistry, 1992. **267**(17): p. 12106-15.
3. Wilson, D.W., Wilcox, C.A., Flynn, G.C., Chen, E., Kuang, W.J., Henzel, W.J., Block, M.R., Ullrich, A., and Rothman, J.E., *A fusion protein required for vesicle-mediated transport in both mammalian cells and yeast.* Nature, 1989. **339**(6223): p. 355-9.
4. Hammer, J.A. and Wu, X.S., *Rabs grab motors: defining the connections between Rab GTPases and motor proteins.* Current Opinion in Cell Biology, 2002. **14**(1): p. 69-75.
5. Peränen, J., Auvinen, P., Virta, H., Wepf, R., and Simons, K., *Rab8 promotes polarized membrane transport through reorganization of actin and microtubules in fibroblasts.* The Journal of Cell Biology, 1996. **135**(1): p. 153-67.
6. Short, B., Preisinger, C., Schaletzky, J., Kopajtich, R., and Barr, F.A., *The Rab6 GTPase regulates recruitment of the dynactin complex to Golgi membranes.* Current Biology, 2002. **12**(20): p. 1792-5.
7. Cai, H., Reinisch, K., and Ferro-Novick, S., *Coats, tethers, Rabs, and SNAREs work together to mediate the intracellular destination of a transport vesicle.* Developmental Cell, 2007. **12**(5): p. 671-82.
8. Sztul, E. and Lupashin, V., *Role of vesicle tethering factors in the ER-Golgi membrane traffic.* FEBS letters, 2009. **583**(23): p. 3770-83.
9. Grosshans, B.L., Ortiz, D., and Novick, P., *Rabs and their effectors: achieving specificity in membrane traffic.* Proceedings of the National Academy of Sciences of the United States of America, 2006. **103**(32): p. 11821-7.
10. Rothman, J.E., *Mechanisms of intracellular protein transport.* Nature, 1994. **372**(6501): p. 55-63.
11. Roth, T.F. and Porter, K.R., *Yolk protein uptake in the oocyte of the mosquito aedes Aegypti. L.* The Journal of Cell Biology, 1964. **20**: p. 313-32.
12. Pearse, B.M., *Coated vesicles from pig brain: purification and biochemical characterization.* Journal of Molecular Biology, 1975. **97**(1): p. 93-8.
13. Letourneur, F., Gaynor, E.C., Hennecke, S., Demolliere, C., Duden, R., Emr, S.D., Riezman, H., and Cosson, P., *Coatomer is essential for retrieval of dilysine-tagged proteins to the endoplasmic reticulum.* Cell, 1994. **79**(7): p. 1199-207.
14. Barlowe, C., Orci, L., Yeung, T., Hosobuchi, M., Hamamoto, S., Salama, N., Rexach, M.F., Ravazzola, M., Amherdt, M., and Schekman, R., *COPII: a membrane coat formed by Sec proteins that drive vesicle budding from the endoplasmic reticulum.* Cell, 1994. **77**(6): p. 895-907.
15. Bonifacino, J.S. and Glick, B.S., *The mechanisms of vesicle budding and fusion.* Cell, 2004. **116**(2): p. 153-66.
16. Ross, E.M. and Gilman, A.G., *Biochemical Properties of Hormone-Sensitive Adenylate Cyclase.* Annual Review of Biochemistry, 1980. **49**(1): p. 533-564.
17. Simon, M.I., Strathmann, M.P., and Gautam, N., *Diversity of G proteins in signal transduction.* Science, 1991. **252**(5007): p. 802-8.

18. Colicelli, J., *Human RAS superfamily proteins and related GTPases.* Science's STKE : Signal Transduction Knowledge Environment, 2004. **2004**(250): p. RE13-RE13.
19. Takai, Y., Sasaki, T., and Matozaki, T., *Small GTP-binding proteins.* Physiological Reviews, 2001. **81**(1): p. 153-208.
20. Milburn, M.V., Tong, L., DeVos, A.M., Brünger, A., Yamaizumi, Z., Nishimura, S., and Kim, S.H., *Molecular switch for signal transduction: structural differences between active and inactive forms of protooncogenic ras proteins.* Science, 1990. **247**(4945): p. 939-45.
21. Vetter, I.R. and Wittinghofer, a., *The guanine nucleotide-binding switch in three dimensions.* Science, 2001. **294**(5545): p. 1299-304.
22. Schmidt, A. and Hall, A., *Guanine nucleotide exchange factors for Rho GTPases: turning on the switch.* Genes & Development, 2002. **16**(13): p. 1587-609.
23. Bernards, A. and Settleman, J., *GAPs in growth factor signalling.* Growth Factors, 2005. **23**(2): p. 143-149.
24. Pylypenko, O., Rak, A., Durek, T., Kushnir, S., Dursina, B.E., Thomae, N.H., Constantinescu, A.T., Brunsveld, L., Watzke, A., Waldmann, H., Goody, R.S., and Alexandrov, K., *Structure of doubly prenylated Ypt1:GDI complex and the mechanism of GDI-mediated Rab recycling.* The EMBO Journal, 2006. **25**(1): p. 13-23.
25. Dirac-Svejstrup, A.B., Sumizawa, T., and Pfeffer, S.R., *Identification of a GDI displacement factor that releases endosomal Rab GTPases from Rab-GDI.* The EMBO Journal, 1997. **16**(3): p. 465-472.
26. Olofsson, B., *Rho guanine dissociation inhibitors: pivotal molecules in cellular signalling.* Cellular Signalling, 1999. **11**(8): p. 545-54.
27. Stenmark, H., *Rab GTPases as coordinators of vesicle traffic.* Nature Reviews. Molecular Cell Biology, 2009. **10**(8): p. 513-25.
28. Zerial, M. and McBride, H., *Rab proteins as membrane organizers.* Nature Reviews. Molecular Cell Biology, 2001. **2**(2): p. 107-17.
29. Herrmann, C., *Ras-effector interactions: after one decade.* Current Opinion in Structural Biology, 2003. **13**(1): p. 122-9.
30. Kirsten, W.H. and Mayer, L.A., *Malignant lymphomas of extrathymic origin induced in rats by murine erythroblastosis virus.* Journal of the National Cancer Institute, 1969. **43**(3): p. 735-46.
31. Harvey, J.J., *An Unidentified Virus which causes the Rapid Production of Tumours in Mice.* Nature, 1964. **204**(4963): p. 1104-1105.
32. Fransson, A., Ruusala, A., and Aspenstrom, P., *Atypical Rho GTPases have roles in mitochondrial homeostasis and apoptosis.* The Journal of Biological Chemistry, 2003. **278**(8): p. 6495-502.
33. Aspenstrom, P., Fransson, A., and Saras, J., *Rho GTPases have diverse effects on the organization of the actin filament system.* The Biochemical Journal, 2004. **377**(Pt 2): p. 327-37.
34. Weis, K., *Regulating access to the genome: nucleocytoplasmic transport throughout the cell cycle.* Cell, 2003. **112**(4): p. 441-51.
35. Donaldson, J.G., Cassel, D., Kahn, R.A., and Klausner, R.D., *ADP-ribosylation factor, a small GTP-binding protein, is required for binding of the coatomer protein*

beta-COP to Golgi membranes. Proceedings of the National Academy of Sciences of the United States of America, 1992. **89**(14): p. 6408-12.
36. Touchot, N., Chardin, P., and Tavitian, A., *Four additional members of the ras gene superfamily isolated by an oligonucleotide strategy: molecular cloning of YPT-related cDNAs from a rat brain library.* Proceedings of the National Academy of Sciences of the United States of America, 1987. **84**(23): p. 8210-4.
37. Goody, R.S., Rak, A., and Alexandrov, K., *The structural and mechanistic basis for recycling of Rab proteins between membrane compartments.* Cellular and Molecular Life Sciences, 2005. **62**(15): p. 1657-70.
38. Wennerberg, K., Rossman, K.L., and Der, C.J., *The Ras superfamily at a glance.* Journal of Cell Science, 2005. **118**(Pt 5): p. 843-6.
39. Bourne, H.R., Sanders, D.A., and McCormick, F., *The GTPase superfamily: conserved structure and molecular mechanism.* Nature, 1991. **349**(6305): p. 117-27.
40. Kjeldgaard, M., Nyborg, J., and Clark, B.F., *The GTP binding motif: variations on a theme.* The FASEB journal : Official Publication of the Federation of American Societies for Experimental Biology, 1996. **10**(12): p. 1347-68.
41. Saraste, M., Sibbald, P.R., and Wittinghofer, A., *The P-loop--a common motif in ATP- and GTP-binding proteins.* Trends in Biochemical Sciences, 1990. **15**(11): p. 430-4.
42. Farnsworth, C.L. and Feig, L.A., *Dominant inhibitory mutations in the Mg(2+)-binding site of RasH prevent its activation by GTP.* Molecular and Cellular Biology, 1991. **11**(10): p. 4822-9.
43. Rensland, H., John, J., Linke, R., Simon, I., Schlichting, I., Wittinghofer, A., and Goody, R.S., *Substrate and Product Structural Requirements for Binding of Nucleotides to H-ras p21: The Mechanism of Discrimination between Guanosine and Adenosine Nucleotides.* Biochemistry, 1995. **34**(2): p. 593-599.
44. Pai, E.F., Krengel, U., Petsko, G.A., Goody, R.S., Kabsch, W., and Wittinghofer, A., *Refined crystal structure of the triphosphate conformation of H-ras p21 at 1.35 A resolution: implications for the mechanism of GTP hydrolysis.* The EMBO Journal, 1990. **9**(8): p. 2351-9.
45. Geyer, M., Schweins, T., Herrmann, C., Prisner, T., Wittinghofer, A., and Kalbitzer, H.R., *Conformational Transitions in p21ras and in Its Complexes with the Effector Protein Raf-RBD and the GTPase Activating Protein GAP†.* Biochemistry, 1996. **35**(32): p. 10308-10320.
46. Sprang, S.R., *Conformational display: a role for switch polymorphism in the superfamily of regulatory GTPases.* Science's STKE : Signal Transduction Knowledge Environment, 2000. **2000**(50): p. pe1-pe1.
47. Jagoe, W.N., Lindsay, A.J., Read, R.J., McCoy, A.J., McCaffrey, M.W., and Khan, A.R., *Crystal structure of rab11 in complex with rab11 family interacting protein 2.* Structure, 2006. **14**(8): p. 1273-83.
48. Corbett, K.D. and Alber, T., *The many faces of Ras: recognition of small GTP-binding proteins.* Trends in Biochemical Sciences, 2001. **26**(12): p. 710-6.
49. Biou, V. and Cherfils, J., *Structural principles for the multispecificity of small GTP-binding proteins.* Biochemistry, 2004. **43**(22): p. 6833-40.
50. Kraulis, P.J., Domaille, P.J., Campbell-Burk, S.L., Van Aken, T., and Laue, E.D., *Solution structure and dynamics of ras p21.GDP determined by heteronuclear*

three- and four-dimensional NMR spectroscopy. Biochemistry, 1994. **33**(12): p. 3515-31.
51. Bock, J.B., Matern, H.T., Peden, A.A., and Scheller, R.H., *A genomic perspective on membrane compartment organization.* Nature, 2001. **409**(6822): p. 839-41.
52. Corbeel, L. and Freson, K., *Rab proteins and Rab-associated proteins: major actors in the mechanism of protein-trafficking disorders.* European Journal of Pediatrics, 2008. **167**(7): p. 723-9.
53. Chavrier, P., Parton, R.G., Hauri, H.P., Simons, K., and Zerial, M., *Localization of low molecular weight GTP binding proteins to exocytic and endocytic compartments.* Cell, 1990. **62**(2): p. 317-29.
54. Takamori, S., Holt, M., Stenius, K., Lemke, E.a., Grønborg, M., Riedel, D., Urlaub, H., Schenck, S., Brügger, B., Ringler, P., Müller, S.a., Rammner, B., Gräter, F., Hub, J.S., De Groot, B.L., Mieskes, G., Moriyama, Y., Klingauf, J., Grubmüller, H., Heuser, J., Wieland, F., and Jahn, R., *Molecular anatomy of a trafficking organelle.* Cell, 2006. **127**(4): p. 831-46.
55. Salminen, A. and Novick, P.J., *A ras-like protein is required for a post-Golgi event in yeast secretion.* Cell, 1987. **49**(4): p. 527-38.
56. McNew, J.A., Parlati, F., Fukuda, R., Johnston, R.J., Paz, K., Paumet, F., Söllner, T.H., and Rothman, J.E., *Compartmental specificity of cellular membrane fusion encoded in SNARE proteins.* Nature, 2000. **407**(6801): p. 153-9.
57. Sinka, R., Gillingham, A.K., Kondylis, V., and Munro, S., *Golgi coiled-coil proteins contain multiple binding sites for Rab family G proteins.* The Journal of Cell Biology, 2008. **183**(4): p. 607-15.
58. Allan, B.B., Moyer, B.D., and Balch, W.E., *Rab1 recruitment of p115 into a cis-SNARE complex: programming budding COPII vesicles for fusion.* Science, 2000. **289**(5478): p. 444-8.
59. Ohya, T., Miaczynska, M., Coskun, U., Lommer, B., Runge, A., Drechsel, D., Kalaidzidis, Y., and Zerial, M., *Reconstitution of Rab- and SNARE-dependent membrane fusion by synthetic endosomes.* Nature, 2009. **459**(7250): p. 1091-7.
60. Carroll, K.S., Hanna, J., Simon, I., Krise, J., Barbero, P., and Pfeffer, S.R., *Role of Rab9 GTPase in facilitating receptor recruitment by TIP47.* Science, 2001. **292**(5520): p. 1373-6.
61. Jedd, G., Mulholland, J., and Segev, N., *Two new Ypt GTPases are required for exit from the yeast trans-Golgi compartment.* The Journal of Cell Biology, 1997. **137**(3): p. 563-80.
62. McLauchlan, H., Newell, J., Morrice, N., Osborne, A., West, M., and Smythe, E., *A novel role for Rab5-GDI in ligand sequestration into clathrin-coated pits.* Current Biology, 1998. **8**(1): p. 34-45.
63. Pagano, A., Crottet, P., Prescianotto-Baschong, C., and Spiess, M., *In vitro formation of recycling vesicles from endosomes requires adaptor protein-1/clathrin and is regulated by rab4 and the connector rabaptin-5.* Molecular Biology of the Cell, 2004. **15**(11): p. 4990-5000.
64. Loubéry, S. and Coudrier, E., *Myosins in the secretory pathway: tethers or transporters?* Cellular and Molecular Life Sciences, 2008. **65**(18): p. 2790-800.
65. Schroer, T.A., Steuer, E.R., and Sheetz, M.P., *Cytoplasmic dynein is a minus end-directed motor for membranous organelles.* Cell, 1989. **56**(6): p. 937-46.

66. Lawrence, C.J., Dawe, R.K., Christie, K.R., Cleveland, D.W., Dawson, S.C., Endow, S.A., Goldstein, L.S., Goodson, H.V., Hirokawa, N., Howard, J., Malmberg, R.L., McIntosh, J.R., Miki, H., Mitchison, T.J., Okada, Y., Reddy, A.S., Saxton, W.M., Schliwa, M., Scholey, J.M., Vale, R.D., Walczak, C.E., and Wordeman, L., *A standardized kinesin nomenclature.* The Journal of Cell Biology, 2004. **167**(1): p. 19-22.
67. Paschal, B.M. and Vallee, R.B., *Retrograde transport by the microtubule-associated protein MAP 1C.* Nature, 1987. **330**(6144): p. 181-3.
68. Tuxworth, R.I. and Titus, M.A., *Unconventional myosins: anchors in the membrane traffic relay.* Traffic, 2000. **1**(1): p. 11-8.
69. Berg, J.S., Powell, B.C., and Cheney, R.E., *A millennial myosin census.* Molecular Biology of the Cell, 2001. **12**(4): p. 780-94.
70. Mehta, A.D., Rock, R.S., Rief, M., Spudich, J.A., Mooseker, M.S., and Cheney, R.E., *Myosin-V is a processive actin-based motor.* Nature, 1999. **400**(6744): p. 590-3.
71. Deretic, D., Huber, L.A., Ransom, N., Mancini, M., Simons, K., and Papermaster, D.S., *rab8 in retinal photoreceptors may participate in rhodopsin transport and in rod outer segment disk morphogenesis.* Journal of Cell Science, 1995. **108 (Pt 1**: p. 215-24.
72. Jordens, I., Marsman, M., Kuijl, C., and Neefjes, J., *Rab proteins, connecting transport and vesicle fusion.* Traffic, 2005. **6**(12): p. 1070-7.
73. Imamura, T., Huang, J., Usui, I., Satoh, H., Bever, J., and Olefsky, J.M., *Insulin-induced GLUT4 translocation involves protein kinase C-lambda-mediated functional coupling between Rab4 and the motor protein kinesin.* Molecular and Cellular Biology, 2003. **23**(14): p. 4892-900.
74. Bielli, A., Thornqvist, P.O., Hendrick, A.G., Finn, R., Fitzgerald, K., and McCaffrey, M.W., *The small GTPase Rab4A interacts with the central region of cytoplasmic dynein light intermediate chain-1.* Biochemical and Biophysical Research Communications, 2001. **281**(5): p. 1141-53.
75. Huang, J., Imamura, T., and Olefsky, J.M., *Insulin can regulate GLUT4 internalization by signaling to Rab5 and the motor protein dynein.* Proceedings of the National Academy of Sciences of the United States of America, 2001. **98**(23): p. 13084-9.
76. Hoepfner, S., Severin, F., Cabezas, A., Habermann, B., Runge, A., Gillooly, D., Stenmark, H., and Zerial, M., *Modulation of receptor recycling and degradation by the endosomal kinesin KIF16B.* Cell, 2005. **121**(3): p. 437-50.
77. Matanis, T., Akhmanova, A., Wulf, P., Del Nery, E., Weide, T., Stepanova, T., Galjart, N., Grosveld, F., Goud, B., De Zeeuw, C.I., Barnekow, A., and Hoogenraad, C.C., *Bicaudal-D regulates COPI-independent Golgi-ER transport by recruiting the dynein-dynactin motor complex.* Nature Cell Biology, 2002. **4**(12): p. 986-92.
78. Echard, A., Jollivet, F., Martinez, O., Lacapere, J.J., Rousselet, A., Janoueix-Lerosey, I., and Goud, B., *Interaction of a Golgi-associated kinesin-like protein with Rab6.* Science, 1998. **279**(5350): p. 580-5.
79. Jordens, I., Fernandez-Borja, M., Marsman, M., Dusseljee, S., Janssen, L., Calafat, J., Janssen, H., Wubbolts, R., and Neefjes, J., *The Rab7 effector protein RILP*

controls lysosomal transport by inducing the recruitment of dynein-dynactin motors. Current Biology, 2001. **11**(21): p. 1680-5.

80. Sahlender, D.A., Roberts, R.C., Arden, S.D., Spudich, G., Taylor, M.J., Luzio, J.P., Kendrick-Jones, J., and Buss, F., *Optineurin links myosin VI to the Golgi complex and is involved in Golgi organization and exocytosis.* The Journal of Cell Biology, 2005. **169**(2): p. 285-95.
81. Hattula, K. and Peranen, J., *FIP-2, a coiled-coil protein, links Huntingtin to Rab8 and modulates cellular morphogenesis.* Current Biology, 2000. **10**(24): p. 1603-6.
82. Lapierre, L.A., Kumar, R., Hales, C.M., Navarre, J., Bhartur, S.G., Burnette, J.O., Provance, D.W., Jr., Mercer, J.A., Bahler, M., and Goldenring, J.R., *Myosin vb is associated with plasma membrane recycling systems.* Molecular Biology of the Cell, 2001. **12**(6): p. 1843-57.
83. Hales, C.M., Vaerman, J.P., and Goldenring, J.R., *Rab11 family interacting protein 2 associates with myosin Vb and regulates plasma membrane recycling.* The Journal of Biological Chemistry, 2002. **277**(52): p. 50415-50421.
84. Fukuda, M., Kuroda, T.S., and Mikoshiba, K., *Slac2-a/melanophilin, the missing link between Rab27 and myosin Va: implications of a tripartite protein complex for melanosome transport.* The Journal of Biological Chemistry, 2002. **277**(14): p. 12432-6.
85. Strom, M., Hume, A.N., Tarafder, A.K., Barkagianni, E., and Seabra, M.C., *A family of Rab27-binding proteins. Melanophilin links Rab27a and myosin Va function in melanosome transport.* The Journal of Biological Chemistry, 2002. **277**(28): p. 25423-30.
86. Westbroek, W., Lambert, J., Bahadoran, P., Busca, R., Herteleer, M.C., Smit, N., Mommaas, M., Ballotti, R., and Naeyaert, J.M., *Interactions of human Myosin Va isoforms, endogenously expressed in human melanocytes, are tightly regulated by the tail domain.* The Journal of Investigative Dermatology, 2003. **120**(3): p. 465-75.
87. Wu, X., Wang, F., Rao, K., Sellers, J.R., and Hammer, J.A., 3rd, *Rab27a is an essential component of melanosome receptor for myosin Va.* Molecular Biology of the Cell, 2002. **13**(5): p. 1735-49.
88. Wu, X.S., Rao, K., Zhang, H., Wang, F., Sellers, J.R., Matesic, L.E., Copeland, N.G., Jenkins, N.A., and Hammer, J.A., 3rd, *Identification of an organelle receptor for myosin-Va.* Nature Cell Biology, 2002. **4**(4): p. 271-8.
89. Desnos, C., Schonn, J.-s., Huet, S., Tran, V.S., El-Amraoui, A., Raposo, G., Fanget, I., Chapuis, C., Ménasché, G., de Saint Basile, G., Petit, C., Cribier, S., Henry, J.-p., and Darchen, F., *Rab27A and its effector MyRIP link secretory granules to F-actin and control their motion towards release sites.* The Journal of Cell Biology, 2003. **163**(3): p. 559-70.
90. El-Amraoui, A., Schonn, J.-S., Küssel-Andermann, P., Blanchard, S., Desnos, C., Henry, J.-p., Wolfrum, U., Darchen, F., and Petit, C., *MyRIP, a novel Rab effector, enables myosin VIIa recruitment to retinal melanosomes.* EMBO Reports, 2002. **3**(5): p. 463-70.
91. Sönnichsen, B., De Renzis, S., Nielsen, E., Rietdorf, J., and Zerial, M., *Distinct membrane domains on endosomes in the recycling pathway visualized by multicolor imaging of Rab4, Rab5, and Rab11.* The Journal of Cell Biology, 2000. **149**(4): p. 901-14.

92. Rivera-Molina, F.E. and Novick, P.J., *A Rab GAP cascade defines the boundary between two Rab GTPases on the secretory pathway.* Proceedings of the National Academy of Sciences of the United States of America, 2009. **106**(34): p. 14408-13.
93. Rink, J., Ghigo, E., Kalaidzidis, Y., and Zerial, M., *Rab conversion as a mechanism of progression from early to late endosomes.* Cell, 2005. **122**(5): p. 735-49.
94. de Renzis, S., Sonnichsen, B., and Zerial, M., *Divalent Rab effectors regulate the sub-compartmental organization and sorting of early endosomes.* Nature Cell Biology, 2002. **4**(2): p. 124-33.
95. Nielsen, E., Christoforidis, S., Uttenweiler-Joseph, S., Miaczynska, M., Dewitte, F., Wilm, M., Hoflack, B., and Zerial, M., *Rabenosyn-5, a novel Rab5 effector, is complexed with hVPS45 and recruited to endosomes through a FYVE finger domain.* The Journal of Cell Biology, 2000. **151**(3): p. 601-12.
96. Christoforidis, S., Miaczynska, M., Ashman, K., Wilm, M., Zhao, L., Yip, S.C., Waterfield, M.D., Backer, J.M., and Zerial, M., *Phosphatidylinositol-3-OH kinases are Rab5 effectors.* Nature Cell Biology, 1999. **1**(4): p. 249-52.
97. Gruenberg, J., *The endocytic pathway: a mosaic of domains.* Nature Reviews. Molecular Cell Biology, 2001. **2**(10): p. 721-730.
98. Polo, S. and Di Fiore, P.P., *Endocytosis Conducts the Cell Signaling Orchestra.* Cell, 2006. **124**(5): p. 897-900.
99. Ceresa, B.P., *Regulation of EGFR endocytic trafficking by rab proteins.* Histology Histopathology, 2006. **21**(9): p. 987-93.
100. Romero Rosales, K., Peralta, E.R., Guenther, G.G., Wong, S.Y., and Edinger, A.L., *Rab7 activation by growth factor withdrawal contributes to the induction of apoptosis.* Molecular Biology of the Cell, 2009. **20**(12): p. 2831-40.
101. Zuchner, S. and Vance, J.M., *Mechanisms of Disease: a molecular genetic update on hereditary axonal neuropathies.* Nature Clinical Practice. Neurology, 2006. **2**(1): p. 45-53.
102. Verhoeven, K., De Jonghe, P., Coen, K., Verpoorten, N., Auer-Grumbach, M., Kwon, J.M., FitzPatrick, D., Schmedding, E., De Vriendt, E., Jacobs, A., Van Gerwen, V., Wagner, K., Hartung, H.-P., and Timmerman, V., *Mutations in the Small GTP-ase Late Endosomal Protein RAB7 Cause Charcot-Marie-Tooth Type 2B Neuropathy.* American Journal of Human Genetics, 2003. **72**(3): p. 722-727.
103. Seabra, M.C., Ho, Y.K., and Anant, J.S., *Deficient geranylgeranylation of Ram/Rab27 in choroideremia.* The Journal of Biological Chemistry, 1995. **270**(41): p. 24420-7.
104. Ménasché, G., Pastural, E., Feldmann, J., Certain, S., Ersoy, F., Dupuis, S., Wulffraat, N., Bianchi, D., Fischer, a., Le Deist, F., and de Saint Basile, G., *Mutations in RAB27A cause Griscelli syndrome associated with haemophagocytic syndrome.* Nature Genetics, 2000. **25**(2): p. 173-6.
105. Coxon, F.P. and Taylor, A., *Vesicular trafficking in osteoclasts.* Seminars in Cell & Developmental Biology, 2008. **19**(5): p. 424-33.
106. Seabra, M.C., Mules, E.H., and Hume, A.N., *Rab GTPases, intracellular traffic and disease.* Trends in Molecular Medicine, 2002. **8**(1): p. 23-30.
107. Chia, W.J. and Tang, B.L., *Emerging roles for Rab family GTPases in human cancer.* Biochimica et Biophysica Acta, 2009. **1795**(2): p. 110-6.

108. Mitra, S., Cheng, K.W., and Mills, G.B., *Rab GTPases implicated in inherited and acquired disorders.* Seminars in Cell & Developmental Biology, 2011. **22**(1): p. 57-68.
109. Shimada, K., Uzawa, K., Kato, M., Endo, Y., Shiiba, M., Bukawa, H., Yokoe, H., Seki, N., and Tanzawa, H., *Aberrant expression of RAB1A in human tongue cancer.* British Journal of Cancer, 2005. **92**(10): p. 1915-1921.
110. Hyvola, N., Diao, A., McKenzie, E., Skippen, A., Cockcroft, S., and Lowe, M., *Membrane targeting and activation of the Lowe syndrome protein OCRL1 by rab GTPases.* The EMBO Journal, 2006. **25**(16): p. 3750-3761.
111. Sklan, E.H., Staschke, K., Oakes, T.M., Elazar, M., Winters, M., Aroeti, B., Danieli, T., and Glenn, J.S., *A Rab-GAP TBC domain protein binds hepatitis C virus NS5A and mediates viral replication.* Journal of Virology, 2007. **81**(20): p. 11096-11105.
112. Derré, I. and Isberg, R.R., *Legionella pneumophila Replication Vacuole Formation Involves Rapid Recruitment of Proteins of the Early Secretory System.* Infection and Immunity, 2004. **72**(5): p. 3048-3053.
113. Yao, R., Wang, Y., Lubet, R.A., and You, M., *Differentially expressed genes associated with mouse lung tumor progression.* Oncogene, 2002. **21**(37): p. 5814-5821.
114. Culine, S., Honore, N., Tavitian, A., and Olofsson, B., *Overexpression of the ras-related rab2 gene product in peripheral blood mononuclear cells from patients with hematological and solid neoplasms.* Cancer Research, 1992. **52**(11): p. 3083-3088.
115. Culine, S., Rousseau-Merck, M.F., Honore, N., Nezelof, C., and Olofsson, B., *Specific expression of the ras-related rab3A gene in human normal and malignant neuroendocrine cells.* Cancer, 1992. **70**(10): p. 2552-2556.
116. Chen, J.S., Kuo, Y.B., Chou, Y.P., Chan, C.C., Fan, C.W., Chen, K.T., Huang, Y.S., and Chan, E.C., *Detection of autoantibodies against Rabphilin-3A-like protein as a potential biomarker in patient's sera of colorectal cancer.* Clinica Chimica Acta, 2011. **412**(15-16): p. 1417-1422.
117. Majó, G., Ferrer, I., Marsal, J., Blasi, J., and Aguado, F., *Immunocytochemical analysis of the synaptic proteins SNAP-25 and Rab3A in human pituitary adenomas. Overexpression of SNAP-25 in the mammosomatotroph lineages.* Journal of Pathology, 1997. **183**(4): p. 440-446.
118. Rotondo, F., Scheithauer, B.W., Kovacs, K., and Bell, D.C., *Rab3B immunoexpression in human pituitary adenomas.* Applied Immunohistochemistry and Molecular Morphology, 2009. **17**(3): p. 185-188.
119. Aligianis, I.A., Johnson, C.A., Gissen, P., Chen, D., Hampshire, D., Hoffmann, K., Maina, E.N., Morgan, N.V., Tee, L., Morton, J., Ainsworth, J.R., Horn, D., Rosser, E., Cole, T.R.P., Stolte-Dijkstra, I., Fieggen, K., Clayton-Smith, J., Mégarbané, A., Shield, J.P., Newbury-Ecob, R., Dobyns, W.B., Graham Jr, J.M., Kjaer, K.W., Warburg, M., Bond, J., Trembath, R.C., Harris, L.W., Takai, Y., Mundlos, S., Tannahill, D., Woods, C.G., and Maher, E.R., *Mutations of the catalytic subunit of RAB3GAP cause Warburg Micro syndrome.* Nature Genetics, 2005. **37**(3): p. 221-223.
120. Kaddai, V., Gonzalez, T., Keslair, F., Grémeaux, T., Bonnafous, S., Gugenheim, J., Tran, A., Gual, P., Le Marchand-Brustel, Y., and Cormont, M., *Rab4b is a small*

GTPase involved in the control of the glucose transporter GLUT4 localization in adipocyte. PLoS ONE, 2009. **4**(4).
121. Kaddai, V., Le Marchand-Brustel, Y., and Cormont, M., *Rab proteins in endocytosis and Glut4 trafficking.* Acta Physiologica, 2008. **192**(1): p. 75-88.
122. Li, Y.Y., Feng, H.C., Yu, C., Rong, Z., Song, Y., Liu, C.X., Wang, W.R., and Pu, L., *Differential expression of RAB5A in human lung adenocarcinoma cells with different metastasis potential.* Clinical and Experimental Metastasis, 1999. **17**(3): p. 213-219.
123. Wang, Y.J., Li, H.Y., Li, Y., and Min, J., *The expression and clinical significance of RABEX-5 and RAB5 in breast cancer.* Journal of Sichuan University (Medical Science Edition), 2011. **42**(2): p. 185-189.
124. Liu, S.S., Chen, X.M., Zheng, H.X., Shi, S.L., and Li, Y., *Knockdown of Rab5a expression decreases cancer cell motility and invasion through integrin-mediated signaling pathway.* Journal of Biomedical Science, 2011. **18**(1).
125. Torres, V.A. and Stupack, D.G., *Rab5 in the regulation of cell motility and invasion.* Current Protein and Peptide Science, 2011. **12**(1): p. 43-51.
126. Yan, H., Jahanshahi, M., Horvath, E.A., Liu, H.Y., and Pfleger, C.M., *Rabex-5 ubiquitin ligase activity restricts Ras signaling to establish pathway homeostasis in drosophila.* Current Biology, 2010. **20**(15): p. 1378-1382.
127. Baskys, A., Bayazitov, I., Zhu, E., Fang, L., and Wang, R., *Rab-mediated endocytosis.* Annals of the New York Academy of Sciences, 2007. **1122**: p. 313-329.
128. Topp, J.D., Gray, N.W., Gerard, R.D., and Horazdovsky, B.F., *Alsin is a Rab5 and Rac1 guanine nucleotide exchange factor.* The Journal of Biological Chemistry, 2004. **279**(23): p. 24612-24623.
129. Pal, A., Severin, F., Lommer, B., Shevchenko, A., and Zerial, M., *Huntingtin-HAP40 complex is a novel Rab5 effector that regulates early endosome motility and is up-regulated in Huntington's disease.* The Journal of Cell Biology, 2006. **172**(4): p. 605-618.
130. Prada-Delgado, A., Carrasco-Marín, E., Peña-Macarro, C., del Cerro-Vadillo, E., Fresno-Escudero, M., Leyva-Cobián, F., and Alvarez-Dominguez, C., *Inhibition of Rab5a exchange activity is a key step for Listeria monocytogenes survival.* Traffic, 2005. **6**(3): p. 252-265.
131. Auer-Grumbach, M., *Hereditary sensory neuropathy type I.* Orphanet Journal of Rare Diseases, 2008. **3**(1): p. 7.
132. Choudhury, A., Dominguez, M., Puri, V., Sharma, D.K., Narita, K., Wheatley, C.L., Marks, D.L., and Pagano, R.E., *Rab proteins mediate Golgi transport of caveola-internalized glycosphingolipids and correct lipid trafficking in Niemann-Pick C cells.* The Journal of Clinical Investigation, 2002. **109**(12): p. 1541-1550.
133. Ginsberg, S.D., Mufson, E.J., Alldred, M.J., Counts, S.E., Wuu, J., Nixon, R.A., and Che, S., *Upregulation of select rab GTPases in cholinergic basal forebrain neurons in mild cognitive impairment and Alzheimer's disease.* Journal of Chemical Neuroanatomy, 2011. **42**(2): p. 102-110.
134. Cataldo, A.M., Mathews, P.M., Boiteau, A.B., Hassinger, L.C., Peterhoff, C.M., Jiang, Y., Mullaney, K., Neve, R.L., Gruenberg, J., and Nixon, R.A., *Down syndrome fibroblast model of Alzheimer-related endosome pathology: Accelerated*

endocytosis promotes late endocytic defects. American Journal of Pathology, 2008. **173**(2): p. 370-384.
135. Batista, D.G.J., Silva, C.F., Mota, R.A., Costa, L.C., Meirelles, M.N.L., Meuser-Batista, M., and Soeiro, M.N.C., *Trypanosoma cruzi modulates the expression of rabs and alters the endocytosis in mouse cardiomyocytes in vitro.* Journal of Histochemistry and Cytochemistry, 2006. **54**(6): p. 605-614.
136. Laezza, C., Bucci, C., Santillo, M., Bruni, C.B., and Bifulco, M., *Control of Rab5 and Rab7 expression by the isoprenoid pathway.* Biochemical and Biophysical Research Communications, 1998. **248**(3): p. 469-472.
137. Chakraborty, A.K., Funasaka, Y., Araki, K., Horikawa, T., and Ichihashi, M., *Evidence that the small GTPase Rab8 is involved in melanosome traffic and dendrite extension in B16 melanoma cells.* Cell and Tissue Research, 2003. **314**(3): p. 381-388.
138. Chi, Z.L., Akahori, M., Obazawa, M., Minami, M., Noda, T., Nakaya, N., Tomarev, S., Kawase, K., Yamamoto, T., Noda, S., Sasaoka, M., Shimazaki, A., Takada, Y., and Iwata, T., *Overexpression of optineurin E50K disrupts Rab8 interaction and leads to a progressive retinal degeneration in mice.* Human Molecular Genetics, 2010. **19**(13): p. 2606-2615.
139. Sato, T., Mushiake, S., Kato, Y., Sato, K., Sato, M., Takeda, N., Ozono, K., Miki, K., Kubo, Y., Tsuji, A., Harada, R., and Harada, A., *The Rab8 GTPase regulates apical protein localization in intestinal cells.* Nature, 2007. **448**(7151): p. 366-369.
140. Lakkaraju, A. and Rodriguez-Boulan, E., *Cell biology: Caught in the traffic.* Nature, 2007. **448**(7151): p. 266-267.
141. Nachury, M.V., Loktev, A.V., Zhang, Q., Westlake, C.J., Peränen, J., Merdes, A., Slusarski, D.C., Scheller, R.H., Bazan, J.F., Sheffield, V.C., and Jackson, P.K., *A Core Complex of BBS Proteins Cooperates with the GTPase Rab8 to Promote Ciliary Membrane Biogenesis.* Cell, 2007. **129**(6): p. 1201-1213.
142. Mosesson, Y., Mills, G.B., and Yarden, Y., *Derailed endocytosis: An emerging feature of cancer.* Nature Reviews. Cancer, 2008. **8**(11): p. 835-850.
143. Ohira, M., Oshitani, N., Hosomi, S., Watanabe, K., Yamagami, H., Tominaga, K., Watanabe, T., Fujiwara, Y., Maeda, K., Hirakawa, K., and Arakawa, T., *Dislocation of Rab13 and vasodilator-stimulated phosphoprotein in inactive colon epithelium in patients with Crohn's disease.* International Journal of Molecular Medicine, 2009. **24**(6): p. 829-835.
144. Jacobsen, M., Repsilber, D., Gutschmidt, A., Neher, A., Feldmann, K., Mollenkopf, H.J., Ziegler, A., and Kaufmann, S.H.E., *Ras-associated small GTPase 33A, a novel T cell factor, is down-regulated in patients with tuberculosis.* Journal of Infectious Diseases, 2005. **192**(7): p. 1211-1218.
145. Jenkins, D., Seelow, D., Jehee, F.S., Perlyn, C.A., Alonso, L.G., Bueno, D.F., Donnai, D., Josifiova, D., Mathijssen, I.M.J., Morton, J.E.V., Ørstavik, K.H., Sweeney, E., Wall, S.A., Marsh, J.L., Nürnberg, P., Passos-Bueno, M.R., and Wilkie, A.O.M., *RAB23 mutations in carpenter syndrome imply an unexpected role for Hedgehog signaling in cranial-suture development and obesity.* American Journal of Human Genetics, 2007. **80**(6): p. 1162-1170.

146. Cohen Jr, M.M., *Perspectives on craniosynostosis: Sutural biology, some well-known syndromes, and some unusual syndromes.* Journal of Craniofacial Surgery, 2009. **20**(SUPPL. 1): p. 646-651.
147. He, H., Dai, F., Yu, L., She, X., Zhao, Y., Jiang, J., Chen, X., and Zhao, S., *Identification and characterization of nine novel human small GTPases showing variable expressions in liver cancer tissues.* Gene Expression, 2002. **10**(5-6): p. 231-242.
148. Hou, Q., Yong, H.W., Grabsch, H., Zhu, Y., Siew, H.L., Ganesan, K., Cross, D., Lay, K.T., Tao, J., Gopalakrishnan, V., Bor, L.T., Oi, L.K., and Tan, P., *Integrative genomics identifies RAB23 as an invasion mediator gene in diffuse-type gastric cancer.* Cancer Research, 2008. **68**(12): p. 4623-4630.
149. Alory, C. and Balch, W.E., *Organization of the Rab-GDI/CHM superfamily: the functional basis for choroideremia disease.* Traffic, 2001. **2**(8): p. 532-43.
150. Wang, J.-S., Wang, F.-B., Zhang, Q.-G., Shen, Z.-Z., and Shao, Z.-M., *Enhanced expression of Rab27A gene by breast cancer cells promoting invasiveness and the metastasis potential by secretion of insulin-like growth factor-II.* Molecular Cancer Research, 2008. **6**(3): p. 372-82.
151. Hendrix, A., Maynard, D., Pauwels, P., Braems, G., Denys, H., Van den Broecke, R., Lambert, J., Van Belle, S., Cocquyt, V., Gespach, C., Bracke, M., Seabra, M.C., Gahl, W.a., De Wever, O., and Westbroek, W., *Effect of the secretory small GTPase Rab27B on breast cancer growth, invasion, and metastasis.* Journal of the National Cancer Institute, 2010. **102**(12): p. 866-80.
152. Hendrix, A., Westbroek, W., Bracke, M., and De Wever, O., *An ex(o)citing machinery for invasive tumor growth.* Cancer Research, 2010. **70**(23): p. 9533-7.
153. Kotzsch, M., Sieuwerts, A.M., Grosser, M., Meye, A., Fuessel, S., Meijer-Van Gelder, M.E., Smid, M., Schmitt, M., Baretton, G., Luther, T., Magdolen, V., and Foekens, J.A., *Urokinase receptor splice variant uPAR-del4/5-associated gene expression in breast cancer: Identification of rab31 as an independent prognostic factor.* Breast Cancer Research and Treatment, 2008. **111**(2): p. 229-240.
154. Di Pietro, S.M. and Dell'Angelica, E.C., *The cell biology of Hermansky-Pudlak syndrome: Recent advances.* Traffic, 2005. **6**(7): p. 525-533.
155. Oiso, N., Riddle, S., Serikawa, T., Kuramoto, T., and Spritz, R., *The rat Ruby (<i>R</i>) locus is <i>Rab38</i>: identical mutations in Fawn-hooded and Tester-Moriyama rats derived from an ancestral Long Evans rat sub-strain.* Mammalian Genome, 2004. **15**(4): p. 307-314.
156. Khosravi-Far, R., Lutz, R.J., Cox, A.D., Conroy, L., Bourne, J.R., Sinensky, M., Balch, W.E., Buss, J.E., and Der, C.J., *Isoprenoid modification of rab proteins terminating in CC or CXC motifs.* Proceedings of the National Academy of Sciences of the United States of America, 1991. **88**(14): p. 6264-8.
157. Anant, J.S., Desnoyers, L., Machius, M., Demeler, B., Hansen, J.C., Westover, K.D., Deisenhofer, J., and Seabra, M.C., *Mechanism of Rab geranylgeranylation: formation of the catalytic ternary complex.* Biochemistry, 1998. **37**(36): p. 12559-68.
158. Wu, S.K., Zeng, K., Wilson, I.A., and Balch, W.E., *Structural insights into the function of the Rab GDI superfamily.* Trends in Biochemical Sciences, 1996. **21**(12): p. 472-6.

159. Pereira-Leal, J.B., Hume, A.N., and Seabra, M.C., *Prenylation of Rab GTPases: molecular mechanisms and involvement in genetic disease.* FEBS letters, 2001. **498**(2-3): p. 197-200.
160. Alory, C. and Balch, W.E., *Molecular basis for Rab prenylation.* The Journal of Cell Biology, 2000. **150**(1): p. 89-103.
161. Fukuda, M., *Distinct Rab binding specificity of Rim1, Rim2, rabphilin, and Noc2. Identification of a critical determinant of Rab3A/Rab27A recognition by Rim2.* The Journal of Biological Chemistry, 2003. **278**(17): p. 15373-80.
162. Olkkonen, V.M. and Stenmark, H., *Role of Rab GTPases in membrane traffic.* International Review of Cytology, 1997. **176**: p. 1-85.
163. Pereira-Leal, J.B. and Seabra, M.C., *The mammalian Rab family of small GTPases: definition of family and subfamily sequence motifs suggests a mechanism for functional specificity in the Ras superfamily.* Journal of Molecular Biology, 2000. **301**(4): p. 1077-87.
164. Pereira-Leal, J.B. and Seabra, M.C., *Evolution of the Rab family of small GTP-binding proteins.* Journal of Molecular Biology, 2001. **313**(4): p. 889-901.
165. Buvelot Frei, S., Rahl, P.B., Nussbaum, M., Briggs, B.J., Calero, M., Janeczko, S., Regan, A.D., Chen, C.Z., Barral, Y., Whittaker, G.R., and Collins, R.N., *Bioinformatic and comparative localization of Rab proteins reveals functional insights into the uncharacterised GTPases Ypt10p and Ypt11p.* Molecular and Cellular Biology, 2006. **26**(19): p. 7299-317.
166. Lee, M.-T.G., Mishra, A., and Lambright, D.G., *Structural mechanisms for regulation of membrane traffic by rab GTPases.* Traffic, 2009. **10**(10): p. 1377-89.
167. Itzen, A. and Goody, R.S., *Key determinants of Rab specificity.* Structure, 2008. **16**(10): p. 1437-9.
168. Ostermeier, C. and Brunger, A.T., *Structural basis of Rab effector specificity: crystal structure of the small G protein Rab3A complexed with the effector domain of rabphilin-3A.* Cell, 1999. **96**(3): p. 363-74.
169. Kukimoto-Niino, M., Sakamoto, A., Kanno, E., Hanawa-Suetsugu, K., Terada, T., Shirouzu, M., Fukuda, M., and Yokoyama, S., *Structural basis for the exclusive specificity of Slac2-a/melanophilin for the Rab27 GTPases.* Structure, 2008. **16**(10): p. 1478-90.
170. Pfeffer, S.R., Dirac-Svejstrup, A.B., and Soldati, T., *Rab GDP Dissociation Inhibitor: Putting Rab GTPases in the Right Place.* The Journal of Biological Chemistry, 1995. **270**(29): p. 17057-17059.
171. Sasaki, T., Kikuchi, A., Araki, S., Hata, Y., Isomura, M., Kuroda, S., and Takai, Y., *Purification and characterization from bovine brain cytosol of a protein that inhibits the dissociation of GDP from and the subsequent binding of GTP to smg p25A, a ras p21-like GTP-binding protein.* The Journal of Biological Chemistry, 1990. **265**(4): p. 2333-7.
172. Ullrich, O., Stenmark, H., Alexandrov, K., Huber, L.A., Kaibuchi, K., Sasaki, T., Takai, Y., and Zerial, M., *Rab GDP dissociation inhibitor as a general regulator for the membrane association of rab proteins.* The Journal of Biological Chemistry, 1993. **268**(24): p. 18143-50.
173. Rak, A., Pylypenko, O., Durek, T., Watzke, A., Kushnir, S., Brunsveld, L., Waldmann, H., Goody, R.S., and Alexandrov, K., *Structure of Rab GDP-*

dissociation inhibitor in complex with prenylated YPT1 GTPase. Science, 2003. **302**(5645): p. 646-50.
174. Rak, A., Pylypenko, O., Niculae, A., Pyatkov, K., Goody, R.S., and Alexandrov, K., *Structure of the Rab7:REP-1 complex: insights into the mechanism of Rab prenylation and choroideremia disease.* Cell, 2004. **117**(6): p. 749-60.
175. Ignatev, A., Kravchenko, S., Rak, A., Goody, R.S., and Pylypenko, O., *A Structural Model of the GDP Dissociation Inhibitor Rab Membrane Extraction Mechanism.* The Journal of Biological Chemistry, 2008. **283**(26): p. 18377-18384.
176. An, Y., Shao, Y., Alory, C., Matteson, J., Sakisaka, T., Chen, W., Gibbs, R.A., Wilson, I.A., and Balch, W.E., *Geranylgeranyl switching regulates GDI-Rab GTPase recycling.* Structure, 2003. **11**(03): p. 347-57.
177. Schalk, I., Zeng, K., Wu, S.K., Stura, E.A., Matteson, J., Huang, M., Tandon, A., Wilson, I.A., and Balch, W.E., *Structure and mutational analysis of Rab GDP-dissociation inhibitor.* Nature, 1996. **381**(6577): p. 42-8.
178. Pfeffer, S. and Aivazian, D., *Targeting Rab GTPases to distinct membrane compartments.* Nature Reviews Molecular Cell Biology, 2004. **5**(11): p. 886-896.
179. Luan, P., Heine, A., Zeng, K., Moyer, B., Greasely, S.E., Kuhn, P., Balch, W.E., and Wilson, I.A., *A New Functional Domain of Guanine Nucleotide Dissociation Inhibitor (α-GDI) Involved in Rab Recycling.* Traffic, 2000. **1**(3): p. 270-281.
180. Zhang, H., *Binding platforms for Rab prenylation and recycling: Rab escort protein, RabGGT, and RabGDI.* Structure, 2003. **11**(03): p. 237-9.
181. Pylypenko, O., Rak, A., Reents, R., Niculae, A., Sidorovitch, V., Cioaca, M.D., Bessolitsyna, E., Thomä, N.H., Waldmann, H., Schlichting, I., Goody, R.S., and Alexandrov, K., *Structure of Rab escort protein-1 in complex with Rab geranylgeranyltransferase.* Molecular Cell, 2003. **11**(2): p. 483-94.
182. Pylypenko, O., Rak, A., Reents, R., Niculae, A., Sidorovitch, V., Cioaca, M.D., Bessolitsyna, E., Thoma, N.H., Waldmann, H., Schlichting, I., Goody, R.S., and Alexandrov, K., *Structure of Rab escort protein-1 in complex with Rab geranylgeranyltransferase.* Molecular Cell, 2003. **11**(2): p. 483-94.
183. Suzanne R, P., *Rab GTPases: master regulators of membrane trafficking.* Current Opinion in Cell Biology, 1994. **6**(4): p. 522-526.
184. Sivars, U., Aivazian, D., and Pfeffer, S.R., *Yip3 catalyses the dissociation of endosomal Rab-GDI complexes.* Nature, 2003. **425**(6960): p. 856-859.
185. Cherfils, J. and Chardin, P., *GEFs: Structural basis for their activation of small GTP-binding proteins.* Trends in Biochemical Sciences, 1999. **24**(8): p. 306-311.
186. Itzen, A. and Goody, R.S., *GTPases involved in vesicular trafficking: structures and mechanisms.* Seminars in Cell & Developmental Biology, 2011. **22**(1): p. 48-56.
187. Carney, D.S., Davies, B.A., and Horazdovsky, B.F., *Vps9 domain-containing proteins: Activators of Rab5 GTPases from yeast to neurons.* Trends in Cell Biology, 2006. **16**(1): p. 27-35.
188. Delprato, A. and Lambright, D.G., *Structural basis for Rab GTPase activation by VPS9 domain exchange factors.* Nature Structural and Molecular Biology, 2007. **14**(5): p. 406-412.
189. Gasper, R., Thomas, C., Reza Ahmadian, M., and Wittinghofer, A., *The Role of the Conserved Switch II Glutamate in Guanine Nucleotide Exchange Factor-Mediated*

Nucleotide Exchange of GTP-Binding Proteins. Journal of Molecular Biology, 2008. **379**(1): p. 51-63.
190. Dong, G., Medkova, M., Novick, P., and Reinisch, K.M., *A Catalytic Coiled Coil: Structural Insights into the Activation of the Rab GTPase Sec4p by Sec2p.* Molecular Cell, 2007. **25**(3): p. 455-462.
191. Sato, Y., Shirakawa, R., Horiuchi, H., Dohmae, N., Fukai, S., and Nureki, O., *Asymmetric Coiled-Coil Structure with Guanine Nucleotide Exchange Activity.* Structure, 2007. **15**(2): p. 245-252.
192. Murata, T., Delprato, A., Ingmundson, A., Toomre, D.K., Lambright, D.G., and Roy, C.R., *The Legionella pneumophila effector protein DrrA is a Rab1 guanine nucleotide-exchange factor.* Nature Cell Biology, 2006. **8**(9): p. 971-977.
193. Ingmundson, A., Delprato, A., Lambright, D.G., and Roy, C.R., *Legionella pneumophila proteins that regulate Rab1 membrane cycling.* Nature, 2007. **450**(7168): p. 365-369.
194. Machner, M.P. and Isberg, R.R., *A bifunctional bacterial protein links GDI displacement to Rab1 activation.* Science, 2007. **318**(5852): p. 974-977.
195. Schoebel, S., Oesterlin, L.K., Blankenfeldt, W., Goody, R.S., and Itzen, A., *RabGDI Displacement by DrrA from Legionella Is a Consequence of Its Guanine Nucleotide Exchange Activity.* Molecular Cell, 2009. **36**(6): p. 1060-1072.
196. Suh, H.-y., Lee, D.-W., Lee, K.-h., Ku, B., Choi, S.-J., Woo, J.-s., Kim, Y.-g., and Oh, B.-h., *Structural insights into the dual nucleotide exchange and GDI displacement activity of SidM/DrrA.* The EMBO Journal, 2010. **29**(2): p. 496-504.
197. Zhu, Y., Hu, L., Zhou, Y., Yao, Q., Liu, L., and Shao, F., *Structural mechanism of host Rab1 activation by the bifunctional Legionella type IV effector SidM/DrrA.* Proceedings of the National Academy of Sciences of the United States of America, 2010. **107**(10): p. 4699-4704.
198. Guo, Z., Ahmadian, M.R., and Goody, R.S., *Guanine nucleotide exchange factors operate by a simple allosteric competitive mechanism.* Biochemistry, 2005. **44**(47): p. 15423-9.
199. Klebe, C., Prinz, H., Wittinghofer, A., and Goody, R.S., *The kinetic mechanism of Ran--nucleotide exchange catalyzed by RCC1.* Biochemistry, 1995. **34**(39): p. 12543-52.
200. Wittinghofer, A., *Phosphoryl transfer in Ras proteins, conclusive or elusive?* Trends in Biochemical Sciences, 2006. **31**(1): p. 20-3.
201. Lassila, J.K., Zalatan, J.G., and Herschlag, D., *Biological phosphoryl-transfer reactions: understanding mechanism and catalysis.* Annual Review of Biochemistry, 2011. **80**: p. 669-702.
202. Scheffzek, K. and Ahmadian, M., *GTPase activating proteins: structural and functional insights 18 years after discovery.* Cellular and Molecular Life Sciences, 2005. **62**(24): p. 3014-3038.
203. Lanzetti, L., Rybin, V., Malabarba, M.G., Christoforidis, S., Scita, G., Zerial, M., and Di Fiore, P.P., *The Eps8 protein coordinates EGF receptor signalling through Rac and trafficking through Rab5.* Nature, 2000. **408**(6810): p. 374-7.
204. Rak, A., Fedorov, R., Alexandrov, K., Albert, S., Goody, R.S., Gallwitz, D., and Scheidig, A.J., *Crystal structure of the GAP domain of Gyp1p: first insights into interaction with Ypt/Rab proteins.* The EMBO Journal, 2000. **19**(19): p. 5105-13.

205. Albert, S. and Gallwitz, D., *Two new members of a family of Ypt/Rab GTPase activating proteins. Promiscuity of substrate recognition.* The Journal of Biological Chemistry, 1999. **274**(47): p. 33186-9.
206. Will, E. and Gallwitz, D., *Biochemical Characterization of Gyp6p, a Ypt/Rab-specific GTPase-activating Protein from Yeast.* The Journal of Biological Chemistry, 2001. **276**(15): p. 12135-12139.
207. Cuif, M.H., Possmayer, F., Zander, H., Bordes, N., Jollivet, F., Couedel-Courteille, A., Janoueix-Lerosey, I., Langsley, G., Bornens, M., and Goud, B., *Characterization of GAPCenA, a GTPase activating protein for Rab6, part of which associates with the centrosome.* The EMBO Journal, 1999. **18**(7): p. 1772-82.
208. Neuwald, A.F., *A shared domain between a spindle assembly checkpoint protein and Ypt/Rab-specific GTPase-activators.* Trends in Biochemical Sciences, 1997. **22**(7): p. 243-244.
209. Nagano, F., Sasaki, T., Fukui, K., Asakura, T., Imazumi, K., and Takai, Y., *Molecular Cloning and Characterization of the Noncatalytic Subunit of the Rab3 Subfamily-specific GTPase-activating Protein.* The Journal of Biological Chemistry, 1998. **273**(38): p. 24781-24785.
210. Tempel, W., Tong, Y., Dimov, S., Bochkarev, A., and Park, H., *First crystallographic models of human TBC domains in the context of a family-wide structural analysis.* Proteins, 2008. **71**(1): p. 497-502.
211. Wittinghofer, A., Scheffzek, K., and Ahmadian, M.R., *The interaction of Ras with GTPase-activating proteins.* FEBS letters, 1997. **410**(1): p. 63-67.
212. Albert, S., Will, E., and Gallwitz, D., *Identification of the catalytic domains and their functionally critical arginine residues of two yeast GTPase-activating proteins specific for Ypt/Rab transport GTPases.* The EMBO Journal, 1999. **18**(19): p. 5216-25.
213. Pan, X., Eathiraj, S., Munson, M., and Lambright, D.G., *TBC-domain GAPs for Rab GTPases accelerate GTP hydrolysis by a dual-finger mechanism.* Nature, 2006. **442**(7100): p. 303-306.
214. Feuerstein, J., Goody, R.S., and Webb, M.R., *The mechanism of guanosine nucleotide hydrolysis by p21 c-Ha-ras. The stereochemical course of the GTPase reaction.* The Journal of Biological Chemistry, 1989. **264**(11): p. 6188-6190.
215. Allin, C., Ahmadian, M.R., Wittinghofer, A., and Gerwert, K., *Monitoring the GAP catalyzed H-Ras GTPase reaction at atomic resolution in real time.* Proceedings of the National Academy of Sciences, 2001. **98**(14): p. 7754-7759.
216. Kötting, C., Blessenohl, M., Suveyzdis, Y., Goody, R.S., Wittinghofer, A., and Gerwert, K., *A phosphoryl transfer intermediate in the GTPase reaction of Ras in complex with its GTPase-activating protein.* Proceedings of the National Academy of Sciences, 2006. **103**(38): p. 13911-13916.
217. Kötting, C., Kallenbach, A., Suveyzdis, Y., Wittinghofer, A., and Gerwert, K., *The GAP arginine finger movement into the catalytic site of Ras increases the activation entropy.* Proceedings of the National Academy of Sciences of the United States of America, 2008. **105**(17): p. 6260-6265.
218. Christoforidis, S., McBride, H.M., Burgoyne, R.D., and Zerial, M., *The Rab5 effector EEA1 is a core component of endosome docking.* Nature, 1999. **397**(6720): p. 621-5.

219. Stroupe, C. and Brunger, A.T., *Crystal Structures of a Rab Protein in its Inactive and Active Conformations.* Journal of Molecular Biology, 2000. **304**(4): p. 585-598.
220. Shirakawa, R., Higashi, T., Tabuchi, A., Yoshioka, A., Nishioka, H., Fukuda, M., Kita, T., and Horiuchi, H., *Munc13-4 is a GTP-Rab27-binding protein regulating dense core granule secretion in platelets.* The Journal of Biological Chemistry, 2004. **279**(11): p. 10730-7.
221. Kanno, E., Ishibashi, K., Kobayashi, H., Matsui, T., Ohbayashi, N., and Fukuda, M., *Comprehensive screening for novel rab-binding proteins by GST pull-down assay using 60 different mammalian Rabs.* Traffic, 2010. **11**(4): p. 491-507.
222. Mishra, A., Eathiraj, S., Corvera, S., and Lambright, D.G., *Structural basis for Rab GTPase recognition and endosome tethering by the C2H2 zinc finger of Early Endosomal Autoantigen 1 (EEA1).* Proceedings of the National Academy of Sciences of the United States of America, 2010. **107**(24): p. 10866-10871.
223. Hou, X., Hagemann, N., Schoebel, S., Blankenfeldt, W., Goody, R.S., Erdmann, K.S., and Itzen, A., *A structural basis for Lowe syndrome caused by mutations in the Rab-binding domain of OCRL1.* The EMBO Journal, 2011. **30**(8): p. 1659-1670.
224. Merithew, E., Hatherly, S., Dumas, J.J., Lawe, D.C., Heller-Harrison, R., and Lambright, D.G., *Structural plasticity of an invariant hydrophobic triad in the switch regions of Rab GTPases is a determinant of effector recognition.* The Journal of Biological Chemistry, 2001. **276**(17): p. 13982-8.
225. Fukuda, M., *Distinct Rab27A binding affinities of Slp2-a and Slac2-a/melanophilin: Hierarchy of Rab27A effectors.* Biochemical and Biophysical Research Communications, 2006. **343**(2): p. 666-74.
226. Bergbrede, T., Chuky, N., Schoebel, S., Blankenfeldt, W., Geyer, M., Fuchs, E., Goody, R.S., Barr, F., and Alexandrov, K., *Biophysical Analysis of the Interaction of Rab6a GTPase with Its Effector Domains.* The Journal of Biological Chemistry, 2009. **284**(5): p. 2628-2635.
227. Chavas, L.M.G., Ihara, K., Kawasaki, M., Torii, S., Uejima, T., Kato, R., Izumi, T., and Wakatsuki, S., *Elucidation of Rab27 recruitment by its effectors: structure of Rab27a bound to Exophilin4/Slp2-a.* Structure, 2008. **16**(10): p. 1468-77.
228. Wu, M., Wang, T., Loh, E., Hong, W., and Song, H., *Structural basis for recruitment of RILP by small GTPase Rab7.* The EMBO Journal, 2005. **24**(8): p. 1491-501.
229. Recacha, R., Boulet, A., Jollivet, F., Monier, S., Houdusse, A., Goud, B., and Khan, A.R., *Structural basis for recruitment of Rab6-interacting protein 1 to Golgi via a RUN domain.* Structure, 2009. **17**(1): p. 21-30.
230. Burguete, A.S., Fenn, T.D., Brunger, A.T., and Pfeffer, S.R., *Rab and Arl GTPase family members cooperate in the localization of the golgin GCC185.* Cell, 2008. **132**(2): p. 286-98.
231. Eathiraj, S., Mishra, A., Prekeris, R., and Lambright, D.G., *Structural basis for Rab11-mediated recruitment of FIP3 to recycling endosomes.* Journal of Molecular Biology, 2006. **364**(2): p. 121-35.
232. Eathiraj, S., Pan, X., Ritacco, C., and Lambright, D.G., *Structural basis of family-wide Rab GTPase recognition by rabenosyn-5.* Nature, 2005. **436**(7049): p. 415-9.

233. Zhu, G., Zhai, P., Liu, J., Terzyan, S., Li, G., and Zhang, X.C., *Structural basis of Rab5-Rabaptin5 interaction in endocytosis.* Nature Structural & Molecular Biology, 2004. **11**(10): p. 975-83.
234. Fukuda, M., *Regulation of secretory vesicle traffic by Rab small GTPases.* Cellular and Molecular Life Sciences, 2008. **65**(18): p. 2801-13.
235. Tolmachova, T., Anders, R., Stinchcombe, J., Bossi, G., Griffiths, G.M., Huxley, C., and Seabra, M.C., *A general role for Rab27a in secretory cells.* Molecular Biology of the Cell, 2004. **15**(1): p. 332-44.
236. Gomi, H., Mori, K., Itohara, S., and Izumi, T., *Rab27b is expressed in a wide range of exocytic cells and involved in the delivery of secretory granules near the plasma membrane.* Molecular Biology of the Cell, 2007. **18**(11): p. 4377-86.
237. Izumi, T., Gomi, H., Kasai, K., Mizutani, S., and Torii, S., *The roles of Rab27 and its effectors in the regulated secretory pathways.* Cell Structure and Function, 2003. **28**(5): p. 465-74.
238. Fukuda, M., *Versatile role of Rab27 in membrane trafficking: focus on the Rab27 effector families.* Journal of Biochemistry, 2005. **137**(1): p. 9-16.
239. Zhao, S., Torii, S., Yokota-Hashimoto, H., Takeuchi, T., and Izumi, T., *Involvement of Rab27b in the regulated secretion of pituitary hormones.* Endocrinology, 2002. **143**(5): p. 1817-24.
240. Barral, D.C., Ramalho, J.S., Anders, R., Hume, A.N., Knapton, H.J., Tolmachova, T., Collinson, L.M., Goulding, D., Authi, K.S., and Seabra, M.C., *Functional redundancy of Rab27 proteins and the pathogenesis of Griscelli syndrome.* The Journal of Clinical Investigation, 2002. **110**(2): p. 247-57.
241. Mizuno, K., Tolmachova, T., Ushakov, D.S., Romao, M., Abrink, M., Ferenczi, M.a., Raposo, G., and Seabra, M.C., *Rab27b regulates mast cell granule dynamics and secretion.* Traffic, 2007. **8**(7): p. 883-92.
242. Ostrowski, M., Carmo, N.B., Krumeich, S., Fanget, I., Raposo, G., Savina, A., Moita, C.F., Schauer, K., Hume, A.N., Freitas, R.P., Goud, B., Benaroch, P., Hacohen, N., Fukuda, M., Desnos, C., Seabra, M.C., Darchen, F., Amigorena, S., Moita, L.F., and Thery, C., *Rab27a and Rab27b control different steps of the exosome secretion pathway.* Nature Cell Biology, 2010. **12**(1): p. 19-30; sup pp 1-13.
243. Gordiyenko, N.V., Fariss, R.N., Zhi, C., and MacDonald, I.M., *Silencing of the CHM gene alters phagocytic and secretory pathways in the retinal pigment epithelium.* Investigative Ophthalmology & Visual Science, 2010. **51**(2): p. 1143-50.
244. Griscelli, C., Durandy, A., Guy-Grand, D., Daguillard, F., Herzog, C., and Prunieras, M., *A syndrome associating partial albinism and immunodeficiency.* The American Journal of Medicine, 1978. **65**(4): p. 691-702.
245. Klein, C., Philippe, N., Le Deist, F., Fraitag, S., Prost, C., Durandy, A., Fischer, A., and Griscelli, C., *Partial albinism with immunodeficiency (Griscelli syndrome).* The Journal of Pediatrics, 1994. **125**(6 Pt 1): p. 886-95.
246. Van Gele, M., Dynoodt, P., and Lambert, J., *Griscelli syndrome: a model system to study vesicular trafficking.* Pigment Cell & Melanoma Research, 2009. **22**(3): p. 268-82.

247. Brzezinska, A.A., Johnson, J.L., Munafo, D.B., Crozat, K., Beutler, B., Kiosses, W.B., Ellis, B.A., and Catz, S.D., *The Rab27a Effectors JFC1/Slp1 and Munc13-4 Regulate Exocytosis of Neutrophil Granules.* Traffic, 2008. **9**(12): p. 2151-2164.
248. Rojo Pulido, I., Nightingale, T.D., Darchen, F., Seabra, M.C., Cutler, D.F., and Gerke, V., *Myosin Va Acts in Concert with Rab27a and MyRIP to Regulate Acute Von-Willebrand Factor Release from Endothelial Cells.* Traffic, 2011. **12**(10): p. 1371-1382.
249. Arimura, N., Kimura, T., Nakamuta, S., Taya, S., Funahashi, Y., Hattori, A., Shimada, A., Ménager, C., Kawabata, S., Fujii, K., Iwamatsu, A., Segal, R.A., Fukuda, M., and Kaibuchi, K., *Anterograde Transport of TrkB in Axons Is Mediated by Direct Interaction with Slp1 and Rab27.* Developmental Cell, 2009. **16**(5): p. 675-686.
250. Fukuda, M., Saegusa, C., and Mikoshiba, K., *Novel splicing isoforms of synaptotagmin-like proteins 2 and 3: identification of the Slp homology domain.* Biochemical and Biophysical Research Communications, 2001. **283**(2): p. 513-9.
251. Fukuda, M. and Mikoshiba, K., *Synaptotagmin-like protein 1-3: a novel family of C-terminal-type tandem C2 proteins.* Biochemical and Biophysical Research Communications, 2001. **281**(5): p. 1226-33.
252. Gaullier, J.M., Simonsen, A., D'Arrigo, A., Bremnes, B., Stenmark, H., and Aasland, R., *FYVE fingers bind PtdIns(3)P.* Nature, 1998. **394**(6692): p. 432-3.
253. Burd, C.G. and Emr, S.D., *Phosphatidylinositol(3)-phosphate signaling mediated by specific binding to RING FYVE domains.* Molecular Cell, 1998. **2**(1): p. 157-62.
254. Fukuda, M., *Synaptotagmin-like protein (Slp) homology domain 1 of Slac2-a/melanophilin is a critical determinant of GTP-dependent specific binding to Rab27A.* The Journal of Biological Chemistry, 2002. **277**(42): p. 40118-24.
255. Nagashima, K., Torii, S., Yi, Z., Igarashi, M., Okamoto, K., Takeuchi, T., and Izumi, T., *Melanophilin directly links Rab27a and myosin Va through its distinct coiled-coil regions.* FEBS letters, 2002. **517**(1-3): p. 233-8.
256. Hattula, K., Furuhjelm, J., Tikkanen, J., Tanhuanpää, K., Laakkonen, P., and Peränen, J., *Characterization of the Rab8-specific membrane traffic route linked to protrusion formation.* Journal of Cell Science, 2006. **119**(23): p. 4866-4877.
257. Coppola, T., Frantz, C., Perret-Menoud, V., Gattesco, S., Hirling, H., and Regazzi, R., *Pancreatic β-cell protein granuphilin binds Rab3 and Munc-18 and controls exocytosis.* Molecular Biology of the Cell, 2002. **13**(6): p. 1906-1915.
258. Kimura, T., Kaneko, Y., Yamada, S., Ishihara, H., Senda, T., Iwamatsu, A., and Niki, I., *The GDP-dependent Rab27a effector coronin 3 controls endocytosis of secretory membrane in insulin-secreting cell lines.* Journal of Cell Science, 2008. **121**(Pt 18): p. 3092-8.
259. Izumi, T., *Physiological roles of Rab27 effectors in regulated exocytosis.* Endocrine Journal, 2007. **54**(5): p. 649-57.
260. Shirataki, H., Kaibuchi, K., Sakoda, T., Kishida, S., Yamaguchi, T., Wada, K., Miyazaki, M., and Takai, Y., *Rabphilin-3A, a putative target protein for smg p25A/rab3A p25 small GTP-binding protein related to synaptotagmin.* Molecular and Cellular Biology, 1993. **13**(4): p. 2061-8.

261. Kuroda, T.S., Fukuda, M., Ariga, H., and Mikoshiba, K., *The Slp homology domain of synaptotagmin-like proteins 1-4 and Slac2 functions as a novel Rab27A binding domain.* The Journal of Biological Chemistry, 2002. **277**(11): p. 9212-8.
262. Tsuboi, T., *Molecular mechanism of attachment process of dense-core vesicles to the plasma membrane in neuroendocrine cells.* Neuroscience Research, 2009. **63**(2): p. 83-8.
263. Wang, J., Takeuchi, T., Yokota, H., and Izumi, T., *Novel rabphilin-3-like protein associates with insulin-containing granules in pancreatic beta cells.* The Journal of Biological Chemistry, 1999. **274**(40): p. 28542-8.
264. Fukuda, M., *Slp4-a/Granuphilin-a Inhibits Dense-core Vesicle Exocytosis through Interaction with the GDP-bound Form of Rab27A in PC12 Cells.* The Journal of Biological Chemistry, 2003. **278**(17): p. 15390-15396.
265. Ren, Q., Wimmer, C., Chicka, M.C., Ye, S., Ren, Y., Hughson, F.M., and Whiteheart, S.W., *Munc13-4 is a limiting factor in the pathway required for platelet granule release and hemostasis.* Blood, 2010. **116**(6): p. 869-77.
266. Fisman, D.N., *Hemophagocytic syndromes and infection.* Emerging Infectious Diseases, 2000. **6**(6): p. 601-8.
267. Elstak, E., de Jong, A., and van der Sluijs, P., *A platform for complementation and characterization of familial haemophagocytic lymphohistiocytosis 3 mutations.* Journal of Immunological Methods, 2011. **365**(1-2): p. 58-66.
268. Kuroda, T.S., Ariga, H., and Fukuda, M., *The actin-binding domain of Slac2-a/melanophilin is required for melanosome distribution in melanocytes.* Molecular and Cellular Biology, 2003. **23**(15): p. 5245-55.
269. Kuroda, T.S. and Fukuda, M., *Rab27A-binding protein Slp2-a is required for peripheral melanosome distribution and elongated cell shape in melanocytes.* Nature Cell Biology, 2004. **6**(12): p. 1195-203.
270. Yu, M., Kasai, K., Nagashima, K., Torii, S., Yokota-Hashimoto, H., Okamoto, K., Takeuchi, T., Gomi, H., and Izumi, T., *Exophilin4/Slp2-a targets glucagon granules to the plasma membrane through unique Ca2+-inhibitory phospholipid-binding activity of the C2A domain.* Molecular Biology of the Cell, 2007. **18**(2): p. 688-96.
271. McAdara Berkowitz, J.K., Catz, S.D., Johnson, J.L., Ruedi, J.M., Thon, V., and Babior, B.M., *JFC1, a novel tandem C2 domain-containing protein associated with the leukocyte NADPH oxidase.* The Journal of Biological Chemistry, 2001. **276**(22): p. 18855-62.
272. Bergerat, A., de Massy, B., Gadelle, D., Varoutas, P.-C., Nicolas, A., and Forterre, P., *An atypical topoisomerase II from archaea with implications for meiotic recombination.* Nature, 1997. **386**(6623): p. 414-417.
273. Catz, S.D., Johnson, J.L., and Babior, B.M., *Characterization of the nucleotide-binding capacity and the ATPase activity of the PIP3-binding protein JFC1.* Proceedings of the National Academy of Sciences of the United States of America, 2001. **98**(20): p. 11230-5.
274. Johnson, J.L., Pacquelet, S., Lane, W.S., Eam, B., and Catz, S.D., *Akt regulates the subcellular localization of the Rab27a-binding protein JFC1 by phosphorylation.* Traffic, 2005. **6**(8): p. 667-81.

275. Lazar, T., Götte, M., and Gallwitz, D., *Vesicular transport: how many Ypt/Rab-GTPases make a eukaryotic cell?* Trends in Biochemical Sciences, 1997. **22**(12): p. 468-472.
276. Bacon, R.A., Salminen, A., Ruohola, H., Novick, P., and Ferro-Novick, S., *The GTP-binding protein Ypt1 is required for transport in vitro: the Golgi apparatus is defective in ypt1 mutants.* The Journal of Cell Biology, 1989. **109**(3): p. 1015-1022.
277. Plutner, H., Cox, A.D., Pind, S., Khosravi-Far, R., Bourne, J.R., Schwaninger, R., Der, C.J., and Balch, W.E., *Rab1b regulates vesicular transport between the endoplasmic reticulum and successive Golgi compartments.* The Journal of Cell Biology, 1991. **115**(1): p. 31-43.
278. Singer-Kruger, B., Stenmark, H., and Zerial, M., *Yeast Ypt51p and mammalian Rab5: counterparts with similar function in the early endocytic pathway.* Journal of Cell Science, 1995. **108**(11): p. 3509-3521.
279. Segev, N. and Gtpases, R., *Ypt and Rab GTPases: insight into functions through novel interactions.* Current Opinion in Cell Biology, 2001. **13**(4): p. 500-11.
280. Gallwitz, D., Donath, C., and Sander, C., *A yeast gene encoding a protein homologous to the human c-has/bas proto-oncogene product.* Nature, 1983. **306**(5944): p. 704-7.
281. Sclafani, A., Chen, S., Rivera-Molina, F., Reinisch, K., Novick, P., and Ferro-Novick, S., *Establishing a role for the GTPase Ypt1p at the late Golgi.* Traffic, 2010. **11**(4): p. 520-32.
282. Jones, S., Newman, C., Liu, F., and Segev, N., *The TRAPP complex is a nucleotide exchanger for Ypt1 and Ypt31/32.* Molecular Biology of the Cell, 2000. **11**(12): p. 4403-11.
283. Wang, W. and Ferro-Novick, S., *A Ypt32p exchange factor is a putative effector of Ypt1p.* Molecular Biology of the Cell, 2002. **13**(9): p. 3336-43.
284. Ortiz, D., Medkova, M., Walch-Solimena, C., and Novick, P., *Ypt32 recruits the Sec4p guanine nucleotide exchange factor, Sec2p, to secretory vesicles; evidence for a Rab cascade in yeast.* The Journal of Cell Biology, 2002. **157**(6): p. 1005-15.
285. Walch-Solimena, C., Collins, R.N., and Novick, P.J., *Sec2p Mediates Nucleotide Exchange on Sec4p and Is Involved in Polarized Delivery of Post-Golgi Vesicles.* The Journal of Cell Biology, 1997. **137**(7): p. 1495-1509.
286. Chen, S.H., Chen, S., Tokarev, A.A., Liu, F., Jedd, G., and Segev, N., *Ypt31/32 GTPases and their novel F-box effector protein Rcy1 regulate protein recycling.* Molecular Biology of the Cell, 2005. **16**(1): p. 178-92.
287. Nava, S., *Coordination of intracellular transport steps by GTPases.* Seminars in Cell & Developmental Biology, 2011. **22**(1): p. 33-38.
288. Benli, M., Doring, F., Robinson, D.G., Yang, X., and Gallwitz, D., *Two GTPase isoforms, Ypt31p and Ypt32p, are essential for Golgi function in yeast.* The EMBO Journal, 1996. **15**(23): p. 6460-75.
289. Casavola, E.C., Catucci, A., Bielli, P., Di Pentima, A., Porcu, G., Pennestri, M., Cicero, D.O., and Ragnini-Wilson, A., *Ypt32p and Mlc1p bind within the vesicle binding region of the class V myosin Myo2p globular tail domain.* Molecular Microbiology, 2008. **67**(5): p. 1051-66.
290. Lipatova, Z., Tokarev, A.A., Jin, Y., Mulholland, J., Weisman, L.S., and Segev, N., *Direct interaction between a myosin V motor and the Rab GTPases Ypt31/32 is*

required for polarized secretion. Molecular Biology of the Cell, 2008. **19**(10): p. 4177-87.

291. Mizuno-Yamasaki, E., Medkova, M., Coleman, J., and Novick, P., *Phosphatidylinositol 4-Phosphate Controls Both Membrane Recruitment and a Regulatory Switch of the Rab GEF Sec2p.* Developmental Cell, 2010. **18**(5): p. 828-840.
292. Jin, Y., Sultana, A., Gandhi, P., Franklin, E., Hamamoto, S., Khan, A.R., Munson, M., Schekman, R., and Weisman, L.S., *Myosin V transports secretory vesicles via a Rab GTPase cascade and interaction with the exocyst complex.* Developmental Cell, in press.
293. Santiago-Tirado, F.H. and Bretscher, A., *Membrane-trafficking sorting hubs: cooperation between PI4P and small GTPases at the trans-Golgi network.* Trends in Cell Biology, 2011. **21**(9): p. 515-525.
294. Medkova, M., France, Y.E., Coleman, J., and Novick, P., *The rab Exchange Factor Sec2p Reversibly Associates with the Exocyst.* Molecular Biology of the Cell, 2006. **17**(6): p. 2757-2769.
295. Guo, W., Roth, D., Walch-Solimena, C., and Novick, P., *The exocyst is an effector for Sec4p, targeting secretory vesicles to sites of exocytosis.* The EMBO Journal, 1999. **18**(4): p. 1071-1080.
296. Horgan, C.P. and McCaffrey, M.W., *The dynamic Rab11-FIPs.* Biochemical Society Transactions, 2009. **37**(Pt 5): p. 1032-6.
297. Roland, J.T., Lapierre, L.A., and Goldenring, J.R., *Alternative Splicing in Class V Myosins Determines Association with Rab10.* The Journal of Biological Chemistry, 2009. **284**(2): p. 1213-1223.
298. Rodriguez, O.C. and Cheney, R.E., *Human myosin-Vc is a novel class V myosin expressed in epithelial cells.* Journal of Cell Science, 2002. **115**(5): p. 991-1004.
299. Ishikura, S. and Klip, A., *Muscle cells engage Rab8A and myosin Vb in insulin-dependent GLUT4 translocation.* American Journal of Physiology - Cell Physiology, 2008. **295**(4): p. C1016-C1025.
300. Kamena, F., Diefenbacher, M., Kilchert, C., Schwarz, H., and Spang, A., *Ypt1p is essential for retrograde Golgi-ER transport and for Golgi maintenance in S. cerevisiae.* Journal of Cell Science, 2008. **121**(Pt 8): p. 1293-302.
301. Singer-Kruger, B., Stenmark, H., Dusterhoft, A., Philippsen, P., Yoo, J.S., Gallwitz, D., and Zerial, M., *Role of three rab5-like GTPases, Ypt51p, Ypt52p, and Ypt53p, in the endocytic and vacuolar protein sorting pathways of yeast.* The Journal of Cell Biology, 1994. **125**(2): p. 283-98.
302. Tsukada, M. and Gallwitz, D., *Isolation and characterization of SYS genes from yeast, multicopy suppressors of the functional loss of the transport GTPase Ypt6p.* Journal of Cell Science, 1996. **109 (Pt 10)**: p. 2471-81.
303. Haas, A., Scheglmann, D., Lazar, T., Gallwitz, D., and Wickner, W., *The GTPase Ypt7p of Saccharomyces cerevisiae is required on both partner vacuoles for the homotypic fusion step of vacuole inheritance.* The EMBO Journal, 1995. **14**(21): p. 5258-70.
304. Arai, S., Noda, Y., Kainuma, S., Wada, I., and Yoda, K., *Ypt11 functions in bud-directed transport of the Golgi by linking Myo2 to the coatomer subunit Ret2.* Current Biology, 2008. **18**(13): p. 987-91.

305. Tisdale, E.J., Bourne, J.R., Khosravi-Far, R., Der, C.J., and Balch, W.E., *GTP-binding mutants of rab1 and rab2 are potent inhibitors of vesicular transport from the endoplasmic reticulum to the Golgi complex.* The Journal of Cell Biology, 1992. **119**(4): p. 749-761.
306. Haas, A.K., Yoshimura, S.-i., Stephens, D.J., Preisinger, C., Fuchs, E., and Barr, F.A., *Analysis of GTPase-activating proteins: Rab1 and Rab43 are key Rabs required to maintain a functional Golgi complex in human cells.* Journal of Cell Science, 2007. **120**(17): p. 2997-3010.
307. Fraser, D.W., Tsai, T.R., Orenstein, W., Parkin, W.E., Beecham, H.J., Sharrar, R.G., Harris, J., Mallison, G.F., Martin, S.M., McDade, J.E., Shepard, C.C., and Brachman, P.S., *Legionnaires' disease: description of an epidemic of pneumonia.* The New England Journal of Medicine, 1977. **297**(22): p. 1189-97.
308. Kagan, J.C. and Roy, C.R., *Legionella phagosomes intercept vesicular traffic from endoplasmic reticulum exit sites.* Nature Cell Biology, 2002. **4**(12): p. 945-954.
309. Kagan, J.C., Stein, M.-p., Pypaert, M., and Roy, C.R., *Legionella subvert the functions of Rab1 and Sec22b to create a replicative organelle.* The Journal of Experimental Medicine, 2004. **199**(9): p. 1201-11.
310. Urwyler, S., Nyfeler, Y., Ragaz, C., Lee, H., Mueller, L.N., Aebersold, R., and Hilbi, H., *Proteome analysis of Legionella vacuoles purified by magnetic immunoseparation reveals secretory and endosomal GTPases.* Traffic, 2009. **10**(1): p. 76-87.
311. Machner, M.P. and Isberg, R.R., *Targeting of Host Rab GTPase Function by the Intravacuolar Pathogen Legionella pneumophila.* Developmental Cell, 2006. **11**(1): p. 47-56.
312. Brombacher, E., Urwyler, S., Ragaz, C., Weber, S.S., Kami, K., Overduin, M., and Hilbi, H., *Rab1 guanine nucleotide exchange factor SidM is a major phosphatidylinositol 4-phosphate-binding effector protein of Legionella pneumophila.* The Journal of Biological Chemistry, 2009. **284**(8): p. 4846-4856.
313. Müller, M.P., Peters, H., Blümer, J., Blankenfeldt, W., Goody, R.S., and Itzen, A., *The Legionella effector protein DrrA AMPylates the membrane traffic regulator Rab1b.* Science, 2010. **329**(5994): p. 946-949.
314. Suh, H.Y., Lee, D.W., Lee, K.H., Ku, B., Choi, S.J., Woo, J.S., Kim, Y.G., and Oh, B.H., *Structural insights into the dual nucleotide exchange and GDI displacement activity of SidM/DrrA.* The EMBO Journal, 2010. **29**(2): p. 496-504.
315. Laemmli, U.K., *Cleavage of structural proteins during the assembly of the head of bacteriophage T4.* Nature, 1970. **227**(5259): p. 680-5.
316. Berman, H.M., Westbrook, J., Feng, Z., Gilliland, G., Bhat, T.N., Weissig, H., Shindyalov, I.N., and Bourne, P.E., *The Protein Data Bank.* Nucleic Acids Research, 2000. **28**(1): p. 235-242.
317. Laskowski, R.A., MacArthur, M.W., Moss, D.S., and Thornton, J.M., *PROCHECK: a program to check the stereochemical quality of protein structures.* Journal of Applied Crystallography, 1993. **26**(2): p. 283-291.
318. Emsley, P. and Cowtan, K., *Coot: model-building tools for molecular graphics.* Acta Crystallographica. Section D, Biological Crystallography, 2004. **60**(Pt 12 Pt 1): p. 2126-32.

319. Kabsch, W., *Automatic processing of rotation diffraction data from crystals of initially unknown symmetry and cell constants.* Journal of Applied Crystallography, 1993. **26**(6): p. 795-800.
320. Vagin, A. and Teplyakov, A., *MOLREP: an Automated Program for Molecular Replacement.* Journal of Applied Crystallography, 1997. **30**: p. 1022-1025.
321. Sultana, A., Jin, Y., Dregger, C., Franklin, E., Weisman, L.S., and Khan, A.R., *The activation cycle of Ypt32 reveals structural determinants of effector recruitment and GDI binding.* FEBS letters, 2011. 585 (22): p. 3520-3527.
322. Murshudov, G.N., Vagin, A.A., and Dodson, E.J., *Refinement of macromolecular structures by the maximum-likelihood method.* Acta Crystallographica. Section D, Biological Crystallography, 1997. **53**(Pt 3): p. 240-55.
323. Collaborative Computational Project, N., *The CCP4 suite: programs for protein crystallography.* Acta Crystallographica. Section D, Biological Crystallography, 1994. **50**(Pt 5): p. 760-3.
324. Delano, W.L., *The PyMOL Molecular Graphics System*. 2002, DeLano Scientific.
325. Otwinowski, Z. and Minor, W., *[20] Processing of X-ray diffraction data collected in oscillation mode*, in *Methods in enzymology*, Charles W. Carter, Jr., Editor. 1997, Academic Press. p. 307-326.
326. Edgar, R.C., *MUSCLE: multiple sequence alignment with high accuracy and high throughput.* Nucleic Acids Research, 2004. **32**(5): p. 1792-1797.
327. Bond, C.S. and Schuttelkopf, A.W., *ALINE: a WYSIWYG protein-sequence alignment editor for publication-quality alignments.* Acta Crystallographica. Section D, Biological Crystallography, 2009. **65**(Pt 5): p. 510-2.
328. Menasche, G., Feldmann, J., Houdusse, A., Desaymard, C., Fischer, A., Goud, B., and de Saint Basile, G., *Biochemical and functional characterization of Rab27a mutations occurring in Griscelli syndrome patients.* Blood, 2003. **101**(7): p. 2736-42.
329. Chavas, L.M.G., Torii, S., Kamikubo, H., Kawasaki, M., Ihara, K., Kato, R., Kataoka, M., Izumi, T., and Wakatsuki, S., *Structure of the small GTPase Rab27b shows an unexpected swapped dimer.* Acta Crystallographica. Section D, Biological Crystallography, 2007. **63**(Pt 7): p. 769-79.
330. Davis, G.D., Elisee, C., Newham, D.M., and Harrison, R.G., *New fusion protein systems designed to give soluble expression in Escherichia coli.* Biotechnology and Bioengineering, 1999. **65**(4): p. 382-8.
331. Schoebel, S., Blankenfeldt, W., Goody, R.S., and Itzen, A., *High-affinity binding of phosphatidylinositol 4-phosphate by Legionella pneumophila DrrA.* EMBO Reports, 2010. **11**(8): p. 598-604.
332. Shirane, M. and Nakayama, K.I., *Protrudin Induces Neurite Formation by Directional Membrane Trafficking.* Science, 2006. **314**(5800): p. 818-821.
333. Johnson, J.L., Ellis, B.a., Noack, D., Seabra, M.C., and Catz, S.D., *The Rab27a-binding protein, JFC1, regulates androgen-dependent secretion of prostate-specific antigen and prostatic-specific acid phosphatase.* The Biochemical Journal, 2005. **391**(Pt 3): p. 699-710.
334. Shiba, T., Koga, H., Shin, H.W., Kawasaki, M., Kato, R., Nakayama, K., and Wakatsuki, S., *Structural basis for Rab11-dependent membrane recruitment of a family of Rab11-interacting protein 3 (FIP3)/Arfophilin-1.* Proceedings of the

National Academy of Sciences of the United States of America, 2006. **103**(42): p. 15416-15421.
335. De Marco, V., Stier, G., Blandin, S., and de Marco, A., *The solubility and stability of recombinant proteins are increased by their fusion to NusA.* Biochemical and Biophysical Research Communications, 2004. **322**(3): p. 766 - 771.
336. Stenmark, H. and Olkkonen, V.M., *The Rab GTPase family.* Genome Biology, 2001. **2**(5): p. 3007.1-3007.7.
337. Fernandes, H., Franklin, E., Recacha, R., Houdusse, A., Goud, B., and Khan, A.R., *Structural aspects of Rab6-effector complexes.* Biochemical Society Transactions, 2009. **37**(Pt 5): p. 1037-41.
338. Li, B.X., Satoh, A.K., and Ready, D.F., *Myosin V, Rab11, and dRip11 direct apical secretion and cellular morphogenesis in developing Drosophila photoreceptors.* The Journal of Cell Biology, 2007. **177**(4): p. 659-669.
339. Fan, G.-H., Lapierre, L.A., Goldenring, J.R., Sai, J., and Richmond, A., *Rab11-Family Interacting Protein 2 and Myosin Vb Are Required for CXCR2 Recycling and Receptor-mediated Chemotaxis.* Molecular Biology of the Cell, 2004. **15**(5): p. 2456-2469.
340. Hales, C.M., Vaerman, J.-P., and Goldenring, J.R., *Rab11 Family Interacting Protein 2 Associates with Myosin Vb and Regulates Plasma Membrane Recycling.* Journal of Biological Chemistry, 2002. **277**(52): p. 50415-50421.